Application of Endostatin Using Nonviral Gene Delivery Toward the Regeneration of Articular Cartilage

by

Lily Jeng

M.S. Biomedical Engineering
University of Limerick, 2006

B.S. Biomedical Engineering
North Carolina State University, 2005

SUBMITTED TO THE DEPARTMENT OF BIOLOGICAL ENGINEERING IN PARTIAL FULFILLMENT OF THE REQUIREMENTS FOR THE DEGREE OF

DOCTOR OF PHILOSOPHY IN BIOLOGICAL ENGINEERING
AT THE
MASSACHUSETTS INSTITUTE OF TECHNOLOGY

JUNE 2011

Signature of Author: _____
Department of Biological Engineering
May 9, 2011

Certified by: _____
Myron Spector
Professor of Orthopaedic Surgery (Biomaterials), Harvard Medical School
Senior Lecturer, Department of Mechanical Engineering, MIT
Thesis Co-Supervisor

_____
Ioannis V. Yannas
Professor of Mechanical and Biological Engineering, MIT
Thesis Co-Supervisor

Accepted by: _____
Forest M. White
Associate Professor of Biological Engineering
Chair, Biological Engineering Graduate Program Committee

A committee consisting of the following members has examined this doctoral thesis:

Thesis Committee Chair: Alan J. Grodzinsky, D.Sc.
Title: Professor of Biological, Electrical, and Mechanical Engineering, MIT

Thesis Supervisor: Myron Spector, Ph.D.
Title: Professor of Orthopaedic Surgery (Biomaterials), Harvard Medical School
Senior Lecturer, Department of Mechanical Engineering, MIT

Thesis Co-Advisor, Biological Engineering: Ioannis V. Yannas, Ph.D.
Title: Professor of Mechanical and Biological Engineering, MIT

Thesis Committee Member: Bjorn R. Olsen, M.D., Ph.D.
Title: Hersey Professor of Cell Biology, Harvard School of Dental Medicine

Application of Endostatin Using Nonviral Gene Delivery Toward the Regeneration of Articular Cartilage

by

Lily Jeng

Submitted to the Department of Biological Engineering on May 18, 2011 in Partial Fulfillment of the Requirements for the Degree of Doctor of Philosophy in Biological Engineering

ABSTRACT

Articular cartilage is avascular, and defects have limited capacity for spontaneous healing. Angiogenesis may interfere with maturation of naturally avascular tissues. Our rationale is that the use of endostatin, a potent angiogenesis inhibitor, will facilitate the formation of hyaline cartilage during regeneration. The objective of this thesis was to develop a system with a novel approach for treating cartilage defects, namely endostatin-producing cartilaginous constructs. The constructs were engineered using nonviral gene therapy, through evaluation of select variables, including regulators (culture media, endostatin plasmid load, method of pEndo lipoplex incorporation, and oxygen tension), scaffold formulation, and cell type. We also investigated select aspects of the *in vivo* cartilage defect model in which the construct can be implanted, including the post-surgical rehabilitation protocol and the use of osteogenic protein (OP)-1.

The principal achievement was the engineering of endostatin-expressing cartilaginous constructs *in vitro* using chondrocytes and mesenchymal stem cells, collagen sponge-like scaffolds and hydrogels, and chondrogenic medium. Peaks in endostatin protein were observed during the first few days of culture, followed by decreases. The endostatin levels were comparable to therapeutic levels *in vitro* and physiological levels *in vivo*. Most of the endostatin protein was released into the expended medium; little retention was observed, including in scaffolds supplemented with heparan sulfate, chondroitin sulfate, and heparin.

In vivo work examining chondral defects in the goat knee demonstrated that long-term post-operative immobilization, even with periodic passive motion exercise, resulted in significant joint degeneration. Cell-seeded scaffolds were observed in the defect 2 months following implantation and short-term immobilization, and yielded results at least as good as historical data obtained using other treatment techniques, including autologous chondrocyte implantation and microfracture, suggesting that a cell-seeded scaffold is a viable option for cartilage repair. There was no significant benefit of multiple treatments of OP-1 on chondral defects. Neovascularization was observed in the largely fibrous reparative tissue filling the chondral defects, providing further rationale for the use of endostatin.

A notable finding was the observation of laminin and type IV collagen, 2 common basement membrane molecules, in both *in vitro* engineered cartilaginous constructs and *in vivo* cartilage repair samples.

Thesis Co-Supervisor: Myron Spector
Title: Professor of Orthopaedic Surgery (Biomaterials), Harvard Medical School
Senior Lecturer, Department of Mechanical Engineering, MIT

Thesis Co-Supervisor: Ioannis V. Yannas
Title: Professor of Mechanical and Biological Engineering, MIT

ACKNOWLEDGEMENTS

Research is not a solitary endeavor, and this thesis could not have happened without the support of many people, to whom I am grateful.

I am incredibly appreciative to Dr. Myron Spector. It has been an absolute pleasure to work with you. You are an excellent teacher and mentor, engaging me in stimulating discussions while allowing me to learn and explore. Thank you for all of your advice and support, and for sharing your passion for research.

Thank you to Dr. Ioannis Yannas for your valuable suggestions.

Dr. Bjorn Olsen, thank you for all of your excellent advice.

Dr. Alan Grodzinsky, thank you for your wonderful insight, especially in all things cartilage.

Dr. Hu-Ping Hsu, thank you for teaching me about animal surgery and allowing me to learn hands-on, and for helpful advice along the way.

Alix Weaver, thank you for all your assistance with the nitty-gritty details involved with doing research and experiments.

Dr. Naomi Fukai and Dr. Donald Glotzer, thank you for your technical assistance and willingness to help.

Dr. Robert Padera, thank you for your pathology expertise.

To the VA Tissue Engineering Laboratories, including Cathy Bolliet, Thomas Cheriyan, Rahmat Cholas, Paul Elias, Casper Foldager, Tadanao Funakoshi, Cathal Kearney, Teck Chuan Lim, Carol Lucchesi, Daniel Macaya, Karen Ng, Roman Perez, Kristy Shine, Xiaodan Sun, Wei Seong Toh, Erica Ueda, Scott Vickers, Tzu-Wei Wang, Hsi-Chin Wu, Malcolm Xing, and all other students, postdoctoral fellows, and visiting scientists, thank you for all of your help, for the interesting conversations, and for making my time at the lab a great one.

To labs at the VA Boston Healthcare System and MIT, thank you for allowing me the use of your equipment.

Thank you to my family and friends, especially my mom, my dad, and Jeff, for their love and support. I couldn't have done it without you.

Financial support provided for this research is gratefully acknowledged: Department of Veterans Affairs; the National Science Foundation; and the Siebel Foundation.

TABLE OF CONTENTS

LIST OF FIGURES

LIST OF TABLES

CHAPTER 1: INTRODUCTION

The material presented in this chapter was adapted from the following publication, with permission of Elsevier Inc.:

Jeng L, Ng kee Kwong F, Spector M. Articular cartilage. In Atala A., Lanza R., Thomson J., Nerem R. (Eds.), Principles of Regenerative Medicine, 2nd ed (pp. 761-777). San Diego: Elsevier, 2011.

1.1. Articular Cartilage

1.1.1. Structure and Function

Articular cartilage is a specialized form of hyaline cartilage. It is normally resistant to vascularization and contains no blood vessels, as well as lacking nerves and lymphatics, instead receiving its nutrients largely from the synovial fluid. It is a connective tissue located at the ends of long bones in synovial joints, such as the hip and the knee. It resides in an environment of low oxygen around 5% [1] and intermittent loading. Cartilage provides a low-friction, load-bearing surface capable of resisting peak stress levels up to 18 MPa [2]. Its major components include chondrocytes and water trapped in a dense extracellular matrix (ECM) rich in collagens (primarily type II collagen), proteoglycans consisting of chondroitin sulfate, keratin sulfate, dermatan sulfate, and heparan sulfate (HS) glycosaminoglycans (GAGs) [3], and other noncollagenous proteins [4]. Chondrocytes, which are crucial for the synthesis and turnover of the cartilage ECM, are the only cell type present in articular cartilage. They are found at a low cell density of 10,000 cells/mm^3, representing 2% of the total cartilage volume, and exhibit low mitotic activity [5].

The extracellular matrix can be further divided into the thin pericellular matrix immediately surrounding the chondrocytes, the territorial matrix encapsulating the cell and pericellular matrix, and the abundant interterritorial matrix [6]. Articular cartilage is not generally thought of as having a traditional basement membrane structure, a specialized form of extracellular matrix. However, the presence of basement membrane molecules, including laminin [7-9], type IV collagen [8], perlecan [8, 10-13], nidogen [8], and type XVIII collagen/endostatin [14], have been reported in the ECM of normal adult articular cartilage. These molecules have generally been found to be localized to the pericellular matrix, resulting in

discussions of the pericellular matrix as a functional equivalent of the basement membrane in articular cartilage [8]. It is thought that basement membrane molecules, such as perlecan, may have important structural and organizational roles in normal articular cartilage, as they can interact with a number of the anchoring and fibrillar proteins in cartilage extracellular matrix [13]. Chondrocytes have also been shown to express several cell surface integrins that bind type IV collagen, laminin, and perlecan, and the basement membrane components may play important roles in chondrocyte survival and differentiation and may aid cells in sensing and responding to changes in their biomechanical environment by modulating signal transduction events [8, 13].

1.1.2. Clinical Problem

Cartilage defects are a common source of pain and/or loss of function in patients presenting to the orthopedic clinic. While any joint can be affected, the joint most commonly affected is the knee. A chondral lesion was found in 63% of a large series of over 31,000 arthroscopic procedures performed in patients with a symptomatic knee [15].

These defects can be divided according to their etiology or morphology. Focal injuries typically occur as a result of a sporting injury and hence tend to affect the younger population. Focal defects can be further subdivided into chondral or osteochondral lesions, depending on the depth of the defect. Chondral lesions, also known as partial thickness lesions, lie entirely within the cartilage and do not penetrate into the sub-chondral bone. In the adult, defects of this nature do not regenerate because of the lack of cells which could participate in the repair process. Osteochondral defects penetrate through the vascularized subchondral bone and some spontaneous repair occurs as mesenchymal chondroprogenitor cells invade the lesion and form cartilage. However, full-thickness defect repair is only transient and the novel tissue formed does

not have the functional properties of native hyaline cartilage [16]. On the other hand, degenerative chondral changes typically occur in the older population as a result of arthritic changes. They often involve a large area of the affected joint, but start off as a focal lesion initially. This thesis will focus on focal chondral defects.

In 1743, Hunter stated that cartilage, once destroyed, cannot be repaired, and this observation has not changed much since [17]. It is generally agreed that adult articular cartilage exhibits poor healing potential because none of the normal inflammatory and reparative processes of the body are available to repair the tissue. Furthermore, chondrocytes which are surrounded by an extracellular matrix cannot freely migrate to the site of injury from an intact healthy site, unlike most tissues [18], and there is no provisional fibrin clot filling the defect into which cells can migrate. Full-thickness defects induce mesenchymal chondroprogenitor cells to differentiate into repair tissue, but this is predominantly fibrous in nature and degenerates with time. Damage, caused by disease, injury, or repetitive loading, presents a significant orthopedic challenge—defects do not heal spontaneously to their original quality; rather, untreated defects lead to pain, inflammation, decrease in mobility, loss of large amounts of cartilage tissue, and the onset of osteoarthritis.

1.1.3. Current Clinical Treatments

Current clinical treatment strategies, including microfracture, osteochondral autografting, and autologous chondrocyte implantation, focus primarily on symptomatic relief.

1.1.3.1. Microfracture

An array of marrow-stimulation techniques, including abrasion arthroplasty, drilling, and microfracture, have been used to treat cartilage defects. Microfracture, a technique commonly used in the clinic, involves the creation of small holes in the underlying bone to allow blood, bone marrow, and marrow-derived MSCs into the cartilage defect site [19, 20]. More recently, a collagen membrane has been applied over microfracture-treated defects in order to contain the blood clot and marrow-derived MSCs, in the procedure referred to as "autologous matrix-induced chondrogenesis" (AMIC) [21].

1.1.3.2. Osteochondral Autografting

Osteochondral autografting involves implanting small cylindrical cartilage-bone grafts from non-weight-bearing cartilage at the periphery of the joint into cartilage defects [22].

1.1.3.3. Autologous Chondrocyte Implantation (ACI)

Since first published in 1994 [23], techniques of cell isolation, expansion in culture, and implantation have remained essentially the same. Cartilage (150–300mg) is harvested arthroscopically from a minimally load-bearing area of the upper aspect or the medial condyle of the affected knee. The biopsy is then transported to a laboratory facility using a transport media. Chondrocytes are isolated using standard techniques. After a certain period of cell expansion (11–21 days [24], depending upon the growth kinetics) a certain number of cells (e.g. minimally 12 million for Genzyme's Carticel procedure) are provided in a serum-free and gentamycin-free transport medium.

Using a medial or lateral parapatellar incision, the defect is debrided to the level of

normal-appearing surrounding cartilage. The integrity of the tidemark needs to be maintained in order to avoid infiltration of undifferentiated mesenchymal stem cells (MSCs) which could contribute to the formation of fibrocartilagenous repair tissue [25]. A periosteal flap is harvested from the anterior aspect of the proximal tibia or distal femur, formed to the shape of the lesion, and sutured to the rim of the defect. The chondrocyte suspension is subsequently injected under the periosteal flap and the border of periosteal cover sealed using fibrin glue. Post-operative rehabilitation protocols generally involve continuous passive motion and limited weight bearing for an extended time. Cooperation of the patient in this respect is essential for a favorable outcome and is difficult to control. This contributes to difficulty in evaluating outcome data.

There are several second generation variations of this technique. In one variation, an off-the-shelf porcine type I/III collagen membrane has been used in place of the periosteal membrane [26]. Its outer surface is smooth, facilitating a low-friction surface. Its inner surface, which is porous due to large gaps among collagen fibers, can accommodate the seeding of cultured chondrocytes, in a procedure referred to as "matrix-assisted autologous chondrocyte implantation" (MACI). In other work, a hyaluronan-based sponge-like scaffold seeded with autologous chondrocytes has been used to fill a cartilage defect site [27]. Both studies found comparable short-term outcomes among the various methods.

1.1.3.4. Clinical Outcomes

Clinical results at follow-ups ranging from 2 to 11 years indicated good to excellent results for 67% of microfracture cases examined in one study [28], 91% of osteochondral autografting cases [29], and 84% of autologous chondrocyte implantation cases [30]. However, the reparative tissue is often observed to be fibrocartilaginous in nature and lacking the

biochemical and biomechanical properties of normal articular cartilage, and it is unclear if the tissue is able to withstand joint loading over the longer term [31]. Focal defects can also lead to degeneration of the entire joint and the need for total joint replacements. While prostheses significantly reduce pain and increase mobility, they are subject to wear, produce problematic debris, are not sufficient for physically active individuals, and eventually fail.

1.2. Tissue Engineering and Regenerative Medicine

Tissue engineering and regenerative medicine provide a potential new solution for treating cartilage defects by utilizing a combination of scaffolds, cells, and regulators to engineer and regenerate new tissue. In this thesis, the term tissue engineering will be used to refer to both tissue engineering and regenerative medicine.

1.2.1. Scaffolds

Scaffolds can be made of synthetic polymers, such as polyglycolides, polylactides, polyorthoesters, and polyanhydrides, or naturally derived biological materials, such as collagen, gelatin, alginate, and hyaluronan. Ideally, scaffolds should be biocompatible, bioresorbable, highly porous with interconnected pores, encourage cell attachment and proliferation, and match the mechanical properties of the surrounding native tissue [32]. Collagen provides an attractive scaffold material choice, as it is one of the most abundant proteins in the body and is naturally recognized by cells. Several studies have investigated the use of collagen scaffolds for the regeneration of various tissues, including dermis [33], peripheral nerve [34], lung [35], heart [36], tendon [37], and articular cartilage [38, 39]. Among different collagen types, type II

collagen scaffolds have been found to promote chondrogenesis compared to type I collagen scaffolds [40, 41].

The physical presentation of scaffolds can vary, such as porous sponge-like scaffolds or gel-like hydrogel scaffolds. In a comparison of several matrix materials (synthetic materials like polylactic acid and naturally-occurring polymers like collagen gel and porous collagen), Grande *et al.* showed a marked variability of the chondrocyte response [42]. Bioabsorbable polymers such as polyglycolic acid (PGA) enhanced proteoglycan synthesis, whereas collagen matrices stimulated synthesis of collagen.

The scaffold alone has not yet been used for treatment of articular cartilage in humans. In animal work with a canine model, type I collagen scaffolds implanted in a chondral defect resulted in 37% filling of the total defect after 15 weeks, with the reparative tissue consisting of a combination of fibrous tissue and fibrocartilage but no hyaline or articular cartilage [43]. A chondral defect treated with microfracture plus implantation of a type II collagen scaffold resulted in 86% filling of the total defect after 15 weeks; however, the reparative tissue was comprised primarily of fibrocartilage, some fibrous tissue, and less than 2% hyaline or articular cartilage [44]. These findings suggest that the scaffold alone is not sufficient for regenerating articular cartilage defects back to their original quality.

1.2.2. Cells

The addition of cells to the scaffolds has been shown to result in improved repair compared to the scaffold alone—a canine study found 88% filling of the original defect, with the reparative tissue consisting of 42% hyaline cartilage, 15 weeks following implantation [38]. No one optimal cell source has been agreed upon; instead, several different cell sources are being

researched for use in articular cartilage applications: chondrocytes and chondroprogenitor cells from various sources, such as periosteum, perichondrium, synovium, adipose, muscle, bone marrow, and the embryo [45-49].

1.2.2.1. Chondrocytes

Chondrocytes comprise the single cellular component of adult hyaline cartilage and are considered to be terminally differentiated, thus being highly specialized. In articular cartilage, their main function is to maintain the cartilage matrix, synthesizing types II, IX, and XI collagen; the large aggregating proteoglycan, aggrecan (which consists of glycosaminoglycans (GAGs) attached to a protein core); the smaller proteoglycans, biglycan and decorin; and specific and non-specific matrix proteins that are expressed at defined stages during growth and development. This makes them a suitable cell type for a cell-based treatment of chondral defects. However, there are also disadvantages to using chondrocytes—they are available in very limited quantities, tend to dedifferentiate during two-dimensional culture *in vitro*, and are associated with donor site morbidity at the site of cartilage harvest [50].

Chondrocytes, in addition to cells from other musculoskeletal tissues, have also been shown to synthesize lubricin [51]. Lubricin is an important glycoprotein in the joint, having been found to act as boundary lubrication at the surfaces of articular cartilage [52] and to provide chondroprotective effects by dissipating strain energy resulting from loading [53]. However, lubricin has not yet been extensively studied in tissue engineered-constructs.

1.2.2.2. Mesenchymal Stem Cells (MSCs)

An alternative cell source, mesenchymal stem cells (MSCs) derived from the bone marrow, is also of interest. MSCs are multipotent progenitor cells capable of differentiating into bone, cartilage, muscle, tendon, ligament, and other connective tissues, and they can be expanded in monolayer while retaining their differentiation potential [54].

1.2.2.3. Embryonic Stem (ES) Cells

Embryonic stem (ES) cells are less differentiated than MSCs, with the potential to generate all cell types in the body, and have the almost unlimited capacity to self-renew in culture. However, the use of these cells for cartilage applications is not as common as other cell types. Early research in this area has demonstrated the chondrogenic potential of ES cells [49]. The optimal culture conditions needed to differentiate ES cells down the chondrogenic lineage have not been identified. This area is actively being researched; for example, one study showed that TGF-β1, insulin, ascorbic acid, and BMP-2—many of the same regulators used in the culture of chondrocytes and MSCs—induced chondrogenic differentiation of ES cells as evidenced by the expression of collagen type IIB and aggrecan [55]. Other studies have found that co-culture of ES cells with articular chondrocytes enhances the chondrocytic commitment of the ES cells [56, 57].

A few *in vivo* studies have shown that ES cells [58, 59] and ES cell-derived chondrogenic cells [60] implanted into animals resulted in improved healing and the formation of cartilaginous tissue. However, Wakitani *et al.* found teratoma formation in the knee joints of mice with severe combined immunodeficiency following transplantation of ES cells into the joints [61], highlighting important safety concerns regarding the use of ES cells. It also raises the question of

whether ES cells should be pre-differentiated *in vitro* prior to transplantation. Clearly, much more basic research is needed into ES cells before their efficacy for cartilage tissue engineering can be evaluated. While the potential of ES cells is interesting, they are outside of the scope of this thesis.

1.2.3. Regulators

Regulators, including both soluble and mechanical factors, have been shown to aid in the induction and development of cartilage formation [62].

1.2.3.1. Soluble Regulators

Several soluble regulators have been identified for their beneficial effects in cartilage applications, including bone morphogenetic factors (BMPs), fibroblast growth factor (FGF)-2, and transforming growth factor (TGF)-β. BMPs are a family of cytokines known for their ability to induce bone and cartilage formation, making them particularly appealing for use in osteochondral defects [62]. In particular, BMP-2 and BMP-7 stimulate ECM formation, increasing the expression levels of tissue inhibitor of matrix metalloproteinases (TIMP)-1, Sox9, type II collagen, and aggrecan [63-65]. FGF-2 has been shown to increase cell proliferation and reduce the expression of a dedifferentiated fibroblastic phenotype [66]. TGF-β is one of the most used growth factors for cartilage and has been shown to induce chondrogenesis of adult MSCs and stimulate ECM synthesis and chondrocyte proliferation [67-71]. It has been suggested that the different isoforms of TGF-β play different roles in cartilage development—TGF-β1 participates in cell-cell interactions during initial condensation of progenitor cells, TGF-β2 is involved in hypertrophic differentiation, and TGF-β3 aids in MSC differentiation [62, 72, 73].

1.2.3.2. Mechanical Regulators

Mechanical regulators, such as hydrostatic pressure and dynamic compression, mimic the cues cells receive *in vivo* and may serve to promote ECM synthesis and accumulation and enhance nutrient transport if applied within specific ranges; however, mechanical regulators are outside the scope of this project [62].

1.3. Angiogenesis

1.3.1. Angiogenesis in Normal Physiological Processes

Angiogenesis is a part of several physiological processes, including embryogenesis, wound healing, and the female reproductive cycle [74]. In normal skeletal development, angiogenesis plays a pivotal role coordinating the transformation from cartilage to bone during endochondral ossification, and potent angiogenic molecules, such as vascular endothelial growth factor (VEGF), have been found to be present in growth plate cartilage [75]. The wound healing response in adults consists of three classic phases: inflammation, proliferation, and remodeling. Angiogenesis, which is critical for a successful repair response, is generally considered to occur during the proliferative stage. Specifically, the newly formed blood vessels participate in granulation tissue formation and support the reparative tissue with nutrition and oxygen as the tissue remodels and matures [76].

1.3.2. Angiogenesis Inhibition in Normal Articular Cartilage

The process of angiogenesis is tightly regulated by the balance between promoters and inhibitors of angiogenesis [77]. Normal mature (adult) articular cartilage contains no blood vessels and actively resists vascular invasion, possibly due to the generation of anti-angiogenic factors by chondrocytes [86]. Several angiogenesis inhibitors have been identified in cartilage, including troponin I [78], chondromodulin I [79], TIMPs [80], metastatin [81], and endostatin [14].

During embryonic development, cartilage formation is associated with avascularity. In the early stages of the process, vascular regression is observed in areas in which cartilage will form, whereas blood vessels in the remainder of the mesenchyme are unaffected [82]. Yin *et al.* found that vascular regression is required for chondrogenesis, in a chick embryo model, and it was hypothesized that the regression is a result of anti-angiogenic molecules produced by mesenchymal cells [83]. Following vascular regression, the mesenchyme then undergoes prechondrogenic condensation, resulting in a localized increase in cell density and rounded mesenchymal cells in close contact [83, 84]. The cells differentiate into chondrocytes, cartilaginous extracellular matrix is synthesized, and cartilage tissue is formed [83]. It should be noted that the environment remains avascular throughout this process [83]. Namba and colleagues found that chondral defects in a fetal lamb model were capable of undergoing complete spontaneous regeneration without scar tissue (or fibrocartilage) formation, in the absence of blood products and without any observed inflammatory response [85].

1.3.3. Angiogenesis Associated with Adult Articular Cartilage Repair

The presence of blood vessels in articular cartilage has been observed during the cartilage healing response in adults. Research suggests that the vascular endothelial cells may have the potential to undergo an endothelial-to-mesechymal transition and conversion into multipotent stem-like cells, which has implications for tissue engineering [87]. However, angiogenesis in articular cartilage may present problems. The physical presence of vessels may compromise the mechanical properties of cartilage [74]. Enzymes normally involved in neovascularization, such as collagenase (matrix metalloproteinase-1, MMP-1) can disrupt and degrade the extracellular matrix of articular cartilage [74]. Blood vessels may also represent a chemical barrier to chondrogenesis, through release of anti-chondrogenic factors from vascular endothelial cells or from those circulating in the blood [88, 89].

Recent studies have investigated angiogenesis inhibitors, such as Flt-1 [97], endostatin [98], and suramin [99], for the regulation of angiogenesis during the repair process and to try to improve cartilage regeneration. Two such studies {Kubo, 2009 #168}{Matsumoto, 2009 #461} have demonstrated improved cartilage formation in repair models in which an anti-angiogenic factor (Flt-1) was delivered.

1.3.4. Angiogenesis Associated with Articular Cartilage Degradation

Angiogenesis in articular cartilage is believed to be a key contributor to the symptoms and pathology associated with osteoarthritis (OA) [90]. Osteoarthritic cartilage has been shown to lose its resistance to vascular invasion compared to normal articular cartilage, with associated deposition of new collagen types I and X and loss of staining for proteoglycans [86, 91]. In the early stages of OA, vascular redistribution in the subchondral bone can lead to the advancement

of vessels into the cartilage. As the vessels invade, new bone and sensory nerves can also develop around the channels, contributing to the formation of osteophytes and the sensation of pain [92]. VEGF—a peptide that attracts endothelial cells during wound healing, is involved in the inflammatory process, and may also increase the production of MMPs while decreasing the production of TIMPs—is thought to have a significant role during the progression of OA [90]. Increased expression of VEGF and its receptor, VEGF receptor 2 (VEGF-R2), have been detected in chondrocytes in the superficial zone of osteoarthritic cartilage compared to healthy articular cartilage [93]. Chronic synovial inflammation, commonly associated with rheumatoid arthritis but also seen in OA, is also accompanied by angiogenesis. Specifically, proinflammatory cytokines, such as tumor necrosis factor (TNF)-α and interleukin (IL)-1, act as pro-angiogenic factors as they stimulate the production of VEGF via the c-Jun N-terminal kinase (JNK) signaling pathway [90, 94]. Strongly decreased oxygen levels and cartilage hypoxia, additional hallmarks of osteoarthritic cartilage, are also associated with angiogenesis—hypoxic conditions activate hypoxia-inducible transcription factor (HIF)-1α, which is known to induce upregulation of VEGF in chondrocytes via the p38 mitogen-activated protein (MAP) kinase pathway [94, 95]. In addition, mechanical overload, one of the causative factors for OA, has also been shown to induce VEGF expression in chondrocytes [96].

1.3.5. Basis of Rationale for Angiogenesis Inhibition During Cartilage Regeneration

The rationale for the supposition that an anti-angiogenic factor (*viz.*, endostatin) will favor the formation of hyaline (articular) cartilage in cartilage defects is based on findings : 1) in embryonic development of cartilage that cartilage formed only in areas in which there was vascular regression; 2) in adult articular cartilage that inhibition of angiogenesis improved

cartilage formation; and 3) in adult articular cartilage that vascular invasion of cartilage was associated with cartilage degeneration.

1.4. Endostatin

Endostatin is arguably one of the most potent and most widely researched angiogenesis inhibitors. It is a 20 kDa carboxy-terminal proteolytic fragment that was first isolated from conditioned media from a murine hemangioendothelioma [100]. It is located at the noncollagenous (NC) 1 domain of the basement membrane molecule collagen XVIII [101-103] and is cleaved by cathepsins and MMPs [104, 105]. Endostatin is present in the circulation of normal individuals around 35 ng/ml [106]. It has been shown to strongly inhibit endothelial cell proliferation and migration and prevent the formation of blood vessels in a biphasic dose-response curve, with reported concentrations around 100-200 ng/ml for proliferation inhibition and 0.1-10 ng/ml for migration inhibition [100, 107-109] Endostatin has been of particular interest as a proposed method to control tumorigenesis, having been shown to prevent growth and promote regression of tumors in mice at doses from 1.5 to 50 mg/kg with no observed toxicity or acquired drug resistance [110]. In addition to its anti-angiogenic properties, endostatin also appears to affect other processes, having recently been shown to inhibit neurogenesis [111, 112].

The exact mechanism by which endostatin inhibits angiogenesis is unclear. Endostatin has been shown to directly interact with VEGF-R2, leading to decreased endothelial cell motility, proliferation, and survival [113]. Endostatin can bind with integrin $\alpha_5\beta_1$ on the cell surface of proliferating endothelial cells, inhibiting signaling pathways mediated by MAP kinases, such as extracellular signal-regulated kinase (ERK)-1 and p38, and resulting in

decreased cell migration. When endostatin binds to $\alpha_5\beta_1$, it can also activate tyrosine kinases of the Src family, causing subsequent disruption of the actin cytoskeleton, cell focal contacts, and deposition of fibronectin matrix, thus lowering cell migration and adhesion [114-116]. Endostatin has also been observed to modulate the intracellular pathways Wnt/β-catenin [117] and calcium signaling [118] and can inhibit some MMPs, having been specifically shown to bind with MMP-2 and -9 [119, 120]. Endostatin can downregulate cyclin D1 and arrest the endothelial cell cycle progression at the G_1 phase [121]. Genome-wide expression profiling has shown that endostatin downregulates many known pro-angiogenic genes, such as HIF-1α and TNF-α, and upregulates many anti-angiogenic genes in human microvascular endothelial cells [122]. While the mechanism is of great research interest, it is outside of the scope of this proposal.

1.4.1. Endostatin in Articular Cartilage

Endostatin levels in articular cartilage have been found to be the highest in fetal cartilage (964 pg/mg fresh weight), lower in normal adult cartilage (228 pg/mg), and lowest in osteoarthritic cartilage (147 pg/mg) [14]. Chondrocytes were found to synthesize endostatin *in vitro* and *in vivo*. Research suggests that endostatin promotes anabolic activity in cartilage. Recombinant human endostatin was shown to promote chondrocyte adhesion and proliferation and led to an upregulation of the transcription of type II collagen, TIMP-1, and type XVIII collagen and a downregulation of type I collagen and MMP-9 *in vitro* [123].

1.4.2. Endostatin in the Regulation of Endochondral Ossification

Endostatin retards cartilage resorption during endochondral ossification and reduces bone formation. In one study, BMP-supplemented gelatine gels implanted in the hamstring muscles with VEGF, endostatin, both, or neither led to significant ectopic bone formation for all groups. The endostatin group demonstrated a decrease in proportional area of bone tissue/osseous nodule, reduction in cartilage-resorbing osteooclasts, and decrease in blood vessel density/field when compared to the VEGF group after 3 weeks [124].

1.5. Nonviral Gene Transfer

While developments in cloning technology have led to the identification of many proteins, such as endostatin, that may be of value for tissue engineering, protein-based therapies, such as the use of TGF-β in the culture medium, are difficult and expensive to administer effectively. Many of these factors have a short half-life—the half-life of the endostatin protein *in vivo* is on the order of several hours—and would require frequent administration [125]. Targeted delivery can be difficult, leading to the use of high dosages that could have serious unintentional side effects for other tissues. Advances in molecular biology have allowed for the use of the gene precursors of these proteins for gene therapy [126-132], enabling the body to produce sustained, regulated levels of proteins in a local area.

Naked DNA is generally not taken up by cells, necessitating the use of gene delivery agents, including viral and nonviral vectors. Viral vectors, such as retroviruses, adenoviruses, and lentiviruses, are widely used due to their high transfection efficiencies around 80-90%, compared to 40-50% for nonviral agents [133]. One group studied the effects of chondrocytes transduced using an adenovirus vector encoding for IGF-1 on healing in equine cartilage defects

[134]. They found an increased amount of hyaline-like tissue filling the defects compared to controls filled with thin and irregular fibrous tissue. In another study, adeno-associated virus-TGF-β1-transduced MSCs implanted into osteochondral defects of athymic rats resulted in improved cartilage repair at 12 weeks [135].

When using nonviral vectors, including liposomes, DNA-ligand complexes, magnetic nanoparticles, electroporation, and gene guns, the DNA tends to remain episomal (not integrated into the host cell chromosomes), resulting in transient expression of the gene product [136, 137]. However, concerns regarding the safety, possible mutagenesis, and immunogenicity of viral vectors have led to increasing popularity of nonviral vectors, which have been shown to trigger little inflammatory response, are simple to synthesize, and have large carrying capacity. One commonly used nonviral agent, cationic liposomes, spontaneously associates with negatively charged DNA due to charge interactions, forming lipoplexes. These membrane-bound plasmids can then be internalized by cells for transfection [138]. Prior work in our lab has found that lipoplexes result in higher transfection efficiencies than other nonviral vectors, such as chitosan (unpublished). One group [139] transfected chondrocytes using a nonviral, lipid-mediated agent carrying the FGF-2 gene and implanted the genetically engineered cells into osteochondral defects. They found enhanced articular cartilage repair after 14 weeks without adverse effects.

In general, there are two strategies for gene therapy: a direct *in vivo* method or an indirect *ex vivo* method. With the *in vivo* method, the vector is directly injected into either the bloodstream for systemic delivery or the tissue of choice for local delivery, making it simple to perform clinically. The *ex vivo* method involves transfecting cells cultured outside the body and then reimplanting the cells into the patient. The second method is more complex but allows for more targeted delivery to specific cells [140]. Modified cationic liposomes have already been

demonstrated to successfully transfect cells of orthopedic importance, including chondrocytes, with TGF-β both *in vivo* [141] and *ex vivo* [142] and with IGF-1 *ex vivo* [130]. A novel technique that has recently been developed for nonviral gene delivery is gene-activated matrix, in which biomaterial scaffolds are used as carriers—they are supplemented with the genetic material and implanted into the defect site, allowing for transfection of cells migrating into the scaffold [143].

1.6. Objectives

The overall objective of this thesis project was to investigate a collagen scaffold-based method of endostatin delivery, toward the regeneration of articular cartilage. The rationale for endostatin, a novel approach to treating cartilage defects, was that the inhibition of blood vessel development in reparative cartilaginous tissue may lead to the formation of hyaline cartilage and improved healing of a focal defect in articular cartilage. In addition, it has been shown that endostatin can influence other processes, such as promoting anabolic activity in cartilage [123] and acting as an antagonist against pain sensing nerve fibers [111, 112], making the application of endostatin in articular cartilage promising for its multiple potential targets.

It was hypothesized that MSC- and chondrocyte-seeded constructs cultured in chondrogenic medium (CM) could form cartilaginous material and overexpress endostatin protein, and that manipulation of select variables, including plasmid load, method of lipoplex incorporation, oxygen tension, scaffold formulation, and crosslinking agent, would affect the development of the engineered constructs. It was also hypothesized that long-term joint immobilization with intermittent passive motion exercise, implantation of cell-seeded scaffolds,

and the use of osteogenic protein (OP)-1 would result in an *in vivo* focal chondral defect model suitable for testing the engineered constructs.

The following specific aims were developed to test these hypotheses:

1. Evaluate the *in vitro* chondrogenic differentiation of mesenchymal stem cells (MSCs) in endostatin plasmid (pEndo)-supplemented collagen scaffolds using chondrogenic medium, compared to control nonchondrogenic medium, in order to engineer endostatin-producing cartilaginous constructs (Chapter 2).
2. Investigate the effects of factors that could potentially influence MSC- and chondrocyte-seeded pEndo-supplemented sponge constructs *in vitro*, specifically the effects of oxygen tension (5% versus 21%), sponge material (type I/III versus type II collagen), and GAG supplementation (heparan sulfate and chondroitin sulfate) on the endostatin expression profile and development of cartilaginous material (Chapter 3).
3. Investigate the effects of factors that could potentially influence endostatin-producing hydrogel constructs *in vitro*, specifically the effects of select crosslinking agents (transglutaminase-2, microbial transglutaminase, and genipin) and GAG supplementation (heparin-agarose beads) on the endostatin expression profile and development of cartilaginous material (Chapter 4).
4. Develop an *in vivo* chondral defect model in the goat knee that would be suitable for testing the engineered constructs, by evaluating the effects of post-surgical rehabilitation (long-term joint immobilization with intermittent passive motion exercise), cell-seeded scaffolds, and osteogenic protein (OP)-1 on cartilage regeneration (Chapter 5).

CHAPTER 2: *IN VITRO* CHONDROGENIC DIFFERENTIATION TO FORM ENDOSTATIN-EXPRESSING CARTILAGINOUS CONSTRUCTS

The material presented in this chapter was adapted from the following publication, with permission of Mary Ann Liebert, Inc.:

Jeng L, Olsen BR, Spector M. Engineering endostatin-producing cartilaginous constructs for cartilage repair using nonviral transfection of chondrocyte-seeded and mesenchymal-stem-cell-seeded collagen scaffolds. Tissue Eng Part A 16(10): 3011-21, 2010.

2.1. Introduction

Unlike most tissues, articular cartilage, a specialized form of hyaline cartilage, is normally resistant to vascularization and contains no blood vessels. If articular cartilage is damaged, the tissue exhibits only limited healing potential. Damage may be accompanied by the invasion of blood vessels from the underlying subchondral bone into the cartilage; osteoarthritic cartilage has been shown to lose its resistance to vascular invasion compared to normal articular cartilage [91]. Moreover, angiogenesis in articular cartilage is believed to be a key contributor to the symptoms and pathology associated with osteoarthritis [90]. The active resistance of normal articular cartilage to neovascularization and the associations of angiogenesis with pathological conditions in cartilage suggest that angiogenesis may interfere with cartilage regeneration and may play a critical role in cartilage degeneration.

Early investigations examining the use of various anti-angiogenic factors, such as Flt-1, endostatin, and suramin, in articular cartilage tissue engineering include the use of soluble Flt-1 to block vascular endothelial growth factor in osteochondral defects [97], the use of nonviral gene therapy to engineer MSCs to overexpress endostatin [98], and a proof-of-concept study demonstrating that by inhibiting angiogenesis with suramin, an environment promoting the exclusive production of cartilage could be created in the space between the tibia and the periosteum [99].

The objective of this study was to engineer *in vitro* a collagen scaffold-based cartilaginous construct overexpressing a potent anti-angiogenic factor, endostatin, using nonviral transfection and small amounts of plasmid to address safety issues. The construct could serve as an implant for defects in the articular surface of joints, providing an immature cartilage for subsequent maturation *in vivo*, and endostatin-expressing cells to prevent vascular invasion.

Endostatin is a 20 kDa proteolytic fragment located at the COOH-terminal of type XVIII collagen that has been shown to strongly inhibit endothelial cell proliferation and migration and prevent the formation of blood vessels [100]. It is synthesized by chondrocytes *in vitro* and *in vivo* [123] and has been found in articular cartilage *in vivo* [14].

Previous work in our laboratory showed that collagen scaffolds supplemented with lipoplexes containing 20 μg of pEndo and cultured in nonchondrogenic growth medium facilitated the production of endostatin by goat MSCs to amounts that begin to achieve what may be therapeutic levels for articular cartilage [98]. However, the chondrogenic potential of these cell-seeded pEndo-supplemented constructs has not been investigated. In this study, we investigated the chondrogenic potential of the engineered constructs in chondrogenic medium, CM, versus control nonchondrogenic medium, NCM. We also investigated the effects of the following select variables on endostatin expression profile and select measures of chondrogenesis, in this study cell morphology and glycosaminoglycan (GAG) and type II collagen content: plasmid load, with an emphasis on small amounts for safety; and method of nonviral vector, lipoplex, incorporation.

2.2. Materials and Methods

2.2.1. Plasmid Propagation and Isolation

The human endostatin plasmid (pEndo) vector *pCEP-Pu AC7* and the propogation and isolation protocol have been previously described [98]. Briefly, plasmid was obtained by heat shock transformation of *Escherichia coli* DH5α competent cells (Invitrogen, Carlsbad, CA, USA) and isolation using a Mega QIAfilter™ Plasmid kit (Qiagen, Valencia, CA, USA).

2.2.2. Cell Isolation and Two-Dimensional Monolayer Expansion

MSCs were isolated from heparinized bone marrow aspirates from the iliac crests of adult Spanish goats. Adherent cells were expanded in monolayer using a standard MSC expansion medium consisting of low glucose Dulbecco's modified Eagle's medium (DMEM-LG), containing 10% (v/v) fetal bovine serum (FBS) and 1% penicillin/streptomycin (PS) (Invitrogen), and supplemented with 10 ng/ml fibroblast growth factor (FGF)-2 (R&D Systems, Minneapolis, MN, USA). The cells were incubated in one of two conditions: (1) a humidified chamber at 37°C, 5% CO_2, and atmospheric (standard) O_2 (approximately 21%) or (2) a humidified chamber at 37°C, 5% CO_2, and 5% (low) O_2. MSCs were grown through two subcultures to obtain passage 2 (P2) cells.

2.2.3. Scaffold Fabrication

Scaffolds were prepared using 0.5% (w/v) porcine type I/III collagen (Geistlich Biomaterials, Wolhusen, Switzerland). Porous sheets (~1.5 mm thick) were fabricated by freeze-drying (VirTis, Gardiner, NY, USA) as previously described [98]. The sheets were then sterilized and lightly crosslinked by dehydrothermal treatment using a vacuum greater than 30 inHg at a temperature of 105°C. Disks (8 mm in diameter and 1.5 mm in thickness) were cut from the porous sheets using a dermal biopsy punch.

2.2.4. Experimental Design

Caprine MSCs were subcultured twice (P2) and transfected with lipoplexes prepared with human endostatin plasmid (Table 2.1).

1) In the first experiment, MSCs expanded at 21% O_2 were seeded into endostatin lipoplex-supplemented type I/III collagen (CI) scaffolds and cultured in nonchondrogenic medium (NCM) or chondrogenic medium (CM) for 22 days at 21% O_2. The CM was composed of DMEM-HG, 1% nonessential amino acids (v/v), 1% HEPES buffer, 1% penicillin/streptomycin/L-glutamine, 1.25 mg/ml of bovine serum albumin (BSA) (Invitrogen), and 1X ITS+1 (Sigma), and supplemented with 10 ng/ml TGF-β1, 100 nM dexamethasone (Sigma), and 0.1 mM L-ascorbic acid 2-phosphate. The NCM consisted of DMEM-LG containing 10% FBS and 1% PS. The variables included the plasmid amount and the culture medium used for 3-D scaffold culture.

2) In the second experiment, MSCs expanded at 21% O_2 were seeded into endostatin lipoplex-supplemented type I/III collagen scaffolds and cultured for 22 days at 21% O_2 in CM. The variable was the method of carbodiimide crosslinking.

The principal outcome variable was the amount of endostatin released by the cells, recovered in the medium.

Table 2.1 Summary of the experimental design.

Exp. #	Lipoplex Incorporation[1]	pEndo (μg)	Culture Medium[2]	Evaluation Method (n)
1	Half X-L	4 20	NCM CM	ELISA (2-3) Histochemical (1)
2	None X-L Half X-L All X-L	20	CM	ELISA (6) Histochemical (2)

[1] X-L, crosslinked
[2] NCM, nonchondrogenic medium; CM, chondrogenic medium

2.2.5. Preparation of Collagen Scaffolds Incorporating GenePORTER 2/Endostatin Plasmid Complexes (Lipoplexes)

Endostatin plasmid was encapsulated in a lipid-mediated transfection reagent, GenePORTER™ 2 (GP2) (Gene Therapy Systems, Inc., San Diego, CA, USA) following the manufacturer's instructions.

In the first experiment, a ratio of μl of GP2:μg of pEndo of 3.5 was used. Our previous work showed that there was no significant effect of GP2:pEndo ratio (3.5, 7, and 10) on endostatin levels [98]. Lipoplexes were prepared using 4 and 20 μg of pEndo and incorporated into type I/III collagen scaffolds using 2 steps. Half of the lipoplex solution was pipetted on one side of the scaffold and incubated for 10 min. A 1 ml aliquot of an aqueous carbodiimide solution consisting of 0.6 mM 1-ethyl-3-(3-dimethylaminopropyl) carbodiimide hydrochloride and 0.6 mM N-hydroxysuccinimide (Sigma Chemical Co., St. Louis, MO, USA) was added to the scaffold, followed by incubation for 30 minutes. The same carbodiimide solution concentration was used for the second experiment as well. Excess carbodiimide was removed by soaking the scaffolds in PBS for 1 hour. Then, the other half of the lipoplex solution was added to the second side of the scaffold and incubated for 10 min. Scaffolds with no lipoplex served as controls.

In the second experiment, 20 μg of pEndo and a GP2:pEndo ratio of 3.5 were used. Three different methods were used for incorporation and crosslinking of the endostatin lipoplexes to type I/III collagen scaffolds. For the group in which none of the lipoplex was crosslinked to the scaffold, the scaffolds were incubated in carbodiimide for 30 minutes and soaked in PBS for 1 hour to remove excess carbodiimide. Then, half of the lipoplex solution was added to each side, with an incubation period of 10 minutes for each side. For the group in

which half of the lipoplex solution was crosslinked to the scaffold, half of the lipoplex solution was added to one side, the scaffolds were incubated for 10 minutes, carbodiimide was added for an incubation period of 30 minutes, the scaffolds were soaked in PBS for 1 hour to remove excess carbodiimide, and the other half of the lipoplex solution was added to the second side for 10 minutes. For the group in which all of the lipoplex was crosslinked, half of the lipoplex solution was added to each side, with an incubation period of 10 minutes for each side, followed by incubation in carbodiimide for 30 minutes and PBS for 1 hour. Control scaffolds with no lipoplex supplementation were also prepared.

2.2.6. Transfection and Culture in Three-Dimensional Collagen Scaffolds

Collagen scaffolds were placed in agarose-coated wells for cell seeding. P2 cells were trypsinized and resuspended in DMEM-LG. One million MSCs were pipetted onto each side of the scaffold, with an incubation period of 10 minutes at 21% O_2 for each side, for a total of 2 million cells seeded per scaffold. All constructs were then incubated in 0.5 ml of DMEM-LG for 4 hrs to allow for transfection. Following transfection, all constructs were cultured in chondrogenic medium (CM) for the remainder of the experiment, with the exception of control scaffolds in the first experiment cultured in nonchondrogenic growth medium (NCM).

Every 1-3 days, expended medium was collected and frozen at -20°C until analysis, and fresh medium was added. Cultures were terminated after 22 days for histological examination and biochemical analysis.

2.2.7. Endostatin Detection in the Medium

Endostatin protein in the culture medium was measured using a sandwich enzyme-linked immunosorbent assay (ELISA) kit for human endostatin protein (R&D Systems, Minneapolis, MN) following the manufacturer's instructions.

2.2.8. Histological and Immunohistochemical Evaluation

Constructs allocated for histology were fixed in 10% formalin or 4% paraformaldehyde for at least 3 hrs, processed and embedded in paraffin, and sectioned by microtomy. The sections were mounted on glass slides and stained with hematoxylin and eosin (H&E) and Safranin-O using standard histological techniques.

Endostatin and type II collagen distribution were examined immunohistochemically using an anti-type II collagen mouse monoclonal antibody (CIIC1, 1:150 dilution, Developmental Studies Hybridoma Bank, University of Iowa, Iowa City, IA, USA) and an anti-endostatin rabbit polyclonal antibody (1:40 dilution, Millipore, Billerica, MA, USA). The immunohistochemical staining was performed using the Dako Autostainer (DakoCytomation, Carpinteria, CA, USA) and the peroxidase-aminoethyl carbazole (AEC)-based Envision+ kit (Dako) following the manufacturer's recommendations.

2.2.9. Statistical Analysis

Data are presented as the mean ± standard error of the mean (SEM). Analysis of variance (ANOVA) and Fisher's protected least squares difference (PLSD) post-hoc testing were performed using StatView software (SAS Institute Inc, Cary, NC, USA). Statistical significance

was set at $p < 0.05$.

2.3. Results

The effects of plasmid load and culture medium (first experiment) and method of nonviral vector incorporation (second experiment) on endostatin expression and chondrogenesis of MSC-seeded constructs were investigated. Our experience with the seeding method indicated that approximately 65% of the cells were retained in the scaffold 1 day post-seeding.

2.3.1. MSC-Seeded Type I/III Constructs Cultured in Chondrogenic and Nonchondrogenic Media

2.3.1.1. Endostatin Detection in the Medium

The MSC-seeded type I/III collagen control groups, which received no lipoplex and were not transfected, displayed no notable endostatin in the medium (data not shown). Endostatin released into the medium of MSC-seeded, lipoplex-supplemented type I/III constructs increased to a peak in the first week of culture and then decreased to low levels (Figure 2.1). The kinetics of expression was similar for constructs supplemented with 4 and 20 μg of plasmid. While the cumulative endostatin release at 6 days for the 20 μg pEndo group in CM (90 ± 20 ng/ml) was around 2-fold higher than in NCM, the results were not statistically significant ($p = 0.181$, power = 0.249), likely owing to variation. For the 3-day collection period ending at day 6, the endostatin level of constructs with 20 μg of plasmid in CM reached 45 ± 10 ng/ml, the highest level seen in the experiment (Figure 2.1). Where $n = 2$, error bars were not calculated.

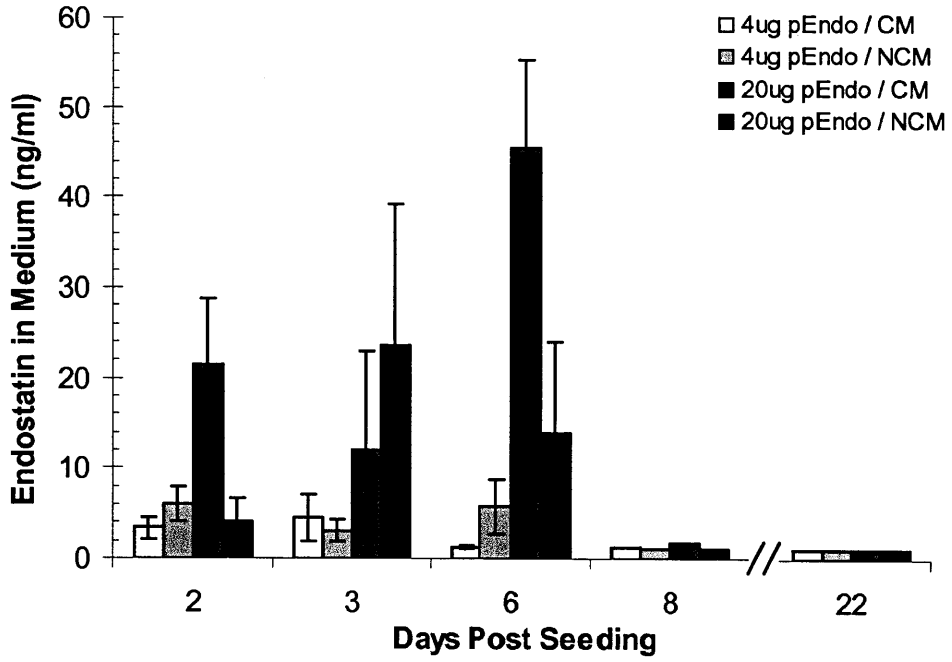

Figure 2.1 Endostatin in the medium of cell-seeded, lipoplex-supplemented collagen constructs and control constructs. MSC-seeded type I/III constructs cultured in CM and NCM (n = 3 for first 6 days of lipoplex-supplemented scaffolds; n = 2 for all others).

Three-factor ANOVA for the cumulative endostatin data from the first 6 days (including the controls with no plasmid) revealed significant effects of plasmid load ($p < 0.0001$; power = 1.0) and collection period ($p = 0.045$, power = 0.596) on endostatin level, but failed to find a significant effect of medium type ($p = 0.181$, power = 0.249). Fisher's PLSD post-hoc testing demonstrated a significant difference in endostatin level between the group treated with 20 μg pEndo and the other 2 groups.

2.3.1.2. Histological and Immunohistochemical Evaluation

Immunohistochemical evaluation of the cell-seeded constructs collected 6 days post-seeding demonstrated positive staining for endostatin for a few cells in the lipoplex-supplemented scaffolds, cultured in CM and NCM (Figure 2.2a), suggesting that most of the endostatin protein was not retained in the engineered constructs. Samples cultured in CM,

collected at the termination of the 22-day culture period, revealed many cells that were rounded and resided in lacunae, typical characteristics of chondrocyte morphology, for scaffolds cultured in CM (Figure 2.2b). Cells could be seen dispersed throughout the construct entrapped in newly synthesized extracellular matrix, with very little original scaffold material remaining (Figure 2.2b and c). The fibrous appearance of the matrix was consistent with fibrocartilage. There were only a few small areas demonstrating a hyaline matrix. MSC-seeded constructs, both lipoplex-supplemented and controls, cultured in CM showed intense positive staining with Safranin-O (Figure 2.2d), indicating the presence of sulfated glycosaminoglycans (GAGs), and stained positively for type II collagen (Figure 2.2e). Constructs cultured in NCM did not display cells with a chondrocytic morphology and did not stain for GAG or type II collagen (data not shown).

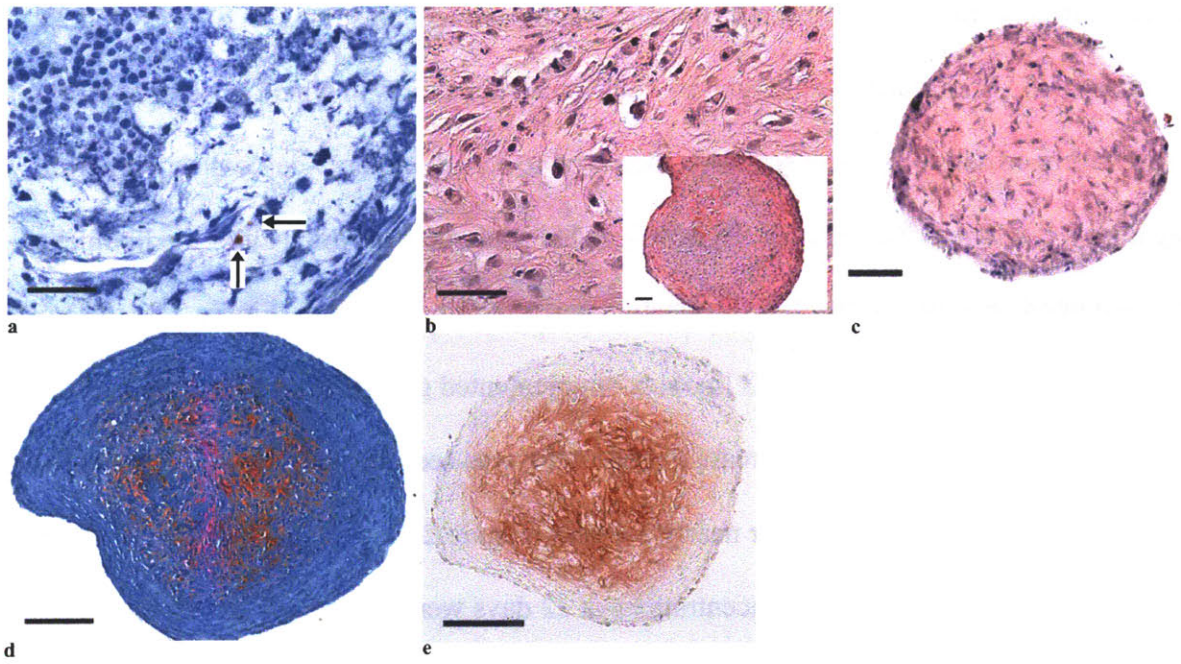

Figure 2.2 Micrographs of histological sections of MSC-seeded constructs cultured in CM and NCM.

- **a. Endostatin immunohistochemistry of MSC-seeded CI scaffold supplemented with 20 µg pEndo after 6 days of culture in NCM (red chromogen indicates positive stain). Scale bar, 50 µm.**
- **b. Hematoxylin and eosin stain of the interior of MSC-seeded CI scaffold supplemented with 4 µg pEndo after 22 days of culture in CM. Scale bar, 50 µm, 40x magnification. Inset shows the section at lower magnification, scale bar, 100 µm.**
- **c. Hematoxylin and eosin stain of the surface of MSC-seeded CI scaffold supplemented with 4 µg pEndo after 22 days of culture in CM. Scale bar, 100 µm.**
- **d. Safranin-O staining of GAG for MSC-seeded CI scaffold supplemented with 4 µg pEndo after 22 days of culture in CM (red chromogen indicates sulfated GAGs). Scale bar, 200 µm.**
- **e. Type II collagen immunohistochemistry of MSC-seeded CI scaffold supplemented with 4 µg pEndo after 22 days of culture in CM (red indicates positive stain). Scale bar, 200 µm.**

2.3.2. Crosslinking Modification of the Type I/III Collagen Scaffold for Retaining the Lipoplex

2.3.2.1. Endostatin Detection in the Medium

Substantial overexpression of endostatin, released into the expended medium, was observed for the MSC-seeded, lipoplex-supplemented constructs compared to non-supplemented controls (Figure 2.3). Endostatin levels of the lipoplex-supplemented constructs were not

noticeably different than the control non-lipoplex-supplemented constructs on days 20 and 22 (data not shown). Endostatin synthesized by cell-seeded constructs in which none or half of the lipoplexes were crosslinked to the scaffolds increased to a peak by the 2-day collection period ending at day 4, whereas the peak for the MSC-seeded constructs in which all of the lipoplexes were crosslinked occurred on the 2-day collection period ending on day 6 (Figure 2.3). The peak amounts per collection period for the 3 lipoplex-supplemented groups were comparable, around 13 ng/ml (Figure 2.3). A gradual decrease in endostatin was seen in the following 2 weeks, but sustained expression was observed for nearly 3 weeks (Figure 2.3).

The cumulative endostatin concentrations at 22 days were similar for all pEndo lipoplex-supplemented groups, around 55 ng/ml. The average 6-day cumulative endostatin in the half crosslinked (20μg) group (30 ± 5 ng/ml; Figure 2.3) was lower than that recorded in the first experiment (90 ± 20 ng/ml; Figure 2.1).

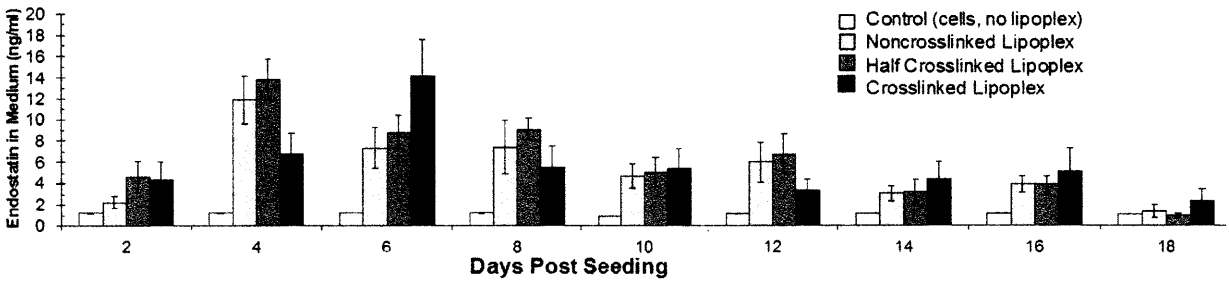

Figure 2.3 Endostatin in the medium of cell-seeded, lipoplex-supplemented collagen constructs and control constructs. Modification of the scaffold via crosslinking none, half, or all of the lipoplexes (n = 6), in MSC-seeded type I/III constructs cultured in CM.

Two-factor ANOVA for the data from the 3 lipoplex-supplemented groups revealed a significant effect of collection period ($p = <0.0001$, power = 1) on endostatin level. The effect of crosslinking method ($p = 0.50$; power = 0.162) on endostatin level did not achieve statistical significance. However, for the endostatin protein peak day data of the 3 lipoplex-supplemented groups, one-factor ANOVA revealed a significant effect of crosslinking method on peak day ($p <$

0.0001; power = 1). Fisher's PLSD post-hoc testing demonstrated a significant difference in peak day between the group in which all the lipoplexes were crosslinked to the scaffold and the other 2 groups.

2.4. Discussion

In this study, we engineered endostatin-expressing cartilaginous constructs *in vitro* using a small amount of pEndo in lipoplex-supplemented scaffolds. An increase and peak in endostatin protein in the expended medium during the first week of culture was seen in each of the 2 experiments, followed by a decrease to low levels, suggesting that overexpression of endostatin could be sustained for at least several days using the nonviral vector. It takes some time before protein product is made from the lipoplexes—the cells must internalize the pEndo lipoplexes, transport them to the nucleus, and transcribe and translate the message into protein that is released and accumulated in the surrounding medium [138]. It also takes some time for the cells to attach to the scaffolds. These events may contribute to the observation that it takes a few days before peak endostatin levels are seen. Since nonviral transfection is being used, the endostatin plasmid is not integrated into the cell's genome and passed on during replication. This means that with cell turnover, the transfected cells that die are not replaced with more transfected cells overexpressing endostatin. Plasmids can also be degraded. These events can result in decreases in the endostatin expression profile over time. The results also suggest that most of the endostatin protein was released into the surrounding media and was not retained in the constructs. Previous work using the same plasmid to produce recombinant endostatin demonstrated the functionality of the protein product [109].

Of note is that the endostatin levels released by the constructs were comparable to physiological values found in human serum, approximately 30 ng/ml [106], and to levels shown to inhibit endothelial cell migration *in vitro*, reported to be 0.1 – 10 ng/ml [109]. The largest observed maximum endostatin level per collection period in this study and maximum total amount of endostatin released over the duration of the experiment occurred in experiment #1, with values of 45 ng/ml and 95 ng, respectively. Given the short half-life of endostatin *in vivo*, the total endostatin in a contained defect at a given time would likely consist of protein synthesized and accumulated over the past few hours [125].

The average amount of endostatin produced per cell cannot be commented on because it is unclear how many cells were present at the time of synthesis. The percentage of cells that were transfected was not determined in this study and requires further work. One potential method for determining the percentage of cells that are actually transfected would be the use of a plasmid encoding for both endostatin and GFP; however, this plasmid was not available. A prior experiment in our lab using a GFP plasmid alone in the same lipoplex system incorporated into collagen scaffolds imaged GFP expression in chondrocytes grown in the scaffolds, but did not quantify transfection efficiency [131].

In experiment #1, plasmid load was found to affect endostatin levels, with higher amounts of plasmid resulting in higher amounts of endostatin protein.

To our knowledge, no studies have yet reported on the effects of endostatin on MSCs. Of note, this study found that endostatin transfection using lipoplex-supplemented scaffolds did not appear to inhibit the chondrogenic potential of MSCs. Chondrogenesis was observed in the engineered constructs cultured in CM for 3 weeks—MSC-seeded constructs were seen to have

cells that expressed chondrocyte morphology and contained areas rich in type II collagen and sulfated GAGs.

It is not yet clear why select groups repeated under the same experimental conditions yielded different expression levels. While the cells were from the same goat donors, unrecognized differences in the thawing and growth of the cells for the various experiments may have affected their response to the lipoplex. Another possible reason could be the incidental loss of activity of one or more of the reagents.

It is recognized that a small sample size (around 2-3) was sometimes used, and that the experiment could benefit from a larger sample size in the future. It should be noted that quantitative assessment (biochemical analysis) using a small sample size was generally accompanied by qualitative assessment (histology), providing confirmation of the findings.

It is possible that the cells are producing endogenous goat endostatin protein, in addition to the endostatin protein produced as a result of transfection using a plasmid encoding for human endostatin. The anti-human endostatin antibody used for immunohistochemical staining did not stain goat tissue samples (unpublished data), suggesting that the antibody does not recognize and bind to goat endostatin, if endogenous endostatin is synthesized by goat MSCs. The ELISA assay kit used in this study was designed to measure human endostatin protein, and it is unclear if it is capable of detecting endostatin produced by other species.

While the timing of endostatin release necessary for articular cartilage repair applications is not yet known, the ability to manipulate the endostatin expression profile, such as through the use of different carbodiimide crosslinking procedures for lipoplex retention in experiment #2, will be of value. Both the lipoplexes and the collagen protein contain amine and carboxyl groups in their molecular structure, and there exists the potential for formation of peptide bonds with the

aid of carbodiimide crosslinking. Previous work in our lab [131] showed that scaffolds that were treated with carbodiimide after supplementing with plasmid did not exhibit passive bolus release of plasmid like scaffolds treated with carbodiimide prior to plasmid supplementation did, but work has not yet been performed to confirm covalent attachment of lipoplexes to collagen scaffolds.

Safranin-O staining was used to stain for sulfated GAGs, with the assumption that the sulfated GAGs are on aggrecan. However, it is possible that the sulfated GAGs could be related to other proteoglycans. One suggestion for the future could be the use of an aggrecan antibody, to confirm the presence of aggrecan in the extracellular matrix.

In the present study, we engineered endostatin-producing constructs using nonviral transfection of MSC-seeded, pEndo lipoplex-supplemented collagen constructs and showed that cells retained their chondrogenic capacity. The endostatin expression profile and degree of chondrogenesis were altered through the manipulation of select variables, including plasmid load, method of lipoplex incorporation, and medium type. The quantity and duration of endostatin protein necessary for cartilage repair is unknown, and more studies are needed in this area. Other potential strategies to increase the duration of sustained production include modifications to the nonviral vector. Given the associations of angiogenesis and pathological conditions in normally avascular cartilage, a pEndo-supplemented scaffold provides a promising off-the-shelf product that could be used to treat patients, possibly in conjunction with other repair options, to inhibit angiogenesis, improve healing of a focal defect, and prevent further cartilage degeneration.

CHAPTER 3: ENGINEERING ENDOSTATIN-EXPRESSING CARTILAGINOUS CONSTRUCTS USING SPONGE SCAFFOLDS

The material presented in this chapter was adapted from the following publication, with permission of Mary Ann Liebert, Inc.:

Jeng L, Olsen BR, Spector M. Engineering endostatin-producing cartilaginous constructs for cartilage repair using nonviral transfection of chondrocyte-seeded and mesenchymal-stem-cell-seeded collagen scaffolds. Tissue Eng Part A 16(10): 3011-21, 2010.

3.1. Introduction

When studying articular cartilage, standard cell culture protocols generally utilize a humidified incubator at 37°C, with a gas composition of 5% carbon dioxide and 95% air, resulting in approximately 21% ambient oxygen. However, both the bone marrow and articular cartilage environments *in vivo* typically experience much lower oxygen tensions around 5% [144]. Interestingly, some studies suggest that hypoxia induces endostatin production [145-148], whereas other studies observed that hypoxia downregulates endostatin [149, 150].

Some studies have shown that *in vitro* culture of chondrocytes at physiologic oxygen tension (~5%) stimulates cell proliferation, type II collagen production, proteoglycan synthesis, and redifferentiation of dedifferentiated cells while decreasing type I collagen production compared to culture at 21% ambient oxygen [151-153]; however, other work suggests that cultured chondrocytes need ~21% oxygen for ideal growth, and that lower oxygen levels result in depressed proteoglycan and DNA synthesis [154, 155]. *In vitro* culture of MSCs at low oxygen (<10%) enhances proliferation [156], upregulates the expression of genes associated with chondrogenesis, including Sox9 [157], and prolongs cell lifespan [158], but there is discrepancy regarding how low oxygen affects MSC differentiation potential [159].

Previous studies have investigated the utility of type I/III and type II collagen scaffolds for the regeneration of articular cartilage [40]. Of particular interest is the use of the collagen scaffolds for nonviral gene delivery [131, 160]; however, prior studies have not yet investigated the differences between type I/III and II collagen as delivery vehicles for nonviral vectors.

Given that 5% oxygen tension is closer to normoxia for cartilage *in vivo* and appears to play an important role in the function of cells, we propose to study the effects of 5% oxygen tension on endostatin biosynthesis and development of cartilaginous material.

Endostatin binding and retention are also of interest, the rationale being that the binding of proteins protects them from proteolytic degradation and creates a reservoir of the proteins for sustained release in a local area, thus potentially increasing the local concentration and amount of time during which the proteins are present [161, 162]. Much research, both *in vitro* and *in vivo*, has focused on the retention of proteins, such as growth factors with short half-lives, often delivered directly via a heparan sulfate or heparin construct, to bind and extend their presence in the desired location [162-165]. Unlike conventional protein retention studies, this thesis presents a modified situation, in which the protein of interest, endostatin, is introduced using genetically modified cells, rather than direct delivery of the protein.

Endostatin has been shown to have multiple binding partners. The protein has been found to bind to heparin and to its physiological ligand heparan sulfate (HS) with moderate binding affinities. Specifically, human recombinant endostatin has been found to bind to heparin with an affinity constant, K_D, of 1.96 μM and to HS with a K_D, of 2.2 μM [166], and mouse recombinant endostatin has been found to bind to heparin with a K_D of 0.3 μM [167]. Two clusters of arginine residues on endostatin have been identified as binding sites for heparin and HS [167]. Chondroitin sulfate (CS) has also been shown to be a partner of endostatin, through non-covalent interactions [168]. It has been suggested that the interaction of endostatin with heparan sulfate may play a role in the anti-angiogenic activity of endostatin [167, 169, 170].

HS and CS are sulfated glycosaminoglycans (GAGs). HS and CS are found in normal articular cartilage [3]. HS is also found on HS-bearing proteins in the extracellular matrix, including type XVIII collagen [171]. HS consists of a sulfated repeating disaccharide unit, most commonly glucuronic acid linked to N-acetylglucosamine [172]. CS consists of alternating sugars, glucuronic acid and N-acetylgalactosamine [172]. Previous work suggests that not all

chondroitin sulfates are the same; for example, CS from different sources have been shown to have different molecular weights, affecting the amount of GAG that is grafted onto collagen molecules during scaffold synthesis [173, 174].

Small amounts of GAGs (~10% of the scaffold weight), such as HS and heparin, have been incorporated into scaffolds [175-178] and utilized for protein binding and retention studies *in vitro* and *in vivo*, given the known moderate binding affinities between HS/heparin and a number of proteins [162, 163, 165, 179]. Previous work suggests that the incorporation of GAG, such as CS, into collagen sponge-like scaffolds can affect the properties of the collagen slurry (aqueous phase of scaffold preparation), results in more interconnected pores (unpublished data), and decreases the degradation rate of the scaffolds [180] compared to scaffolds without CS. HS-, CS-, and heparin-incorporated scaffolds have also been shown to stimulate chondrogenesis for cartilage tissue engineering, including increased cell viability and proliferation, and increased type II collagen and proteoglycan retention [181-184].

Our supposition was that the following select variables may affect the endostatin expression and retention and select measures of chondrogenesis, in this study cell morphology and glycosaminoglycan (GAG) and type II collagen content: collagen scaffold material (type I/III versus II), oxygen tension, recognizing that articular cartilage levels are low, estimated to range from 1% to 7% [1], and GAG (HS and CS) supplementation of collagen sponges. These studies were conducted using caprine chondrocyte- and marrow stromal cell (also referred to as mesenchymal stem cell, MSC)-seeded constructs, recognizing the advantage with respect to procurement of the latter.

3.2. Materials and Methods

3.2.1. Plasmid Propagation and Isolation

The endostatin plasmid (pEndo) vector *pCEP-Pu AC7* and the propogation and isolation protocol have been previously described [98]. Briefly, plasmid was obtained by heat shock transformation of *Escherichia coli* DH5α competent cells (Invitrogen, Carlsbad, CA, USA) and isolation using a Mega QIAfilter™ Plasmid kit (Qiagen, Valencia, CA, USA).

3.2.2. Cell Isolation and Two-Dimensional Monolayer Expansion

MSCs were isolated from heparinized bone marrow aspirates from the iliac crests of adult Spanish goats. Adherent cells were expanded in monolayer using a standard MSC expansion medium consisting of low glucose Dulbecco's modified Eagle's medium (DMEM-LG), containing 10% (v/v) fetal bovine serum (FBS) and 1% penicillin/streptomycin (PS) (Invitrogen), and supplemented with 10 ng/ml fibroblast growth factor (FGF)-2 (R&D Systems, Minneapolis, MN, USA). The cells were incubated in one of two conditions: (1) a humidified chamber at 37°C, 5% CO_2, and atmospheric (standard) O_2 (approximately 21%) or (2) a humidified chamber at 37°C, 5% CO_2, and 5% (low) O_2. MSCs were grown through two subcultures to obtain passage 2 (P2) cells.

Chondrocytes were isolated from articular cartilage shavings obtained from non-articulating regions of the trochlear ridges and trochlear notch of the left knee of an adult Spanish goat. Cells were expanded in monolayer culture using a standard chondrocyte expansion medium consisting of high glucose Dulbecco's modified Eagle's medium (DMEM-HG), containing 1% nonessential amino acids (v/v), 1% HEPES buffer, 1% penicillin/streptomycin/L-

glutamine, and 10% FBS (Invitrogen), and supplemented with 1 ng/ml transforming growth factor (TGF)-β1, 5 ng/ml FGF-2, and 10 ng/ml platelet-derived growth factor (PDGF)-ββ (R&D Systems). The cells were incubated at in a humidified chamber at 37°C, 5% CO_2, and 21% O_2 and grown through two subcultures to obtain P2 cells.

3.2.3. Scaffold Fabrication

Scaffolds were prepared, using 0.5% (w/v) porcine type I/III collagen (CI) (Geistlich Biomaterials, Wolhusen, Switzerland) and 1% porcine type II collagen (CII) (Geistlich Biomaterials). The 0.5% CI scaffolds were also additionally supplemented with GAGs: (1) 0.5% CI supplemented with 7% chondroitin sulfate (CS) (w/w relative to CI) (Sigma Chemical Co., St. Louis, MO, USA); and (2) 0.5% CI supplemented with 7% heparan sulfate (HS) (w/w relative to CI) (Sigma). Collagen, and CS and HS GAGs as appropriate, was blended in 0.001N hydrochloric acid. The slurry was degassed and poured into molds, and porous sponge-like sheets (~1.5 mm thick) were fabricated by freeze-drying (VirTis, Gardiner, NY, USA) and sterilized using dehydrothermal treatment as previously described [98]. The sheets were then sterilized and lightly crosslinked by dehydrothermal treatment using a vacuum greater than 30 inHg at a temperature of 105°C. Disks (8 mm in diameter and 1.5 mm in thickness) were cut from the porous sheets using a dermal biopsy punch and stored in a desiccator cabinet until ready for lipoplex incorporation.

3.2.4. Experimental Design

Caprine MSCs and chondrocytes were subcultured twice (P2) and transfected with lipoplexes prepared with human endostatin plasmid.

1) In the first experiment, MSCs and chondrocytes from the same goat were seeded into endostatin lipoplex-supplemented CI or CII scaffolds, without additional GAG supplementation. The cultures were maintained for 20 days in CM. The CM was composed of DMEM-high glucose, 1% nonessential amino acids (v/v), 1% HEPES buffer, 1% penicillin/streptomycin/L-glutamine, 1.25 mg/ml of bovine serum albumin (BSA) (Invitrogen), and 1X ITS+1 (Sigma), and supplemented with 10 ng/ml transforming growth factor (TGF)-β1, 100 nM dexamethasone (Sigma), and 0.1 mM L-ascorbic acid 2-phosphate. Four different oxygen groups were cultured: (1) MSCs expanded in 2-D monolayer at 21% (standard) O_2 and cultured in 3-D scaffolds at 21% (21%-21%), (2) chondrocytes expanded in 2-D at 21% and cultured in 3-D at 21% (21%-21%), (3) chondrocytes expanded in 2-D at 21% and cultured in 3-D at 5% (low) (21%-5%), and (4) MSCs expanded in 2-D at 5% and cultured in 3-D at 5% (5%-5%). The variables included the cell type, scaffold collagen type, and oxygen tension.

2) In the second experiment, MSCs were seeded into endostatin lipoplex-incorporating CI, CI-CS, and CI-HS sponge-like scaffolds and cultured in CM, using 21% O_2 throughout the entire experiment. The variable was GAG supplementation of the CI sponge.

The principal outcome variable was the amount of endostatin released by the cells, recovered in the medium.

3.2.5. Preparation of Collagen Scaffolds Incorporating GenePORTER 2/Endostatin Plasmid Complexes (Lipoplexes)

Endostatin plasmid was encapsulated in a lipid-mediated transfection reagent, GenePORTER™ 2 (GP2) (Gene Therapy Systems, Inc., San Diego, CA, USA) following the manufacturer's instructions.

In the first experiment, 20 μg of pEndo and a GP2:pEndo ratio of 2.5 were used. Half of the lipoplex solution was added to each side with 20 minute incubations, followed by carbodiimide incubation for 30 minutes using a 1 ml aliquot of an aqueous carbodiimide solution consisting of 0.6 mM 1-ethyl-3-(3-dimethylaminopropyl) carbodiimide hydrochloride and 0.6 mM N-hydroxysuccinimide (Sigma Chemical Co., St. Louis, MO, USA). Scaffolds were rinsed and maintained in PBS until cell seeding. Both type I/III and type II collagen scaffolds, with no additional GAG, were supplemented with lipoplexes. Scaffolds with no lipoplex served as controls.

In the second experiment, lipoplexes were prepared and incorporated into the porous sponge-like scaffolds, 20 μg of pEndo per scaffold and a GP2:pEndo ratio of 3.5, using 2 steps. Half of the lipoplex solution was pipetted on one side of the scaffold and incubated for 10 min. The other half of the lipoplex solution was added to the second side of the scaffold and incubated for 10 min. A 1 ml aliquot of an aqueous carbodiimide solution consisting of 0.6 mM 1-ethyl-3-(3-dimethylaminopropyl) carbodiimide hydrochloride and 0.6 mM N-hydroxysuccinimide (Sigma) was added to the scaffold, followed by incubation for 30 minutes. Excess carbodiimide was removed by soaking the scaffolds in PBS for 1 hour. CI scaffolds, with and without GAG supplementation, were used. Scaffolds with no lipoplex served as controls.

3.2.6. Transfection and Culture in Three-Dimensional Collagen Scaffolds

The collagen sponge-like scaffolds were placed in agarose-coated wells for cell seeding. P2 cells were trypsinized and resuspended in DMEM-LG. Two million MSCs or chondrocytes were pipetted onto each side of the scaffold and incubated at 5% or 21% O_2, as appropriate, for 10-30 minutes for each side, for a total of 4 million cells seeded per scaffold (5 μg pEndo per 1 million cells). All constructs were then incubated in DMEM-LG at 5% or 21% O_2, as appropriate, to allow for no more than 4 hrs of transfection. Following transfection, all constructs were cultured at 5% or 21% O_2, as appropriate, in chondrogenic medium (CM) for the remainder of the experiment.

Every 1-3 days, expended medium was collected and frozen at -20°C until analysis, and fresh CM was added. Cultures were terminated on select days for histological examination and biochemical analysis.

3.2.7. Endostatin Detection in the Medium

Endostatin protein in the culture medium was measured using a sandwich enzyme-linked immunosorbent assay (ELISA) kit for human endostatin protein (R&D Systems, Minneapolis, MN) following the manufacturer's instructions.

3.2.8. Analysis of DNA and GAG Content

Constructs were lyophilized and enzymatically digested overnight using proteinase K (Roche Diagnostics, Indianapolis, IN). Determination of the DNA content was carried out using the Picogreen dye assay kit (Molecular Probes, Inc., Eugene, OR, USA) according to the manufacturer's instructions. Previous work in our laboratory found that the average DNA

content was 5.6 pg DNA/cell for goat MSCs and 7.7 pg DNA/cell for goat chondrocytes. The sulfated GAG content was determined by the dimethylmethylene blue (DMMB) dye assay, with a standard curve obtained using chondroitin-6-sulfate from shark cartilage (Sigma).

3.2.9. Histological and Immunohistochemical Evaluation

Constructs allocated for histology were fixed in 4% paraformaldehyde for at least 3 hrs, processed and embedded in paraffin, and sectioned by microtomy. The sections were mounted on glass slides and stained with hematoxylin and eosin (H&E), Safranin-O, and Masson's trichrome using standard histological techniques.

Endostatin and type II collagen distribution were examined immunohistochemically using an anti-type II collagen mouse monoclonal antibody (CIIC1, 1:150 dilution, final concentration 4 μg/ml, Developmental Studies Hybridoma Bank, University of Iowa, Iowa City, IA, USA) and an anti-endostatin rabbit polyclonal antibody (1:40 dilution, final concentration 17 μg/ml, Millipore, Billerica, MA, USA). The immunohistochemical staining was performed using the Dako Autostainer (DakoCytomation, Carpinteria, CA, USA) and the peroxidase-aminoethyl carbazole (AEC)-based Envision+ kit (Dako) following the manufacturer's recommendations.

3.2.10. Statistical Analysis

Data are presented as the mean ± standard error of the mean (SEM). Analysis of variance (ANOVA) and Fisher's protected least squares difference (PLSD) post-hoc testing were performed using StatView software (SAS Institute Inc, Cary, NC, USA). Statistical significance was set at $p < 0.05$.

3.3. Results

The effects of cell type, oxygen tension, and scaffold collagen type (first experiment) and incorporation of heparan sulfate and chondroitin sulfate into sponge scaffolds (second experiment) on endostatin expression and retention and chondrogenesis of cell-seeded constructs were evaluated. Our experience with the seeding method indicated that ~65% of the cells were retained in the porous sponge-like scaffold 1 day after seeding.

3.3.1. Cell Type, Oxygen Tension, and Scaffold Collagen Type

3.3.1.1. Endostatin Detection in the Medium

Endostatin released into the medium of cell-seeded, lipoplex-supplemented scaffolds increased to a peak during the first week, followed by a gradual decrease (Figure 3.1a and b). Notable endostatin levels could be measured in several of the groups even after 17 days (Figure 3.1a and b). The cumulative endostatin concentrations at day 17 ranged from 3 to 11 ng/ml. The highest endostatin level in the experiment was observed to be 3.8 ± 0.3 ng/ml for 21%-21% MSCs cultured on type II collagen scaffolds for the 3-day collection period ending on day 3 (Figure 3.1a). MSC-seeded constructs resulted in higher endostatin levels than chondrocyte-seeded constructs during the initial week after transfection, and constructs cultured in 3-D scaffolds at standard oxygen showed more endostatin compared with those cultured at low oxygen (Figure 3.1a and b). For constructs cultured at low oxygen, after the first 3 days, endostatin expression levels for MSCs were higher in the type II collagen versus the type I collagen scaffolds (Figure 3.1a). For standard oxygen, there was no notable effect of scaffold type on expression (Figure 3.1a and b).

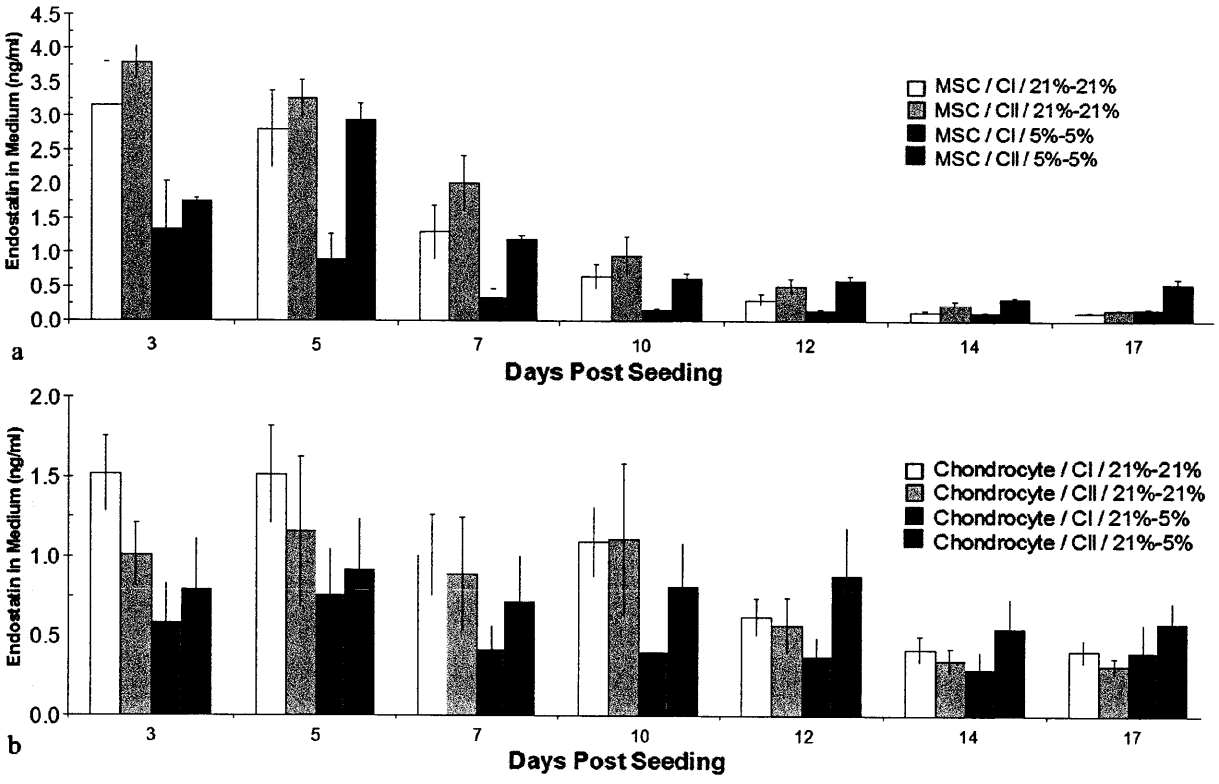

Figure 3.1 Endostatin in the medium of cell-seeded, lipoplex-supplemented collagen constructs and control constructs.

a. **MSCs cultured at standard and low oxygen in type I/III and type II collagen scaffolds in CM (n = 3).**
b. **Chondrocytes cultured at standard and low oxygen in type I/III and type II collagen scaffolds in CM (n = 3).**

Including all data, 5-factor ANOVA demonstrated significant effects of 3-D oxygen tension, collagen scaffold type, cell type, plasmid load (0 vs. 20 μg), and collection period on endostatin level ($p < 0.0001$, power = 1). Analyzing data for the 2 cell types separately, 4-factor ANOVA revealed significant effects of oxygen tension, collagen scaffold type, plasmid load, and collection period ($p < 0.0001$, power = 1) on endostatin level of the 21%-21% and the 21%-5% MSCs. For the data for the 21%-21% and the 21%-5% chondrocytes, 4-factor ANOVA demonstrated significant effects of oxygen tension ($p = 0.002$, power = 0.913), plasmid load ($p < 0.0001$, power = 1), and collection period ($p = 0.0002$, power = 0.991) on endostatin level. The

effect of collagen scaffold type ($p = 0.57$; power = 0.086) on endostatin level did not achieve statistical significance.

3.3.1.2. Biochemical Analysis of DNA and GAG Content

Biochemical analyses of cell-seeded samples terminated after 20 days of culture found that the GAG density (GAG content per volume) of the constructs ranged from less than 10% to about 150% of that in native cartilage (Figure 3.2a and b); the value for the normal GAG density that was used is 15.8 $\mu g/mm^3$ [185]. No notable GAG (<2%) was detected in non-cell-seeded controls (data not shown). Higher percentages of GAG were observed in chondrocyte-seeded constructs, compared to the respective MSC-seeded scaffolds, and the GAG density was higher in the type I/III collagen constructs compared to the type II collagen constructs (Figure 3.2a and b). Biochemical findings also indicated that constructs cultured at standard oxygen resulted in higher percentages of GAG compared to those at low oxygen (Figure 3.2a and b). It was apparent in the chondrocyte-seeded constructs that there was a higher GAG density in scaffolds with endostatin-expressing cells compared to the scaffolds with no lipoplex (Figure 3.2b).

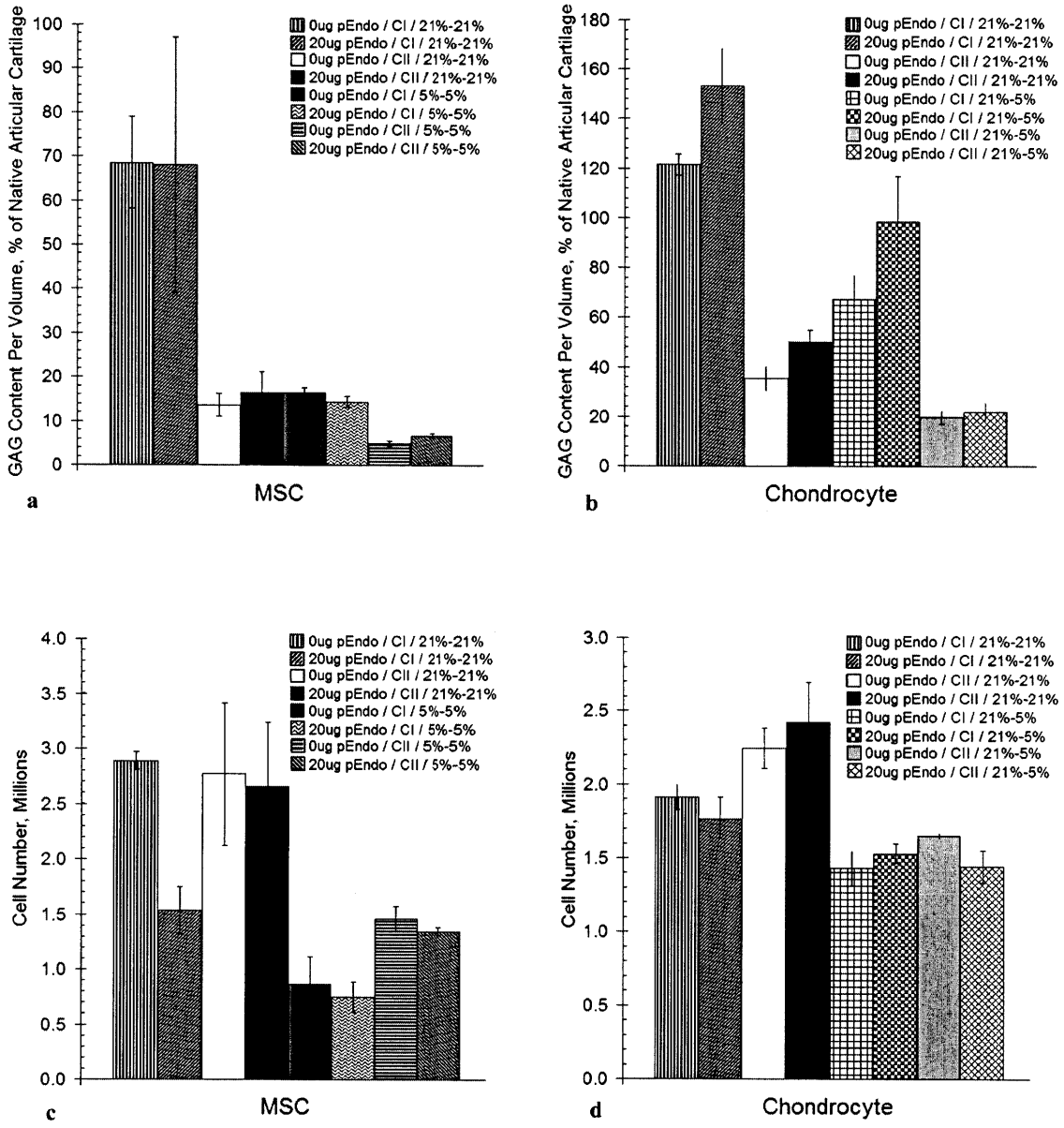

Figure 3.2 Biochemical analyses of MSC- and chondrocyte-seeded constructs cultured at standard and low oxygen (n = 3 for all samples except CI / 21%-21% MSCs, where n = 2).

- **a. Percentage GAG content per volume compared to native articular cartilage in the MSC-seeded samples after 20 days of culture.**
- **b. Percentage GAG content per volume compared to native articular cartilage in the chondrocyte-seeded samples after 20 days of culture**
- **c. Cell numbers in the MSC-seeded samples after 20 days of culture, estimated from the DNA content.**
- **d. Cell numbers in the chondrocyte-seeded samples after 20 days of culture, estimated from the DNA content.**

Including all data for the cell-seeded constructs, 4-factor ANOVA demonstrated significant effects of 3-D oxygen tension ($p < 0.0001$, power = 1), collagen scaffold type ($p < 0.0001$, power = 1), cell type ($p < 0.0001$, power = 1), and plasmid load ($p = 0.0290$, power = 0.597) on the percentage of GAG. Analyzing data for the 21%-21% and the 5%-5% MSCs, 3-factor ANOVA revealed significant effects of oxygen tension ($p < 0.0001$, power = 1) and collagen scaffold type ($p < 0.0001$, power = 1), but not plasmid load ($p = 0.9278$; power = 0.051), on the percentage of GAG. For the data for the 21%-21% and the 21%-5% chondrocytes, 3-factor ANOVA again demonstrated significant effects of oxygen tension ($p < 0.0001$, power = 1) and collagen scaffold type ($p < 0.0001$, power = 1) on the percentage of GAG. Plasmid load was also found to have a significant effect ($p = 0.011$, power = 0.778).

At the end of the 20-day culture period, the number of MSCs and chondrocytes in the cell-seeded scaffolds ranged from about 0.5 to 2.75 million cells per scaffold (Figure 3.2c and d), compared to the 4 million cells seeded. More cells were found in the scaffolds cultured at standard oxygen compared to those cultured at low oxygen (Figure 3.2c and d). A larger number of MSCs than chondrocytes were seen in the 21%-21% group at the termination of the culture period (Figure 3.2c and d). Including all data for the cell-seeded constructs, 4-factor ANOVA demonstrated significant effects of 3-D oxygen tension ($p < 0.0001$, power = 1) and collagen scaffold type ($p = 0.0042$, power = 0.866) on cell number, but failed to find a significant effect of plasmid load ($p = 0.1097$, power = 0.342) or cell type ($p = 0.8984$, power = 0.052). Including the data for the 21%-21% and the 5%-5% MSCs, 3-factor ANOVA revealed a significant effect of oxygen tension ($p = 0.0001$, power = 1) on cell number but failed to find significant effect of collagen scaffold type ($p = 0.055$, power = 0.485) or plasmid load ($p = 0.131$, power = 0.308). For the 21%-21% and the 21%-5% chondrocytes, 3-factor ANOVA demonstrated significant

effects of oxygen tension ($p < 0.0001$, power = 1) and collagen scaffold type ($p = 0.011$, power = 0.775) on cell number and found no significant effect of plasmid load ($p = 0.845$, power = 0.054).

3.3.1.3. Histological and Immunohistochemical Evaluation of the Constructs

Immunohistochemical analysis of the constructs cultured for 20 days revealed the presence of newly-synthesized extracellular matrix staining strongly positive for sulfated GAG (Figure 3.3a) and type II collagen (Figure 3.3b), generally around the periphery of the constructs. Few areas of newly-synthesized matrix were observed in the centers of the constructs. Cells were distributed throughout the constructs, and much of the original collagen scaffold could still be seen (Figure 3.3a, b, and c). Some of the cells in the GAG- and type II collagen-rich matrix appeared rounded in lacunae; many had a fibroblast-like appearance (without lacunae) (Figure 3.3a). The fibrous appearance of the matrix was consistent with fibrocartilage and fibrous tissue. The Safranin-O staining results of the 20-day samples correlated with the biochemical findings, in that increasing amounts of positive staining for sulfated GAG were seen in constructs with increasing percentages of GAG. The amount and distribution of positive staining for type II collagen (Figure 3.3b) correlated with that of the GAG staining. Masson's trichrome staining indicated the presence of collagen around the periphery of the constructs, in the same areas where positive staining for type II collagen was observed in the newly-synthesized matrix (Figure 3.3b and c). Many of the struts of the collagen scaffold stained red (Figure 3.3c), likely due to a difference in tension of the collagen struts compared to that found in the collagen in the matrix [186].

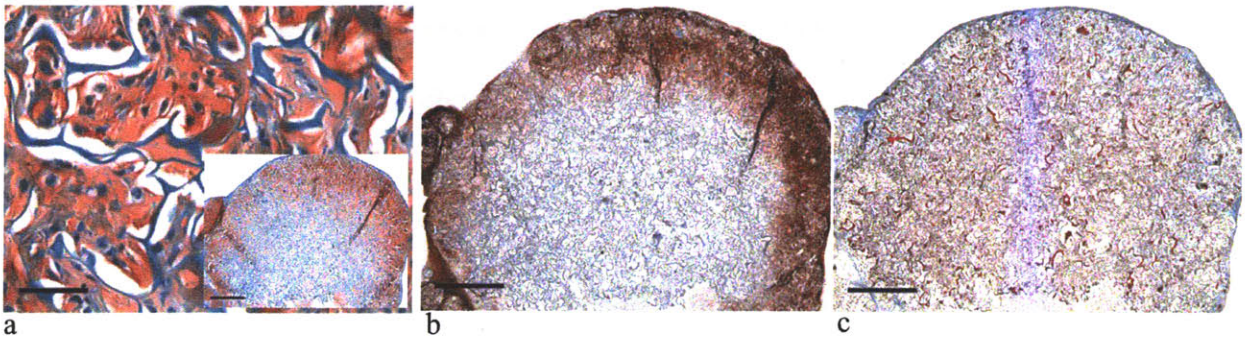

Figure 3.3 Micrographs of chondrocyte-seeded CI scaffold construct supplemented with 20 μg pEndo, after 20 days of culture at standard oxygen.

- **a. Safranin-O staining of GAG (red chromogen indicates sulfated GAGs). Scale bar, 50 μm. Inset shows the section at lower magnification, scale bar, 500 μm.**
- **b. Type II collagen immunohistochemistry (brownish-red chromogen indicates positive stain). Scale bar, 500 μm.**
- **c. Masson's trichrome staining of (blue chromogen indicates collagen, red chromogen indicates cytoplasm, and black chromogen indicates nuclei). Scale bar, 500 μm.**

3.3.2. Scaffold Supplementation with Chondroitin Sulfate and Heparan Sulfate

3.3.2.1. Endostatin Detection in the Medium

Endostatin released into the medium of MSC-seeded, lipoplex-incorporating constructs increased to a peak in the first week of culture and then decreased to low levels (Figure 3.4). The endostatin levels of the 2 groups that received additional GAG supplementation were comparable, and the levels of both groups were lower than those of the group that did not receive additional GAG supplementation at all collection periods (Figure 3.4). The cumulative endostatin level at day 20 was much higher for the non-GAG-supplemented group (97 ng/ml) than for both GAG-supplemented groups (28 ng/ml for CI-CS, 9 ng/ml for CI-HS). The highest endostatin level in the experiment was observed to be 29 ng/ml at the 3-day collection period ending on day 4, for the lipoplex-incorporating CI control group (Figure 3.4). The

nontransfected MSC-seeded control group, which received no lipoplex and was not transfected, displayed no notable endostatin protein in the medium (Figure 3.4).

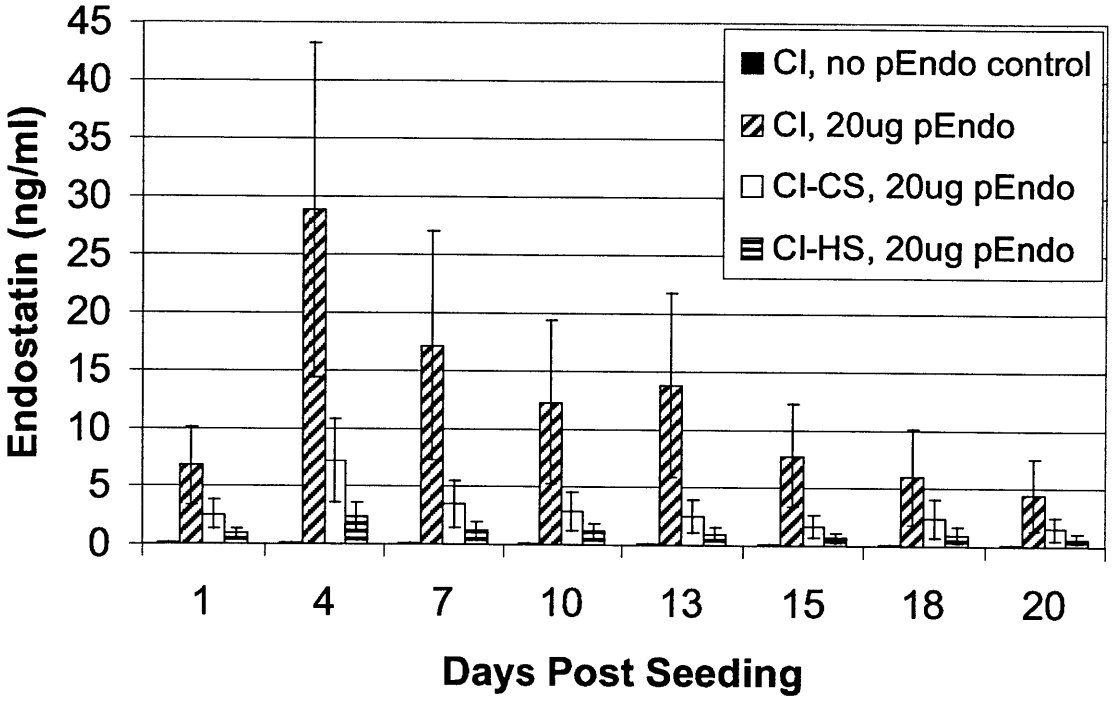

Figure 3.4 Endostatin measured in the expended medium of cell-seeded collagen sponge-like scaffold constructs supplemented with chondroitin sulfate and heparan sulfate (n = 2-4).

Two-factor ANOVA of the lipoplex-incorporating groups revealed significant effects of collection period ($p = 0.0012$, power = 0.98) and GAG supplementation ($p < 0.0001$, power = 1) on endostatin levels in the expended medium. Fisher's *post hoc* PLSD testing demonstrated a significant difference between the CI control constructs and the 2 GAG-supplemented constructs.

3.3.2.2. Histological/Immunohistochemical Evaluation of the Constructs

Four days after seeding, cells could be seen in the pores of the sponge-like scaffold, often clustered together (Figure 3.5a, b, and c). Positive staining for endostatin for a few cells was seen in the lipoplex-incorporating constructs at day 4 (Figure 3.5a, b, and c). Similar sparse

staining was seen at days 14, 20, and 28 (data not shown). No staining was observed in the controls that did not receive lipoplex (data not shown).

After 20 days, all constructs demonstrated areas of positive staining for type II collagen (Figure 3.5d, e, and f) and sulfated GAG (Figure 3.5g, h, and i). Higher magnification of a Safranin-O-stained section (Figure 3.5h) revealed the fibrous appearance of the newly-formed extracellular matrix. Cells were in close proximity to each other, and some cells appeared rounded and resided in lacunae, characteristic morphology of chondrocytes (Figure 3.5h). The outermost layer of the constructs, which was several cells thick, consisted of cells with a flattened, elongated, fibroblast-like morphology, and did not stain for type II collagen or sulfated GAG (Figure 3.5h). A few residual struts of the sponge-like scaffold could be seen, in the interior portion of the construct (Figure 3.5h).

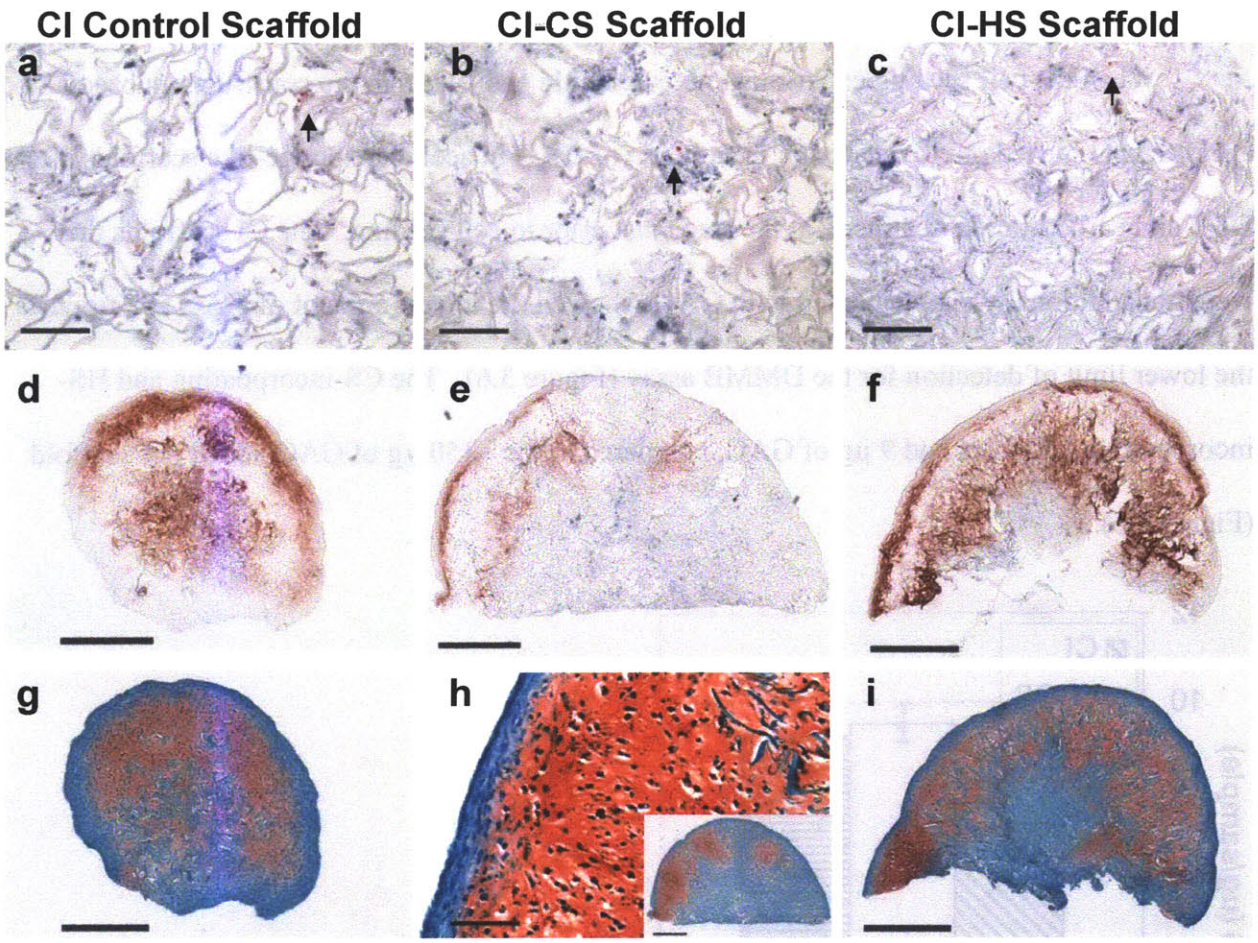

Figure 3.5 Micrographs of histological sections of MSC-seeded, pEndo lipoplex-incorporating sponge-like constructs, with and without additional GAG supplementation.

a. **Endostatin immunohistochemistry (arrows, red chromogen) of CI control construct, without additional GAG supplementation, 4 days after seeding. Scale bar, 100 μm.**
b. **Endostatin immunohistochemistry of CI-CS construct 4 days after seeding. Scale bar, 100 μm.**
c. **Endostatin immunohistochemistry of CI-HS construct 4 days after seeding. Scale bar, 100 μm.**
d. **Type II collagen immunohistochemistry of CI control construct after 20 days of culture in CM (brownish-red chromogen indicates positive stain). Scale bar, 500 μm.**
e. **Type II collagen immunohistochemistry of CI-CS construct after 20 days of culture in CM. Scale bar, 500 μm.**
f. **Type II collagen immunohistochemistry of CI-HS construct after 20 days of culture in CM. Scale bar, 500 μm.**
g. **Safranin-O staining for GAG of CI control scaffold (red chromogen indicates sulfated GAGs). Scale bar, 500 μm.**
h. **Safranin-O staining for GAG of CI-CS scaffold. Scale bar, 100 μm. Inset shows the section at lower magnification, scale bar, 500 μm.**
i. **Safranin-O staining for GAG of CI-HS scaffold. Scale bar, 500 μm.**

3.3.2.3. Biochemical Analysis of GAG Content

When the cell seeding experiment revealed little endostatin in the constructs, subsequent analysis was carried out to determine the amount of GAG in acellular sponge-like scaffolds after DHT and carbodiimide treatment, at the stage just prior to cell seeding. The CI scaffolds that were not additionally supplemented with GAGs showed the lowest amount of GAG at 7 μg, near the lower limit of detection for the DMMB assay (Figure 3.6). The CS-incorpoating and HS-incorporating scaffolds had 9 μg of GAG, compared to the ~150 μg of GAG added per scaffold (Figure 3.6).

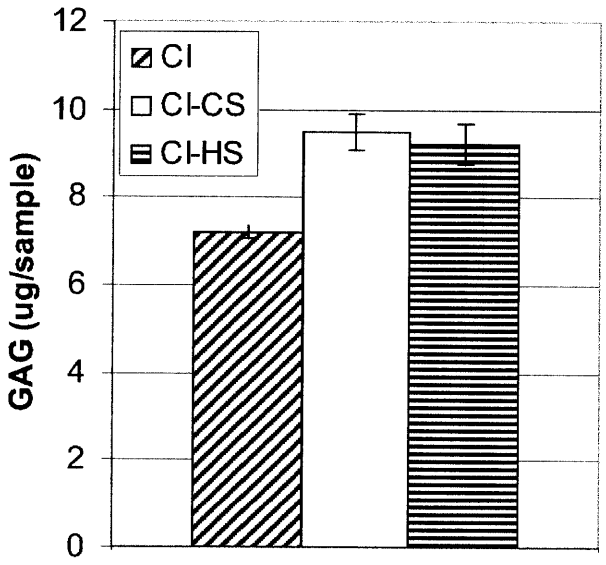

Figure 3.6 Biochemical analysis of acellular sponge-like scaffolds, just prior to cell seeding. Average GAG per sponge-like scaffold (n = 4-5).

3.4. Discussion

In this study, we engineered endostatin-expressing cartilaginous constructs *in vitro* using a small amount of pEndo in lipoplex-supplemented sponge scaffolds. A peak in endostatin protein in the expended medium during the first week of culture was seen in each of the groups, followed by a decrease, suggesting that overexpression of endostatin could be sustained for at

least several days using the nonviral vector. Similar kinetics of endostatin expression were found in this experiment and those in Chapter 2 despite differences in the GP2:pEndo ratio and number of seeded cells. The maximum endostatin level per collection period in this study was ~30 ng/ml, similar to physiological levels [106].

Endostatin overexpression was affected by a number of variables in the first experiment. MSC- and chondrocyte-seeded constructs were found to behave differently. MSC-seeded constructs were generally observed to have more endostatin in the expended medium in the initial week following transfection compared to chondrocytes. Oxygen tension was found to play an important role, significantly affecting endostatin expression. In this experiment, 5% oxygen resulted in lower endostatin levels compared to 21% oxygen. How oxygen tension affects endostatin production is unclear—some studies have found that low oxygen induced endostatin production [146], whereas other studies have observed that low oxygen downregulated endostatin [149]. Similarly, the mechanism by which these variables are affecting endostatin overexpression, whether they are affecting gene transfection efficiency in general or whether they are specific to endostatin production, is not known. These issues remain to be addressed in future studies.

Chondrogenesis was observed in the engineered constructs cultured in CM for 3 weeks. The constructs were not homogeneous—cartilaginous material was found in regions of the constructs. The GAG density reported in this study was calculated using the entire volume of the construct; if GAG density were calculated using only the volume of the GAG-rich regions, the density would be higher. For experiment #1, chondrocyte-seeded scaffolds demonstrated greater degrees of chondrogenesis than MSC-seeded scaffolds after the same amount of time in culture, likely due to MSCs requiring time to first differentiate down the chondrogenic lineage. The

correlation between the GAG per cell cannot be commented on because it is unclear how many cells were present when the GAG was synthesized, and the amount of GAG that was lost to the medium cannot be accounted for.

Another finding from the first experiment of this study was that chondrocyte-seeded, lipoplex-supplemented constructs were observed to have higher percentages of GAG per volume compared to chondrocyte-seeded, non-lipoplex-supplemented controls, which achieved statistical significance. This suggests that endostatin may stimulate chondrocyte production of sulfated GAGs, and thus supports previous observations that *in vitro* exposure to recombinant human endostatin protein promoted the anabolic activity of articular chondrocytes [123]. This phenomenon was not seen for MSC-seeded constructs. However, in our study the percentage increase for the chondrocyte-seeded constructs varied only from 2% to 32%. Our contemporaneous negative control for endostatin expression and chondrogenesis were the cells alone. A control scaffold incorporating a lipoplex containing an irrelevant DNA was not included in the study, because our own prior study [98] demonstrated that increasing the lipid in the lipoplex had no significant effect on endostatin expression. There was no reason to expect that the lipid alone would induce endostatin expression or increase GAG production; therefore, this control was not performed. Our own data and the absence of prior studies demonstrating that lipid alone would affect endostatin levels and GAG synthesis make it unlikely that the absence of a lipid control is a confounding factor in the interpretation of the effects of various factors on endostatin expression and chondrogenesis.

A higher GAG percentage and more positive staining of newly-synthesized matrix for type II collagen and GAG were seen when using type I/III collagen scaffolds compared to type II collagen in the first experiment. It is possible that the weight percentage of collagen used when

fabricating the scaffolds (1% type II collagen versus 0.5% type I/III collagen), and not only the collagen type, may account for the observed differences in GAG percentages.

Oxygen tension was also found to have a significant effect on chondrogenesis and cell number in the first experiment. Both MSC- and chondrocyte-seeded constructs cultured at 21% oxygen demonstrated more chondrogenesis than in those cultured at 5%. Additionally, more cells were observed in the standard oxygen constructs after 20 days of culture than in the low oxygen constructs, even though the same number of cells was initially seeded onto each scaffold, suggesting that low oxygen may result in decreased cell proliferation or viability. It should be noted that the oxygen level actually experienced by the cell is often unrecognized by investigators and may not be the same as the oxygen level in the gas phase, and this may contribute to differences between our findings and previous work as well as discrepancies within the literature itself [187].

Given that 5% oxygen tension is closer to normoxia for cartilage *in vivo*, these findings could have implications for endostatin expression and chondrogenesis of cells transfected by the endostatin lipoplex-supplemented scaffolds in an *in vivo* setting. However, it is important to note that the *in vivo* environment has many other soluble and mechanical factors that were not simulated in our *in vitro* setting. Here, only the effects of oxygen tension during 3-D culture of the constructs were investigated. Future work is needed to address the role of oxygen tension during 2-D monolayer expansion of the cells for subsequent use in tissue engineered constructs; for example, the fact that the chondrocytes were expanded in monolayer at 21% oxygen and not at 5% oxygen may have contributed to the GAG results seen in this study [188]. It is also possible that 21% oxygen may be preferable for MSCs compared to 5% oxygen, and that 5% oxygen may be more desirable only once MSCs differentiate into chondrocyte-like cells.

As mentioned in other studies, the extent of lipoplex cytotoxicity is unclear [189]; however, no significant effect of lipoplex was seen on cell number after 3 weeks in culture, suggesting that there are no long-term negative effects of lipoplexes on cell viability.

For the constructs in the GAG supplementation experiment, endostatin levels in the expended medium were significantly lower for the GAG-supplemented constructs than for the non-supplemented constructs at all collection periods. The structural and mechanical properties of scaffolds have been shown to influence cell behavior [175, 190-192], and it has been suggested that the addition of GAGs in collagen sponge-like scaffolds modifies the properties of the scaffolds [173, 176]. In this study, the addition of HS and CS may have affected the properties of the scaffolds, and thus the behavior of the cells during the process of obtaining, transcribing, and translating the genetic material into the final protein product, possibly contributing to the differences seen in endostatin production levels.

The addition of HS and CS in the second experiment of this study did not have a beneficial effect on endostatin retention as hypothesized. Positive staining for endostatin was seen for only a few cells in the GAG-supplemented sponges, suggesting that the protein amounts in the engineered constructs were negligible, and qualitatively, there were no notable differences among the 3 sponge groups. This is in contrast with other *in vitro* and *in vivo* binding and retention studies. Il Choi *et al.* showed sustained release of human growth hormone (hGH) from hGF-loaded heparin-based hydrogels *in vitro*, with ~60% of the loaded hGH released over a 2-week period, compared to 100% release of the loaded hGH from control constructs without heparin by 10 days [163]. Chung *et al.* demonstrated sustained release of lysozyme from lysozyme-loaded heparin-functionalized PLGA nanoparticles *in vitro* over 20 days, compared to release of all protein from a control PLGA nanoparticle with no heparin in only 7 days [164].

McGonigle *et al.* loaded heparin hydrogels with osteoprotegerin (OPG), a pro-angiogenic factor, and found that the more crosslinked the OPG-loaded gel, the more delayed the release of the protein from the construct *in vitro* [165]. The authors also found that implantation of OPG-loaded heparin gels, which retained OPG for at least 2 weeks *in vivo*, led to a 2-fold increase in neovascularization compared to control gels in a mouse model [165]. Pieper *et al.* synthesized HS-supplemented collagen scaffolds and loaded them with FGF, a growth factor with angiogenic properties [162]. They found that HS resulted in a 3-fold increase in initial FGF loading compared to a collagen scaffold alone, and that HS aided in retention of FGF *in vitro*—after 4 weeks of incubation, 53% of FGF was released from HS-supplemented scaffolds, compared to 64% from non-supplemented controls [162]. The constructs were implanted subcutaneously in rats, and the FGF-loaded, HS-supplemented constructs resulted in the most angiogenesis *in vivo*, compared to controls without HS [162].

A possible reason for the lack of endostatin binding and retention is low retention of HS and CS in the scaffolds. The small amount of GAGs (9 μg per scaffold) measured in the sponges just prior to cell seeding was unexpected, as previous studies have demonstrated the ability to fabricate scaffolds with GAG compositions similar to the GAG percentage intended for this study (7 wt %) [173, 176, 178]. It is not entirely clear why the heparan sulfate and chondroitin sulfate were not retained in the sponges just prior to cell seeding. It has been shown that chondroitin sulfates and heparan sulfates vary depending on the species of origin and the manufacturing process used to obtain the GAG, including differences in molecular weights, and evidence from previous work suggests that these differences can affect the amount of GAG that is grafted on the collagen [172-174]. It is possible that only small amounts of the GAGs used in this study formed crosslinks with the collagen during DHT treatment. Loss of GAGs due to

elution may have occurred when the sponges were immersed in an aqueous carbodiimide solution following DHT treatment. The finding from this experiment suggests that not all GAGs lend themselves to crosslinking well to collagen. A modified protocol using heparin-agarose beads in hydrogels was developed for endostatin protein retention, to ensure that GAG was retained in the constructs at the time of cell seeding (Chapter 4).

In general, GAG supplementation in the second experiment did not have a beneficial effect on chondrogenesis, likely due to the lack of the presence of the GAGs.

In this study, we engineered endostatin-producing constructs using nonviral transfection of MSC- and chondrocyte-seeded, pEndo lipoplex-supplemented collagen constructs. The endostatin expression profile and degree of chondrogenesis were altered through the manipulation of select variables, including oxygen tension and collagen scaffold type. The addition of HS and CS did not have beneficial effects on endostatin production and retention or chondrogenesis. Based on the current results, the optimal group of experimental conditions for sponge-like scaffold constructs appears to be MSCs seeded in 0.5% type I/III collagen scaffolds, supplemented with 5 μg of pEndo per 1 million cells, and cultured at 21% oxygen, balancing considerations of high levels of overexpression and sustained production over an extended period of time; however, this should not completely rule out consideration of other conditions tested, such as type II collagen scaffolds.

CHAPTER 4: ENGINEERING ENDOSTATIN-EXPRESSING CARTILAGINOUS CONSTRUCTS USING HYDROGELS

4.1. Introduction

In previous chapters, we utilized pre-formed sponge-like scaffolds. We were able to develop endostatin-producing tissue-engineered constructs, but there are some challenges associated with sponges, including challenges with cell seeding and the need for open knee surgery to implant the constructs.

Hydrogels are being researched as an alternative scaffold for cartilage regeneration [193, 194]. Similarly to sponges, gels can be made using natural and synthetic polymers, including type I collagen, and have been shown to result in cartilaginous constructs [195]. Unlike sponges, the average pore size of gels is generally much smaller [175, 196]. Gels are injectable, facilitating the use of minimally invasive surgical techniques and resulting in less surgical trauma compared to sponge implantation. Gels can also take any shape, allowing them to more easily fill defects of any geometry. However, there are also disadvantages with gels, including limitations in terms of mechanical strength, which could lead to an inability to bear high loads *in vivo* [197].

The gels can be covalently crosslinked, if desired, increasing the mechanical strength of the scaffolds and providing a potential method by which to control the degradation rate [176, 198, 199]. Commonly used synthetic crosslinking agents for biologic tissue fixation include glutaraldehyde and carbodiimide; however, these reagents are toxic to cells and would not allow for *in situ* crosslinking of cell-seeded scaffolds [198]. Crosslinking agents that can be used safely with cells, such as transglutaminases and genipin, have been receiving increased attention in recent years; prior studies have not directly compared transglutaminases and genipin.

Transglutaminase-2 (TG-2, tissue transglutaminase, tTG, mammalian) is an 88 kDa calcium-dependent enzyme that catalyzes post-translational modification of specific protein

substrates through its active cysteine site, resulting in the formation of covalent bonds between primary amines and glutamine residues [200-202]. This enzyme participates in a wide variety of physiological processes, such as blood coagulation and extracellular matrix assembly, and has also been reported to have therapeutic benefits, such as protection against ischemic stroke [203, 204]. TG-2 has been shown to be noncytotoxic at 100 μg/ml [205]. It is found naturally in the body in endothelial cells at high levels and has also been reported in chondrocytes and articular cartilage, and many cartilage matrix molecules are crosslinking substrates for TG-2 [201, 206-210]. It has been used to crosslink scaffolds for cartilage tissue engineering applications [210], although there is debate in the literature regarding the extent of its effectiveness at crosslinking collagen scaffolds [211, 212]. TG-2 has also been shown to bind to endostatin with a high affinity (K_D = 6.8 nM), at the same arginine residues on endostatin that also bind to heparin and heparan sulfate [202]. The endostatin binding site on TG-2 is believed to be separate from its active cysteine site [202].

Microbial transglutaminase (mTG) is primarily known for its industrial applications, including its use as a food protein crosslinking agent [213]. It appears to have a cysteine active site similar to that of TG-2 [213], and both mTG and TG-2 seem to introduce similar amounts of crosslink per unit activity [205]. However, the overall mTG enzyme bears little homology with TG-2. mTG is a 38 kDa enzyme that does not require calcium, and its physiological role is unclear [213]. It has been used to crosslink scaffolds [214] and to bond articular cartilage [215]. This enzyme has been shown to be noncytotoxic when crosslinking scaffolds at 100 μg/ml [205, 214].

Genipin (GP) is a naturally occurring crosslinking agent from the *Gardenia jasminoides* plant that has been found to crosslink functional amine groups [198]. It has been suggested that

GP has anti-inflammatory and anti-fibrotic properties [216-218]. It has been shown to be non-cytotoxic, generally at small concentrations under 0.5 mM [198, 218, 219]; for example, no adverse reactions were noted following the use of GP *in vivo* in a rat knee [220]. GP has been used in traditional Chinese medicine [221], used to crosslink scaffolds for articular cartilage tissue engineering [219, 220], used to bond articular cartilage [215], and added exogenously in culture medium for engineered cartilage [218].

Since the GAG-supplemented sponge-like scaffolds resulted in little GAG retention just prior to cell seeding, a modified protocol using heparin-agarose beads was developed for endostatin protein retention in hydrogels. Heparin has been added to scaffolds using other methods. Beamish *et al.* loaded poly(ethylene glycol) diacrylate (PEGDA) hydrogel scaffolds with heparin by soaking the scaffolds overnight in buffer consisting of 2 mg/ml heparin [222]. Il Choi *et al.* functionalized heparin by adding thiol, and then reacted it with PEGDA to make a heparin-based hydrogel [163]. Chung *et al.* mixed heparin with poly(glycolide-co-lactide) (PLGA) in the aqueous phase of preparation to make 2.4% and 4.7% (wt %) heparin-functionalized PLGA nanoparticles and showed that over 80% (0.94 – 1.71 mg) of the heparin was located on the nanoparticle surface layer [164]. Elia *et al.* synthesized thiol-modified forms of hyaluronic acid (HA), gelatin, and heparin, then made PEGDA-crosslinked HA-based hydrogels containing 0.03% and 0.3% (wt %) heparin [223]. Here, the rationale for using heparin-agarose beads was that the beads would be physically entrapped in the gels, since they are substantially larger than the pores of the hydrogels, thus ensuring incorporation of GAG into the scaffolds.

Heparin, best known for its use as an anticoagulant, is a highly-sulfated GAG, similar in structure to heparan sulfate, though generally more sulfated and less acetylated than HS.

Heparin consists of a repeating disaccharide unit, most commonly 2-O-sulfated iduronic acid and 6-O-sulfated, N-sulfated glucosamine [172]. Heparin covalently bound to the surface of agarose beads is commonly used in columns to bind and purify proteins, including endostatin [100, 166].

Previously, our lab has shown that endostatin-expressing cartilaginous constructs can be engineered using pre-formed sponge-like scaffolds [98, 224]. In this study, the ability to engineer similar constructs using hydrogels, with various covalent crosslinking agents and heparin-agarose beads, was evaluated.

4.2. Materials and Methods

4.2.1. Plasmid Propagation and Isolation

The endostatin plasmid (pEndo) vector *pCEP-Pu AC7* and the propagation and isolation protocol have been previously described [98]. Briefly, plasmid was obtained by heat shock transformation of *Escherichia coli* DH5α competent cells (Invitrogen, Carlsbad, CA, USA) and isolation using a Mega QIAfilter™ Plasmid kit (Qiagen, Valencia, CA, USA).

4.2.2. Cell Isolation and Two-Dimensional Monolayer Expansion

MSCs were isolated from heparinized bone marrow aspirates from the iliac crests of adult Spanish goats. Adherent cells were expanded in monolayer using a standard MSC expansion medium consisting of low glucose Dulbecco's modified Eagle's medium (DMEM-LG), containing 10% (v/v) fetal bovine serum (FBS) and 1% penicillin/streptomycin (PS) (Invitrogen), and supplemented with 10 ng/ml fibroblast growth factor (FGF)-2 (R&D Systems, Minneapolis, MN, USA). The cells were incubated in a humidified chamber at 37°C, 5% carbon

dioxide, and atmospheric oxygen. MSCs were grown through two subcultures to obtain passage 2 (P2) cells.

4.2.3. Scaffold Fabrication

Six groups of hydrogel scaffolds were prepared: (1) 0.2% (w/v) rat tail type I collagen (BD Biosciences, San Jose, CA, USA); (2) 0.2% type I collagen incorporating 100 μg/ml transglutaminase (TG)-2 (Sigma); (3) 0.2% type I collagen incorporating 100 μg/ml microbial transglutaminase (mTG) (Ajinomoto, Fort Lee, NJ, USA); (4) 0.2% type I collagen incorporating 0.25 mM genipin (GP, Wako, Richmond, VA, USA); (5) 0.2% type I collagen incorporating 0.25 mM GP and control agarose beads (without heparin) (Sigma); and (6) 0.2% type I collagen incorporating 0.25 mM GP and 10% (weight of heparin/weight of collagen) heparin-agarose type I beads (Sigma). The volume of agarose beads and heparin-agarose beads added to the hydrogels was determined by the amount of heparin attached to the heparin-agarose beads; for this experiment, 0.16 ml of beads were added per ml of hydrogel mixture. The molecular weight of the heparin was reported by the manufacturer to be around 25 kDa. All beads were washed in sterile water to remove any preservatives prior to adding to the hydrogel mixtures. For all hydrogel groups, 1 M sodium hydroxide (Fisher, Pittsburgh, PA, USA) was added to the hydrogel mixture to obtain a final pH of 7.4, and expansion medium (with no FGF-2) and phosphate-buffered saline (PBS, Sigma) were used as fillers to bring the mixture up to the desired total volume. For the TG-2 group, 5 mM calcium chloride (Sigma) and 2 mM dithiothreitol (Sigma) were also added to the mixture. All hydrogel groups were kept on ice until ready for cell seeding and gel casting.

4.2.4. Experimental Design

Caprine MSCs were subcultured twice (P2) and transfected with lipoplexes prepared with human endostatin plasmid.

1) In the first experiment, monolayer-transfected MSCs were seeded in hydrogels, which were covalently crosslinked using TG-2, mTG, and GP. Control MSCs that were not transfected were also seeded. No beads were added to any of the hydrogels. The variable was the crosslinking agent.

2) In the second experiment, monolayer-transfected MSCs were seeded in genipin-crosslinked hydrogel scaffolds incorporating control agarose beads or heparin-agarose beads and cultured in CM. Non-bead-supplemented hydrogel controls were used. Control MSCs transfected using a plasmid encoding for green fluorescent protein (GFP) were also seeded. The variable was the incorporation of the heparin-agarose beads.

The principal outcome variable was the amount of endostatin released by the cells.

4.2.5. Transfection with GenePORTER 2/Endostatin Plasmid Complexes (Lipoplexes) and Cell Seeding and Culture

Plasmid encoding for human endostatin and for GFP were encapsulated in a lipid-mediated transfection reagent, GenePORTER™ 2 (GP2) (Gene Therapy Systems, Inc., San Diego, CA, USA) following the manufacturer's instructions.

P2 MSCs were transfected in monolayer using the lipoplexes, using the same ratio of plasmid to cells (5 μg pEndo/1 million cells) as was used for sponge-like scaffold transfection in Chapter 3. The cells were incubated in DMEM-LG for 4 hours to allow for transfection, and then expansion medium (with no FGF-2) was added to the cell flasks for overnight incubation.

In the first experiment, the day after transfection, the transfected cells were added to the hydrogel mixtures (crosslinked using TG-2, mTG, or GP) at a seeding density of 0.8 million cells/ml. No beads were added to any of the hydrogels. Control constructs seeded with nontransfected cells were also prepared.

In the second experiment, the day after transfection, the transfected cells were added to the different hydrogel groups (no additional crosslinker control with no beads, GP-crosslinked control with no beads, GP and control beads, and GP and heparin-agarose beads) at a seeding density of 0.8 million cells/ml. Additional control groups were prepared: (1) constructs with no beads, seeded with pGFP lipoplex-transfected MSCs (5 μg pGFP/1 million cells) and (2) genipin-crosslinked non-cell-seeded constructs.

For both experiments, hydrogels were cast by pipetting 0.5 ml of the cell-seeded mixtures into each well of a 24-well plate and incubating at 37°C, to create constructs with a diameter of 16 mm and a thickness of ~2 mm. The constructs were incubated overnight in expansion medium (with no FGF-2). Constructs were switched to chondrogenic medium the day after cell seeding and cultured in CM for the remainder of the experiments. Every 1-3 days, expended medium was collected and frozen at -20°C until analysis, and fresh CM was added. The constructs were cultured in 1 ml of medium. Cultures were terminated on select days for histological examination and biochemical analysis.

4.2.6. Endostatin Detection in the Constructs and the Medium

Select constructs were collected for homogenization. Homogenizing medium was prepared by dissolving 1 Complete Mini protease inhibitor cocktail tablet (Roche, Indianapolis, IN, USA) per 7 ml of PBS. Constructs were cut into small pieces, as needed, using a safety razor

blade. Each construct was placed in a homogenizing vessel containing 500 µl of homogenizing medium and homogenized using the Tissue-Tearor tissue homogenizer (Biospec, Bartlesville, OK) at 30,000 RPM for 1 min on ice. The homogenate was then centrifuged at 10,000-13,000 rcf for 5-8 mins to remove debris and insoluble materials, and the supernatant was stored at -20°C until analysis.

Endostatin protein in the homogenized constructs and in the expended culture medium was measured using a sandwich enzyme-linked immunosorbent assay (ELISA) kit for human endostatin protein (R&D Systems, Minneapolis, MN) following the manufacturer's instructions.

4.2.7. Analysis of DNA and GAG Content

Constructs were lyophilized and enzymatically digested overnight using proteinase K (Roche Diagnostics, Indianapolis, IN). Determination of the DNA content was carried out using the Picogreen dye assay kit (Molecular Probes, Inc., Eugene, OR) according to the manufacturer's instructions. Previous work in our laboratory found that the average DNA content was 5.6 pg DNA/cell for goat MSCs. The sulfated GAG content was determined by the dimethylmethylene blue (DMMB) dye assay [225], with a standard curve obtained using chondroitin-6-sulfate from shark cartilage (Sigma).

4.2.8. Histological and Immunohistochemical Evaluation

Constructs allocated for histology were fixed in 4% paraformaldehyde for at least 3 hrs, processed and embedded in paraffin, and sectioned by microtomy. The sections were mounted on glass slides and stained with Safranin-O using standard histological techniques.

Immunohistochemical evaluation was carried out. Endostatin was examined using an anti-endostatin rabbit polyclonal antibody (final concentration 17 μg/ml, Millipore, Billerica, MA, USA). Type II collagen distribution was examined immunohistochemically using an anti-type II collagen mouse monoclonal antibody (CIIC1, final concentration 4 μg/ml, Developmental Studies Hybridoma Bank, University of Iowa, Iowa City, IA, USA). Laminin and type IV collagen, common basement membrane molecules, were also examined immunohistochemically, using an anti-laminin rabbit polyclonal antibody (final concentration 27 μg/ml, Abcam) and an anti-type IV collagen rabbit polyclonal antibody (final concentration 17 μg/ml, Abcam), respectively. The immunohistochemical staining was performed using the Dako Autostainer (DakoCytomation, Carpinteria, CA, USA) and the peroxidase-aminoethyl carbazole (AEC)-based Envision+ kit (Dako) following the manufacturer's recommendations.

4.2.9. Statistical Analysis

Data are presented as the mean ± standard error of the mean (SEM). Analysis of variance (ANOVA) and Fisher's protected least squares difference (PLSD) *post hoc* testing were performed using StatView software (SAS Institute Inc, Cary, NC, USA). Statistical significance was set at $p < 0.05$.

4.3. Results

The effects of crosslinking agents (first experiment) and incorporation of heparin-agarose beads (second experiment) on endostatin expression and chondrogenesis of MSC-seeded constructs were evaluated. Our experience with the seeding method indicated that ~100% of the cells were present in the hydrogels, 1 day after seeding.

4.3.1. Crosslinking Agents

4.3.1.1. Endostatin Detection in the Constructs and Expended Medium

Endostatin released into the expended medium of hydrogel constructs seeded with pEndo lipoplex-transfected MSCs showed a peak during the first several days of culture, followed by a decrease to lower levels during the third week (Figure 4.1). The highest endostatin level of the experiment, 18 ng/ml (a total of 18 ng of endostatin in the expended medium), was measured on the 3-day collection period ending on day 4, for the GP-crosslinked group (Figure 4.1). The cumulative endostatin level at 21 days was highest for the GP-crosslinked group (64 ng/ml) and lowest for mTG-crosslinked group (28 ng/ml); the cumulative release for the TG-2-crosslinked group was 51 ng/ml. The endostatin levels for the nontransfected controls were negligible (data not shown).

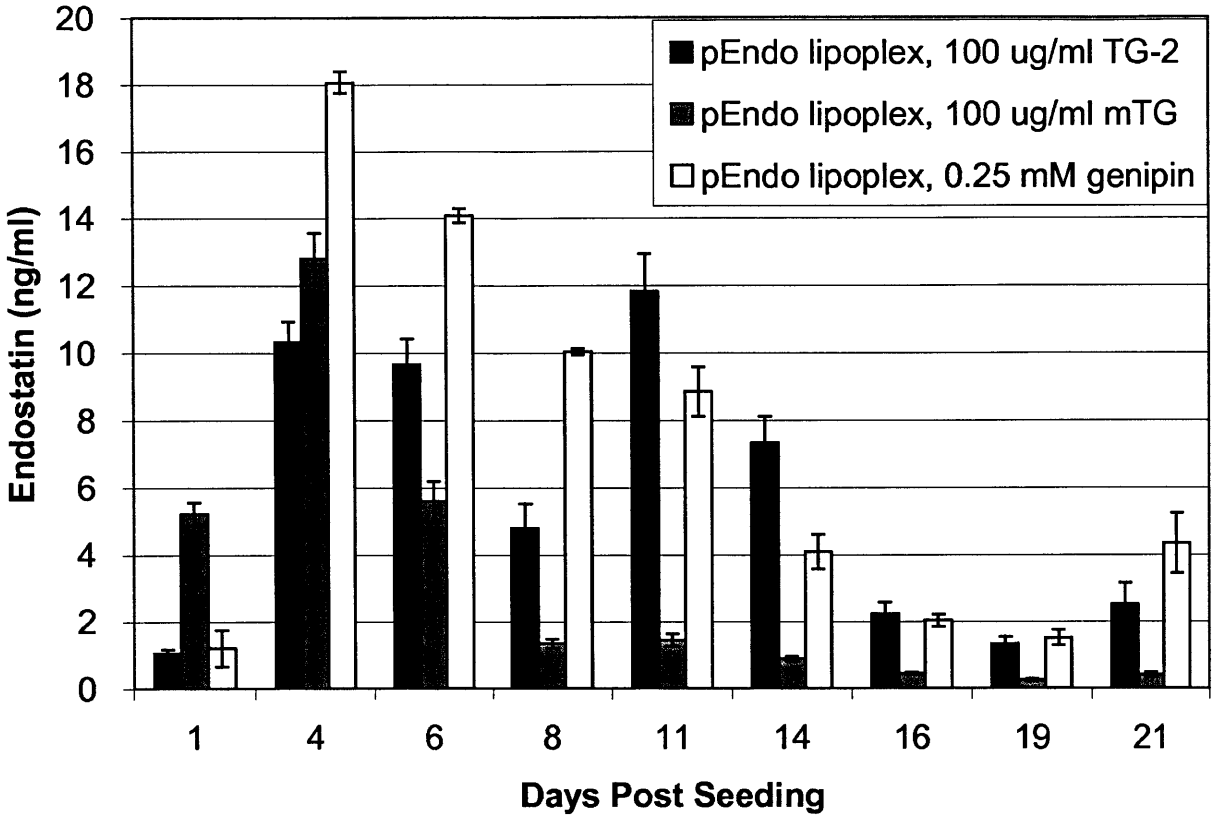

Figure 4.1 Endostatin in the expended medium of cell-seeded collagen hydrogel constructs crosslinked using select crosslinking agents, including TG-2, mTG, and GP (n = 6).

Including all pEndo lipoplex-transfected groups, 2-factor ANOVA indicated significant effects of crosslinking agent and collection period ($p < 0.0001$, power = 1 for both) on endostatin levels. Fisher's *post hoc* PLSD testing demonstrated significant differences among all 3 crosslinking agent groups.

Endostatin amounts within the homogenized constructs were very small, with a maximum measured amount of only 0.13 ng of protein (Table 4.1). The amount of endostatin for the nontransfected controls was negligible (data not shown). The amounts of protein in the homogenized constructs were very small compared to the endostatin amounts in the expended medium. Including all pEndo lipoplex-transfected groups, 2-factor ANOVA indicated a

significant effect of crosslinking agent (p = 0.0002, power = 0.997) on endostatin amount, but failed to find a significant effect of collection period (p = 0.186, power = 0.324). Fisher's *post hoc* PLSD testing demonstrated a significant difference between mTG and the other 2 groups.

Table 4.1 Endostatin protein amounts (ng) measured in homogenized cell-seeded collagen hydrogel constructs crosslinked using select crosslinking agents, including TG-2, mTG, and GP (values are endostatin amounts in ng; n = 3).

Time, days	pEndo Lipoplex		
	100 µg/ml TG-2	100 µg/ml mTG	0.25 mM GP
1	0.02 ± 0.004	0.07 ± 0.006	0.13 ± 0.009
6	0.09 ± 0.008	0.03 ± 0.002	0.06 ± 0.014
21	0.12 ± 0.024	0.01 ± 0.003	0.04 ± 0.002

4.3.1.2. Biochemical Analysis of DNA and GAG Content

Biochemical analyses of samples terminated after 21 days of culture revealed similar cell numbers among the groups, between 1.2 and 1.5 million cells per construct (Figure 4.2). These values represented an increase in cell number over time, compared to the 0.4 million cells seeded. There were no notable differences among the different crosslinking agents. Two-factor ANOVA failed to find significant effects of transfection (p = 0.22, power = 0.21) or crosslinking agent (p = 0.55, power = 0.13) on cell number.

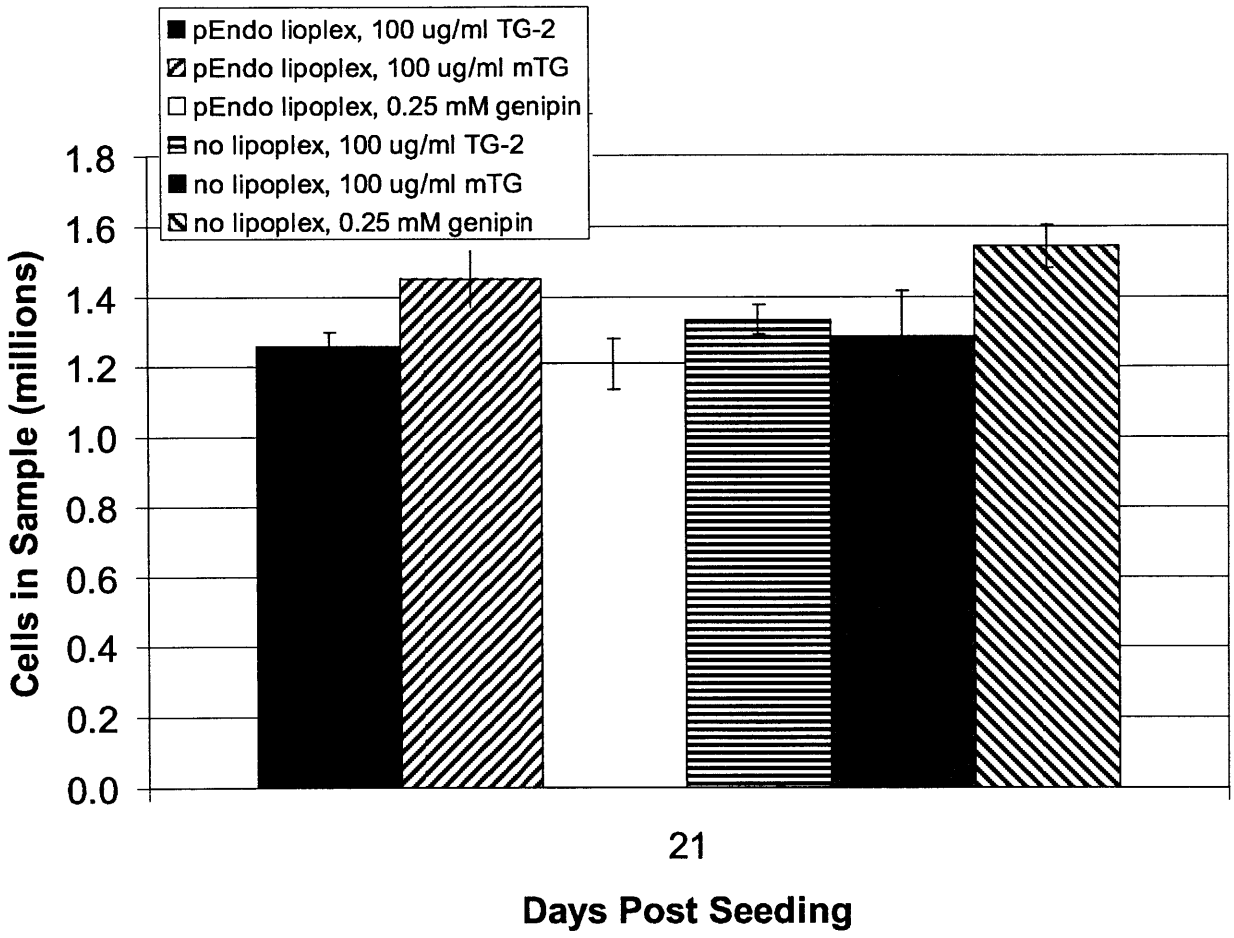

Figure 4.2 Cell numbers in the MSC-seeded collagen hydrogel constructs crosslinked using select agents, including TG-2, mTG, and GP, after 21 days of culture, estimated from the DNA content (n = 3).

For this experiment, the amount of GAG was recorded per volume, as a percentage of that of native goat articular cartilage. The GAG content per volume of native goat articular cartilage has previously been shown to be 15.8 $\mu g/mm^3$ [185]. One day after seeding, no notable GAG was measured in the constructs (data not shown). All groups displayed notable amounts of GAG after 3 weeks of culture, with a wide range from 64% to over 200% that of native cartilage (Fig. 2b). The nontransfected, GP-crosslinked group displayed a remarkably high GAG

percentage compared to the other groups (Fig. 2b). Two-factor ANOVA found significant effects of transfection ($p < 0.0001$, power =1) and crosslinking agent ($p < 0.0001$, power =1) on GAG percentage. Fisher's *post hoc* PLSD testing demonstrated a significant difference between the GP-crosslinked group and the other 2 groups.

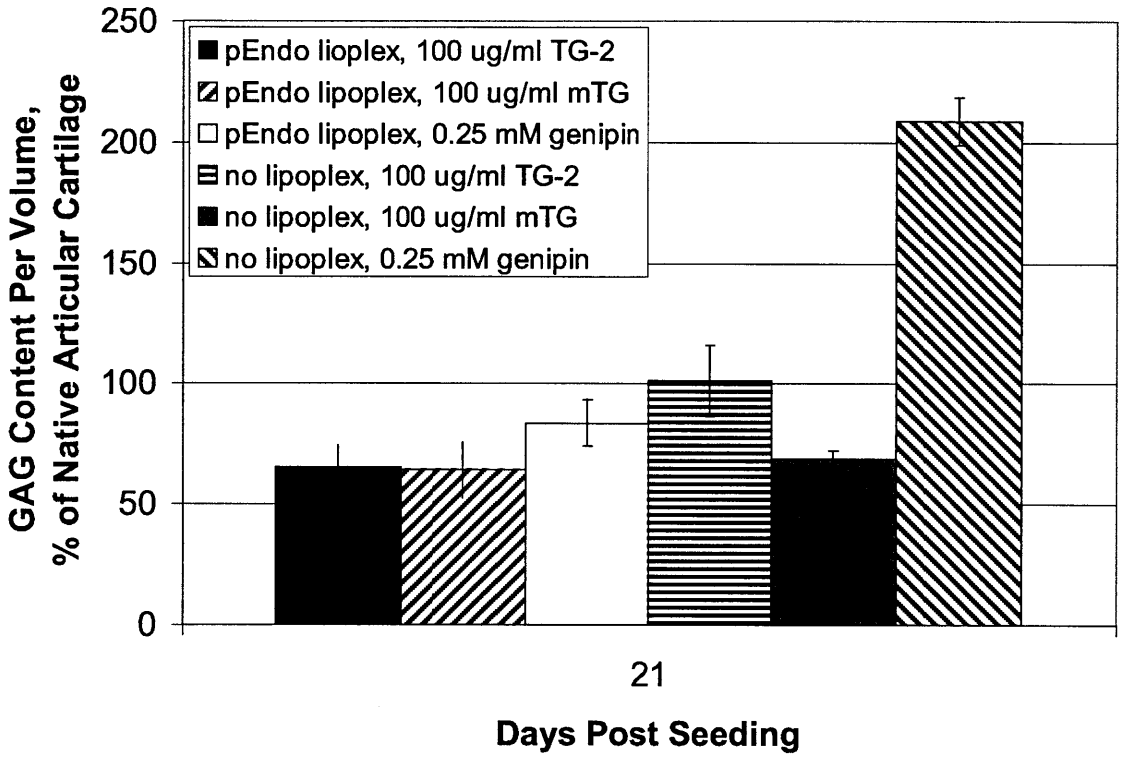

Figure 4.3 Percentage GAG content per volume compared to native articular cartilage in the MSC-seeded collagen hydrogel constructs crosslinked using select agents, including TG-2, mTG, and GP, after 21 days of culture (n = 3).

4.3.1.3. Histological Evaluation of the Constructs

Qualitative observation for endostatin in the constructs revealed only a few positive cells throughout the 3-week culture period (Figure 4.4a), consistent with the low quantitative levels seen with the homogenization results.

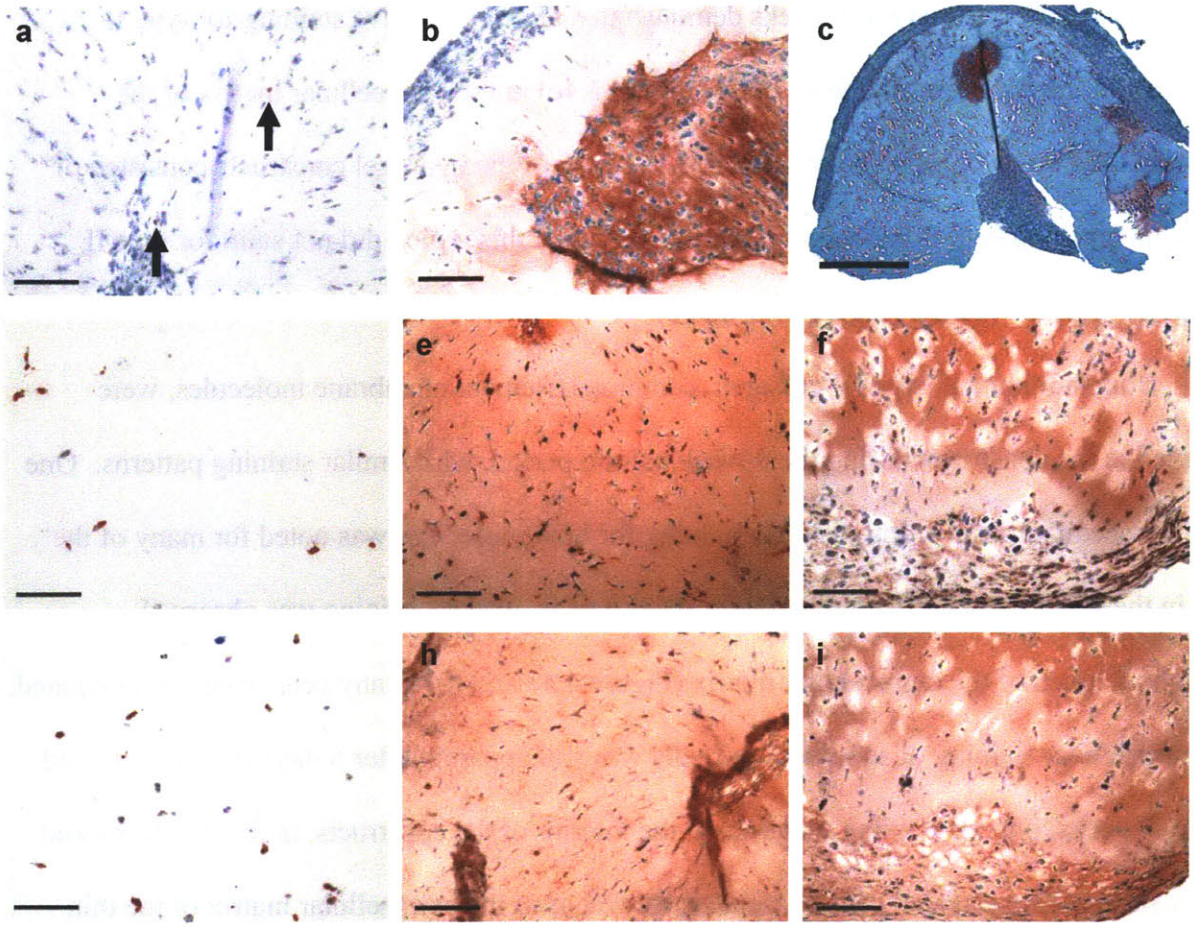

Figure 4.4 Micrographs of histological sections of TG-2 crosslinked hydrogel constructs seeded with transfected MSCs.

a. **Endostatin immunohistochemistry (arrows, red chromogen) of TG-2-crosslinked gel seeded with transfected MSCs, 21 days after seeding. Scale bar, 100 μm.**
b. **Type II collagen immunohistochemistry (red) of GP-crosslinked gel seeded with nontransfected MSCs, 21 days after seeding. Scale bar, 100 μm.**
c. **Safranin-O staining (red) of GP-crosslinked gel seeded with nontransfected MSCs, 21 days after seeding. Scale bar, 500 μm.**
d. **Laminin immunohistochemistry (red) of TG-2-crosslinked gel seeded with transfected MSCs, 1 day after seeding. Scale bar, 100 μm.**
e. **Laminin immunohistochemistry (red) of TG-2-crosslinked gel seeded with transfected MSCs, 6 days after seeding. Scale bar, 100 μm.**
f. **Laminin immunohistochemistry (red) of TG-2-crosslinked gel seeded with transfected MSCs, 21 days after seeding. Scale bar, 100 μm.**
g. **Type IV collagen immunohistochemistry (red) of TG-2-crosslinked gel seeded with transfected MSCs, 1 day after seeding. Scale bar, 100 μm.**
h. **Type IV collagen immunohistochemistry (red) of TG-2-crosslinked gel seeded with transfected MSCs, 6 days after seeding. Scale bar, 100 μm.**
i. **Type IV collagen immunohistochemistry (red) of TG-2-crosslinked gel seeded with transfected MSCs, 21 days after seeding. Scale bar, 100 μm.**

Constructs cultured for 3 weeks demonstrated areas of positive staining for type II collagen (Figure 4.4b) and sulfated GAGs (Figure 4.4c) in the extracellular matrix of the construct. A thin layer, several cells thick, at the edge of the hydrogel constructs consisted of cells with an elongated, fibroblast-like morphology, and this region did not stain for type II collagen or sulfated GAGs (Figure 4.4b and c).

Both laminin and type IV collagen, common basement membrane molecules, were observed in the constructs during the 3-week culture period, with similar staining patterns. One day after seeding, positive intracellular staining for both molecules was noted for many of the cells in the constructs (Figure 4.4d and g). After 6 days, diffuse staining was observed throughout much of the extracellular matrix (Figure 4.4e and h). Many cells appeared elongated, and intracellular staining of several of the cells was still apparent after 6 days (Figure 4.4e and h). At 3 weeks, intense staining was seen in the interior of the constructs, in the interterritorial matrix surrounding rounded cells in lacunae, as well as in the extracellular matrix of the thin layer at the periphery of the constructs (Figure 4.4f and i). Cell aggregation was noted in all gels, as the cells went from being widely spaced apart 1 day after seeding (Figure 4.4d) to being close in proximity after 1 week (Figure 4.4e and f), and there were no notable differences in cell aggregation among the different crosslinking agent groups.

4.3.2. Gels Incorporating Heparin-Agarose Beads

4.3.2.1. General Observations of the Hydrogels

Constructs were examined using light microscopy. Immediately after seeding, rounded cells (Figure 4.5) were noted in all groups, and beads could be seen dispersed throughout the hydrogels of the bead-incorporating groups (Figure 4.5b and c).

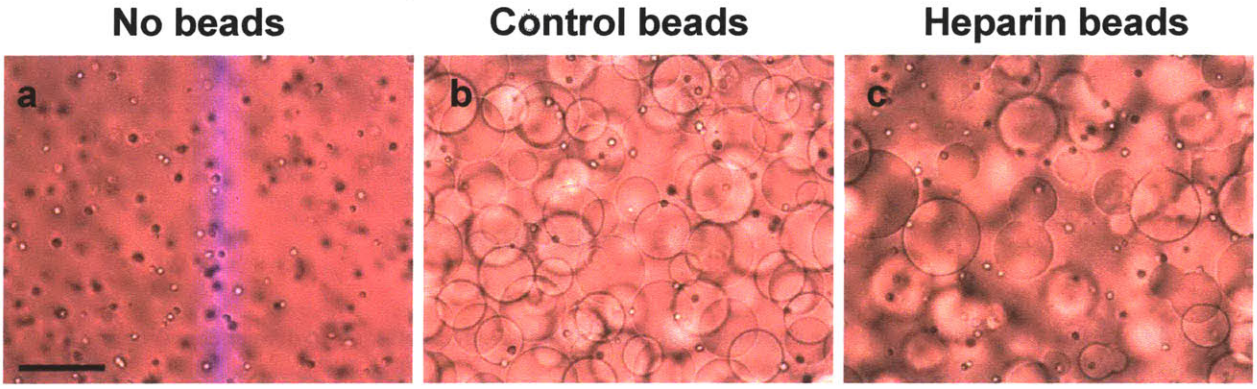

Figure 4.5 Light microscopy images of hydrogel constructs seeded with pEndo lipoplex-transfected MSCs and crosslinked with genipin, with and without beads. Each image is represented at identical magnification; scale bar, 200 μm.

4.3.2.2. Endostatin Detection in the Constructs and Expended Medium

Endostatin released into the medium of hydrogel constructs seeded with pEndo lipoplex-transfected MSCs increased to a peak in the first week of culture and then decreased (Figure 4.6), similar to the endostatin expression profile seen with the sponge-like scaffolds. The highest endostatin level of the experiment was 11 ng/ml (a total of 11 ng of endostatin in the expended medium), measured on the 3-day collection period ending on day 5, for the genipin-crosslinked group with no beads (Figure 4.6). The cumulative endostatin levels at day 21 ranged from 31 ng/ml (heparin-agarose bead group) to 36 ng/ml (control agarose bead group). The endostatin levels for the pGFP controls were negligible (data not shown).

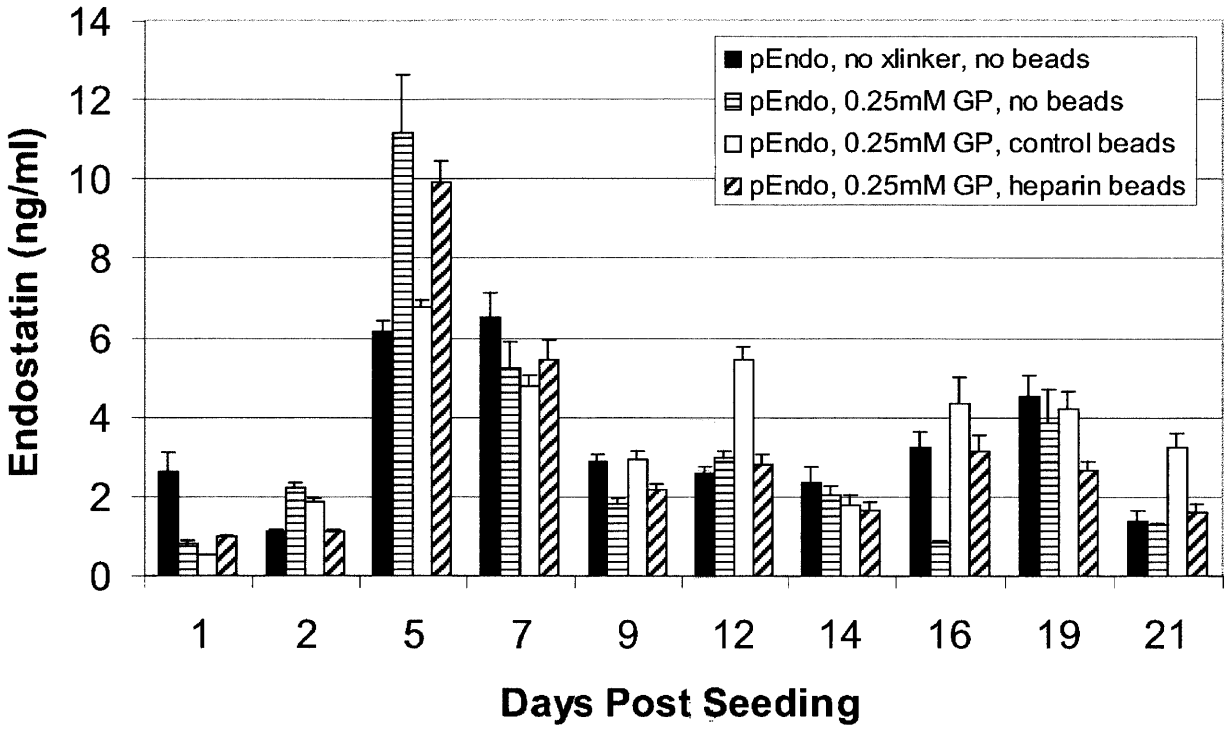

Figure 4.6 Endostatin measured in the expended medium of cell-seeded collagen hydrogel constructs incorporating heparin-agarose beads (n = 6).

Including all groups with no beads, 3-factor ANOVA revealed significant effects of plasmid (pEndo versus pGFP) ($p < 0.0001$, power = 1) and collection period ($p < 0.0001$, power = 1) on endostatin levels in the expended medium, but failed to find an effect of crosslinking agent ($p = 0.74$, power = 0.06). Including all genipin-crosslinked constructs seeded with pEndo lipoplex-transfected cells, 2-factor ANOVA revealed significant effects of collection period ($p < 0.0001$, power = 1) and bead incorporation ($p = 0.046$, power = 0.59) on endostatin levels. Fisher's *post hoc* PLSD testing demonstrated a significant difference between the control agarose bead group and the heparin-agarose bead group.

Endostatin amounts within the homogenized constructs were very small, ranging from 0.06 to 0.41 ng of protein (Table 4.2). The amount of endostatin for the pGFP controls was

negligible (data not shown). The amounts of protein in the homogenized constructs were very small compared to the endostatin amounts in the expended medium. Including all groups with no beads, 3-factor ANOVA revealed significant effects of plasmid (pEndo versus pGFP) ($p < 0.0001$, power = 1), collection period ($p < 0.0001$, power = 1), and crosslinking agent ($p = 0.01$, power = 0.78) on endostatin amounts. Fisher's *post hoc* PLSD testing demonstrated a significant difference among all 3 days. Including all genipin-crosslinked constructs seeded with pEndo lipoplex-transfected cells, 2-factor ANOVA revealed a significant effect of collection period ($p < 0.0001$, power = 1) on endostatin amounts, but failed to find a significant effect of bead incorporation ($p = 0.19$, power = 0.32). Fisher's *post hoc* PLSD testing demonstrated a significant difference between day 21 and the other 2 days.

Table 4.2 Endostatin protein amounts (ng) measured in homogenized cell-seeded collagen hydrogel constructs incorporating heparin-agarose beads (values are endostatin amounts in ng; n = 3).

Time, days	pEndo Lipoplex			
	No Crosslinker, No Beads	0.25 mM GP, No Beads	0.25 mM GP, Control Beads	0.25 mM GP, Heparin Beads
1	0.19 ± 0.008	0.36 ± 0.039	0.27 ± 0.048	0.1 ± 0.003
7	0.06 ± 0.004	0.06 ± 0.008	0.3 ± 0.061	0.41 ± 0.049
21	0.11 ± 0.018	0.15 ± 0.023	0.11 ± 0.022	0.07 ± 0.021

4.3.2.3. Biochemical Analysis of DNA and GAG Content

An average of 0.4 million cells were measured in the constructs the day after seeding, suggesting that ~100% of the cells seeded in the hydrogels were retained in the constructs, as mentioned earlier (Figure 4.7). After one week, there was generally an increase in cell number, ranging from 0.4 to 0.9 million cells per construct (Figure 4.7). The highest cell numbers were seen in the 21-day constructs, with values ranging from 0.7 to 1.3 million cells per construct (Figure 4.7). Where n = 2, error bars were not calculated.

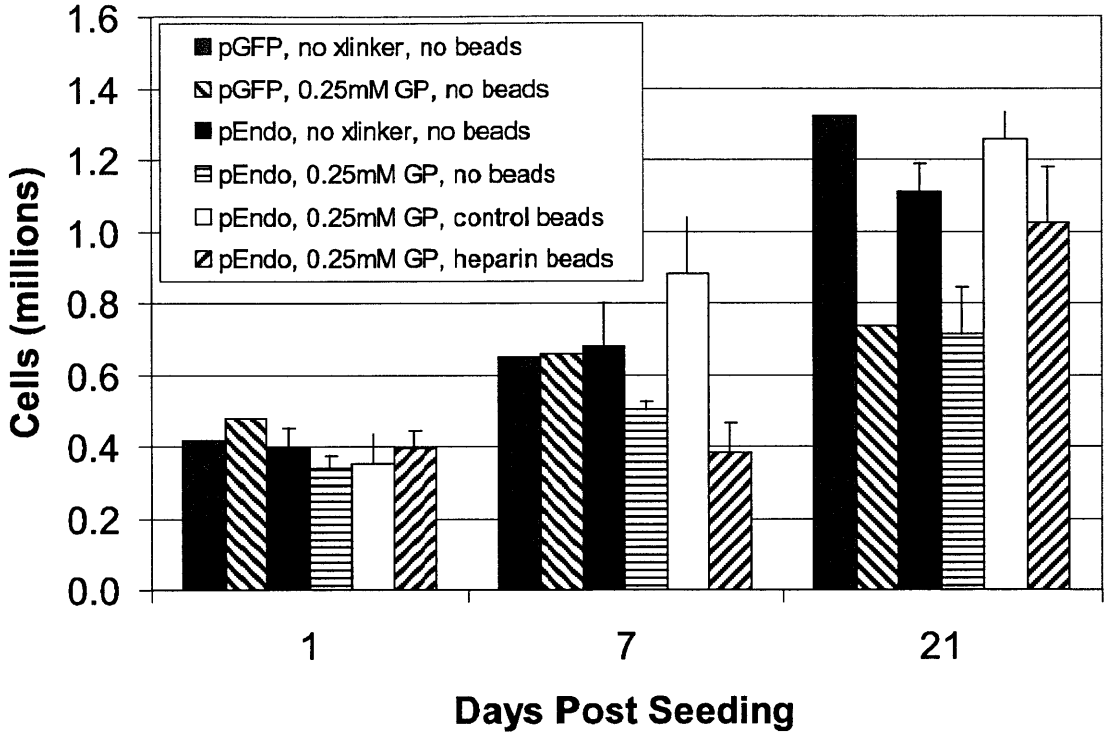

Figure 4.7 Biochemical analysis of MSC-seeded constructs. Cell numbers in the collagen hydrogel constructs incorporating heparin-agarose beads, estimated from the DNA content (n = 2-3).

Including all groups without beads, 3-factor ANOVA revealed significant effects of collection period ($p < 0.0001$, power = 1) and crosslinking agent ($p = 0.001$, power = 1) on cell number, but failed to find an effect of plasmid ($p = 0.1$, power = 0.36). Fisher's *post hoc* PLSD testing demonstrated a significant difference among all 3 days. Including all constructs seeded with genipin-crosslinked pEndo lipoplex-transfected cells, 2-factor ANOVA revealed significant effects of collection period ($p < 0.0001$, power = 1) and bead incorporation ($p = 0.003$, power = 0.93). Fisher's *post hoc* PLSD testing demonstrated a significant difference among all 3 days and between the control agarose bead group and the other 2 groups.

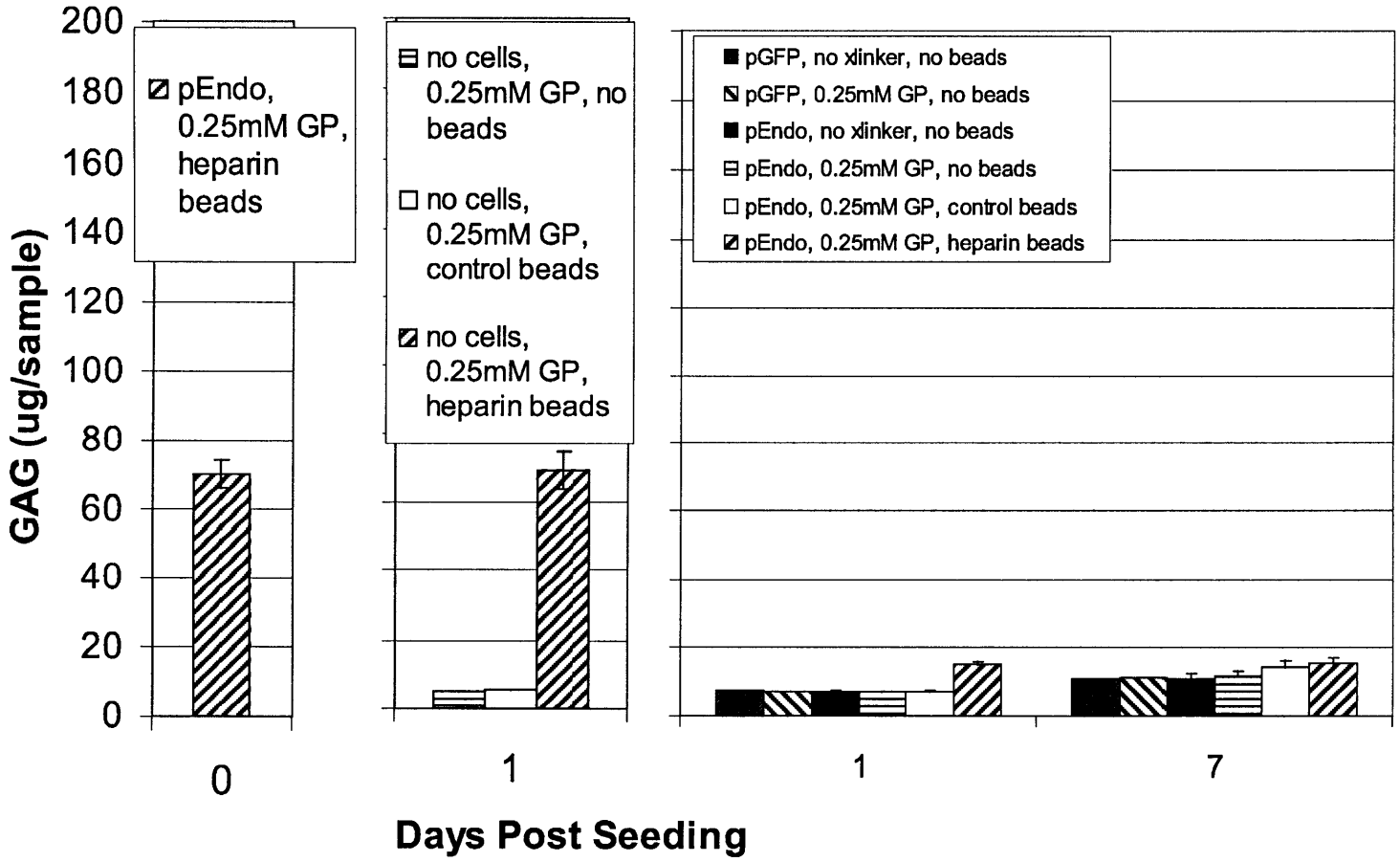

Figure 4.8 Biochemical analysis of MSC-seeded constructs (and non-cell-seeded controls, as indicated) during the first week of culture. Average GAG per construct for the collagen hydrogel constructs incorporating heparin-agarose beads (n = 5-6 for non-cell-seeded controls, n = 2-3 for all other samples).

One and seven days after seeding, little GAG (<15 μg per sample) was detected in all groups without heparin-agarose beads (Figure 4.8). For the heparin-agarose bead group, 70 μg of GAG was measured in the constructs immediately after cell seeding and gel casting, compared to the 100 μg of heparin added (Figure 4.8). After one day, the non-cell-seeded heparin-agarose group had 70 μg of GAG, while the cell-seeded heparin-agarose groups at days 1 and 7 had much smaller amounts of GAG, around 15 μg per construct (Figure 4.8). Where n = 2, error bars were not calculated.

For the 21 day constructs, the GAG density was reported as a percentage of that of native goat articular cartilage, based on average measured dimensions. All groups without beads showed notable GAG amounts, ranging from 50% to 120% of that of normal goat articular cartilage (Figure 4.9). The bead-incorporating groups showed very low percentages of GAG, less than 10% of normal cartilage (Figure 4.9). Where n = 2, error bars were not calculated.

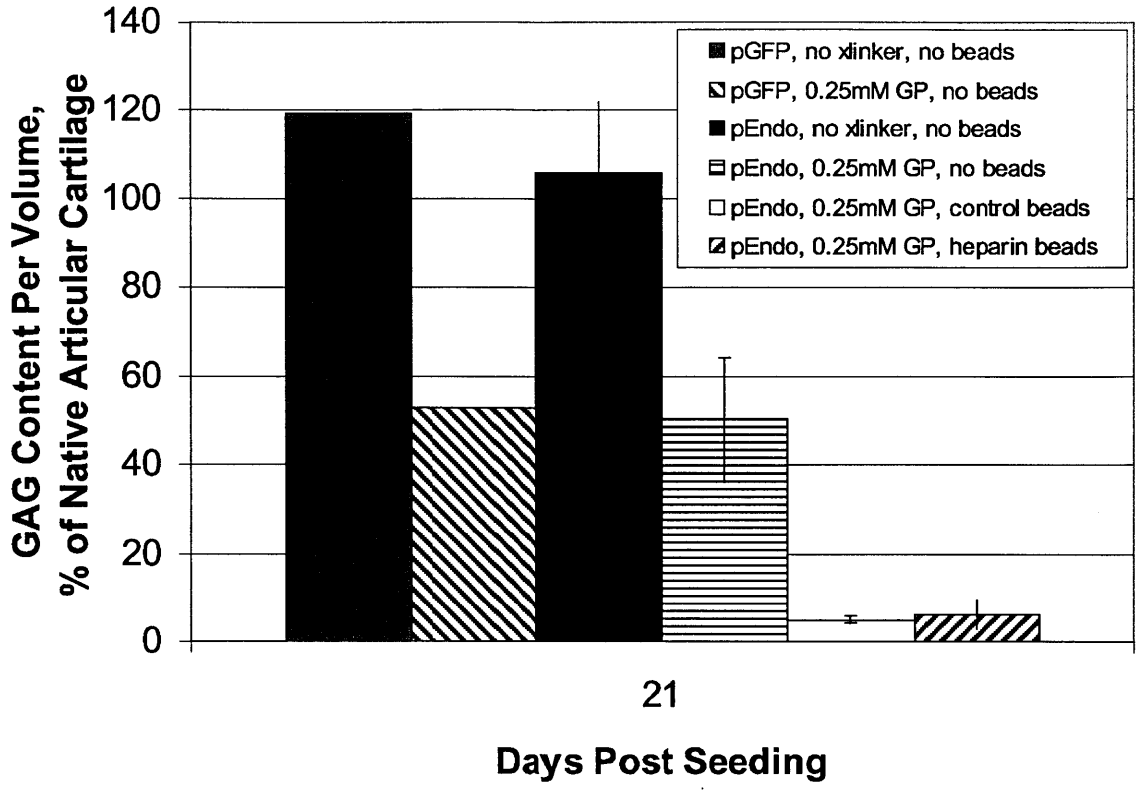

Figure 4.9 Biochemical analysis of MSC-seeded constructs after 21 days of culture. Percentage GAG content per volume compared to native articular cartilage for the collagen hydrogel constructs incorporating heparin-agarose beads (n = 2-3).

For the 21 day samples, including all cell-seeded groups without beads, 2-factor ANOVA revealed a significant effect of crosslinking agent ($p = 0.003$, power = 0.97) on GAG percentage, but failed to find an effect of plasmid ($p = 0.57$, power = 0.08). Including all genipin-crosslinked constructs seeded with pEndo lipoplex-transfected cells, 1-factor ANOVA revealed a significant effect of bead incorporation ($p = 0.014$, power = 0.86) on GAG percentage. Fisher's *post hoc* PLSD testing demonstrated a significant difference between the group with no beads and both other groups.

4.3.2.4. Histological/Immunohistochemical Evaluation of the Constructs

Immunohistochemical analysis for endostatin in the constructs revealed a few cells showing positive staining 1 day after seeding for all pEndo lipoplex-transfected groups (Figure 4.10a, b, and c). At day 7 after seeding, sparse positive staining was seen in the 2 bead-incorporating groups (Figure 4.10e and f), and by day 21, virtually no positive staining was noted (Figure 4.10g, h, and i). Cell aggregation was noted in the gels with no beads, as the cells went from being spaced apart 1 day after seeding (Figure 4.10a) to being closer in proximity by 1 week (Figure 4.10d and g). This phenomenon has also been reported with sponge-like scaffolds [190]. Cells in the bead-incorporating gels, on the other hand, remained spaced apart throughout the 3-week culture period (Figure 4.10b, c, e, f, h, and i).

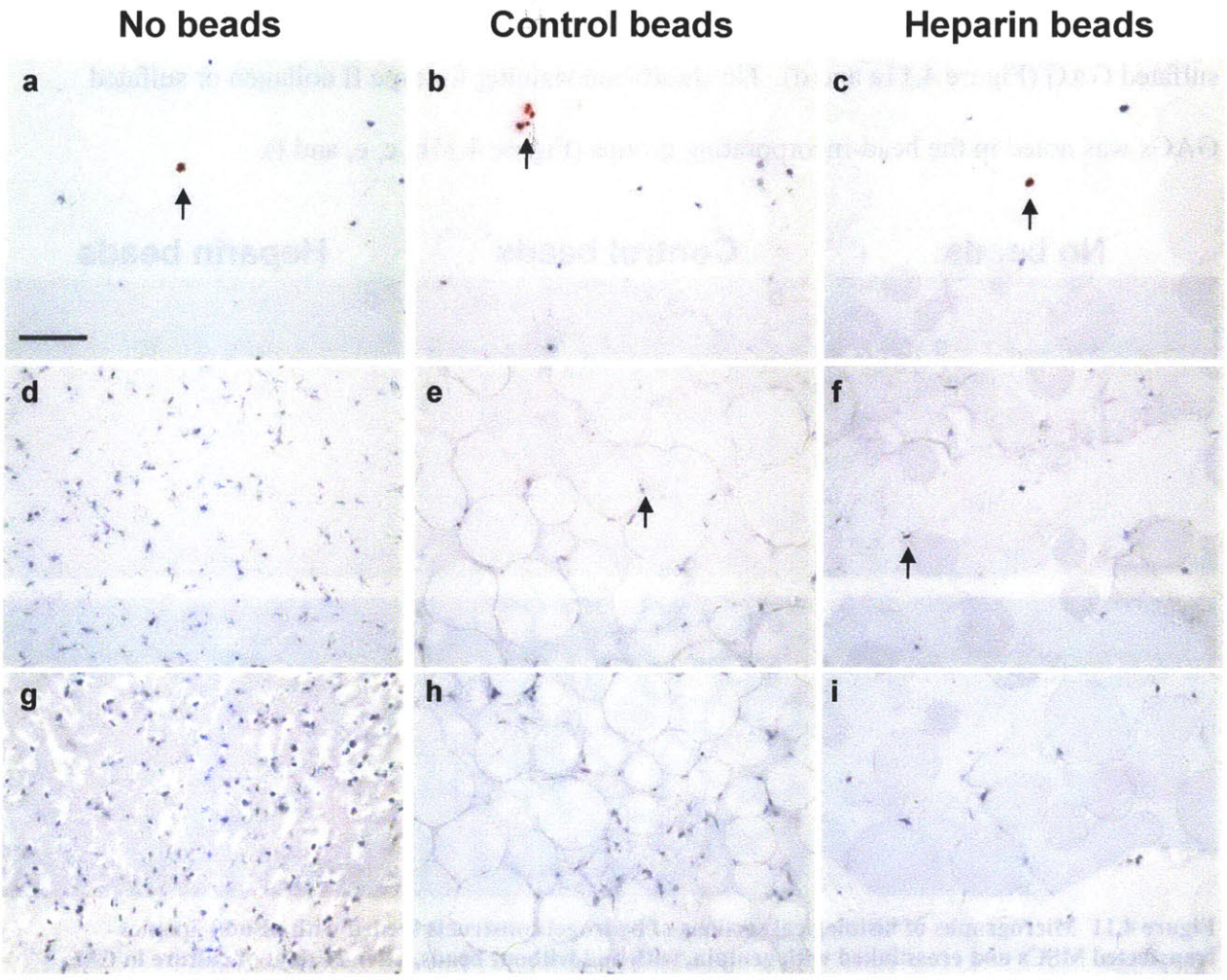

Figure 4.10 Endostatin immunohistochemistry (arrows, red chromogen) of hydrogel constructs seeded with pEndo lipoplex-transfected MSCs and crosslinked with genipin, with and without beads. Each image is represented at identical magnification; scale bar, 100 μm. Top row, 1 day after seeding; middle row, 7 days after seeding; bottom row, 21 days after seeding.

Positive staining for type II collagen and sulfated GAGs was seen in the non-bead-incorporating group at 21 days, near the periphery of the constructs for both molecules (Figure 4.11a and d). In the interior of the constructs, type II collagen was also observed in some areas of the interterritorial matrix within the construct (Figure 4.11a), while sulfated GAGs were found in the pericellular matrix surrounding the cells (Figure 4.11d). Similarly to the sponge-like scaffold constructs, a thin layer at the edge of the hydrogel constructs consisted of cells with an

elongated, fibroblast-like morphology, and this region did not stain for type II collagen or sulfated GAG (Figure 4.11a and d). No significant staining for type II collagen or sulfated GAGs was noted in the bead-incorporating groups (Figure 4.11b, c, e, and f).

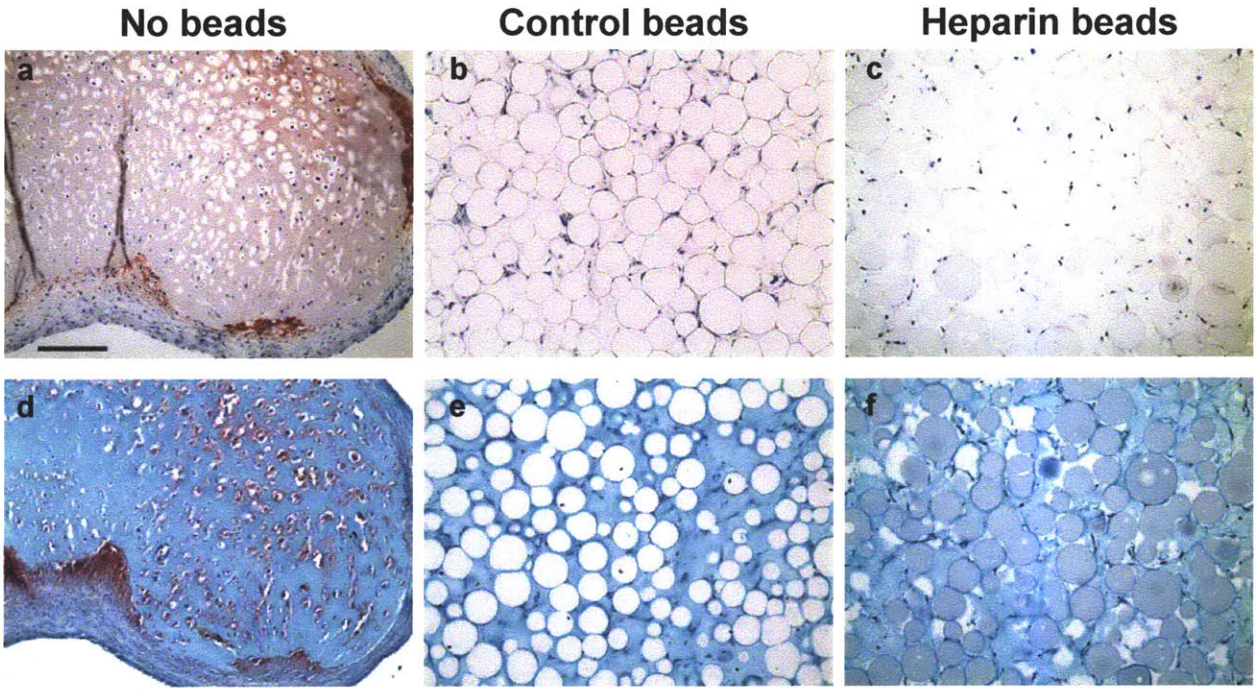

Figure 4.11 Micrographs of histological sections of hydrogel constructs seeded with pEndo lipoplex-transfected MSCs and crosslinked with genipin, with and without beads, after 21 days of culture in CM. Each image is represented at identical magnification; scale bar, 200 μm. Top row, type II collagen immunohistochemistry (brownish-red chromogen); bottom row, Safranin-O (red indicates sulfated GAGs).

Cells were distributed throughout the constructs of all groups (Figure 4.11); many of those in the group without beads appeared rounded and resided in lacunae (Figure 4.11a and d), whereas more elongated cells were frequently seen in both bead-incorporating groups (Figure 4.11b, c, e, and f). Beads were clearly visible throughout the 3-week culture period in both the control agarose and heparin-agarose groups (Figure 4.10b, c, e, f, h, i and Figure 4.11b, c, e, f).

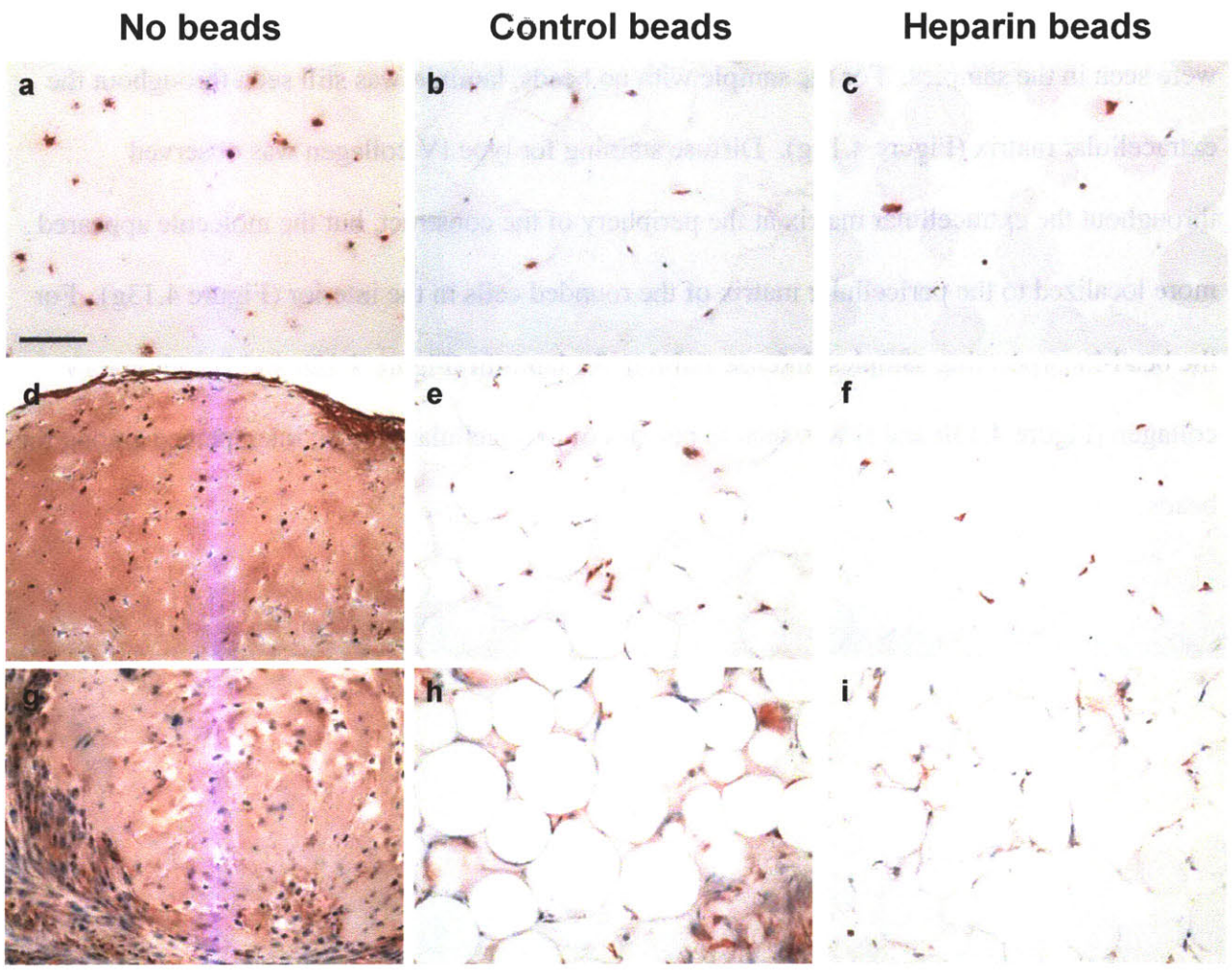

Figure 4.12 Laminin immunohistochemistry (red chromogen) of hydrogel constructs seeded with pEndo lipoplex-transfected MSCs and crosslinked with genipin, with and without beads. Each image is represented at identical magnification; scale bar, 100 μm. Top row, 1 day after seeding; middle row, 7 days after seeding; bottom row, 21 days after seeding.

Laminin (Figure 4.12) and type IV collagen (Figure 4.13) were observed in all samples throughout the 3-week culture period. One day after seeding, positive intracellular staining for both basement membrane molecules was noted in many of the cells in the constructs (Figure 4.12a, b, c and Figure 4.13a, b, c). After 1 week, type IV collagen was still restricted to the cells for all samples (Figure 4.13d, e, and f), and staining of the bead-incorporating constructs for laminin showed the same pattern (Figure 4.12e and f); however, remarkable staining for laminin throughout the extracellular matrix, as well as some intracellular staining, was noted for the

sample with no beads (Figure 4.12d). By 3 weeks, larger areas of laminin and type IV collagen were seen in the samples. For the sample with no beads, laminin was still seen throughout the extracellular matrix (Figure 4.12g). Diffuse staining for type IV collagen was observed throughout the extracellular matrix at the periphery of the construct, but the molecule appeared more localized to the pericellular matrix of the rounded cells in the interior (Figure 4.13g). For the bead-incorporating samples, intense staining for laminin (Figure 4.12h and i) and type IV collagen (Figure 4.13h and i) was seen in patches of extracellular matrix, interspersed among the beads.

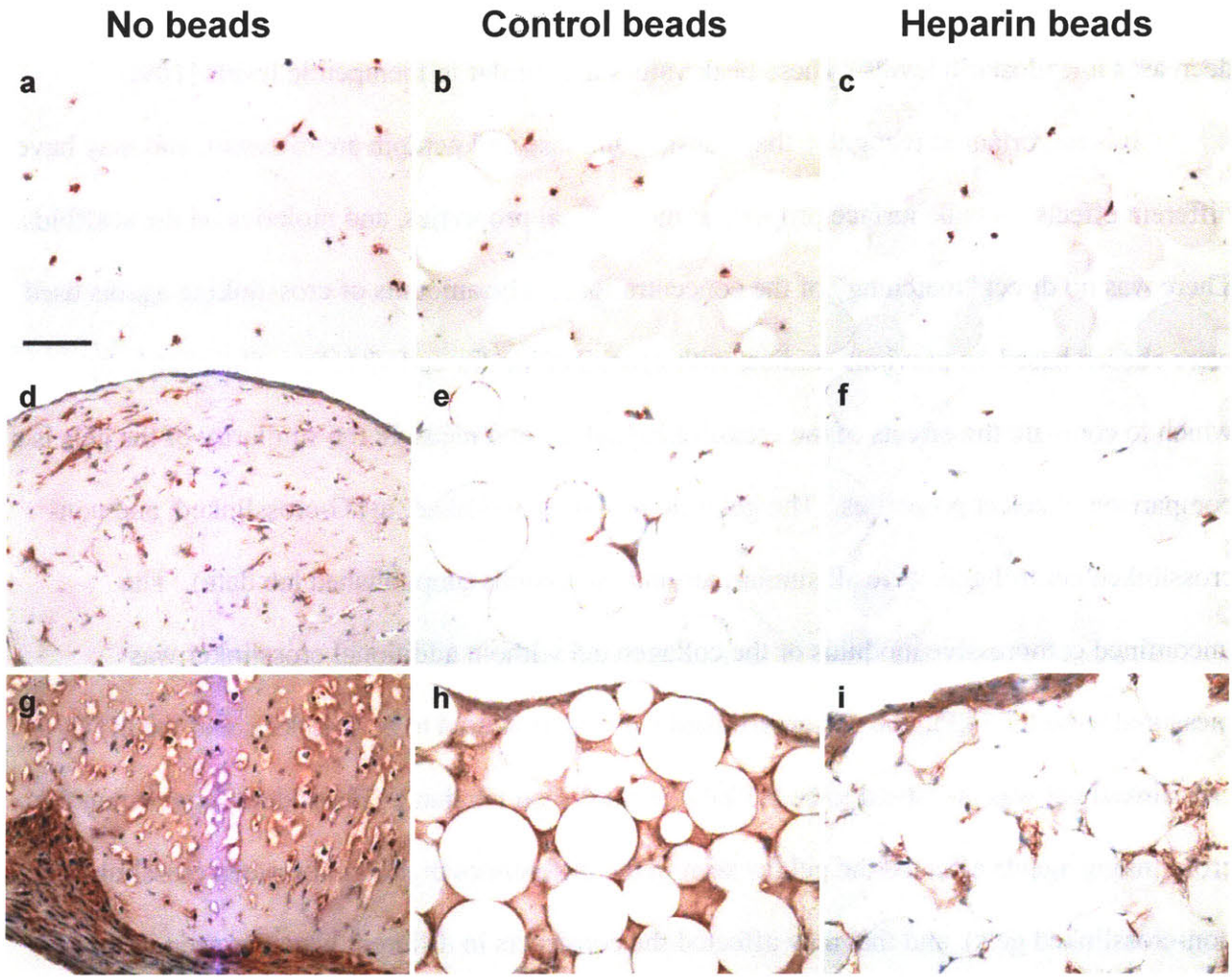

Figure 4.13 Type IV collagen immunohistochemistry (red chromogen) of hydrogel constructs seeded with pEndo lipoplex-transfected MSCs and crosslinked with genipin, with and without beads. Each image is represented at identical magnification; scale bar, 100 μm. Top row, 1 day after seeding; middle row, 7 days after seeding; bottom row, 21 days after seeding.

4.4. Discussion

In this study, we engineered endostatin-expressing cartilaginous constructs *in vitro* using hydrogels covalently crosslinked with transglutaminase-2, microbial transglutaminase, and genipin. Only a small amount of pEndo (5 μg of plasmid per 1 million cells) was used, for safety considerations. General trends in the expression profiles of the expended medium were similar among the different groups, and similar to those seen with sponge-like scaffolds. Peak values

(ranging from 7 to 18 ng/ml) occurred during the first few collection periods, followed by decreases in endostatin levels. These peak values are similar to therapeutic levels [109].

It is important to recognize that transglutaminase and genipin are different, and may have different effects on bulk/surface properties, mechanical properties, and moieties on the scaffolds. There was no direct "matching" of the concentrations. The amounts of crosslinking agents used were chosen based on previous studies, with consideration for cell viability. One metric by which to compare the effects of the crosslinking agents and measure the similarity of the gels is a comparison of select properties. The gel time for GP-crosslinked, mTG-crosslinked, and non-crosslinked control gels were all similar, around 50 seconds (unpublished lab data). The unconfined compressive modulus of the collagen gel without additional crosslinker was measured to be 0.25 kPa, the GP-crosslinked gel was measured to be 0.45 kPa, and the mTG-crosslinked gel was measured to be 0.5 kPa (unpublished lab data). These data suggest that the crosslinking agents affected the gel (as seen in the differences in moduli between crosslinked and non-crosslinked gels), and that they affected the constructs in different ways (as seen in the differences in moduli between different crosslinking agents). The differences among the unconfined compressive modulus values are small compared to that of native articular cartilage, reported to be 314 kPa [185].

Much higher endostatin amounts were detected in the expended media than in the homogenized constructs, and little staining for endostatin was seen in the constructs, suggesting that not much of the protein was retained in the engineered constructs. Of note is the observation that the covalently-crosslinked hydrogels did not appear to impede movement of the protein through the scaffold, as notable levels of endostatin were detected in the expended medium. The measured endostatin protein levels in the homogenized constructs were near the lower limit of

detection of the ELISA assay. It is possible that these measurements represent the endostatin protein that was recently produced by the cells and had not yet diffused out of the constructs. It is not entirely clear why differences in endostatin amounts within the constructs were observed among the different groups. In the first experiment, it is possible that residual amounts of TG-2, which has been shown to have one of the strongest binding affinities with endostatin, remained in the constructs and bound to endostatin, contributing to the higher protein levels measured in the constructs at 21 days. In the second experiment, it is possible that residual amounts of GP remained in the construct and crosslinked small amounts of endostatin to the construct, resulting in the higher protein levels compared to the group with no additional crosslinking agent. Biological variation may have also contributed to the observed differences.

In experiment #1, the crosslinking agents affected the endostatin levels in the expended medium, with 0.25 mM GP resulting in the highest cumulative endostatin, and 100 μg/ml mTG resulting in the lowest. This finding suggests that crosslinking agents may affect the development of endostatin-producing constructs. One study demonstrated that GP can directly alter cell metabolism, including inhibition of TGF-β-induced Smad and p38 mitogen-activated protein kinase (MAPK) signaling [217]. Another study, which found that GP added as a medium supplement during *in vitro* culture of chondrocyte-seeded agarose gels resulted in enhanced mechanical properties of the engineered cartilage and protected against interleukin-1α-induced degradation, hypothesized that these were indirect effects, due primarily to modulation of the nature of ECM deposition and not to direct alterations of the cell [218]. In this study, it is unknown if the crosslinking agents, including GP, TG-2, and mTG, had a direct or indirect effect on MSC behavior (*i.e.* endostatin production); for example, it is possible that the crosslinking

agents had an indirect effect on cell behavior, through change in the mechanical stiffness of the scaffolds [191, 192].

The MSC-seeded constructs demonstrated the capacity to undergo chondrogenic differentiation, as indicated by the increase in GAG for all groups over the 3-week culture period. This is in agreement with other studies demonstrating chondrogenesis in gels crosslinked using transglutaminase [210] and GP [218, 219]. Qualitatively, there were areas in the constructs that showed signs of chondrogenesis (positive staining for type II collagen and sulfated GAGs and chondrocyte morphology). Quantitatively, genipin did not promote chondrogenesis, compared to noncrosslinked controls in experiment #2. Dare *et al.* [219] and Lima *et al.* [218] failed to find notable increases in matrix molecule content (GAG and collagen) in GP-crosslinked chondrocyte-seeded constructs compared to controls, suggesting that GP does not stimulate chondrogenesis. In experiment #1 of this study, GP-crosslinked constructs were found to have a higher percentage of sulfated GAGs compared to the transglutaminase-crosslinked constructs.

The cell numbers at 3 weeks were comparable for all groups and were increased compared to the initial seeding density, indicating that the cells were undergoing proliferation. At 3 weeks, genipin-crosslinked groups did not have notably higher cell numbers than the non-crosslinked controls in experiment #2, suggesting that genipin did not stimulate proliferation, similar to what other studies have reported. Dare *et al.* observed that GP-crosslinked fibrin gels did not stimulate human articular chondrocyte proliferation compared to control gels without additional crosslinking [219]. Lima *et al.* also found that GP supplementation did not stimulate proliferation of bovine chondrocytes [218]. Kitano *et al.* found that genipin did not stimulate cell proliferation in subconjuctival fibroblasts [226] and the α-TN4 lens epithelial cell line [217].

In experiment #1 of this study, no single crosslinking agent stimulated goat MSC proliferation compared to the others.

We report on the distribution of 2 common basement membrane molecules, laminin and type IV collagen, in engineered cartilaginous constructs. The diffuse staining pattern seen in this study is different than the localized pericellular matrix staining that has previously been reported in normal articular cartilage [8], demonstrating that the constructs being engineered *in vitro* are not the same as normal cartilage. However, the staining pattern seen here is reminiscent of those seen in cartilage development and disease. Diffuse generalized staining for many basement membrane molecules, including laminin, type IV collagen, and perlecan, has been reported throughout the extracellular matrix during knee joint maturation, with no apparent organization of the molecules in the pericellular matrix [8, 13]. Staining for perlecan in osteoarthritic cartilage is also not localized to the pericellular matrix, and has been reported in the interterritorial matrix [227]. This discovery may provide insight into the development of tissue engineered constructs.

Hydrogels incorporating heparin-agarose beads were successfully cast, and analysis of the immobilized heparin content revealed that the majority of the heparin that was added was present in the gels. However, the addition of heparin did not have a beneficial effect on endostatin retention in the hydrogels. Much higher endostatin amounts were detected in the expended media than in the homogenized constructs, and little staining for endostatin was seen in the constructs, suggesting that little endostatin was retained in the engineered constructs. Biochemical analysis of the gels indicated that when cells were also added into the hydrogel constructs, the amount of heparin drastically decreased even though the beads were still present. The addition of cells genetically modified to deliver protein, rather than direct delivery of the

protein in conventional protein retention studies, added to the complexity of the system and may have contributed to the decrease in GAG levels after cell seeding. It is possible that the cells may have internalized the heparin or released molecules that degraded the heparin; for example, heparin has been found to be endocytosed by the hyaluronic acid receptor for endocytosis (HARE), found in several cell types [228], and heparin can be degraded by nitric oxide, which has been shown to be produced by MSCs [229, 230].

GAG supplementation in the second experiment did not have a beneficial effect on chondrogenesis. This was likely due to the lack of retention of heparin following cell seeding. The incorporation of nondegradable agarose beads may have also contributed to an inhibition of chondrogenesis. Previous work suggests that cell-mediated contraction/aggregation promotes chondrogenesis [190]. These interactions are reminiscent of the precartilage condensation process during embryonic development [231]. In this study, the beads may have acted as a physical barrier and hindered the ability of the cells to contract and aggregate, resulting in inhibition of chondrogenesis.

Nonviral gene therapy techniques have already been shown to result in locally sustained levels of protein, as evidenced in this thesis as well as in the literature [131, 160, 224]. We employed retention techniques to attempt to gain additional control of the availability of the endostatin but were unsuccessful, likely due in part to the additional complexities introduced through the use of cells. While the heparin-agarose bead-incorporating constructs in this study did not aid in endostatin retention using engineered MSCs, the heparin-agarose bead-incorporating gels could be of potential benefit for other retention applications using direct delivery of the proteins.

In this study, we engineered endostatin-producing cartilaginous constructs using covalently-crosslinked hydrogels, demonstrating that gels are a feasible scaffold option. Of the conditions tested, 0.25 mM GP yielded the best results; however, TG-2 and mTG should be not ruled out as alternative crosslinking agents, as they also resulted in cartilaginous constructs overexpressing endostatin protein. Future work is needed for a comprehensive comparison of the various crosslinking agents, using a range of concentrations for each agent. Also, given TG-2's high binding affinity with endostatin, it may be of interest to determine a method to retain the TG-2 in the constructs in future studies, to serve as a method of binding endostatin. The addition of heparin-agarose beads did not have beneficial effects on endostatin production and retention or chondrogenesis. These gel-based constructs will be of value for future *in vivo* work investigating the use of endostatin for cartilage repair.

CHAPTER 5: EVALUATION OF AN *IN VIVO* CARTILAGE DEFECT MODEL, FOR FUTURE IMPLANTATION OF ENDOSTATIN-EXPRESSING CONSTRUCTS

PART 1: LONG-TERM JOINT IMMOBILIZATION WITH INTERMITTENT PASSIVE MOTION EXERCISE

5.1. Introduction

The rehabilitation protocol following surgical treatment of chondral defects in the knee is important, as it can affect the cartilage repair process and the retention of reparative tissue or implanted constructs in a defect site.

Historically, long-term rigid immobilization was the standard. One benefit was that it minimized the dislodgment of potential tissue filling the defect site. However, studies have found notable cartilage degeneration and necrosis, osteophyte formation, and decreases in water and glycosaminoglycans (GAGs), generally after about 6-9 weeks of rigid immobilization [232-234]. Previous work has also shown random collagen fiber growth and an increase in collagen crosslinks following immobilization, resulting in random points of fixation, increased joint stiffness, and loss of range of motion (ROM) [235].

To attempt to overcome the negative effects observed with long-term rigid immobilization, the application of movement early after surgery, in a controlled fashion, has been implemented. Currently in the clinical setting, continuous passive motion (CPM), a procedure in which an external motorized apparatus moves the joint, providing passive exercise, and physiotherapy, including ROM and muscle strengthening exercises, are frequently initiated immediately following total knee arthroplasty [236, 237]. Early mobilization has been shown to result in a decrease in joint stiffness and the need for pain medication, and an increase in ROM of the joint, particularly flexion [237]. Various modified versions of clinical post-operative treatment have been utilized in animal studies. Custom-designed devices are often assembled—

some apply movement to the limb [236, 238, 239], while other devices are designed to rigidly immobilize the joint [240, 241].

Goats are an attractive animal model for articular cartilage repair studies for reasons of articular cartilage thickness (approximately 1-2 mm), which more closely approaches the thickness found in humans than that of smaller laboratory animal models, such as rabbits (typically < 0.5 mm), and the loading of the joint [242]. Recent work using goats has demonstrated the value of the animal model for investigating the healing of osteochondral defects [243] and the retention of periosteal flaps for autologous chondrocyte implantation [244]. Other work has used goats for the assessment of donor cell and matrix survival in fresh articular cartilage allografts [245], the resurfacing of articular cartilage by chondrocytes derived from bone marrow [246], biodegradable implants for the treatment of osteochondral defects [247], and repair of cartilage lesions using selected biological implants [248].

In this study, we evaluated the effects of long-term rigid immobilization of the joint using an external fixation device, with removal of the device every 1-2 weeks to allow for intermittent manual passive motion exercises, following microfracture treatment of chondral defects in the goat knee. This rehabilitation protocol was adapted from the clinical setting. The goal of this study was to investigate the effects of the post-surgical rehabilitation protocol on the cartilage repair process.

5.2. Materials and Methods

5.2.1. Animal Model

Four skeletally mature female goats (ages 2 to 5 years) were used in this study. The animal experiment was approved by the Veterans Administration Animal Care Committee. All implantations were performed on the right knee of the animal under general anesthesia and using sterile conditions. The joint was opened by an anteromedial approach, and the patella was displaced laterally to expose the trochlea. Two 4-mm chondral defects were created in the trochlear groove as previously described [241]. The two defects were located approximately 1 and 2 cm proximal to the intercondylar notch, slightly lateral or medial to the midline. A dermal punch was used to create the outline of the defects. All noncalcified cartilage was removed from the defects by lightly scraping the calcified cartilage surface using a curet, with the aid of loupe visualization.

Microfracture was performed by forcing the straight pointed end of a microsurgical pick into the subchondral bone with a twisting motion. Six equally spaced penetrations, each approximately 1 mm in diameter, were made in each defect. Before closing the joint capsule, bleeding vessels were clamped and cauterized. The knee joint was closed by zero point suturing.

The knee was immobilized by external fixation (IMEX Veterinary, Longview, TX) (Figure 5.1) until sacrifice. Pins, 2 in the femur and 2 in the tibia, were inserted through the skin and into the bone. Bars parallel to the femur and tibia were secured to the pins, and then 2 other bars, parallel to each other, were put in place to rigidly fix the joint. Under anesthesia, the 2 bars parallel to each other were removed once every 1-2 weeks, followed by 20 minutes of manual passive motion exercise. Minor bleeding and skin wounds observed following exercise were treated.

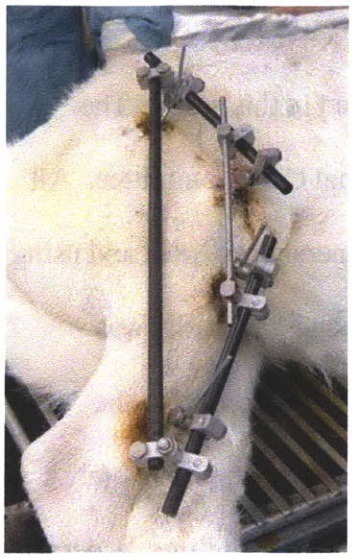

Figure 5.1 Photograph of immobilized joint with external fixation device.

5.2.2. Histological and Immunohistochemical Evaluation

At necropsy, *in vivo* defects were removed from the joints, fixed in 10% formalin, and decalcified using ethylenediamine tetraacetic acid (EDTA). All samples were processed and embedded in paraffin, and sectioned by microtomy. The sections were mounted on glass slides and stained with hematoxylin and eosin (H&E) and Safranin-O using standard histological techniques.

Select sections underwent immunohistochemical staining. Types I and II collagen distribution were examined immunohistochemically using an anti-type I collagen mouse monoclonal antibody (I-8H5 CP17, final concentration of 5 μg/ml, Calbiochem, Gibbstown, NJ, USA) and an anti-type II collagen mouse monoclonal antibody (CIIC1, final concentration 4 μg/ml, Developmental Studies Hybridoma Bank, University of Iowa, Iowa City, IA, USA). Staining for lubricin was done using anti-lubricin mouse monoclonal antibody (S.679, final concentration 4.6 μg/ml, Dr. T. Schmid, Rush University Medical Center, Chicago, Illinois). Distribution of von Willebrand factor (vWF) and CD31, common markers for endothelial cells,

was examined using an anti-vWF rabbit polyclonal antibody (final concentration 16.5 μg/ml, Dako, Carpinteria, CA, USA) and an anti-CD31 rabbit polyclonal (final concentration 21 μg/ml, Abcam, Cambridge, MA, USA). Laminin and type IV collagen, common basement membrane molecules, were also examined immunohistochemically, using an anti-laminin rabbit polyclonal antibody (final concentration 27 μg/ml, Abcam) and an anti-type IV collagen rabbit polyclonal antibody (final concentration 17 μg/ml, Abcam). All staining was performed using the Dako Autostainer (Dako) and the peroxidase-aminoethyl carbazole (AEC)-based Envision+ kit (Dako) following the manufacturer's recommendations.

5.2.3. Histomorphometry

Histomorphometric analysis of specific tissue types filling the defect was carried out on one H&E-stained section from the center portion of each defect. Previous work found that the inter-observer error associated with this quantitative histological method was generally less than the inter-animal variation in the results[249]. Digital micrographs were taken of the defect and surrounding tissues. The total cross-sectional area of the original defect and the percentages of fibrous tissue, fibrocartilage, and hyaline cartilage filling the original defect were measured using ImageJ software (NIH, Bethesda, MD). Tissue types were classified according to textbook appearance of cell morphology and extracellular matrix structure as previously described[241]. In many of the samples, surrounding tissue "flowed" into the peripheral areas of the defect. These regions were classified separately as matrix flow. The percentage of bone ingrowth into the defect sites was also evaluated. When the percentages do not add up to 100%, it is due to rounding of values.

5.2.4. Quantitative Evaluation of Tissue Bonding

The linear percentages of the base of the defect to which the healing tissue was bonded and of the height of the edges of the repair tissue on the left and right sides of the defect that were bonded to the adjacent cartilage were determined.

5.2.5. Statistical Analysis

Data are presented as the mean ± standard error of the mean (SEM). Contingency tables and analysis of variance (ANOVA) were performed using StatView software (SAS Institute Inc, Cary, NC, USA). Statistical significance was set at $p < 0.05$.

5.3. Results

5.3.1. General Gross Evaluations

One animal died at 2 weeks, before reaching the proscribed sacrifice time of 6 weeks, unrelated to the cartilage repair; the other 3 animals went to term (Table 5.1).

Table 5.1 Gross findings at necropsy.

Goat #	Duration, wks	Jt. Condition at Sacrifice*
203	2	Normal
197	6	Degenerative
205[1]	6	Degenerative
206	6	Degenerative

[1] Infection at proximal pin on femur
* $p < 0.05$

During the first 2 weeks after surgery, no significant stiffness was noted during passive motion exercise. Beginning 3-4 weeks post-surgery and at subsequent weeks, initial stiffness during flexion was observed to varying degrees, ranging from slight loss of range of motion to complete inability to flex the knee joint. In cases of slight stiffness, normal range of motion was regained after a few times of normally moving the knee back and forth, so that the stiffness was no longer noticeable; in the case of complete loss of range of motion, the joint had to be strongly forced to flex, and cracking within the joint could be heard, likely the breaking of newly-formed collagen crosslinks [235].

Occasional pin loosening, bending, or breakage was noted. Occasional minor bleeding was sometimes seen around the pins securing the external fixation device to the leg, at the surface of the skin, following passive motion exercise, likely due to movement of the skin around the pin during exercise. A skin infection was noted at the proximal pin on the femur, at the skin surface 5 weeks post-surgery for one of the goats, and remained until sacrifice (Table 5.1). No other infection was noted.

At the time of sacrifice, the immobilized joint of the 2-week animal appeared normal (Figure 5.2a), and the immobilized joints of all 6-week animals showed significant signs of degeneration (Figure 5.2b), characterized by areas of articular cartilage loss, ingrowth of the surrounding synovial tissue into the joint space, fibrous adhesions, and discoloration (Table 5.1). Contingency tables of necropsy findings revealed a significant difference in joint condition between 2 weeks and 6 weeks (chi square $p = 0.046$). At 2 weeks, the defect was clearly distinguishable from the surrounding tissue, and there was almost no reparative tissue in the defect (Figure 5.2a). At 6 weeks, there was more tissue compared to 2 weeks, but still incomplete filling of the defects (Figure 5.2b).

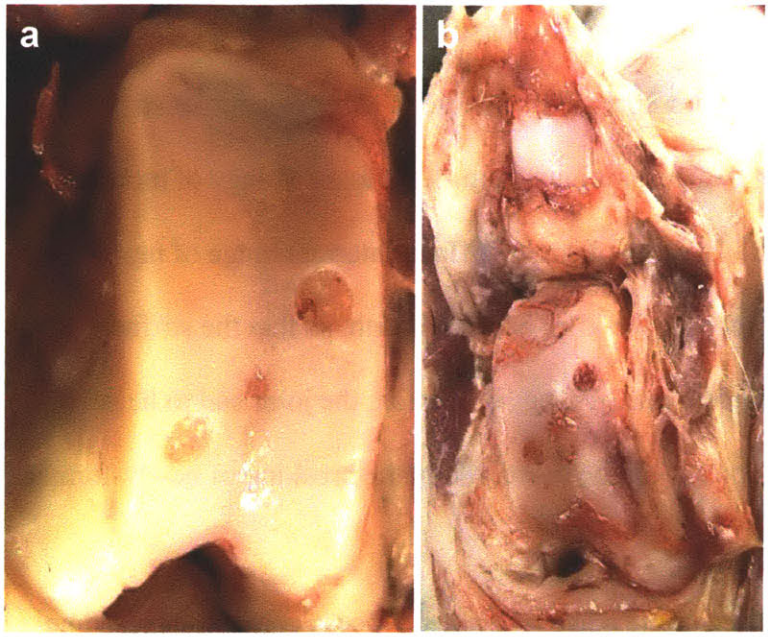

Figure 5.2 Photographs of joints immediately after sacrifice; (a) two-week survival period and (b) six-week survival period.

5.3.2. Histological and Immunohistochemical Evaluation

Most of the defect sites (7 of 8 defects) had clearly defined boundaries when viewed microscopically, and the reparative tissue was easily distinguishable from the surrounding articular cartilage and underlying bone (Figure 5.3a). The sample in which the defect site was not distinguishable was collected at 6 weeks. Degeneration of the cartilage around the defect confounded histomorphometry, and this sample was thus excluded from histomorphometric analysis. Some bonding was observed between the reparative tissue and the surrounding host tissue, but notable gaps were also noted (Figure 5.3a). The extracellular matrix of the tissue filling the defect sites had a distinct fibrous appearance (Figure 5.3b), and the surface often appeared uneven and fibrillated (Figure 5.3b), with small fragments (Figure 5.3c) and fissures (Figure 5.3d) present.

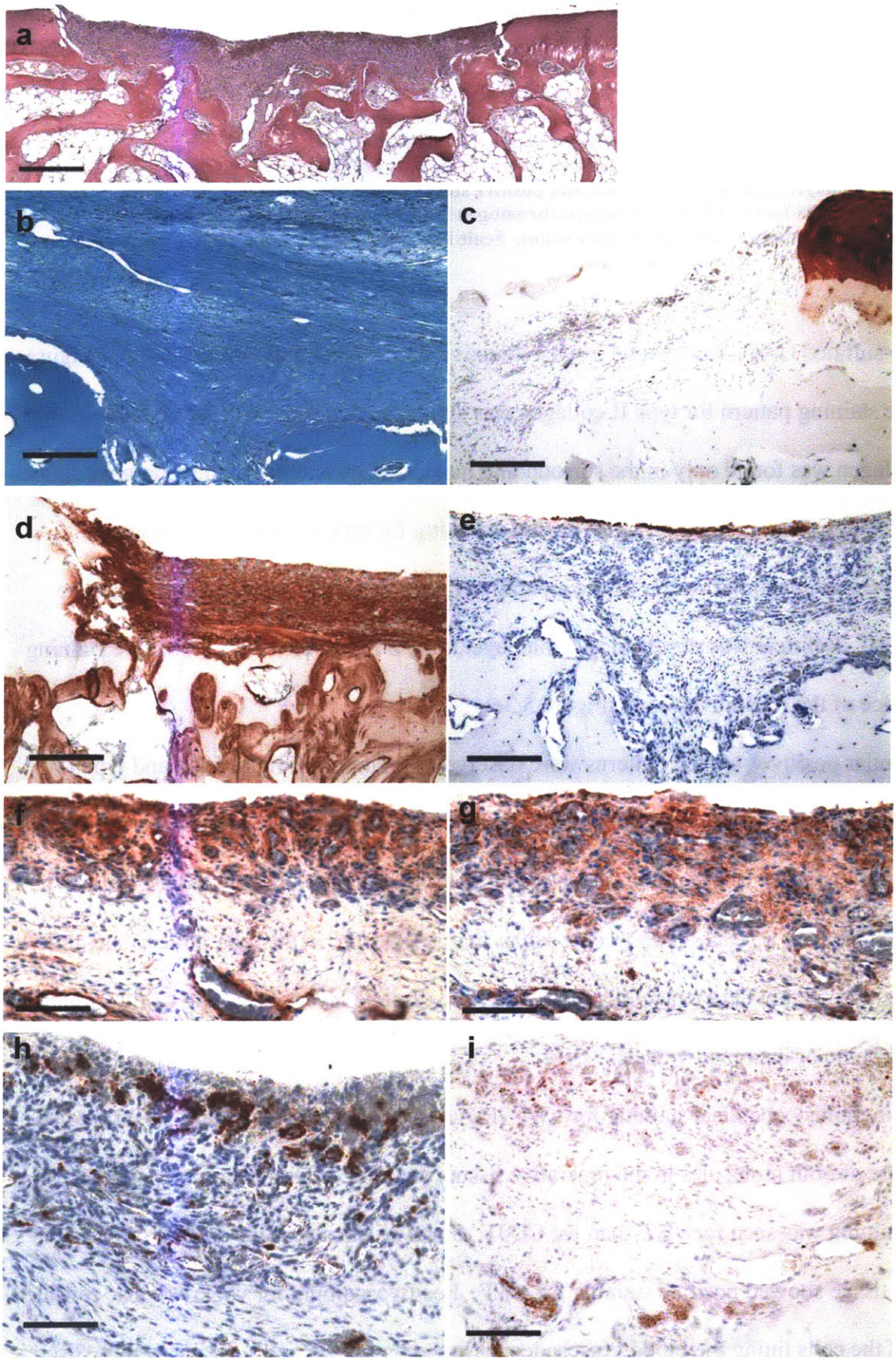
a
b
c
d
e
f
g
h
i

Figure 5.3 Micrographs of *in vivo* reparative tissues, after 6 weeks.

a. H&E. Scale bar, 500 μm.
b. Safranin-O (red chromogen indicates sulfated GAGs). Scale bar, 200 μm.
c. Type II collagen (red chromogen indicates positive stain). Scale bar, 200 μm.
d. Type I collagen (red chromogen indicates positive stain). Scale bar, 200 μm.
e. Lubricin (red chromogen indicates positive stain). Scale bar, 200 μm.
f. Laminin (red chromogen indicates positive stain). Scale bar, 100 μm.
g. Type IV collagen (red chromogen indicates positive stain). Scale bar, 100 μm.
h. von Willebrand factor (vWF) (red-brown chromogen indicates positive stain). Scale bar, 100 μm.
i. CD31 (red chromogen indicates positive stain). Scale bar, 100 μm.

No sulfated GAGs were found in the reparative tissue using Safranin-O staining (Figure 5.3b). The staining pattern for type II collagen was similar to that seen with Safranin-O, in that type II collagen was found only in the surrounding host cartilage and not in the reparative tissues filling the defects (Figure 5.3c). Intense positive staining for type I collagen was seen throughout the extracellular matrix of the reparative tissue, as well as in the underlying bone (Figure 5.3d). Lubricin was observed as a thin layer, only a few cells thick, of positive staining at the surface of the reparative tissue (Figure 5.3e).

Similar positive staining patterns were observed for laminin (Figure 5.3f) and type IV collagen (Figure 5.3g) in the reparative tissue. Interestingly, staining was noted near the surface of the reparative tissue, to a depth of 100-200 μm, not only lining the blood vessels, but also as a diffuse positive stain throughout the extracellular matrix. Deeper in the reparative tissue, little to no staining was seen in the extracellular matrix; a thin, discrete layer of staining could still be seen lining some of the blood vessels.

Immunohistochemical staining for vWF (Figure 5.3h) and CD31 (Figure 5.3i) revealed the presence of both molecules in the reparative tissue, but with different staining patterns. More positive staining was seen for vWF than for CD31. Small clusters near the surface of the reparative tissue showed positive staining for vWF. Positive staining for vWF was also revealed in some of the cells lining the blood vessels deeper in the tissue, generally seen as a thin, discrete

layer. Only a few cells lining some of the blood vessels, generally near the surface, showed positive staining for CD31.

5.3.3. Histomorphometric Evaluation of Reparative Tissue

At 2 weeks post-surgery, 17 ± 3% of the defect cross-sectional area was filled with reparative tissue, of which the majority was fibrous tissue (Table 5.2). No hyaline cartilage or fibrocartilage was seen. By 6 weeks, the amount of reparative tissue filling the defect increased to 70 ± 7% (Table 5.2). The majority of the reparative tissue was still fibrous tissue; small amounts of hyaline cartilage (1 ± 1%) and fibrocartilage (7 ± 7%) were observed (Table 5.2). Slight bone ingrowth (5 ± 4%) was also noted at 6 weeks (Table 5.2).

Table 5.2 Histomorphometry results. Values reported as percentage of defect cross-sectional area.

Survival Time, wks	Hyaline Cartilage	Fibro-cartilage	Fibrous Tissue	Matrix Flow	Bone Ingrowth	Total Fill
2 (n = 2*)	0 ± 0	0 ± 0	14 ± 4	3 ± 1	0 ± 0	17 ± 3
6 (n = 5)	1 ± 1	7 ± 7	52 ± 6	5 ± 1	5 ± 4	70 ± 7

* n, number of defects

Two-factor ANOVA indicated a significant effect of survival time on total fill ($p = 0.027$, power = 0.764), but failed to find a significant effect on the amount of hyaline cartilage ($p = 0.703$, power = 0.061), fibrocartilage ($p = 0.703$, power = 0.061), fibrous tissue ($p = 0.067$, power = 0.485), matrix flow ($p = 0.652$, power = 0.065), or bone ingrowth ($p = 0.0567$, power = 0.075). ANOVA also failed to find a significant effect of defect location on any of the outcome variables ($p >> 0.05$), suggesting that each of the defect sites could be treated as an independent sample.

5.3.4. Quantitative Evaluation of the Bonding of the Reparative Tissue to the Adjacent Tissue

Bonding between the reparative tissue and the surrounding host tissue was observed (Table 5.3). At 2 and 6 weeks post-surgery, about half of the reparative tissue was bonded to the underlying subchondral bone. At 2 weeks post-surgery, over 70% of the reparative tissue was bonded to the adjacent cartilage, whereas 45-72% of the reparative tissue was bonded to the adjacent cartilage at 6 weeks.

Table 5.3 Bonding of reparative tissue. Values reported as percentage of defect cross-sectional area.

Survival Time, wks	Bonding of Height with Adjacent Cartilage (Left Side)*	Bonding of Height with Adjacent Cartilage (Right Side)*	Bonding of Base
2 (n = 2 defects)	78 ± 22	93 ± 7	52 ± 34
6 (n = 5 defects)	45 ± 20	72 ± 20	51 ± 15

* Height of repair tissue in apposition with adjacent cartilage divided by total height of repair tissue

5.4. Discussion

Significant joint degeneration, including areas of articular cartilage loss, ingrowth of the surrounding synovial tissue into the joint space, fibrous adhesions, and discoloration, was observed in this study. Previous work in our lab using the same external fixation device for a short-term period (10 days) in a canine model of cartilage repair, some of which were treated using microfracture, followed by normal ambulation until sacrifice have generally reported little degeneration of the surrounding joint [38, 43, 44, 241, 249]. In contrast, negative effects of long-term post-operative immobilization have been previously reported in other animal studies [232-235], suggesting that the long-term joint immobilization protocol in this study likely

resulted in the joint degeneration seen. Even though 20 minutes of periodic passive motion exercise was manually carried out every 1-2 weeks following removal of the parallel bars of the external fixation device in this study, the passive motion exercise did not appear to have been enough to overcome the negative effects of immobilization.

While the results of this study suggest an increase in frequency and/or duration of the passive motion exercise for potentially decreasing cartilage degeneration, the possibility of infection must also be considered. The skin surrounding the external fixation device pins moved during exercise, resulting in bleeding and the formation of fresh open wounds at the surface of the skin, and creating opportunities for infection. In this study, infection was already noted in one of three 6-week animals. If more passive motion exercise were carried out, there would likely also be an undesirable increase in the likelihood of infection.

Even though the overall condition of the joints at 6 weeks showed severe degeneration, it should be noted that approximately 70% of the defect sites were filled with reparative tissue, and generally over half of the reparative tissue showed bonding with the surrounding host tissue. In a canine study of microfracture-treated chondral defects, 56 ± 12% of the defects were filled with reparative tissue 15 weeks post-operatively [44], compared to control data from another canine study showing only 41 ± 4.3% total fill 1.5 months after defect creation [249], suggesting that the microfracture treatment in this study is comparable with other findings following microfracture, and that the treatment still encouraged formation of new tissue compared to an untreated control.

The reparative tissue was composed largely of fibrous tissue, consistent with the positive staining seen for type I collagen; virtually no hyaline cartilage, consistent with the lack of staining for type II collagen and sulfated GAGs, was seen.

Laminin and type IV collagen are major constituents of basement membranes, including those found in blood vessels. Healthy articular cartilage is not normally thought of as having a traditional basement membrane, but studies have shown that many of the common basement membrane molecules are found in the pericellular matrix of chondrocytes, suggesting that the pericellular matrix may be a functional equivalent of the basement membrane in cartilage [7-10]. In this study, positive staining for laminin and type IV collagen was not localized to the pericellular matrix of the reparative tissue, but was instead seen near the surface as diffuse staining throughout the extracellular matrix of the tissue filling the defects. The differences in staining pattern for laminin and type IV collagen between normal articular cartilage and the reparative tissue seen here serves to further highlight that the tissue filling the defect sites in this study is histologically different from normal cartilage.

The staining pattern for lubricin seen in the reparative tissue in this study, as a thin layer at the articulating surface of the tissue, resembles that observed in normal articular cartilage [250], suggesting that other properties of the reparative tissue may be similar to normal cartilage. Similarly, a study examining the presence of lubricin in repair tissue filling chondral and osteochondral defects, following autologous chondrocyte implantation, also found positive staining mostly at the surface [251]. Lubricin is known for its important role in joint lubrication in normal cartilage [53, 252] and may also facilitate joint tribology during repair; however, its exact role during cartilage repair is unclear [52, 253]

Blood vessels were evident in the repair tissue, as noted through visual observation of the histological sections and positive staining for vWF and CD31. The fact that normal articular cartilage is naturally avascular, and given the associations between angiogenesis and cartilage degradation [86, 90, 91, 93, 94], provide rationale for the inhibition of neovascularization in the

reparative tissue during cartilage repair and regeneration [97, 98, 224]. It should be noted that the staining patterns were different between vWF and CD31—more cells lining vessels stained for vWF than for CD31, and additional small clusters near the surface stained for vWF but not for CD31. This finding illustrates the difficulty of relying on immunohistochemical staining alone to visualize blood vessels in our samples, and commends the additional use of general histological observation. A recent study showing that vascular endothelial cells can transform into multipotent stem-like cells via an activin-like kinase-2 (ALK2) receptor-dependent mechanism found that the endothelial cells demonstrated slight reduction in vWF expression and significant reduction in CD31 expression during the transition process [87]. It is possible that the endothelial cells in the reparative tissue in this study may also be undergoing ALK2-dependent endothelial-to-mesenchymal transition, explaining the staining pattern observed. These potential stem-like cells may have implications for cartilage repair and regeneration.

The results of this study suggest that post-operative long-term immobilization of the joint using an external fixation device with periodic removal of the device and manual passive motion exercise is detrimental in animal studies of cartilage repair, when balancing considerations of infection and joint degeneration, and this protocol is not recommended for future work. Instead, an alternative to be considered is the use of short-term immobilization using an external fixation device followed by removal of the device and normal ambulation.

PART 2: CELL-SEEDED SCAFFOLDS FOR THE TREATMENT OF CHONDRAL DEFECTS

5.5. Introduction

Current clinical treatments for damaged articular cartilage include microfracture [19] and autologous chondrocyte implantation (ACI) [25], which focus primarily on symptomatic relief. The reparative tissue formed is often observed to be fibrocartilaginous in nature and lacking the biochemical and biomechanical properties of normal articular cartilage, and it is unclear if the tissue is able to withstand joint loading over the longer term [31].

Tissue engineering and regenerative medicine provide a potential new solution for treating cartilage defects by utilizing a combination of scaffolds and cells, along with regulators, to engineer and regenerate new tissue. Given the phenomenon of chondrocyte dedifferentiation in monolayer culture [50], there has been increasing interest in three-dimensional systems for cell culture and *in vivo* delivery. These systems provide a structure more similar to what is found *in vivo* and can aid in the phenotypic stability of the chondrocytes. Various cell-seeded scaffolds have been implanted *in vivo*, including chondrocyte-seeded types I and II collagen sponge-like scaffolds in a dog model [38, 43, 44], chondrocyte- and MSC-seeded collagen sponge-like scaffolds in a sheep model [254], chondrocyte-seeded hyaluronan-based sponge-like scaffolds in humans [27, 255], chondrocyte-seeded type II collagen gel in a rabbit model [256], and MSC-seeded collagen gels in humans [257]. These studies have generally found that cell-seeded scaffolds result in better results compared to controls and microfracture-treated defects, including more repair tissue filling the defect sites and better histological scores.

In this study, autologous chondrocyte-seeded type II collagen scaffolds were engineered *in vitro* to form a known amount of glycosaminoglycan (GAG) [185], with a goal of 75% GAG

compared to normal articular cartilage, resulting in a construct of some maturity, prior to implantation in a caprine model. GAG content was used as a quantitative measure of the degree of chondrogenesis. Our rationale for achieving a construct with 75% GAG prior to implantation is based on prior work [38, 44] showing that chondrocyte-seeded type II collagen scaffolds cultured *in vitro* for 4 weeks prior to implantation resulted in more hyaline cartilage and more total reparative tissue filling the defect site compared to type II collagen scaffolds seeded with chondrocytes within 12 hours of implantation, suggesting that implantation of a more mature cartilaginous construct may yield better healing *in vivo*. This *in vivo* study serves as a cell-seeded construct control without endostatin overexpression, in which we investigated retention of the implanted construct and its effects on cartilage repair.

5.6. Materials and Methods

5.6.1. Cell Isolation and Two-Dimensional Monolayer Expansion

Autologous chondrocytes were isolated from articular cartilage shavings obtained from non-articulating regions of the stifle joints (left knee) of four skeletally mature female goats (ages 2 to 5 years). The animal experiment was approved by the Veterans Administration Animal Care Committee. Cells were expanded in monolayer culture using a standard chondrocyte expansion medium consisting of high glucose Dulbecco's modified Eagle's medium (DMEM-HG), containing 1% nonessential amino acids (v/v), 1% HEPES buffer, 1% penicillin/streptomycin/L-glutamine, and 10% FBS (Invitrogen, Carlsbad, CA, USA), and supplemented with 1 ng/ml transforming growth factor (TGF)-β1, 5 ng/ml FGF-2, and 10 ng/ml platelet-derived growth factor (PDGF)-ββ (R&D Systems, Minneapolis, MN, USA). The cells

were incubated in a humidified chamber at 37°C, 5% CO_2, and 21% O_2 and grown through two subcultures to obtain P2 cells.

5.6.2. Scaffold Fabrication

Scaffolds were prepared using 1% porcine type II collagen (Geistlich Biomaterials, Wolhusen, Switzerland) as previously described [185]. Briefly, porous sheets (~2.5 mm thick) were fabricated by freeze-drying (VirTis, Gardiner, NY, USA). The sheets were sterilized and lightly crosslinked by dehydrothermal treatment using a vacuum greater than 30 inHg at a temperature of 105°C. Disks (8 mm in diameter and 2.5 mm in thickness) were cut from the sheets using a dermal biopsy punch. The scaffolds were incubated in 2.5 ml of an aqueous carbodiimide solution consisting of 1-ethyl-3-(3-dimethylaminopropyl) carbodiimide hydrochloride and N-hydroxysuccinimide (Sigma Chemical Co., St. Louis, MO, USA) at a molar ratio of 5:2:5 (EDAC:NHS:COOH, relative to the carboxyl contained in the collagen scaffold) for 2 hours and then washed with phosphate buffered saline (PBS, Invitrogen).

5.6.3. Cell Seeding and Culture in Collagen Scaffolds

Collagen scaffolds were placed in agarose-coated wells for cell seeding. P2 cells were trypsinized and resuspended in DMEM-LG. Two million chondrocytes were pipetted onto one side of the scaffold and incubated for 10 minutes, followed by the addition of 2 million cells on the second side for 30 minutes, for a total of 4 million cells seeded per scaffold. Then, chondrogenic medium (CM), as previously described [190], was added to each well.

Media was changed every 2-3 days, and constructs were cultured for 35 days and then trimmed to 4-mm diameter using a biopsy punch prior to implantation. Additional constructs

were terminated after 1 (n = 24) and 35 (n = 22) days for biochemical analysis and histological examination.

5.6.4. Analysis of DNA and Glycosaminoglycan (GAG) Content

Constructs cultured *in vitro* were lyophilized and enzymatically digested overnight using proteinase K (Roche Diagnostics, Indianapolis, IN). The DNA content was measured using the Picogreen dye assay kit (Molecular Probes, Inc., Eugene, OR, USA) according to the manufacturer's instructions. The sulfated GAG content was measured using the dimethylmethylene blue (DMMB) dye assay, with a standard curve obtained using chondroitin-6-sulfate from shark cartilage (Sigma).

5.6.5. Surgical Implantation in Animal Model

All implantations were performed on the right knee of the animal under general anesthesia and using sterile conditions. The joint was opened by an anteromedial approach, and the patella was displaced laterally to expose the trochlea. Two 4-mm chondral defects were created in the trochlear groove as previously described [241]. The two defects were located approximately 1.25 and 2.25 cm proximal to the intercondylar notch, slightly lateral or medial to the midline. A dermal punch was used to create the outline of the defects. All noncalcified cartilage was removed from the defects by lightly scraping the calcified cartilage surface using a curet, with the aid of loupe visualization. The autologous cell-seeded constructs were fit into the defects and secured using sutures. The knee joint was closed by zero point suturing.

The knee was immobilized by external fixation (IMEX Veterinary, Longview, TX) for the first 8 days after surgery, followed by normal ambulation until sacrifice.

5.6.6. Histological and Immunohistochemical Evaluation

Constructs cultured *in vitro* and allocated for histology were fixed in 10% neutral buffered formalin. *In vivo* defects were removed from the joints, fixed in 10% formalin, and decalcified using ethylenediamine tetraacetic acid (EDTA). All samples were processed and embedded in paraffin, and sectioned by microtomy. The sections were mounted on glass slides and stained with hematoxylin and eosin (H&E) and Safranin-O using standard histological techniques.

Types I and II collagen distribution were examined immunohistochemically using an anti-type I collagen mouse monoclonal antibody (I-8H5 CP17, final concentration of 5 μg/ml, Calbiochem, Gibbstown, NJ, USA) and an anti-type II collagen mouse monoclonal antibody (CIIC1, final concentration 4 μg/ml, Developmental Studies Hybridoma Bank, University of Iowa, Iowa City, IA, USA). Staining for lubricin was done using anti-lubricin mouse monoclonal (S.679, final concentration 4.6 μg/ml, Dr. T. Schmid, Rush University Medical Center, Chicago, Illinois). Laminin and type IV collagen were also examined immunohistochemically, using an anti-laminin rabbit polyclonal antibody (final concentration 27 μg/ml, Abcam, Cambridge, MA, USA) and an anti-type IV collagen rabbit polyclonal antibody (final concentration 17 μg/ml, Abcam). All staining was performed using the Dako Autostainer (DakoCytomation, Carpinteria, CA, USA) and the peroxidase-aminoethyl carbazole (AEC)-based Envision+ kit (Dako) following the manufacturer's recommendations.

5.6.7. Histomorphometry

Histomorphometric analysis of specific tissue types filling the defect was carried out on one H&E-stained section from the center portion of each defect. Previous work found that the inter-observer error associated with this quantitative histological method was generally less than the inter-animal variation in the results [249]. Digital micrographs were taken of the defect and surrounding tissues. The total cross-sectional area of the original defect and the percentages of fibrous tissue, fibrocartilage, and hyaline cartilage filling the original defect were measured using ImageJ software (NIH, Bethesda, MD). Tissue types were classified according to textbook appearance of cell morphology and extracellular matrix structure as previously described [241]. In many of the samples, surrounding tissue "flowed" into the peripheral areas of the defect. These regions were classified separately as matrix flow. The percentage of bone ingrowth into the defect sites was also evaluated. When the percentages do not add up to 100%, it is due to rounding of values.

5.6.8. Quantitative Evaluation of Tissue Bonding

The linear percentages of the base of the defect to which the healing tissue was bonded and of the height of the edges of the repair tissue on the left and right sides of the defect that were bonded to the adjacent cartilage were determined.

5.6.9. Statistical Analysis

Data are presented as the mean ± standard error of the mean (SEM). Analysis of variance (ANOVA) was performed using StatView software (SAS Institute Inc, Cary, NC, USA).

Statistical significance was set at $p < 0.05$.

5.7. Results

5.7.1. Biochemical Analysis of the In Vitro Constructs

One day after seeding, the average number of chondrocytes in the cell-seeded scaffolds (n = 24) was 2.0 ± 0.2 million cells (Figure 5.4), compared to the 4 million cells seeded; the average DNA content for goat chondrocytes used is 7.7 pg DNA/cell [258]. This indicates that approximately 50% of the cells were retained in the scaffolds 1 day post-seeding. At the time of implantation, after 35 days of culture, the average number of chondrocytes in the cell-seeded scaffolds (n = 22) increased to 3.5 ± 0.2 million cells (Figure 5.4). One-factor ANOVA indicated a significant effect of culture time ($p < 0.0001$, power = 1) on cell number.

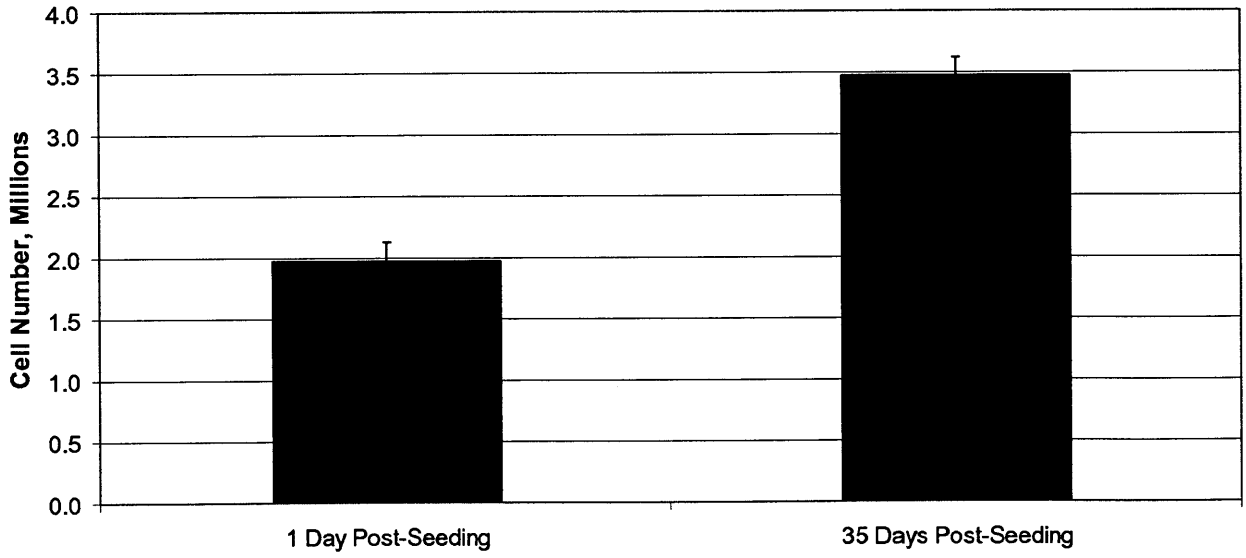

Figure 5.4 Cell numbers in the in vitro-cultured constructs, estimated from the DNA content (n = 24 for 1 day samples, n = 22 for 35 day samples).

One day after seeding, the average GAG density (GAG content per volume) of the constructs (n = 24) was 13 ± 1% of that in native cartilage (Figure 5.5); 15.8 mg/mm^3 was the value used for the normal GAG density [185]. At the time of implantation, after 35 days of culture, the average GAG density (n = 22) was much higher, at 88 ± 7% (Figure 5.5). One-factor ANOVA indicated a significant effect of culture time ($p < 0.0001$, power = 1) on the GAG percentage.

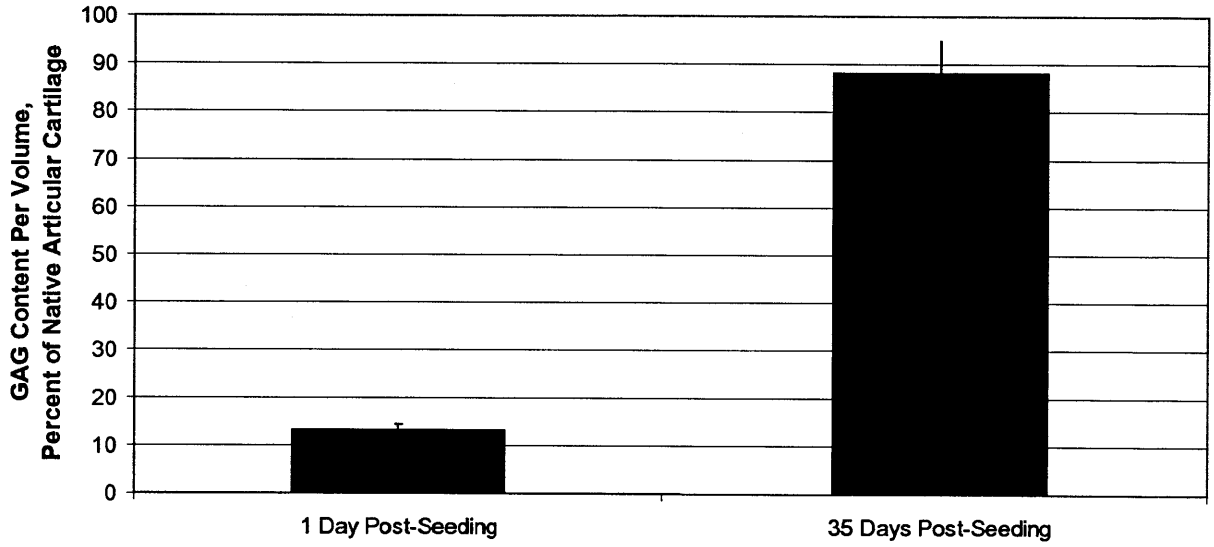

Figure 5.5 Percentage GAG content per volume in the in vitro-cultured constructs, compared to native goat articular cartilage (n = 24 for 1 day samples, n = 22 for 35 day samples).

5.7.2. Histological Evaluation of the In Vitro Constructs

Immunohistochemical evaluation of the cell-seeded constructs collected 1 day post-seeding revealed cells distributed throughout porous scaffolds (Figure 5.6a and b). Of note was the positive intracellular staining for laminin (Figure 5.6a) and type IV collagen (Figure 5.6b), suggesting that some of the cultured chondrocytes were synthesizing laminin and type IV

collagen *in vitro*. No notable staining for either molecule was noted on the collagen scaffold itself.

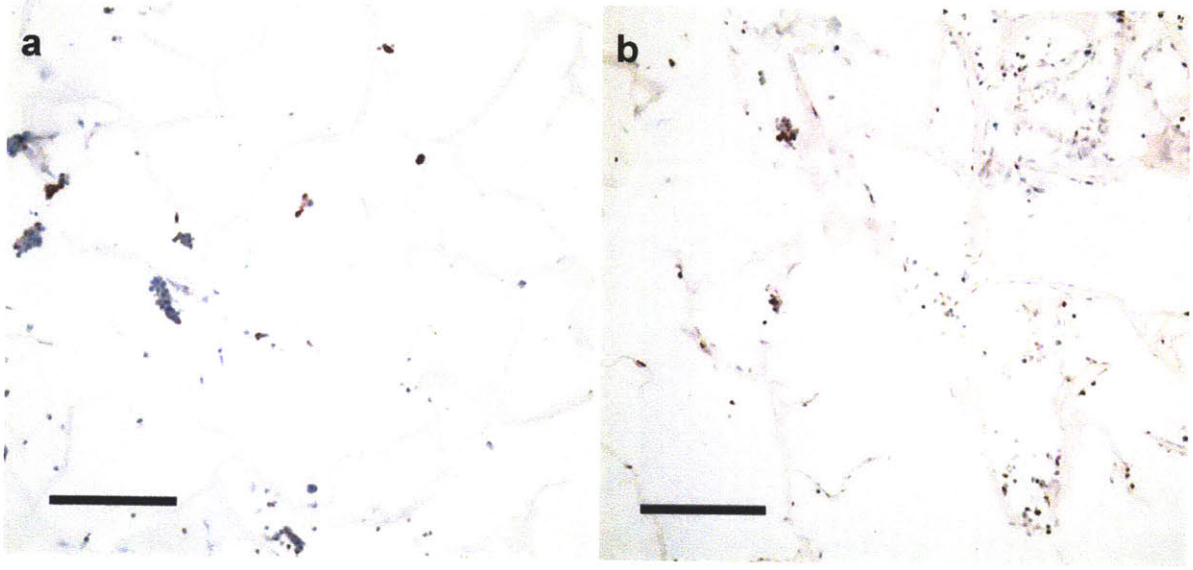

Figure 5.6 In vitro-cultured constructs, 1 day post-seeding, stained for (a) laminin and (b) type IV collagen. Scale bar, 200 μm.

Constructs collected at the time of implantation revealed cells, many rounded and in lacunae, residing in newly-synthesized extracellular matrix (Figure 5.7a). Residual struts from the collagen scaffold could be seen (Figure 5.7a). The newly-synthesized extracellular matrix stained for sulfated GAGs (Figure 5.7a) and type II collagen (Figure 5.7b). Interestingly, large areas of the extracellular matrix also stained for laminin (Figure 5.7c) and type IV collagen (Figure 5.7d); the residual collagen struts did not stain (Figure 5.7c and d). Little to no positive staining for lubricin was seen in the *in vitro*-cultured constructs (data not shown).

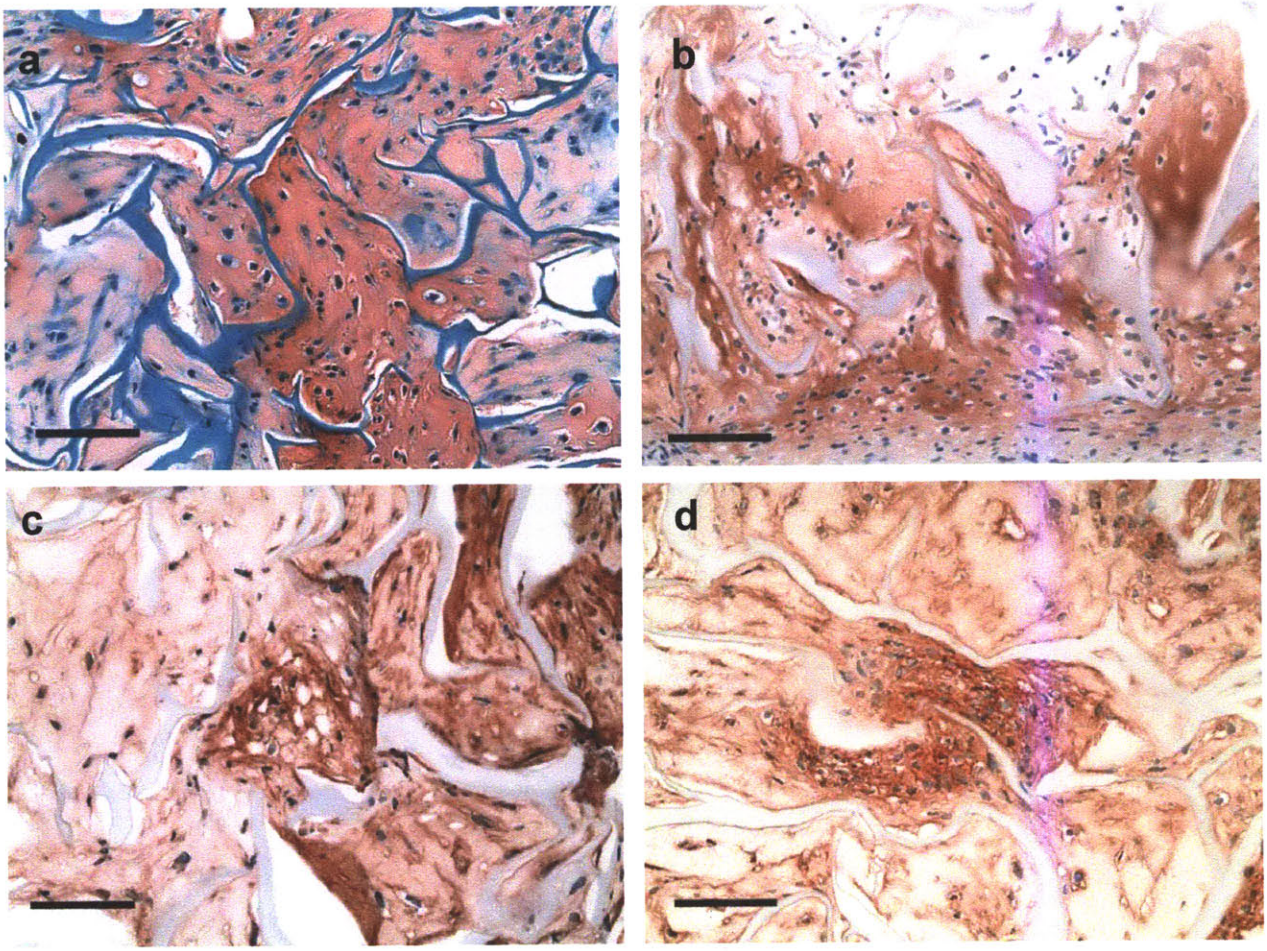

Figure 5.7 In vitro-cultured constructs at the time of implantation, 35 days post-seeding, stained for (a) sulfated GAGs (Safranin-O), (b) type II collagen, (c) laminin, and (d) type IV collagen. Scale bar, 100 μm.

5.7.3. Laminin and Type IV Collagen Distribution in Normal Goat Articular Cartilage

As seen in Figure 5.8, positive staining for both molecules was observed in normal goat articular cartilage, found as an intense and distinct layer in the pericellular matrix. Faint staining was also observed around many of the cells in the territorial matrix, while negligible staining was seen in the interterritorial matrix (Figure 5.8a and b).

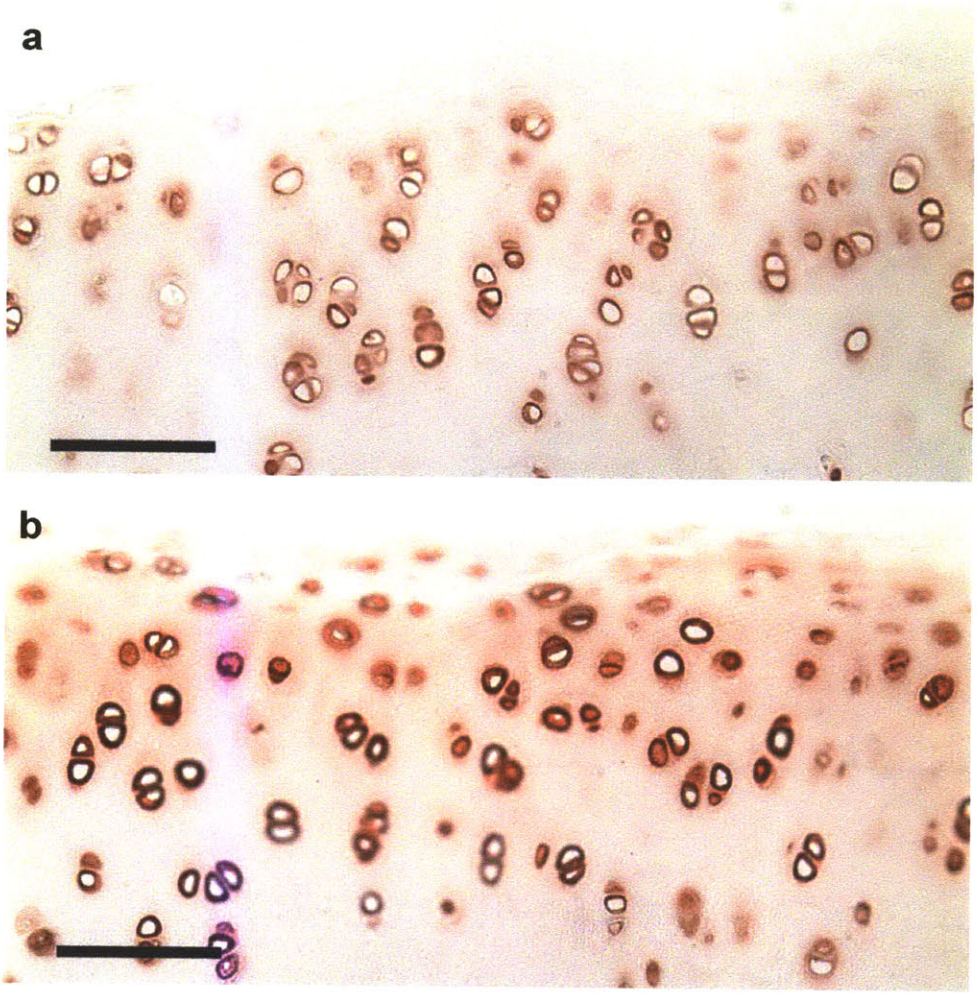

Figure 5.8 Normal goat articular cartilage, stained for (a) laminin and (b) type IV collagen. Scale bar, 100 μm.

5.7.4. Gross and Histological Assessment of In Vivo Cartilage Repair

One animal died at 7 weeks, before reaching the proscribed sacrifice time of 8 weeks, unrelated to the cartilage repair; the other 3 animals went to term.

Gross examination revealed normal joint condition at sacrifice. All defect sites were clearly identifiable, and the surrounding cartilage appeared mostly normal (Figure 5.9a). Residual collagen struts from the implanted scaffolds could be observed in some of the defects (Figure 5.9a and b).

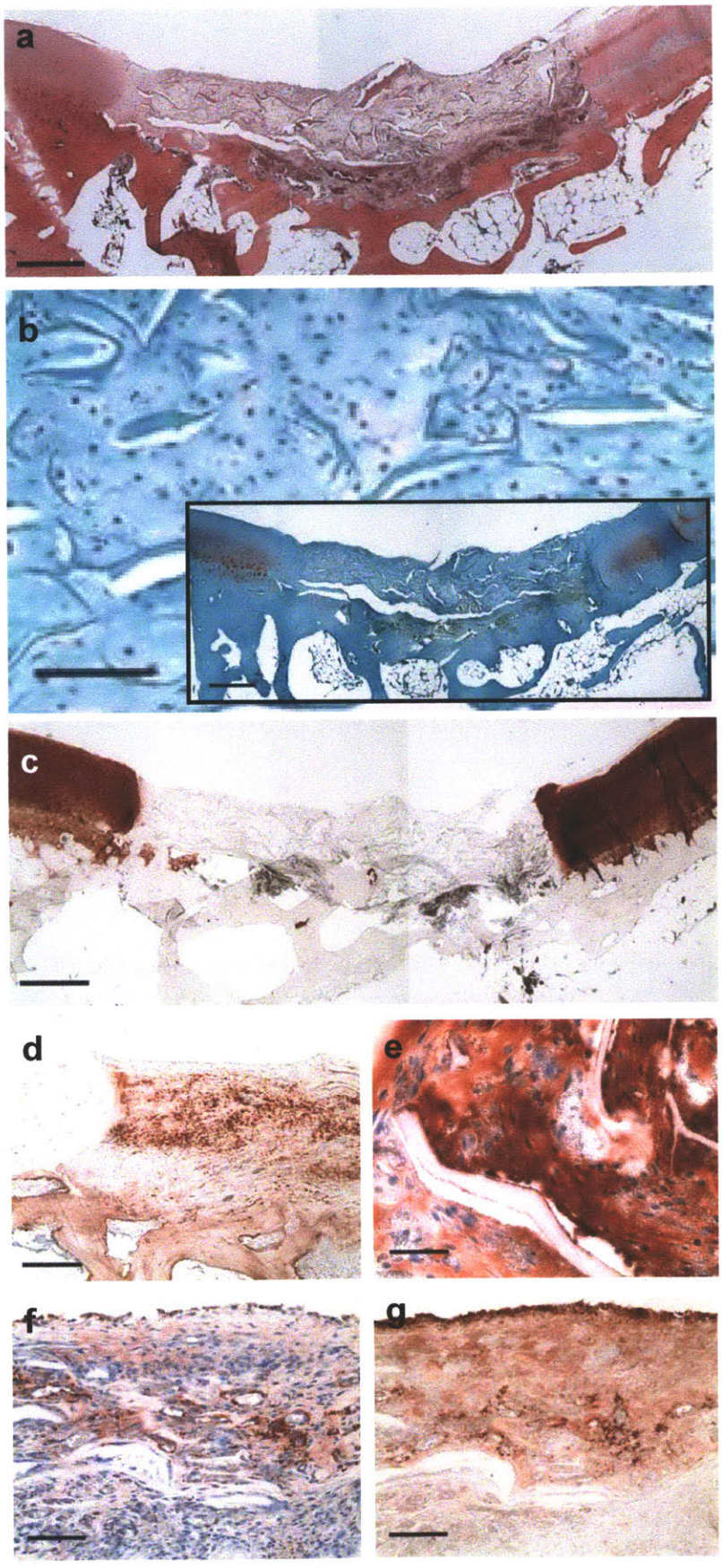
a
b
c
d
e
f
g

Figure 5.9 In vivo reparative tissue, 7-8 weeks post-surgery.

a. **H&E. Scale bar, 500 μm.**
b. **Safranin-O (red chromogen indicates sulfated GAGs). Scale bar, 100 μm. Inset shows the section at lower magnification, scale bar, 500 μm.**
c. **Type II collagen (red chromogen indicates positive stain). Scale bar, 500 μm.**
d. **Type I collagen (red chromogen indicates positive stain). Scale bar, 200 μm.**
e. **Lubricin (red chromogen indicates positive stain). Scale bar, 50 μm.**
f. **Laminin (red chromogen indicates positive stain). Scale bar, 100 μm.**
g. **Type IV collagen (red chromogen indicates positive stain). Scale bar, 100 μm.**

The staining pattern for sulfated GAGs and type II collagen were similar. Some positive staining for sulfated GAGs was seen in the extracellular matrix, typically in the middle and deep zones of the surrounding articular cartilage, while little to no staining was observed in the reparative tissue (Figure 5.9b). Intense positive staining for type II collagen was observed throughout the extracellular matrix of the cartilage surrounding the defect site (Figure 5.9c). There was no notable staining for type II collagen in the reparative tissue (Figure 5.9c).

Positive staining for type I collagen was present in large areas of the extracellular matrix of the reparative tissue filling the defect sites (Figure 5.9d).

Lubricin was also noted in the reparative tissue (Figure 5.9e). Staining intensity varied from sample to sample, but was generally seen in the extracellular matrix. Discrete surface staining was also noted on the residual collagen struts.

Of note was the presence of laminin (Figure 5.9f) and type IV collagen (Figure 5.9g) in the *in vivo* reparative tissue. Intense staining was seen on the surface and surrounding some of the newly-forming blood vessels in the reparative tissue. Diffuse staining was also noted throughout large areas of the extracellular matrix.

5.7.5. Histomorphometric Evaluation of Reparative Tissue

On average, 69 ± 5% of the defect site was filled with reparative tissue 7-8 weeks post-implantation (Table 5.4). The reparative tissue consisted primarily of fibrous tissue and a small

amount of fibrocartilage. No hyaline cartilage was found filling the defect. Negligible amounts of matrix flow and bone ingrowth (<4% of the total defect site) were noted.

Table 5.4 Histomorphometry results. Values reported as percentage of defect cross-sectional area.

Survival Time, wks	Hyaline Cartilage	Fibro-cartilage	Fibrous Tissue	Matrix Flow	Bone Ingrowth	Total Fill
7-8 (n = 8 defects)	0 ± 0	6 ± 2	57 ± 5	3 ± 1	2 ± 1	69 ± 5

Two-factor ANOVA indicated that defect location (proximal or distal) had a significant effect on bone ingrowth ($p = 0.02$, power = 0.85), but failed to find a significant effect on the percentages of fibrocartilage ($p = 0.83$, power = 0.05), fibrous tissue ($p = 0.13$, power = 0.30), matrix flow ($p = 0.31$, power = 0.15), or total fill ($p = 0.13$, power = 0.30). ANOVA also revealed no significant effect of survival time on any of the outcome variables ($p >> 0.05$).

5.7.6. Quantitative Evaluation of the Bonding of the Reparative Tissue to the Adjacent Tissue

Nearly complete bonding was noted between the left (91 ± 5%) and right (87 ± 7%) sides of the reparative tissue and the surrounding cartilage 7-8 weeks post-implantation (Table 5.5). Significant bonding was also observed at the base of the reparative tissue (72 ± 8%) (Table 5.5).

Table 5.5 Bonding of reparative tissue. Values reported as percentages.

Survival Time, wks	Bonding of Height with Adjacent Cartilage (Left Side)*	Bonding of Height with Adjacent Cartilage (Right Side)*	Bonding of Base
7-8 (n = 8 defects)	91 ± 5	87 ± 7	72 ± 8

* Height of repair tissue in apposition with adjacent cartilage divided by total height of repair tissue

5.8. Discussion

To our knowledge, no studies have yet reported on the distribution of laminin and type IV collagen in normal adult goat articular cartilage. The pericellular staining pattern observed in goat articular cartilage in this study is similar to what has been reported in the literature for other species, including cow [8], mouse [8, 9], and human [7].

The notable finding of this study is the observation of laminin and type IV collagen, 2 common basement membrane molecules, in both *in vitro* engineered cartilaginous constructs and *in vivo* cartilage repair samples. The *in vitro* staining pattern reported here is similar to what was reported in an earlier chapter of this thesis on MSC-seeded gels cultured *in vitro*. Widespread and extensive staining for the 2 molecules was observed throughout the extracellular matrix of *in vitro*-cultured constructs (5 weeks) and *in vivo* samples, different than the localized pericellular staining pattern seen in normal adult articular cartilage [8], suggesting that the engineered constructs and reparative tissue being formed *in vitro* and *in vivo* are different than normal articular cartilage. Again, the similarity in staining patterns seen in our study and in maturing [8, 13] and osteoarthritic cartilage [227] may suggest that aspects of the cartilage repair process are recapitulating either normal joint maturation or matrix remodeling events and repair following the onset of osteoarthritis. Further work is needed to elucidate the role of basement membrane molecules during cartilage repair and regeneration.

In agreement with previous work showing that chondrocytes can synthesize laminin and type IV collagen *in vitro* [259], chondrocytes cultured *in vitro* in this study were also capable of synthesizing the 2 molecules, even though a number of the cells appeared de-differentiated. It has also been shown that chondrocytes can synthesize the molecules *in vivo* [8]; however, the

source of the laminin and type IV collagen in the reparative tissue in this study was not investigated.

In this study, we engineered cartilaginous constructs *in vitro* and implanted them into chondral defects in the goat knee. At sacrifice 7-8 weeks post-implantation, nearly 70% of the defect site was filled with reparative tissue, and over 70% of the reparative tissue was bonded to the adjacent host tissue. The composition of the reparative tissue largely consisted of fibrous tissue and some fibrocartilage. Other studies in our lab have investigated cartilage repair using a number of techniques. An untreated defect in a canine model revealed 41 ± 4.3% total fill 1.5 months after defect creation; 3 months after defect creation, 34 ± 6.9% of the defect was filled with reparative tissue, with up to 51 ± 11% bonding to the surrounding host tissue [249]. In the same study, a defect treated using ACI resulted in 41 ± 10% total fill after 1.5 months, and 48 ± 6.5% total fill and up to 76 ± 12% bonding after 3 months [249]. In another canine study, a microfracture-treated defect showed 56 ± 12% total fill 15 weeks after treatment, consisting of a mixture of fibrocartilage and fibrous tissue, and 25 ± 9% bonding to the adjacent cartilage [44]. The findings of this study showed results at least as good as our historical data obtained using other treatment techniques, including ACI and microfracture, suggesting that a cell-seeded scaffold is a viable option for cartilage repair.

Cell-seeded scaffolds have been utilized in other studies. Nehrer and coworkers [43] found that autologous chondrocyte-seeded type I collagen matrices implanted in dogs within 12 hours of seeding resulted in 51 ± 12% filling of the defect site after 15 weeks, and type II collagen matrices resulted in 58 ± 10%. Breinan *et al.* [44] showed that autologous chondrocyte-seeded type II collagen matrices implanted in chondral defects in dog knees within 12 hours of seeding yielded 62 ± 13% filling of the defect site and 34 ± 8% bonding to the adjacent cartilage

after 15 weeks. Lee *et al.* [38] found that chondrocyte-seeded type II collagen matrices implanted in dogs after 4 weeks of *in vitro* culture resulted in 88 ± 6% filling of the defect site and 64 ± 12% bonding to the adjacent tissue after 15 weeks. Our results are generally comparable to these previously published studies. It should be noted that differences existed in animal survival time and the *in vitro* culture conditions among the studies, likely accounting for the differences seen in total fill.

Chondrogenesis was observed in the engineered constructs, prior to implantation, as indicated by the cell morphology and the presence of GAG and type II collagen at 35 days. The GAG density of the constructs was measured at the time of implantation, providing a measure of the maturity of the construct. In this study, fairly mature constructs were engineered, with a GAG density of 88%, close to our target of 75% GAG. The constructs also contained areas of hyaline-like cartilage at the time of implantation into cartilage defects. However, no hyaline cartilage was noted in the *in vivo* reparative tissue, suggesting that the transplanted hyaline-like cartilage did not survive following implantation, and that its initial presence in the defect site did not stimulate the formation of new hyaline cartilage during remodeling, by 7-8 weeks post-implantation. This is in contrast with autologous osteochondral mosaicplasty studies showing the consistent survival of the transplanted hyaline cartilage [29].

While other work has shown that lubricin can be synthesized by chondrocytes *in vitro* [260], little to no lubricin was observed in the engineered constructs in this study. Significant lubricin was observed in the extracellular matrix of the *in vivo* reparative tissue and was likely from the surrounding synovium [261], though it is possible that some cells in the reparative tissue were also responsible for contributing to the observed lubricin [51]. The presence of lubricin in the *in vivo* cartilage repair model is of note, though its role is unclear—it may be

important for facilitating the tribology of the reparative tissue, it may be a response to injury, or its anti-adhesive role may have implications for bonding and integration during repair [52, 253].

Retention of constructs and repair tissue in a load-bearing site is important. Previous work in our lab demonstrated that implants sutured in the knee joints of 2 goats were located in their defect sites 1 and 2 weeks following implantation, suggesting that the suturing method is sufficient for retention of the construct during both external fixation (first week) and normal ambulation (following week) [262]. Residual scaffold struts were seen in defects 2 months after implantation in this study, further affirming construct retention using suturing and short-term immobilization followed by normal ambulation.

In the present study, we implanted *in vitro*-cultured constructs with a known GAG density into chondral defects in the goat knee, and demonstrated improvement in quantity of reparative tissue compared to untreated historical controls. We report the novel finding of laminin and type IV collagen during the engineering and regeneration of articular cartilage, with different staining patterns than that seen in normal articular cartilage. This discovery may have implications for cell behavior, including growth, migration, and differentiation, during cartilage tissue engineering and regeneration.

PART 3: EFFECTS OF OSTEOGENIC PROTEIN (OP)-1 ON MICROFRACTURE-TREATED CHONDRAL DEFECTS

5.9. Introduction

The introduction of a molecule that could promote chondrocyte metabolism, such as osteogenic protein (OP)-1, could be used in concert with endostatin to potentially improve the cartilage repair process. OP-1, also known as bone morphogenetic protein (BMP)-7, is a member of the transforming growth factor (TGF)-β superfamily and is primarily known for its bone induction activity [263]. Clinically, it is used for bone applications, including spinal fusion and fracture repair. However, the benefits of osteogenic protein (OP)-1 in promoting chondrocyte metabolism *in vitro* commend it for cartilage repair. It has been found in normal articular cartilage [264] and has been shown to be synthesized by articular chondrocytes [265]. *In vitro* studies indicate that OP-1 is involved in the maintenance of normal cartilage homeostasis [266], promotes anabolic pathways, including stimulation of type II collagen and aggrecan synthesis [267], and protects against catabolic factors, such as interleukin-1 [268-270]. Also of note are prior experiments which have demonstrated the effects of BMP-7 in stimulating the expression of lubricin [271-273], which has been demonstrated to be a critical lubricating glycoprotein in diarthrodial joints and which may play other roles as an anti-adhesion molecule.

There are several potential OP-1 protein delivery methods. One popular method that has been investigated involves the use of a collagen matrix as a carrier of OP-1 [274, 275], while another potential method is the implantation of an osmotic pump for continuous delivery of OP-1 [276, 277]. However, for clinical use, periodic injections provide a more attractive option, as it is a technically simple procedure that maintains the presence of the protein over an extended period.

The half-life of OP-1 is on the order of hours [278].

The objective of this study was to evaluate the effects of OP-1 on the amount and composition of the reparative tissue induced by a microfracture procedure in a goat model.

5.10. Materials and Methods

5.10.1. Animal Model

Thirteen skeletally mature female goats (ages 2 to 5 years) were used in the study. The animal experiment was approved by the Veterans Administration Animal Care Committee. Prior to surgery, the goats were examined roentgenographically to ensure that there was no preexisting degenerative joint disease of the knee.

All operations were performed on the right knee (stifle joint) of the animal under general anesthesia and using sterile conditions. The joint was opened by an anteromedial approach, and the patella was displaced laterally to expose the trochlea. Two 4-mm chondral defects were created in the trochlear groove as previously described [241]. The two defects were located approximately 1.25 and 2.25 cm proximal to the intercondylar notch, slightly lateral or medial to the midline. A dermal punch was used to create the outline of the defects. All noncalcified cartilage was removed from the defects by lightly scraping the calcified cartilage surface using a curet, with the aid of loupe visualization.

Microfracture was performed by forcing the straight pointed end of a microsurgical pick into the subchondral bone with a twisting motion. Six equally spaced penetrations, each approximately 1 mm in diameter, were made in each defect. Before closing the joint capsule, bleeding vessels were clamped and cauterized. The knee joint was closed by zero point suturing.

Under anesthesia, the joints were injected with 1 mg of OP-1 in 1 ml of vehicle (Stryker Biotech, Hopkinton, MA) using an 18 gage needle (Group II) three times: immediately post-operative, and at 8 and 20-21 days, post-operative. Control animals received injections of the vehicle alone (Group I). The knee was immobilized by external fixation (IMEX Veterinary, Longview, TX) for the first 8 days after surgery, followed by normal ambulation until euthanasia.

5.10.2. Tissue Processing and Staining

At necropsy, the joints were grossly examined and photographed. Joints that were found to have new bone formation were also examined roentgenographically. Defects and capsule tissue were removed from the joints, fixed in 10% neutral buffered formalin, and decalcified using ethylenediamine tetraacetic acid (EDTA). The samples were dehydrated and embedded in paraffin so that cross-sections of the samples spanning from the surface down into the tissue were obtained during sectioning with a microtome. Microtomed sections were deparaffinized and stained with hematoxylin and eosin (H&E), Safranin-O for sulfated glycosaminoglycans (GAGs), and Masson's trichrome for total collagen using standard techniques. Sections were also stained immunohistochemically for lubricin and type II collagen using anti-lubricin (S.679, final concentration of 4.6 μg/ml, Dr. T. Schmid, Rush University Medical Center, Chicago, Illinois) and anti-type II collagen (CIIC1, final concentration of 4 μg/ml, Developmental Studies Hybridoma Bank, University of Iowa, Iowa City, IA) mouse monoclonal antibodies, respectively, using the Dako Autostainer (DakoCytomation, Carpinteria, CA). Briefly, deparaffinized sections were digested in 0.1% protease for 40 mins, quenched with peroxidase blocking reagent (Dako) for 10 mins, blocked with blocking solution (Dako) for 10 mins, and incubated with the primary antibodies for 30 mins. Labeling was developed using streptavidin-

HRP and aminoethyl carbazole (AEC) following the manufacturer's instructions (Dako), and sections were counterstained with Mayer's hematoxylin. Negative controls were incubated with mouse IgG2a and IgG2b at the same concentrations as the primary antibodies, instead of the primary antibodies.

5.10.3. Histomorphometry

Histomorphometric analysis of specific tissue types filling the defect was carried out on one H&E-stained section from the center portion of each defect. Previous work found that the inter-observer error associated with this quantitative histological method was generally less than the inter-animal variation in the results [249]. Digital micrographs were taken of the defect and surrounding tissues. The total cross-sectional area of the original defect and the percentages of fibrous tissue, fibrocartilage, and hyaline cartilage filling the original defect were measured using ImageJ software (NIH, Bethesda, MD). Tissue types were classified according to textbook appearance of cell morphology and extracellular matrix structure as previously described [241]. Briefly, fibrous tissue was defined by the presence of elongated cells not in lacunae surrounded by extracellular matrix with a distinct fibrous appearance. Fibrocartilage consisted of rounded cells in lacunae surrounded by extracellular matrix with a distinct fibrous appearance. Cells in hyaline cartilage were rounded and resided in lacunae, and there were no visible collagen fibers or bundles in the matrix. In many of the samples, surrounding tissue "flowed" into the peripheral areas of the defect. These regions were classified separately as matrix flow. The percentage of bone ingrowth into the defect sites was also evaluated. When the percentages do not add up to 100%, it is due to rounding of values.

5.10.4. Quantitative Evaluation of Tissue Bonding

The linear percentages of the base of the defect to which the healing tissue was bonded and of the height of the edges of the repair tissue on the left and right sides of the defect that were bonded to the adjacent cartilage were determined. The percentage of the length of the subchondral plate with a normal appearance was also quantified. Both the bony plate and the overlying calcified cartilage were required to be free from signs of resorption, fibrous deposition, and mechanical damage.

5.10.5. Statistics

Statistical significance was determined using StatView software (SAS Institute Inc., Cary, NC). Contingency tables were used to determine the statistical significance of OP-1 treatment on joint condition and ossification at 16 weeks. Two-factor analysis of variance (ANOVA) was used to determine the significance of OP-1 treatment and defect location on selected outcome categories for the defects collected at 16 weeks. Significance was set at $p < 0.05$. All results are reported as mean ± standard error of the mean (SEM).

5.11. Results

5.11.1. General Gross Observations

At the time of sacrifice, the majority of the joints appeared normal, and the margins of the defects could generally be grossly distinguished with the naked eye (Figure 5.10). However, 1 of 6 control goats and 2 of 7 OP-1-treated goats showed significant signs of degeneration (Table 5.6), characterized by areas of articular cartilage loss, ingrowth of the surrounding synovial

tissue into the joint space, fibrous adhesions, and discoloration (Figure 5.10). Contingency tables of necropsy findings revealed no significant difference in joint condition between OP-1 treated and control joints at 16 weeks (chi square $p = 0.78$, Fisher's exact $p > 0.99$). The amount of reparative tissue filling the defects varied greatly from defect to defect. Some defects appeared nearly completely filled with white repair tissue, while microfracture holes were still visible in other defects that were filled with little to no tissue (Figure 5.10).

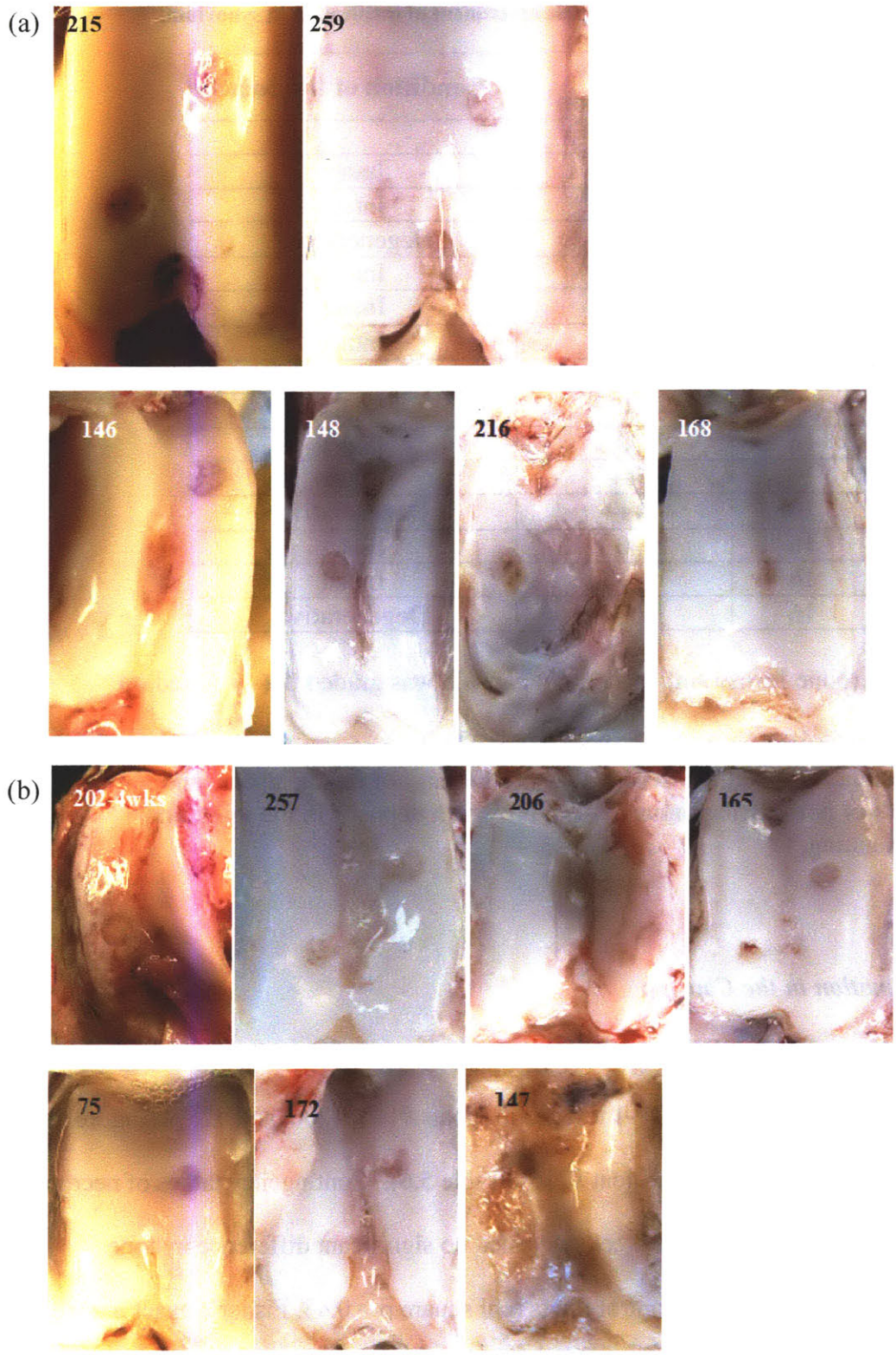

Figure 5.10 Photographs of joints immediately after sacrifice. Gross appearances of defects in Group I (-OP-1) goats (a) and Group II (+OP-1) goats (b).

Table 5.6 Gross findings at necropsy and radiographic assessment of ossification in synovium.

Goat #	Duration, wks	Capsule Ossification[1]	Condition of the Joint
Group I (-OP-1) Control			
215	5.5	0	Intact
259	8.5	0	Intact
216	16	+	Degenerative[2]
168	16	0	Intact
148	16	0	Intact
146	16	0	Intact
Group II (+OP-1)			
202	4	0	Intact
75	16	0	Intact
257	16	++	Intact
206	16	+++	Degenerative
172	16	0	Intact
165	16	+	Intact
147	16	0	Degenerative

[1] Ossification (bone formation) in the joint capsule was graded 0-+++ based on radiographs.

[2] Grossly degenerative joints were characterized by loss of cartilage from the condyles, tibia and patella, discoloration (yellowing) of the meniscus, and overgrowth of non-cartilaginous tissues, brownish deposits in the joint, and variable bleeding.

5.11.2. Bone Formation in the Capsule

Radiographs revealed regions of radiodense features consistent with the appearance of bone in the capsules of 3 goats in the OP-1 test group (goats #165, #206, and #257) (Figure 5.11) as well as in a control synovial capsule (goat #216) (Table 5.6). Contingency tables of necropsy findings for the samples collected at 16 weeks revealed no significant difference in bone formation between OP-1 treated and control joints (chi square $p = 0.43$, Fisher's exact $p = 0.57$).

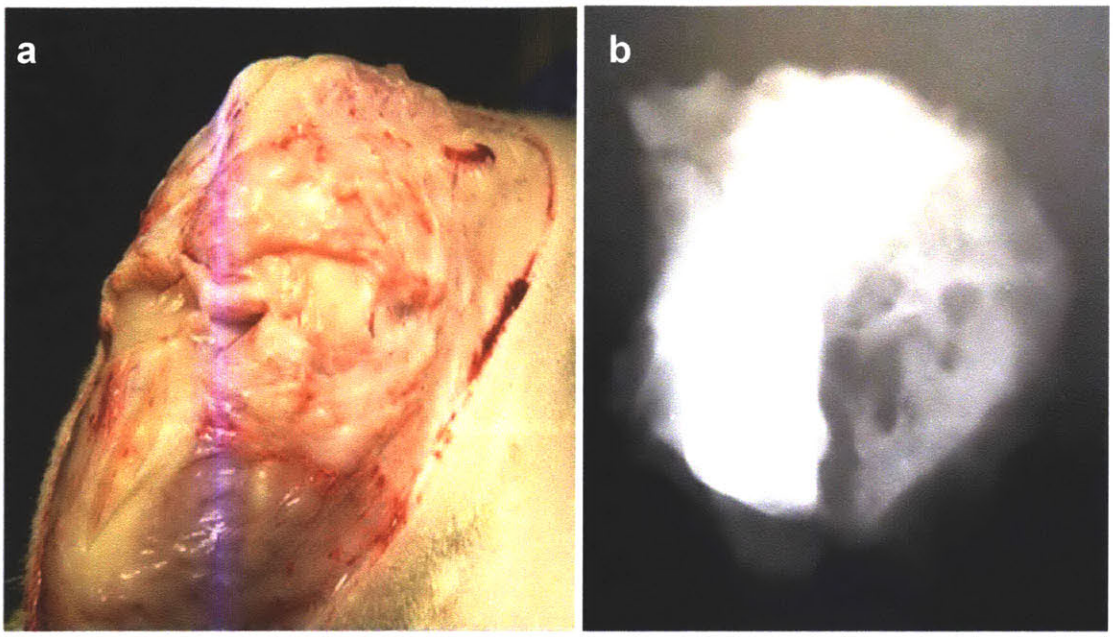

Figure 5.11 Gross observation of new bone formation found in the capsule tissue. Photograph (a) and radiograph (b) of joint from a Group II (+OP-1) goat immediately after sacrifice (#257).

Histological results confirmed the radiological findings. Areas of dense and open trabecular bone were found in the capsular tissue of both the OP-1 test group (Figure 5.12a) and the control group (Figure 5.12b). Vascular spaces in the bone were lined by osteoblasts and contained blood vessels, fibroblasts, and connective tissue (Figure 5.12c). Osteocytes could be seen in the bone tissue (Figure 5.12c and d), and large multinucleated osteoclasts were located in resorption cavities of the bone (Figure 5.12d). Sharpey's fibers were seen extending from the bone into the surrounding tissue (Figure 5.12e and f). Flattened, irregularly shaped cells seen in the surrounding tissue were suggestive of progenitor cells (Figure 5.12e). Cartilaginous tissue was also observed in some areas adjacent to the bone tissue, with rounded cells residing in lacunae, typical morphology of chondrocytes (Figure 5.12g).

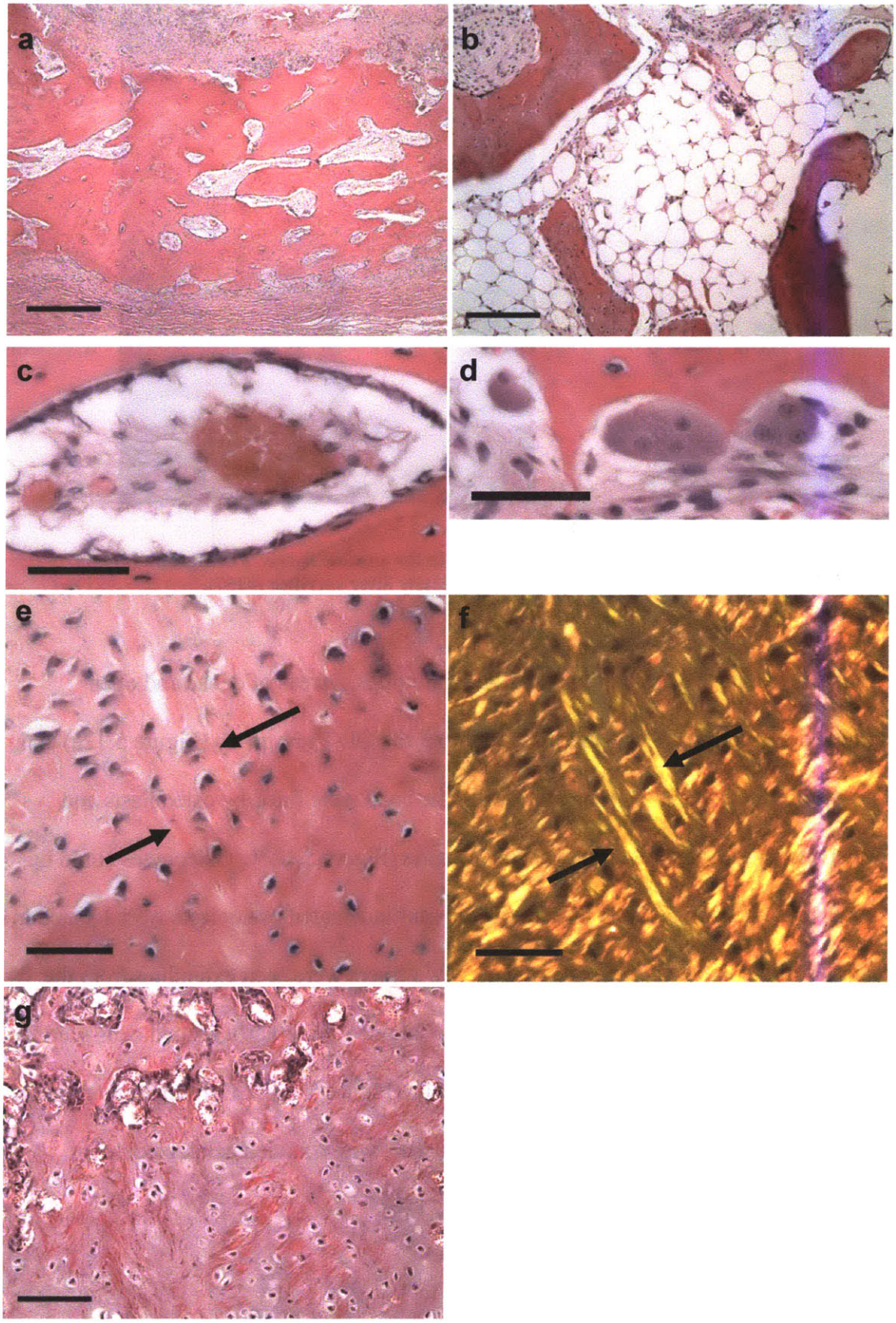
a
b
c
d
e
f
g

Figure 5.12 Micrographs of the capsule tissue. H&E staining.

a. **Medial capsule tissue from a Group II (+OP-1) goat (#206). Scale bar, 500 μm.**
b. **Medial capsule tissue from a Group I (-OP-1) goat (#216). Scale bar, 200 μm.**
c. **Vascular space within an ossicle (goat #206). Scale bar, 50 μm.**
d. **Large multinucleated osteoclasts residing in resorption cavities (goat #206). Scale bar, 50 μm.**
e. **Sharpey's fibers (arrows) observed using standard light (goat #206). Scale bar, 50 μm.**
f. **Sharpey's fibers (arrows) observed using polarized light (goat #206). Scale bar, 50 μm.**
g. **Cartilage found in the capsule tissue (goat #216). Scale bar, 100 μm.**

5.11.3. Qualitative Histological Assessment

Most of the defect sites in the control group (11 of 12 defects) were easily distinguishable from the surrounding articular cartilage (Figure 5.13a), while only 6 of 14 defects in the OP-1 treatment group had clearly defined boundaries when viewed under a microscope. The samples in which the defect sites were not identifiable (Figure 5.13b) were all collected at 16 weeks. Degeneration of the cartilage around the defects, lack of reparative tissue in the defects contributing to incomplete histological sections, and enlargement of the fossa through the base of the groove encroaching on the defects confounded histomorphometry. These samples were thus excluded from histomorphometric analysis.

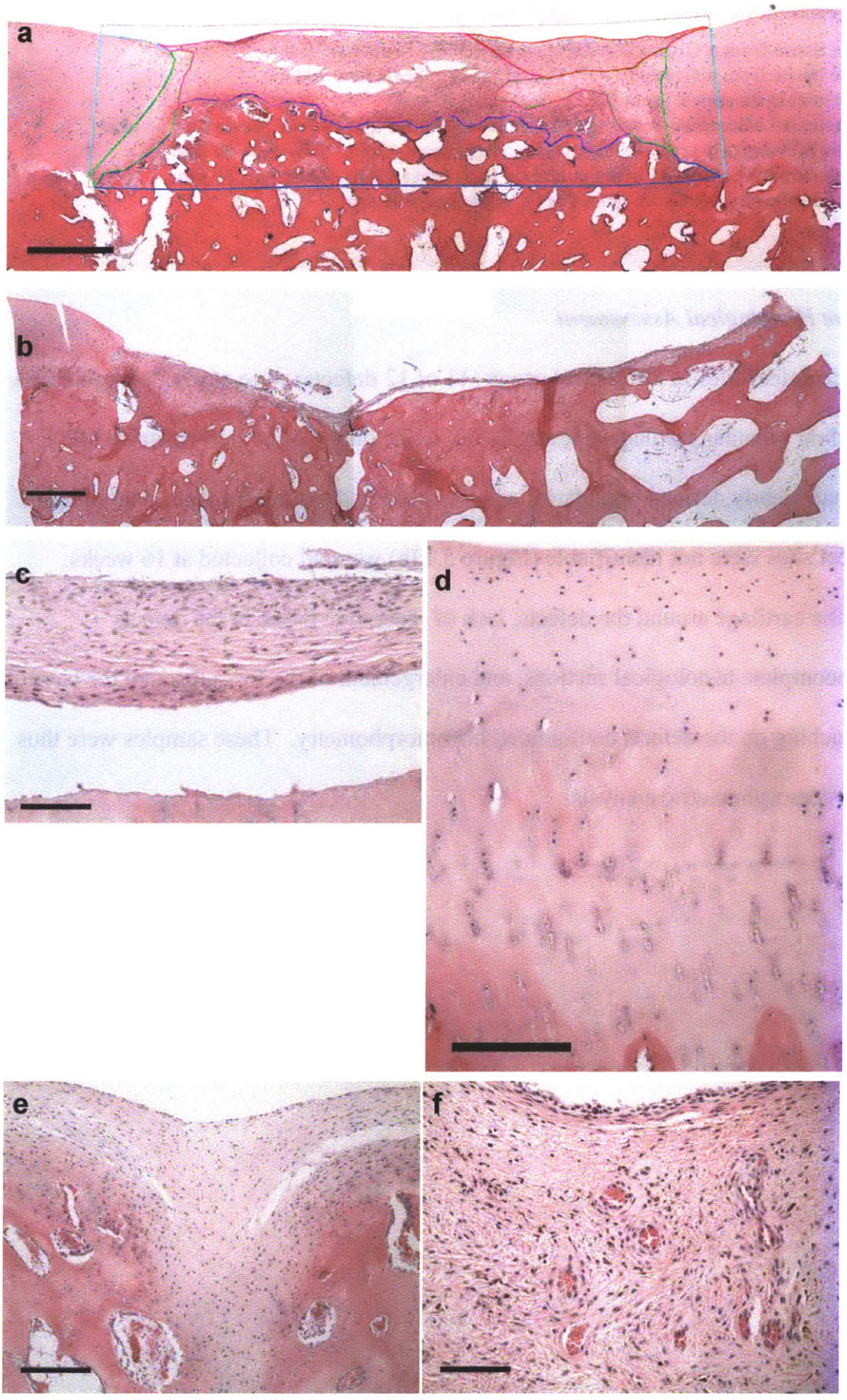
a
b
c
d
e
f

Figure 5.13 H&E micrographs of defects and surrounding tissue.

a. **Proximal defect site of a Group I (-OP-1) goat (#148). The original defect site is outlined, and specific tissue types are further subdivided in order to calculate areal percentages for histomorphometry. Scale bar, 500 μm.**
b. **Distal defect site of a Group II (+OP-1) goat (#75). Scale bar, 500 μm.**
c. **Reparative tissue filling the defect site of a Group I (-OP-1) goat (#215) and the underlying calcified layer. Scale bar, 100 μm.**
d. **Articular cartilage surrounding the defect site of a Group I (-OP-1) goat (#215). Scale bar, 200 μm.**
e. **Reparative tissue found in the proximal defect site and underlying calcified layer of a Group II (+OP-1) goat (#165). Scale bar, 200 μm.**
f. **Vessels seen in the reparative tissue filling the distal defect of a Group I (-OP-1) goat (#216). Scale bar, 100 μm.**

Samples collected at the early timepoints (4-8.5 weeks) generally had less reparative tissue filling the defect sites than those collected at 16 weeks. The tissue filling the early timepoint defects consisted almost entirely of fibrous tissue densely packed with cells (Figure 5.13c). These repair tissues generally showed poor integration with the adjacent tissues, especially a lack of bonding with the underlying calcified layer (Figure 5.13c). The surrounding articular cartilage appeared fairly normal, including columnar arrangements of cells displaying a spherical morphology in well-developed lacunae and a distinct tidemark separating the calcified zone from the noncalcified (Figure 5.13d).

The majority of the reparative tissue filling the 16-week defects was fibrous in nature (fibrocartilage and fibrous tissue), and little hyaline cartilage was observed. These tissues were generally well-integrated with the surrounding tissues (Figure 5.13). Although not flush with the surface of the adjacent cartilage, the defect volume was nearly filled for most of the samples (Figure 5.13a).

It was interesting to note that perhaps the most favorable histological finding of reparative tissue in the defects was from one of the Group II (+OP-1) goats that presented with a degenerative joint and the most extensive capsular ossification (#206).

Notable fractures were observed in the underlying calcified cartilage and subchondral bone in the majority of the early timepoint defects and in several of the 16-week defects. Communication was evident between the defect space and the marrow space of the trabecular bone. Many breaks were filled by repair tissue extending from the original defect site down into the subchondral bone (Figure 5.13e). Neovascularization was evident within reparative tissue filling the defect space, primarily within tissue that was fibrous in nature (Figure 5.13f) and rarely within hyaline-like tissue. Many vessels were present in samples collected at early timepoints, whereas fewer to no vessels were typically seen in the samples collected at 16 weeks.

Type II collagen staining (Figure 5.14a) revealed intense positive staining in the host articular cartilage, while some positive staining for type II collagen was seen in the reparative tissue, and no positive staining was noted in the underlying bone. Safranin-O staining (Figure 5.14b) reflected a similar staining pattern as the type II collagen staining. Positive staining for sulfated GAGs was seen in some areas of the reparative tissue filling the defect site and throughout much of the surrounding host articular cartilage. Masson's trichrome staining (Figure 5.14c) revealed the presence of collagen (blue chromogen) throughout the extracellular matrix of the reparative tissue and surrounding native cartilage. The underlying bone also showed areas of collagen throughout the tissue. Some areas of the reparative tissue stained for collagen using Masson's trichrome stain but did not stain positively for type II collagen, particularly near the surface of the reparative tissue, suggesting the presence of type I collagen, or other collagen type, in the defect.

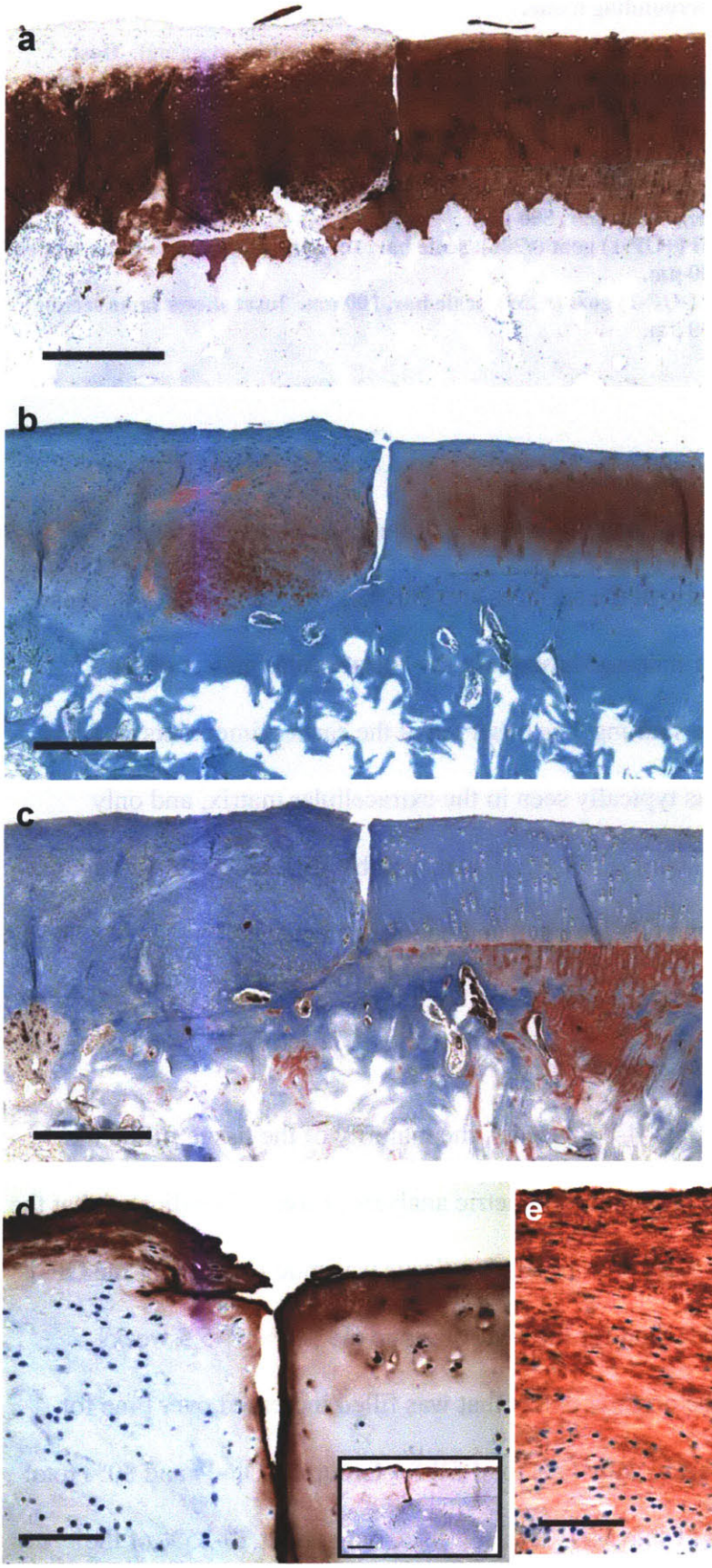
a
b
c
d
e

Figure 5.14 Micrographs of defects and surrounding tissue.

a. **Type II collagen staining of a Group II (+OP-1) goat (#206) (red indicates positive staining). Host articular cartilage is on the right, and reparative tissue filling the defect site is on the left. Scale bar, 500 μm.**
b. **Safranin-O staining of a Group II (+OP-1) goat (#206) (red indicates staining for sulfated GAGs). Scale bar, 500 μm.**
c. **Masson's trichrome staining of a Group II (+OP-1) goat (#206) (blue indicates collagen, red indicates cytoplasm, and black indicates nuclei). Scale bar, 500 μm.**
d. **Lubricin staining (red) of a Group II (+OP-1) goat (#206), scale bar, 100 μm. Inset shows same section at lower magnification, scale bar, 500 μm.**
e. **Lubricin staining (red) of a Group I (-OP-1) goat (#259), scale bar, 100 μm. Inset shows same section at lower magnification, scale bar, 500 μm.**

Repair tissue and host articular cartilage showed positive staining for lubricin, with varying amounts and intensities seen from animal to animal. Some samples revealed a very dense layer of positive staining primarily at the surfaces and crevices (Figure 5.14d), whereas other samples showed diffuse positive staining throughout the extracellular matrix of the reparative tissue (Figure 5.14e). More staining was observed at the earlier timepoints (4-8.5 weeks) than at 16 weeks. Staining was typically seen in the extracellular matrix, and only infrequently appeared as intracellular staining. Generally, no notable differences in amount or intensity of staining were noted between OP-1-treated and control defects.

5.11.4. Histomorphometric Evaluation of Reparative Tissue

At the early timepoints (3 animals, 4-8.5 weeks), the majority of the tissue filling the defects was fibrous tissue (Table 5.7). Histomorphometric analysis (Table 5.7) indicated that the percentage of the defect site that was filled with reparative tissue was much higher for the OP-1 treated group (62 ± 17%, mean ± SEM) than for the control group (19 ± 5%) 4-5.5 weeks postoperatively. The percentage of the original defect that was filled increased over time for both groups and was similar by 16 weeks, with 75% total fill for Group I (-OP-1) and 80% total fill for Group II (+OP-1) at 16 weeks (Table 5.7). By 16 weeks, only about 20-25% of the

reparative tissue consisted of fibrous tissue, whereas the majority of the filling was classified as cartilaginous tissue (fibrocartilage and hyaline cartilage) (Table 5.7). In all cases, less than 20% of the defect site was filled with hyaline cartilage (Table 5.7).

Table 5.7 Summary of the histomorphometric results; as a percentage of the original area of the defect. Eleven out of 12 Group I defects and 6 out of 14 Group II defects were analyzed; the others were not due to generalized joint degeneration or erosion of the adjacent cartilage and a lack of defined defect cross-sectional area.

Group	Time, wks (n*)	Hyaline Cartilage	Fibro-cartilage	Fibrous Tissue	Matrix Flow	Bone Ingrowth	Total Fill
Group I (-OP-1)	5.5 (2)	0 ± 0	0 ± 0	17 ± 5	2 ± 0	0 ± 0	19 ± 5
	8.5 (2)	3 ± 3	10 ± 4	46 ± 12	3 ± 1	6 ± 4	68 ± 8
	16 (7)	17 ± 8	26 ± 6	15 ± 5	4 ± 2	11 ± 5	75 ± 6
Group II (+OP-1)	4 (2)	0 ± 0	0 ± 0	59 ± 17	2 ± 0	0 ± 0	62 ± 17
	16 (4)	6 ± 3	51 ± 19	20 ± 7	2 ± 1	2 ± 1	80 ± 10

* n, number of defects

Two-factor ANOVA indicated that OP-1 treatment had no significant effect on the percentages of hyaline cartilage ($p = 0.37$, power = 0.13), fibrocartilage ($p = 0.23$, power = 0.20), fibrous tissue ($p = 0.57$, power = 0.08), matrix flow ($p = 0.25$, power = 0.19), bone ingrowth ($p = 0.18$, power = 0.24), or total fill ($p = 0.68$, power = 0.07) in the defects collected at 16 weeks. ANOVA also revealed no significant effect of defect location (proximal or distal) on any of the outcome variables ($p >> 0.05$).

Including the data for all animals from the experimental and control groups (including those sacrificed before 16 weeks), a paired comparison of the percentage fill of the proximal defect with the percentage fill of the distal defect in the same animal demonstrated no statistically significant difference (paired Student's t test; $p=0.77$). Separate paired tests of the percentage fill in the proximal and distal defects for the 16-week animals and the 3 goats sacrificed early (*i.e.*, at 4, 5.5, and 8.5 week) also revealed no statistically significant difference

in the percentage fill of the proximal and distal defects (paired Student's t tests; p=0.83 and p=0.88, respectively).

An analysis was performed of the percentage fill of the defects of goats sacrificed less than 8.5 weeks (6 defects) versus those that went to term (16 weeks; 11 defects). Combining data from the experimental and control groups demonstrated a 56% greater fill on the defects at 16 weeks, compared to the early sacrifices (49±6 %, mean ± standard error of the mean, versus 77 ± 16 %), which was statistically significant (p=0.018; power=0.70).

5.11.5. Quantitative Evaluation of Tissue Bonding

Bonding between the reparative tissue and surrounding host tissue was typically seen to increase over time. Although little bonding of the reparative tissue to the base of the defect was seen at the early stage of healing (*i.e.* at 4 and 5.5 weeks), some of the subchondral plate (24-57% of its length) did exhibit a normal appearance (Table 5.8). By 8.5 weeks and later, the majority of the healing tissue was bonded to the base in both groups, and none of the subchondral bone appeared normal (Table 5.8). Generally, good bonding was observed between the edges of the repair tissue on the left and right sides of the defect and the adjacent cartilage in both groups by 8-16 weeks (77-100%), while less bonding was noted at 4 weeks, in which 17-60% of the OP-1-treated healing tissue appeared bonded (Table 5.8).

Table 5.8 Quantitative measurements of defect bonding and normal subchondral bone.

Group	Time, wks	Quantitative Measures (%); Number of Defects in Parenthesis			
		Bonding of Base	Bonding of Height with Adjacent Cartilage (Left Side)*	Bonding of Height with Adjacent Cartilage (Right Side)*	Length of Subchondral Plate with Normal Appearance
Group I (-OP-1)	5.5	3 ± 3 (2)	77 ± 23 (2)	81 ± 3 (2)	57 ± 18 (2)
	8.5	81 ± 19 (2)	82 ± 18 (2)	85 ± 15 (2)	0 ± 0 (2)
	16	91 ± 7 (7)	97 ± 3 (7)	100 ± 0 (8)	0 ± 0 (8)
Group II (+OP-1)	4	0 ± 0 (2)	17 ± 17 (2)	60 ±24 (2)	24 ± 8 (2)
	16	90 ± 6 (4)	100 ± 0 (8)	91 ± 6 (6)	0 ± 0 (12)

* Height of repair tissue in apposition with adjacent articular cartilage divided by total height of repair tissue

5.12. Discussion

In this study, microfracture-treated articular cartilage defects in a caprine model were treated with 3 injections of 1 mg of OP-1 each. A much higher total fill was observed in the OP-1 group (62 ± 17%) compared to the control group (19 ± 5%) after one month, suggesting that the OP-1 treatment may be beneficial during the early stages of cartilage repair. However, there was no significant benefit of multiple treatments of OP-1 on the chondral defects by 16 weeks. The OP-1 and control groups demonstrated comparable results at 4 months, with both showing nearly complete filling (80 ± 10% for the OP-1 treatment compared to 75 ± 6% for the control group), of which little was hyaline cartilage, consistent with findings from other microfracture models [44]. There were 2 defects in the OP-1 treatment group (goat #75) that could not be evaluated due to the fact that the scant amount of reparative tissue in the defects contributed to poor quality histological slides. These defects might have been scored zero with respect to the total fill of the defect, further demonstrating the absence of a positive effect of OP-1 in this study.

Previous work in bone suggests that there is an optimal range of OP-1 doses, dependent on species and location, below which maximal bone volume is not induced and above which excessive and unwanted bone formation occurs [279-281]. It is likely that there also exists an optimal OP-1 concentration for treatment of articular cartilage. Full-thickness cartilage defects in a rabbit model treated with 10 μg of OP-1 was found to stimulate cartilage repair [274]. One study [282] examining the use of OP-1 to treat a model of osteoarthritis in the rabbit knee tested three doses—0.6, 6, and 60 μg—and found improvement of treated knees compared to controls for the 6 and 60 μg groups. In another rabbit osteoarthritis study [276], 250 μg of OP-1, delivered using an Alzet osmotic pump over a period of 6 weeks, resulted in improved healing. A study in dogs [275] found that 350 μg of OP-1 resulted in improved healing of an osteochondral defect. One study using sheep [277] showed that doses of 55 and 170 μg of OP-1 delivered to the chondral defects yielded improved results compared to controls, while another sheep study [278] found that 340 μg of OP-1 protected against further cartilage degeneration. A caprine study found that 30 and 60 μg of OP-1 resulted in extensive filling of a subchondral defect in the knee 4 months after treatment, with a significant relationship noted between OP-1 dosage and amount of aggrecan [283]. Here, the dose used (3 injections each consisting of 1 mg of OP-1, for a total of 3 mg of OP-1) was significantly larger than in previous studies, and may have, in fact, been too high, possibly contributing to the negative outcomes described here.

There are several large animal studies reported in the literature regarding OP-1 treatment for cartilage repair. One of the prior studies performed in sheep [277] employed a categorical evaluation that demonstrated greater than 90% filling of the OP-1-treated defects after 3 months compared to less than 25% in the controls. This study was the one that most dramatically demonstrated a positive effect of OP-1 on cartilage repair. Two other animal investigations that

concluded that OP-1 had a positive effect on cartilage repair [275, 283] reported benefits of OP-1 on select categories that do not relate to the contribution of OP-1 to the amount of tissue in the defect or to the relative amounts of the various tissue types. A fourth study [284], which employed OP-1 overexpressing chondrocytes found that there was no difference in the histologic scores between treated and control defects in an equine model at 8 months. Several factors could be responsible for the difference in the outcome of this animal study compared with those previously reported: species; site of implantation and surgical approach; OP-1 levels maintained in the joint; mode of delivery of the OP-1; and method of evaluation.

A recent study found a synergistic effect of microfracture and OP-1 in treating full-thickness defects in young rabbits that resulted in increased quality and quantity of repair tissue compared to either treatment alone [274]. The differences from our results are likely attributed in part to the age difference of the animals. In the rabbit study, adolescent animals were used, whereas here, skeletally mature animals were employed, preferable since most individuals undergoing cartilage treatment in the clinic are adults.

The observation of ossicle formation in the joint capsule has not been previously reported in other studies investigating OP-1 treatment for articular cartilage damage. Ossification was observed in a higher percentage of the joints receiving OP-1 (50% of 6 joints) than in the control joints (25% of 4 joints), although no statistically significant effect of OP-1 treatment was observed for joint ossification. Two studies in which intra-articular injections of OP-1 were administered into rabbit knees following anterior cruciate ligament transection [282] and into sheep knees following impact injury [278] reported no adverse bone formation. It is unclear what triggered the phenomenon observed in this study, though it may have been influenced by the high dose of OP-1 used, the trauma associated with multiple injections, or the vehicle

employed. The source of the cells that resulted in ossification, whether it be circulating progenitor cells that homed to the site of injury and differentiated, local cells that underwent metaplasia, or some other cell source, is also unknown.

Also of note in this study is the presence of lubricin at the articulating surfaces, including fissures, of both the OP-1-treated and control animals. A small amount of intracellular staining was seen, showing that the cells within the tissue were capable of producing lubricin, but it is possible that the surrounding synovium also contributed to the lubricin seen in the tissue samples [261]. Lubricin is primarily known for its boundary lubricating properties [52], but its exact role during cartilage repair remains unclear.

Evidence of neovascularization was observed in the primarily fibrous reparative tissue, while normal articular cartilage is avascular. It is hypothesized that the angiogenesis observed during cartilage repair may be interfering with the formation of hyaline cartilage, providing a rationale for the use of an angiogenesis inhibitor, such as endostatin [97, 224].

One limitation in this study is that only one treatment regimen, including timing and dosage level of injection, was tested. A study in sheep investigated the timing of therapy and found that (1) intra-articular OP-1 injections immediately following impact injury resulted in focal lesions at the injury site that did not progress into the surrounding tissue, (2) injections on day 21 following injury resulted in limited progression compared to the controls, and (3) injections on day 90 resulted in no improvement compared to the controls, suggesting that OP-1 may be chondroprotective if administered early after a traumatic injury [278].

Many studies have reported on the *in vitro* and *in vivo* benefits of OP-1 for articular cartilage. However, this study found no benefit of this OP-1 treatment protocol on the quantity or quality of reparative tissue formed in a chondral defect following microfracture treatment at

16 weeks, and noted the adverse formation of ossicles in the synovial capsule of several animals, though the cause of bone formation is unclear. These results dissuade against the use of this OP-1 treatment protocol in conjuction with endostatin.

CHAPTER 6: CONCLUSIONS

There is widespread recognition of the importance of angiogenesis in wound healing and tissue repair, but there is little work on the inhibition of angiogenesis for tissue engineering and regenerative medicine and particularly articular cartilage regeneration. The necessity of angiogenesis inhibition for cartilage development, the findings that inhibition of angiogenesis improved cartilage repair in adult articular cartilage, and the associations between angiogenesis and pathological cartilage conditions in adult articular cartilage suggest that angiogenesis may interfere with articular cartilage regeneration and may play a critical role in cartilage degeneration, thus emphasizing the importance of investigating a method to inhibit angiogenesis during the regeneration process. A tissue-engineered, endostatin-producing cartilaginous construct may provide a solution for repairing damaged cartilage tissue and result in an increase in the quality of life for the millions of people who suffer from joint pain. Specifically, the presence of endostatin, an angiogenesis inhibitor, may favor the formation of hyaline (articular) cartilage and improved healing of a focal defect in articular cartilage. Besides its anti-angiogenic properties, it is known that endostatin can influence other processes, including promotion of anabolic activity in cartilage [123] and neurogenesis [111, 112], and the application of endostatin in articular cartilage is promising for its potential multiple effects.

6.1. Summary of Findings and Limitations

In this thesis, we investigated an innovative approach of simultaneous use of the construct as a delivery vehicle for endostatin and for cartilage regeneration. The principal achievement was the development of a system with a novel approach for treating cartilage defects, namely endostatin-producing cartilaginous constructs. The constructs were engineered using nonviral gene therapy, through manipulation of select variables, including regulators

(culture media, endostatin plasmid load, method of pEndo lipoplex incorporation, and oxygen tension), scaffold formulation, and cell type. Specifically, we found that constructs engineered using MSCs and chondrocytes, transfected with 5 μg of plasmid per 1 million cells, and cultured in chondrogenic medium are capable of overexpressing endostatin protein and forming areas of cartilaginous material. Sponge-like scaffolds, as well as hydrogels crosslinked using GP, TG-2, and mTG, are viable options for engineering these endostatin-producing cartilaginous constructs. We began to demonstrate the ability to control the endostatin expression profile, through the method of lipoplex incorporation. The type I collagen scaffold used in this thesis and 21% oxygen are preferable to the type II collagen scaffold used and 5% oxygen. In this thesis, GAG supplementation of the scaffolds, using heparan sulfate, chondroitin sulfate, and heparin, did not have beneficial effects on endostatin production and retention or chondrogenesis. One limitation of this thesis is the small sample size; future work may benefit from larger sample sizes. Another limitation is that only select conditions were tested; for example, only 1 amount of each crosslinking agent was used. Future work could benefit from testing a more extensive range of the variables.

We also investigated select aspects of the *in vivo* cartilage defect model in the goat knee in which the construct can be implanted, including the post-operative rehabilitation protocol and the use of OP-1. We found that cell-seeded scaffolds are retained in the defect for at least 2 months following implantation and short-term immobilization and resulted in a favorable outcome, and that the use of our OP-1 treatment protocol in conjuction with endostatin is not recommended. One limitation is that only one OP-1 treatment regimen, including timing and dosage level of injection, was tested, and it is possible that different OP-1 dosages could result in

more favorable outcomes. Another limitation is that cartilage repair was only examined for up to 16 weeks *in vivo*; the long-term results, over a period of years, are unknown.

There are both similarities and differences between the sponge-like scaffolds and the hydrogels, and strengths and weaknesses of each. The unconfined compressive moduli of the sponges (~0.88kPa [185]) and the gels (<0.5 kPa, unpublished lab data) are both very small compared to that of native articular cartilage (314 kPa [185]). The gel is injectable, resulting in less surgical trauma compared to sponge implantation. However, a lipoplex-supplemented sponge-like scaffold may provide the utility of a one-step off-the-shelf transfection construct, compared to the current two-step process of monolayer transfection and subsequent scaffold seeding for the hydrogel scaffold. Further research is needed to investigate the possibility of a one-step *in situ* transfection process for gels.

It is of interest to compare monolayer-transfected cells in sponges versus gels. Previous work in our lab examined ~0.1 million monolayer-transfected MSCs (10-50 μg pEndo per 1 million cells) seeded per sponge-like scaffold and found peak endostatin levels ranging from approximately 3 to 12 ng/ml [98]. In this work, 0.4 million monolayer-transfected MSCs (5 μg pEndo per 1 million cells) seeded per gel resulted in peak endostatin levels ranging from 6 to 18 ng/ml. The ranges are similar between the sponges and the gels, and the preliminary data may begin to suggest that scaffold form does not have a significant effect on endostatin production of already transfected cells. However, the differences in number of cells used and pEndo/cell ratios make it difficult to draw conclusions, and further investigation is needed in this area.

The endostatin levels in the expended medium of monolayer- versus scaffold-transfected constructs were of comparable magnitudes. However, a much larger number of cells were used with sponges than with gels—four million cells were seeded per sponge-like scaffold construct,

with an estimated 2.6 million cells retained by the next day, and 0.4 million cells were seeded per hydrogel construct. On a per cell basis, the data suggest that monolayer-transfected cells were producing, on average, more endostatin than scaffold-transfected cells. The cellular environment during DNA uptake—endostatin plasmid lipoplexes were presented in a 3-dimensional scaffold environment in the sponge-like scaffold experiment and in a 2-dimensional monolayer environment in the hydrogel experiment—may have contributed to the differences in endostatin production per cell, possibly by affecting the presentation/availability of the lipoplexes or by directly affecting cell behavior [98, 285, 286]. It is important to note that there were differences in other experimental conditions between the sponge experiments and the gel experiments, and further studies are needed to determine if cell-matrix interactions may be used to modulate nonviral gene transfection.

The average amount of endostatin produced per cell in normal adult articular cartilage can be estimated to be around 0.02 pg of endostatin per cell, given 228 pg endostatin/mg cartilage and ~10,000 cells/mm^3 of cartilage [5, 14]. It is unclear what the average endostatin being produced per transfected cell is in this thesis, in part because the percentage of cells that are transfected is unknown. It is speculated that the number of cells that are transfected is small in comparison to the total number of cells in the constructs, and it is possible that the transfected cells produce more endostatin than normal adult chondrocytes. However, further work is needed to compare the amounts of endogenous endostatin versus the amounts produced by the transfected cells.

6.2. Future Directions

Future work is needed to determine the quantity and duration of endostatin protein necessary for cartilage repair and to evaluate *in vivo* cartilage regeneration following implantation of our endostatin-producing collagen scaffold constructs in a chondral defect in the knee joint of a goat model, including the degree of vascularization.

In this thesis, collagen scaffolds were used. Other scaffold materials, both natural and synthetic, could also be considered, such as hyaluronan. It is likely that the scaffold material will affect the development of the constructs, including endostatin expression profiles and chondrogenesis.

The mechanical properties of the engineered constructs and the reparative tissue were not evaluated in this thesis, and future work is needed in this area.

The ability to engineer novel endostatin-producing constructs, which may be used primarily for their angiogenesis inhibition properties, has important implications not only for articular cartilage tissue engineering, but for other avascular tissues, for cancer research applications, and for tissues in which angiogenesis inhibition is desired. For example, prominent vascular infiltration has been implicated in the failure of tissue-engineered auricular cartilage [287], and an endostatin-producing construct could be of value for this application. The role of angiogenesis in tumor growth and the importance of angiogenesis regulation has also been recognized for years in the cancer field [288]. Given that endostatin is one of the most widely researched angiogenesis inhibitors in this area, it follows that a novel endostatin-producing construct could be of interest for this field.

The construct engineered in this thesis could also be modified through the use of other cell types and other plasmids to deliver proteins of choice for a wide range of applications, such as spinal cord regeneration and traumatic brain injury repair.

REFERENCES

1. Zhou, S.D., Z.F. Cui, and J.P.G. Urban, *Factors influencing the oxygen concentration gradient from the synovial surface of articular cartilage to the cartilage-bone interface - A modeling study.* Arthritis and Rheumatism, 2004. **50**(12): p. 3915-3924.
2. Hodge, W.A., et al., *Contact Pressures in the Human Hip-Joint Measured Invivo.* Proceedings of the National Academy of Sciences of the United States of America, 1986. **83**(9): p. 2879-2883.
3. Otsuki, S., et al., *Expression of novel extracellular sulfatases Sulf-1 and Sulf-2 in normal and osteoarthritic articular cartilage.* Arthritis Res Ther, 2008. **10**(3): p. R61.
4. Roughley, P.J., *Articular cartilage and changes in arthritis - Noncollagenous proteins and proteoglycans in the extracellular matrix of cartilage.* Arthritis Research, 2001. **3**(6): p. 342-347.
5. Hunziker, E.B., T.M. Quinn, and H.J. Hauselmann, *Quantitative structural organization of normal adult human articular cartilage.* Osteoarthritis Cartilage, 2002. **10**(7): p. 564-72.
6. Hauselmann, H.J., et al., *Adult human chondrocytes cultured in alginate form a matrix similar to native human articular cartilage.* American Journal of Physiology-Cell Physiology, 1996. **271**(3): p. C742-C752.
7. Durr, J., et al., *Identification and immunolocalization of laminin in cartilage.* Exp Cell Res, 1996. **222**(1): p. 225-33.
8. Kvist, A.J., et al., *The major basement membrane components localize to the chondrocyte pericellular matrix--a cartilage basement membrane equivalent?* Matrix Biol, 2008. **27**(1): p. 22-33.
9. Lee, S.K., et al., *Laminin chain expression by chick chondrocytes and mouse cartilaginous tissues in vivo and in vitro.* Exp Cell Res, 1997. **236**(1): p. 212-22.
10. Vincent, T.L., et al., *FGF-2 is bound to perlecan in the pericellular matrix of articular cartilage, where it acts as a chondrocyte mechanotransducer.* Osteoarthritis and Cartilage, 2007. **15**(7): p. 752-763.
11. Chia, S.L., et al., *Fibroblast Growth Factor 2 Is an Intrinsic Chondroprotective Agent That Suppresses ADAMTS-5 and Delays Cartilage Degradation in Murine Osteoarthritis.* Arthritis and Rheumatism, 2009. **60**(7): p. 2019-2027.
12. Iozzo, R.V., et al., *The biology of perlecan: the multifaceted heparan sulphate proteoglycan of basement membranes and pericellular matrices.* Biochem J, 1994. **302 (Pt 3)**: p. 625-39.
13. Melrose, J., et al., *Perlecan displays variable spatial and temporal immunolocalisation patterns in the articular and growth plate cartilages of the ovine stifle joint.* Histochemistry and Cell Biology, 2005. **123**(6): p. 561-571.
14. Pufe, T., et al., *Endostatin/collagen XVIII - an inhibitor of angiogenesis - is expressed in cartilage and fibrocartilage.* Matrix Biology, 2004. **23**(5): p. 267-276.
15. Curl, W.W., et al., *Cartilage injuries: A review of 31,516 knee arthroscopies.* Arthroscopy, 1997. **13**(4): p. 456-460.
16. Shapiro, F., S. Koide, and M.J. Glimcher, *Cell Origin and Differentiation in the Repair of Full-Thickness Defects of Articular-Cartilage.* Journal of Bone and Joint Surgery-American Volume, 1993. **75A**(4): p. 532-553.

17. Hunter, W., *Of the Structure and Disease of Articulating Cartilages (Reprinted from Philos-Trans-R-Soc-Lond, Vol 42, Pg 514-521, 1743).* Clinical Orthopaedics and Related Research, 1995(317): p. 3-6.
18. Buckwalter, J.A. and H.J. Mankin, *Articular cartilage: Tissue design and chondrocyte-matrix interactions*, in *Instructional Course Lectures, Vol 47 - 1998.* 1998, AMER ACAD ORTHOPAEDIC SURGEONS: Rosemont. p. 477-486.
19. Steadman, J.R., et al., *The microfracture procedure: Rationale, technique, and clinical observations for treatment of articular cartilage defects.* Journal of Sports Traumatology and Related Research, 1998. **20**(2): p. 61-70.
20. Rodrigo, J.J., et al., *Improvement of full-thickness chondral defect healing in the human knee after debridement and microfracture using continuous passive motion.* Am. J. Knee Surg., 1994. **7**(3): p. 109-116.
21. Gille, J., et al., *Mid-term results of Autologous Matrix-Induced Chondrogenesis for treatment of focal cartilage defects in the knee.* Knee Surgery Sports Traumatology Arthroscopy, 2010. **18**(11): p. 1456-1464.
22. Hangody, L., et al., *Arthroscopic autogenous osteochondral mosaicplasty for the treatment of femoral condylar articular defects. A preliminary report.* Knee Surg Sports Traumatol Arthrosc, 1997. **5**(4): p. 262-7.
23. Brittberg, M., et al., *Treatment of Deep Cartilage Defects in the Knee with Autologous Chondrocyte Transplantation.* New England Journal of Medicine, 1994. **331**(14): p. 889-895.
24. Peterson, L., et al., *Two- to 9-year outcome after autologous chondrocyte transplantation of the knee.* Clinical Orthopaedics and Related Research, 2000(374): p. 212-234.
25. Brittberg, M., *Autologous chondrocyte transplantation.* Clinical Orthopaedics and Related Research, 1999(367): p. S147-S155.
26. Bartlett, W., et al., *Autologous chondrocyte implantation versus matrix-induced autologous chondrocyte implantation for osteochondral defects of the knee.* Journal of Bone and Joint Surgery-British Volume, 2005. **87B**(5): p. 640-645.
27. Manfredini, M., et al., *Autologous chondrocyte implantation: A comparison between an open periosteal-covered and an arthroscopic matrix-guided technique.* Acta Orthopaedica Belgica, 2007. **73**(2): p. 207-218.
28. Mithoefer, K., et al., *Chondral resurfacing of articular cartilage defects in the knee with the microfracture technique. Surgical technique.* J Bone Joint Surg Am, 2006. **88 Suppl 1 Pt 2**: p. 294-304.
29. Hangody, L. and P. Fules, *Autologous osteochondral mosaicplasty for the treatment of full-thickness defects of weight-bearing joints: ten years of experimental and clinical experience.* J Bone Joint Surg Am, 2003. **85-A Suppl 2**: p. 25-32.
30. Peterson, L., et al., *Autologous chondrocyte transplantation. Biomechanics and long-term durability.* Am J Sports Med, 2002. **30**(1): p. 2-12.
31. Ochi, M., et al., *Current concepts in tissue engineering technique for repair of cartilage defect.* Artificial Organs, 2001. **25**(3): p. 172-179.
32. Hutmacher, D.W., *Scaffolds in tissue engineering bone and cartilage.* Biomaterials, 2000. **21**(24): p. 2529-2543.
33. Compton, C.C., et al., *Organized skin structure is regenerated in vivo from collagen-GAG matrices seeded with autologous keratinocytes.* Journal of Investigative Dermatology, 1998. **110**(6): p. 908-916.

34. Spilker, M.H., et al., *Contraction of collagen-glycosaminoglycan matrices by peripheral nerve cells in vitro.* Biomaterials, 2001. **22**(10): p. 1085-1093.
35. Chen, P., et al., *Formation of lung alveolar-like structures in collagen-glycosaminoglycan scaffolds in vitro.* Tissue Engineering, 2005. **11**(9-10): p. 1436-1448.
36. Xiang, Z., et al., *Collagen-GAG scaffolds grafted onto myocardial infarcts in a rat model: A delivery vehicle for mesenchymal stem cells.* Tissue Engineering, 2006. **12**(9): p. 2467-2478.
37. Louie, L.K., et al., *Healing of tendon defects implanted with a porous collagen-GAG matrix: Histological evaluation.* Tissue Engineering, 1997. **3**(2): p. 187-195.
38. Lee, C.R., et al., *Effects of a cultured autologous chondrocyte-seeded type II collagen scaffold on the healing of a chondral defect in a canine model.* Journal of Orthopaedic Research, 2003. **21**(2): p. 272-281.
39. Veilleux, N. and M. Spector, *Effects of FGF-2 and IGF-1 on adult canine articular chondrocytes in type II collagen-glycosaminoglycan scaffolds in vitro.* Osteoarthritis and Cartilage, 2005. **13**(4): p. 278-286.
40. Nehrer, S., et al., *Matrix collagen type and pore size influence behaviour of seeded canine chondrocytes.* Biomaterials, 1997. **18**(11): p. 769-76.
41. Buma, P., et al., *Cross-linked type I and type II collagenous matrices for the repair of full-thickness articular cartilage defects--a study in rabbits.* Biomaterials, 2003. **24**(19): p. 3255-63.
42. Grande, D.A., et al., *Evaluation of matrix scaffolds for tissue engineering of articular cartilage grafts.* Journal of Biomedical Materials Research, 1997. **34**(2): p. 211-220.
43. Nehrer, S., et al., *Chondrocyte-seeded collagen matrices implanted in a chondral defect in a canine model.* Biomaterials, 1998. **19**(24): p. 2313-28.
44. Breinan, H.A., et al., *Healing of canine articular cartilage defects treated with microfracture, a type-II collagen matrix, or cultured autologous chondrocytes.* J Orthop Res, 2000. **18**(5): p. 781-9.
45. Kim, H.W. and C.D. Han, *An overview of cartilage tissue engineering.* Yonsei Medical Journal, 2000. **41**(6): p. 766-773.
46. Nicoll, S.B., et al., *Modulation of proteoglycan and collagen profiles in human dermal fibroblasts by high density micromass culture and treatment with lactic acid suggests change to a chondrogenic phenotype.* Connective Tissue Research, 2001. **42**(1): p. 59-+.
47. Zuk, P.A., et al., *Multilineage cells from human adipose tissue: Implications for cell-based therapies.* Tissue Engineering, 2001. 7(2): p. 211-228.
48. Adachi, N., et al., *Muscle derived, cell based ex vivo gene therapy for treatment of full thickness articular cartilage defects.* Journal of Rheumatology, 2002. **29**(9): p. 1920-1930.
49. Kramer, J., et al., *Stem cell-derived chondrocytes for regenerative medicine.* Transplantation Proceedings, 2006. **38**(3): p. 762-765.
50. Gao, J., J.Q. Yao, and A.I. Caplan, *Stem cells for tissue engineering of articular cartilage.* Proceedings of the Institution of Mechanical Engineers Part H-Journal of Engineering in Medicine, 2007. **221**(H5): p. 441-450.
51. Schumacher, B.L., et al., *A novel proteoglycan synthesized and secreted by chondrocytes of the superficial zone of articular cartilage.* Arch Biochem Biophys, 1994. **311**(1): p. 144-52.

52. Schmidt, T.A., et al., *Boundary lubrication of articular cartilage - Role of synovial fluid constituents.* Arthritis and Rheumatism, 2007. **56**(3): p. 882-891.
53. Jay, G.D., et al., *The role of lubricin in the mechanical behavior of synovial fluid.* Proceedings of the National Academy of Sciences of the United States of America, 2007. **104**(15): p. 6194-6199.
54. Otto, W.R. and J. Rao, *Tomorrow's skeleton staff: mesenchymal stem cells and the repair of bone and cartilage.* Cell Proliferation, 2004. **37**(1): p. 97-110.
55. zur Nieden, N.I., et al., *Induction of chondro-, osteo- and adipogenesis in embryonic stem cells by bone morphogenetic protein-2: Effect of cofactors on differentiating lineages.* Bmc Developmental Biology, 2005. **5**: p. 1.
56. Hwang, N.S., S. Varghese, and J. Elisseeff, *Derivation of Chondrogenically-Committed Cells from Human Embryonic Cells for Cartilage Tissue Regeneration.* Plos One, 2008. **3**(6).
57. Bigdeli, N., et al., *Coculture of Human Embryonic Stem Cells and Human Articular Chondrocytes Results in Significantly Altered Phenotype and Improved Chondrogenic Differentiation.* Stem Cells, 2009. **27**(8): p. 1812-1821.
58. Dattena, M., et al., *Sheep embryonic stem-like cells transplanted in full-thickness cartilage defects.* Journal of Tissue Engineering and Regenerative Medicine, 2009. **3**(3): p. 175-187.
59. Wakitani, S., et al., *Embryonic stem cells form articular cartilage, not teratomas, in osteochondral defects of rat joints.* Cell Transplantation, 2004. **13**(4): p. 331-336.
60. Fecek, C., et al., *Chondrogenic derivatives of embryonic stem cells seeded into 3D polycaprolactone scaffolds generated cartilage tissue in vivo.* Tissue Engineering Part A, 2008. **14**(8): p. 1403-1413.
61. Wakitani, S., et al., *Embryonic stem cells injected into the mouse knee joint form teratomas and subsequently destroy the joint.* Rheumatology, 2003. **42**(1): p. 162-165.
62. Chung, C. and J.A. Burdick, *Engineering cartilage tissue.* Advanced Drug Delivery Reviews, 2008. **60**(2): p. 243-262.
63. Frenkel, S.R., et al., *Transforming growth factor beta superfamily members: Role in cartilage modeling.* Plastic and Reconstructive Surgery, 2000. **105**(3): p. 980-990.
64. Park, Y., et al., *BMP-2 induces the expression of chondrocyte-specific genes in bovine synovium-derived progenitor cells cultured in three-dimensional alginate hydrogel.* Osteoarthritis and Cartilage, 2005. **13**(6): p. 527-536.
65. Hicks, D.L., et al., *Effect of bone morphogenetic proteins 2 and 7 on septal chondrocytes in alginate.* Otolaryngology-Head and Neck Surgery, 2007. **136**(3): p. 373-379.
66. Miot, S., et al., *Cartilage tissue engineering by expanded goat articular chondrocytes.* Journal of Orthopaedic Research, 2006. **24**(5): p. 1078-1085.
67. Seyedin, S.M., D.M. Rosen, and P.R. Segarini, *Modulation of Chondroblast Phenotype by Transforming Growth Factor-Beta.* Pathology and Immunopathology Research, 1988. **7**(1-2): p. 38-42.
68. Iwasaki, M., et al., *Transforming Growth-Factor-Beta-1 Stimulates Chondrogenesis and Inhibits Osteogenesis in High-Density Culture of Periosteum-Derived Cells.* Endocrinology, 1993. **132**(4): p. 1603-1608.
69. Kim, S.E., et al., *Porous chitosan scaffold containing microspheres loaded with transforming growth factor-beta 1: Implications for cartilage tissue engineering.* Journal of Controlled Release, 2003. **91**(3): p. 365-374.

70. Rosier, R.N., et al., *Transforming Growth-Factor Beta - an Autocrine Regulator of Chondrocytes.* Connective Tissue Research, 1989. **20**(1-4): p. 295-301.
71. Vivien, D., et al., *Differential-Effects of Transforming Growth-Factor-Beta and Epidermal Growth-Factor on the Cell-Cycle of Cultured Rabbit Articular Chondrocytes.* Journal of Cellular Physiology, 1990. **143**(3): p. 534-545.
72. Tuli, R., et al., *Transforming growth factor-beta-mediated chondrogenesis of human mesenchymal progenitor cells involves N-cadherin and mitogenactivated protein kinase and Wnt signaling cross-talk.* Journal of Biological Chemistry, 2003. **278**(42): p. 41227-41236.
73. Roberts, A.B., et al., *Mesoderm induction in Xenopus laevis distinguishes between the various TGF-beta isoforms.* Growth Factors, 1990. **3**(4): p. 277-86.
74. Ballara, S.C., J.M. Miotla, and E.M. Paleolog, *New vessels, new approaches: angiogenesis as a therapeutic target in musculoskeletal disorders.* Int J Exp Pathol, 1999. **80**(5): p. 235-50.
75. Harada, S., et al., *Induction of Vascular Endothelial Growth-Factor Expression by Prostaglandin E(2) and E(1) in Osteoblasts.* Journal of Clinical Investigation, 1994. **93**(6): p. 2490-2496.
76. Li, J., Y.P. Zhang, and R.S. Kirsner, *Angiogenesis in wound repair: angiogenic growth factors and the extracellular matrix.* Microsc Res Tech, 2003. **60**(1): p. 107-14.
77. Hanahan, D. and J. Folkman, *Patterns and emerging mechanisms of the angiogenic switch during tumorigenesis.* Cell, 1996. **86**(3): p. 353-364.
78. Moses, M.A., et al., *Troponin I is present in human cartilage and inhibits angiogenesis.* Proceedings of the National Academy of Sciences of the United States of America, 1999. **96**(6): p. 2645-2650.
79. Hiraki, Y., et al., *Identification of chondromodulin I as a novel endothelial cell growth inhibitor - Purification and its localization in the avascular zone of epiphysical cartilage.* Journal of Biological Chemistry, 1997. **272**(51): p. 32419-32426.
80. Martelpelletier, J., et al., *Excess of Metalloproteases over Tissue Inhibitor of Metalloprotease May Contribute to Cartilage Degradation in Osteoarthritis and Rheumatoid-Arthritis.* Laboratory Investigation, 1994. **70**(6): p. 807-815.
81. Liu, N.F., et al., *Metastatin: A hyaluronan-binding complex from cartilage that inhibits tumor growth.* Cancer Research, 2001. **61**(3): p. 1022-1028.
82. Feinberg, R.N., C.H. Latker, and D.C. Beebe, *Localized vascular regression during limb morphogenesis in the chicken embryo. I. Spatial and temporal changes in the vascular pattern.* Anat Rec, 1986. **214**(4): p. 405-9.
83. Yin, M. and M. Pacifici, *Vascular regression is required for mesenchymal condensation and chondrogenesis in the developing limb.* Dev Dyn, 2001. **222**(3): p. 522-33.
84. Wilson, D.J., *Development of avascularity during cartilage differentiation in the embryonic limb. An exclusion model.* Differentiation, 1986. **30**(3): p. 183-7.
85. Namba, R.S., et al., *Spontaneous repair of superficial defects in articular cartilage in a fetal lamb model.* J Bone Joint Surg Am, 1998. **80**(1): p. 4-10.
86. Smith, J.O., et al., *Changes in the antiangiogenic properties of articular cartilage in osteoarthritis.* J Orthop Sci, 2003. **8**(6): p. 849-57.
87. Medici, D., et al., *Conversion of vascular endothelial cells into multipotent stem-like cells.* Nature Medicine, 2010. **16**(12): p. 1400-U80.

88. Gamer, L.W., et al., *Gdf11 is a negative regulator of chondrogenesis and myogenesis in the developing chick limb.* Dev Biol, 2001. **229**(2): p. 407-20.
89. Zimmermann, B. and D. Tsambaos, *Evaluation of the sensitive step of inhibition of chondrogenesis by retinoids in limb mesenchymal cells in vitro.* Cell Differ, 1985. **17**(2): p. 95-103.
90. Ashraf, S. and D.A. Walsh, *Angiogenesis in osteoarthritis.* Current Opinion in Rheumatology, 2008. **20**(5): p. 573-580.
91. Fenwick, S.A., P.J. Gregg, and P. Rooney, *Osteoarthritic cartilage loses its ability to remain avascular.* Osteoarthritis Cartilage, 1999. **7**(5): p. 441-52.
92. Imhof, H., et al., *Degenerative joint disease: cartilage or vascular disease?* Skeletal Radiology, 1997. **26**(7): p. 398-403.
93. Pufe, T., et al., *The influence of biomechanical parameters on the expression of VEGF and endostatin in the bone and joint system.* Annals of Anatomy-Anatomischer Anzeiger, 2005. **187**(5-6): p. 461-472.
94. Murata, M., et al., *Distinct signaling pathways are involved in hypoxia- and IL-1-induced VEGF expression in human articular chondrocytes.* Journal of Orthopaedic Research, 2006. **24**(7): p. 1544-1554.
95. Pfander, D., T. Cramer, and B. Swoboda, *Hypoxia and HIF-1 alpha in osteoarthritis.* International Orthopaedics, 2005. **29**(1): p. 6-9.
96. Pufe, T., et al., *Mechanical overload induces VEGF in cartilage discs via hypoxia-inducible factor.* American Journal of Pathology, 2004. **164**(1): p. 185-192.
97. Kubo, S., et al., *Blocking vascular endothelial growth factor with soluble Flt-1 improves the chondrogenic potential of mouse skeletal muscle-derived stem cells.* Arthritis Rheum, 2009. **60**(1): p. 155-65.
98. Sun, X.-D., et al., *Non-viral endostatin plasmid transfection of mesenchymal stem cells via collagen scaffolds.* Biomaterials, 2009. **30**(6): p. 1222-31.
99. Stevens, M.M., et al., *In vivo engineering of organs: the bone bioreactor.* Proc Natl Acad Sci U S A, 2005. **102**(32): p. 11450-5.
100. O'Reilly, M.S., et al., *Endostatin: An endogenous inhibitor of angiogenesis and tumor growth.* Cell, 1997. **88**(2): p. 277-285.
101. Abe, N., et al., *Identification of a Novel Collagen Chain Represented by Extensive Interruptions in the Triple-Helical Region.* Biochemical and Biophysical Research Communications, 1993. **196**(2): p. 576-582.
102. Oh, S.P., et al., *Isolation and Sequencing of Cdnas for Proteins with Multiple Domains of Gly-Xaa-Yaa Repeats Identify a Distinct Family of Collagenous Proteins.* Proceedings of the National Academy of Sciences of the United States of America, 1994. **91**(10): p. 4229-4233.
103. Rehn, M. and T. Pihlajaniemi, *Alpha-1(Xviii), a Collagen Chain with Frequent Interruptions in the Collagenous Sequence, a Distinct Tissue Distribution, and Homology with Type-Xv Collagen.* Proceedings of the National Academy of Sciences of the United States of America, 1994. **91**(10): p. 4234-4238.
104. Marneros, A.G. and B.R. Olsen, *The role of collagen-derived proteolytic fragments in angiogenesis.* Matrix Biology, 2001. **20**(5-6): p. 337-345.
105. Sasaki, T., E. Hohenester, and R. Timpl, *Structure and function of collagen-derived endostatin inhibitors of angiogenesis.* Iubmb Life, 2002. **53**(2): p. 77-84.

106. Kulke, M.H., et al., *Phase II study of recombinant human endostatin in patients with advanced neuroendocrine tumors.* Journal of Clinical Oncology, 2006. **24**(22): p. 3555-3561.
107. Dhanabal, M., et al., *Cloning, expression, and in vitro activity of human endostatin.* Biochemical and Biophysical Research Communications, 1999. **258**(2): p. 345-352.
108. Celik, I., et al., *Therapeutic efficacy of endostatin exhibits a biphasic dose-response curve.* Cancer Res, 2005. **65**(23): p. 11044-50.
109. Yamaguchi, N., et al., *Endostatin inhibits VEGF-induced endothelial cell migration and tumor growth independently of zinc binding.* EMBO J, 1999. **18**(16): p. 4414-23.
110. Sim, B.K., et al., *Zinc ligand-disrupted recombinant human Endostatin: potent inhibition of tumor growth, safety and pharmacokinetic profile.* Angiogenesis, 1999. **3**(1): p. 41-51.
111. Al Ahmad, A., et al., *Endostatin binds nerve growth factor and thereby inhibits neurite outgrowth and neuronal migration in-vitro.* Brain Research, 2010. **1360**: p. 28-39.
112. Nakano-Doi, A., et al., *Bone Marrow Mononuclear Cells Promote Proliferation of Endogenous Neural Stem Cells Through Vascular Niches After Cerebral Infarction.* Stem Cells, 2010. **28**(7): p. 1292-1302.
113. Kim, Y.M., et al., *Endostatin blocks vascular endothelial growth factor-mediated signaling via direct interaction with KDR/Flk-1.* Journal of Biological Chemistry, 2002. **277**(31): p. 27872-27879.
114. Rehn, M., et al., *Interaction of endostatin with integrins implicated in angiogenesis.* Proceedings of the National Academy of Sciences of the United States of America, 2001. **98**(3): p. 1024-1029.
115. Sudhakar, A., et al., *Human tumstatin land human endostatin exhibit distinct antiangiogenic activities mediated by alpha v beta 3 and alpha 5 beta 1 integrins.* Proceedings of the National Academy of Sciences of the United States of America, 2003. **100**(8): p. 4766-4771.
116. Digtyar, A.V., et al., *Endostatin: Current concepts about its biological role and mechanisms of action.* Biochemistry-Moscow, 2007. **72**(3): p. 235-246.
117. Hanai, J., et al., *Endostatin is a potential inhibitor of Wnt signaling.* J Cell Biol, 2002. **158**(3): p. 529-39.
118. Jiang, L., et al., *Intracellular Ca(2+) signaling in endothelial cells by the angiogenesis inhibitors endostatin and angiostatin.* Am J Physiol Cell Physiol, 2001. **280**(5): p. C1140-50.
119. Lee, S.J., et al., *Endostatin binds to the catalytic domain of matrix metalloproteinase-2.* Febs Letters, 2002. **519**(1-3): p. 147-152.
120. Nyberg, P., et al., *Endostatin inhibits human tongue carcinoma cell invasion and intravasation and blocks the activation of matrix metalloprotease-2,-9, and-13.* Journal of Biological Chemistry, 2003. **278**(25): p. 22404-22411.
121. Hanai, J., et al., *Endostatin causes G(1) arrest of endothelial cells through inhibition of cyclin D1.* Journal of Biological Chemistry, 2002. **277**(19): p. 16464-16469.
122. Abdollahi, A., et al., *Endostatin's antiangiogenic signaling network.* Molecular Cell, 2004. **13**(5): p. 649-663.
123. Feng, Y., et al., *Endostatin promotes the anabolic program of rabbit chondrocyte.* Cell Research, 2005. **15**(3): p. 201-206.
124. Sipola, A., et al., *Endostatin inhibits endochondral ossification.* J Gene Med, 2007. **9**(12): p. 1057-64.

125. Herbst, R.S., et al., *Phase I study of recombinant human endostatin in patients with advanced solid tumors.* Journal of Clinical Oncology, 2002. **20**(18): p. 3792-3803.
126. Shuler, F.D., et al., *Increased matrix synthesis following adenoviral transfer of a transforming growth factor beta(1) gene into articular chondrocytes.* Journal of Orthopaedic Research, 2000. **18**(4): p. 585-592.
127. Guo, X.D., et al., *Repair of full-thickness articular cartilage defects by cultured mesenchymal stem cells transfected with the transforming growth factor beta(1) gene.* Biomedical Materials, 2006. **1**(4): p. 206-215.
128. Tong, J.C. and S.L. Yao, *Novel scaffold containing transforming growth factor-beta 1 DNA for cartilage tissue engineering.* Journal of Bioactive and Compatible Polymers, 2007. **22**(2): p. 232-244.
129. Cucchiarini, M., et al., *Improved tissue repair in articular cartilage defects in vivo by rAAV-mediated overexpression of human fibroblast growth factor 2.* Molecular Therapy, 2005. **12**(2): p. 229-238.
130. Madry, H., et al., *Enhanced repair of articular cartilage defects in vivo by transplanted chondrocytes overexpressing insulin-like growth factor I (IGF-I).* Gene Therapy, 2005. **12**(15): p. 1171-1179.
131. Capito, R.M. and M. Spector, *Collagen scaffolds for nonviral IGF-1 gene delivery in articular cartilage tissue engineering.* Gene Therapy, 2007. **14**(9): p. 721-732.
132. Brower-Toland, B.D., et al., *Direct adenovirus-mediated insulin-like growth factor I gene transfer enhances transplant chondrocyte function.* Human Gene Therapy, 2001. **12**(2): p. 117-129.
133. Saraf, A. and A.G. Mikos, *Gene delivery strategies for cartilage tissue engineering.* Advanced Drug Delivery Reviews, 2006. **58**(4): p. 592-603.
134. Goodrich, L.R., et al., *Genetic modification of chondrocytes with insulin-like growth factor-1 enhances cartilage healing in an equine model.* Journal of Bone and Joint Surgery-British Volume, 2007. **89B**(5): p. 672-685.
135. Pagnotto, M.R., et al., *Adeno-associated viral gene transfer of transforming growth factor-beta 1 to human mesenchymal stem cells improves cartilage repair.* Gene Therapy, 2007. **14**(10): p. 804-813.
136. Evans, C.H. and P.D. Robbins, *Possible Orthopedic Applications of Gene-Therapy.* Journal of Bone and Joint Surgery-American Volume, 1995. **77A**(7): p. 1103-1114.
137. Yang, S.Y., et al., *Ex vivo magnetofection with magnetic nanoparticles: A novel platform for nonviral tissue engineering.* Artificial Organs, 2008. **32**(3): p. 195-204.
138. Zuhorn, I.S. and D. Hoekstra, *On the mechanism of cationic amphiphile-mediated transfection. To fuse or not to fuse: Is that the question?* Journal of Membrane Biology, 2002. **189**(3): p. 167-179.
139. Kaul, G., et al., *Local stimulation of articular cartilage repair by transplantation of encapsulated chondrocytes overexpressing human fibroblast growth factor 2 (FGF-2) in vivo.* Journal of Gene Medicine, 2006. **8**(1): p. 100-111.
140. Goessler, U.R., et al., *Perspectives of gene therapy in stem cell tissue engineering.* Cells Tissues Organs, 2006. **183**(4): p. 169-179.
141. Goomer, R.S., et al., *Nonviral in vivo gene therapy for tissue engineering of articular cartilage and tendon repair.* Clinical Orthopaedics and Related Research, 2000(379): p. S189-S200.

142. Goomer, R.S., et al., *High-efficiency non-viral transfection of primary chondrocytes and perichondrial cells for ex-vivo gene therapy to repair articular cartilage defects.* Osteoarthritis and Cartilage, 2001. **9**(3): p. 248-256.
143. Bonadio, J., *Tissue engineering via local gene delivery: Update and future prospects for enhancing the technology.* Advanced Drug Delivery Reviews, 2000. **44**(2-3): p. 185-194.
144. Hung, S.C., et al., *Short-term exposure of multipotent stromal cells to low oxygen increases their expression of CX3CR1 and CXCR4 and their engraftment in vivo.* PLoS ONE, 2007. **2**(5): p. e416.
145. Deininger, M.H., et al., *Endothelial endostatin release is induced by general cell stress and modulated by the nitric oxide/cGMP pathway.* Faseb J, 2003. **17**(10): p. 1267-76.
146. Ghafar, M.A., et al., *Hypoxia and an angiogenic response in the partially obstructed rat bladder.* Lab Invest, 2002. **82**(7): p. 903-9.
147. Macpherson, G.R., et al., *Anti-angiogenic activity of human endostatin is HIF-1-independent in vitro and sensitive to timing of treatment in a human saphenous vein assay.* Mol Cancer Ther, 2003. **2**(9): p. 845-54.
148. Paddenberg, R., et al., *Hypoxia-induced increase of endostatin in murine aorta and lung.* Histochem Cell Biol, 2006. **125**(5): p. 497-508.
149. Wu, P., et al., *Hypoxia down-regulates endostatin production by human microvascular endothelial cells and pericytes.* Biochem Biophys Res Commun, 2001. **288**(5): p. 1149-54.
150. Nasu, K., et al., *Hypoxia simultaneously inhibits endostatin production and stimulates vascular endothelial growth factor production by cultured human endometrial stromal cells.* Fertil Steril, 2004. **82**(3): p. 756-9.
151. Domm, C., et al., *Redifferentiation of dedifferentiated bovine articular chondrocytes in alginate culture under low oxygen tension.* Osteoarthritis and Cartilage, 2002. **10**(1): p. 13-22.
152. Kurz, B., et al., *Tissue engineering of articular cartilage under the influence of collagen I/III membranes and low oxygen tension.* Tissue Engineering, 2004. **10**(7-8): p. 1277-1286.
153. Murphy, C.L. and J.M. Polak, *Control of human articular chondrocyte differentiation by reduced oxygen tension.* Journal of Cellular Physiology, 2004. **199**(3): p. 451-459.
154. Marcus, R.E., *The effect of low oxygen concentration on growth, glycolysis, and sulfate incorporation by articular chondrocytes in monolayer culture.* Arthritis Rheum, 1973. **16**(5): p. 646-56.
155. Lane, J.M., C.T. Brighton, and B.J. Menkowitz, *Anaerobic and aerobic metabolism in articular cartilage.* J Rheumatol, 1977. **4**(4): p. 334-42.
156. Ren, H.Y., et al., *Proliferation and differentiation of bone marrow stromal cells under hypoxic conditions.* Biochemical and Biophysical Research Communications, 2006. **347**(1): p. 12-21.
157. Robins, J.C., et al., *Hypoxia induces chondrocyte-specific gene expression in mesenchymal cells in association with transcriptional activation of Sox9.* Bone, 2005. **37**(3): p. 313-22.
158. Moussavi-Harami, F., et al., *Oxygen effects on senescence in chondrocytes and mesenchymal stem cells: consequences for tissue engineering.* Iowa Orthop J, 2004. **24**: p. 15-20.

159. Rosova, I., et al., *Hypoxic preconditioning results in increased motility and improved therapeutic potential of human mesenchymal stem cells.* Stem Cells, 2008. **26**(8): p. 2173-2182.
160. Samuel, R.E., et al., *Delivery of plasmid DNA to articular chondrocytes via novel collagen-glycosaminoglycan matrices.* Hum Gene Ther, 2002. **13**(7): p. 791-802.
161. Sommer, A. and D.B. Rifkin, *Interaction of Heparin with Human Basic Fibroblast Growth-Factor - Protection of the Angiogenic Protein from Proteolytic Degradation by a Glycosaminoglycan.* Journal of Cellular Physiology, 1989. **138**(1): p. 215-220.
162. Pieper, J.S., et al., *Loading of collagen-heparan sulfate matrices with bFGF promotes angiogenesis and tissue generation in rats.* Journal of Biomedical Materials Research, 2002. **62**(2): p. 185-194.
163. Il Choi, W., et al., *Sustained release of human growth hormone from heparin-based hydrogel.* Biomacromolecules, 2008. **9**(6): p. 1698-1704.
164. Chung, Y.I., G. Tae, and S.H. Yuk, *A facile method to prepare heparin-functionalized nanoparticles for controlled release of growth factors.* Biomaterials, 2006. **27**(12): p. 2621-2626.
165. McGonigle, J.S., et al., *Heparin-regulated delivery of osteoprotegerin promotes vascularization of implanted hydrogels.* Journal of Biomaterials Science-Polymer Edition, 2008. **19**(8): p. 1021-1034.
166. Ricard-Blum, S., et al., *Characterization of endostatin binding to heparin and heparan sulfate by surface plasmon resonance and molecular modeling - Role of divalent cations.* Journal of Biological Chemistry, 2004. **279**(4): p. 2927-2936.
167. Sasaki, T., et al., *Structural basis and potential role of heparin/heparan sulfate binding to the angiogenesis inhibitor endostatin.* Embo J, 1999. **18**(22): p. 6240-8.
168. Faye, C., et al., *The First Draft of the Endostatin Interaction Network.* Journal of Biological Chemistry, 2009. **284**(33): p. 22041-22047.
169. Karumanchi, S.A., et al., *Cell surface glypicans are low-affinity endostatin receptors.* Mol Cell, 2001. **7**(4): p. 811-22.
170. Norrby, K., *Low-molecular-weight heparins and angiogenesis.* Apmis, 2006. **114**(2): p. 79-102.
171. Halfter, W., et al., *Collagen XVIII is a basement membrane heparan sulfate proteoglycan.* Journal of Biological Chemistry, 1998. **273**(39): p. 25404-25412.
172. Salamone, J.C., ed. *Concise Polymeric Materials Encyclopedia.* 1999, CRC Press: Boca Raton.
173. Yannas, I.V., et al., *Design of an Artificial Skin .2. Control of Chemical-Composition.* Journal of Biomedical Materials Research, 1980. **14**(2): p. 107-132.
174. Ellis, D.L. and I.V. Yannas, *Regeneration Templates, Artifical Skin and Nerves.* Polymeric Materials Encyclopedia, ed. J.C. Salamone. 1999, Boca Raton: CRC Press.
175. O'Brien, F.J., et al., *The effect of pore size on cell adhesion in collagen-GAG scaffolds.* Biomaterials, 2005. **26**(4): p. 433-441.
176. Pek, Y.S., et al., *Degradation of a collagen-chondroltin-6-sulfate matrix by collagenase and by chondroitinase.* Biomaterials, 2004. **25**(3): p. 473-482.
177. Anselme, K., H. Petite, and D. Herbage, *Inhibition of Calcification Invivo by Acyl Azide Cross-Linking of a Collagen-Glycosaminoglycan Sponge.* Matrix, 1992. **12**(4): p. 264-273.

178. Pieper, J.S., et al., *Attachment of glycosaminoglycans to collagenous matrices modulates the tissue response in rats.* Biomaterials, 2000. **21**(16): p. 1689-1699.
179. Kim, M., et al., *Heparin-based hydrogel as a matrix for encapsulation and cultivation of primary hepatocytes.* Biomaterials, 2010. **31**(13): p. 3596-3603.
180. Yannas, I.V., et al., *Biologically active collagen-based scaffolds: advances in processing and characterization.* Philosophical Transactions of the Royal Society a-Mathematical Physical and Engineering Sciences, 2010. **368**(1917): p. 2123-2139.
181. San Antonio, J.D., B.M. Winston, and R.S. Tuan, *Regulation of chondrogenesis by heparan sulfate and structurally related glycosaminoglycans.* Dev Biol, 1987. **123**(1): p. 17-24.
182. van Susante, J.L.C., et al., *Linkage of chondroitin-sulfate to type I collagen scaffolds stimulates the bioactivity of seeded chondrocytes in vitro.* Biomaterials, 2001. **22**(17): p. 2359-2369.
183. Kuo, Y.C. and Y.T. Tsai, *Heparin-conjugated scaffolds with pore structure of inverted colloidal crystals for cartilage regeneration.* Colloids and Surfaces B-Biointerfaces, 2011. **82**(2): p. 616-623.
184. Cao, H. and S.Y. Xu, *EDC/NHS-crosslinked type II collagen-chondroitin sulfate scaffold: characterization and in vitro evaluation.* Journal of Materials Science-Materials in Medicine, 2008. **19**(2): p. 567-575.
185. Pfeiffer, E., et al., *The effects of glycosaminoglycan content on the compressive modulus of cartilage engineered in type II collagen scaffolds.* Osteoarthritis Cartilage, 2008. **16**(10): p. 1237-44.
186. Flint, M.H., et al., *The Masson staining of collagen - an explanation of an apparent paradox.* Histochemical Journal, 1975. **7**(6): p. 529-46.
187. Millman, J.R., J.H. Tan, and C.K. Colton, *The effects of low oxygen on self-renewal and differentiation of embryonic stem cells.* Current Opinion in Organ Transplantation, 2009. **14**(6): p. 694-700.
188. Ellis, S.J., et al., *EPR oxygen mapping (EPROM) of engineered cartilage grown in a hollow-fiber bioreactor.* Magn Reson Med, 2001. **46**(4): p. 819-26.
189. Dass, C.R., *Cytotoxicity issues pertinent to lipoplex-mediated gene therapy in-vivo.* Journal of Pharmacy and Pharmacology, 2002. **54**(5): p. 593-601.
190. Vickers, S.M., L.S. Squitieri, and M. Spector, *Effects of cross-linking type II collagen-GAG scaffolds on chondrogenesis in vitro: Dynamic pore reduction promotes cartilage formation.* Tissue Engineering, 2006. **12**(5): p. 1345-1355.
191. Keogh, M.B., F.J. O'Brien, and J.S. Daly, *Substrate stiffness and contractile behaviour modulate the functional maturation of osteoblasts on a collagen-GAG scaffold.* Acta Biomaterialia, 2010. **6**(11): p. 4305-4313.
192. Haugh, M.G., M.J. Jaasma, and F.J. O'Brien, *The effect of dehydrothermal treatment on the mechanical and structural properties of collagen-GAG scaffolds.* Journal of Biomedical Materials Research Part A, 2009. **89A**(2): p. 363-369.
193. Kim, M., et al., *In Vitro Chondrocyte Culture in a Heparin-Based Hydrogel for Cartilage Regeneration.* Tissue Engineering Part C-Methods, 2010. **16**(1): p. 1-10.
194. Bosnakovski, D., et al., *Chondrogenic differentiation of bovine bone marrow mesenchymal stem cells (MSCs) in different hydrogels: Influence of collagen type II extracellular matrix on MSC chondrogenesis.* Biotechnology and Bioengineering, 2006. **93**(6): p. 1152-1163.

195. Noth, U., et al., *Chondrogenic differentiation of human mesenchymal stem cells in collagen type I hydrogels.* Journal of Biomedical Materials Research Part A, 2007. **83A**(3): p. 626-635.
196. Yang, Y.L., S. Motte, and L.J. Kaufman, *Pore size variable type I collagen gels and their interaction with glioma cells.* Biomaterials, 2010. **31**(21): p. 5678-5688.
197. Wallace, D.G. and J. Rosenblatt, *Collagen gel systems for sustained delivery and tissue engineering.* Advanced Drug Delivery Reviews, 2003. **55**(12): p. 1631-1649.
198. Sundararaghavan, H.G., et al., *Genipin-induced changes in collagen gels: Correlation of mechanical properties to fluorescence.* Journal of Biomedical Materials Research Part A, 2008. **87A**(2): p. 308-320.
199. Chvapil, M., et al., *Effect of Collagen Crosslinking on Rate of Resorption of Implanted Collagen Tubing in Rabbits.* Journal of Biomedical Materials Research, 1977. **11**(2): p. 297-314.
200. Bergamini, C.M., *Effects of ligands on the stability of tissue transglutaminase: studies in vitro suggest possible modulation by ligands of protein turn-over in vivo.* Amino Acids, 2007. **33**(3): p. 415-421.
201. Korner, G., et al., *Bovine Aortic Endothelial-Cell Transglutaminase - Enzyme Characterization and Regulation of Activity.* Biochemical Journal, 1989. **262**(2): p. 633-641.
202. Faye, C., et al., *Transglutaminase-2: a new endostatin partner in the extracellular matrix of endothelial cells.* Biochemical Journal, 2010. **427**: p. 467-475.
203. Lorand, L. and R.M. Graham, *Transglutaminases: Crosslinking enzymes with pleiotropic functions.* Nature Reviews Molecular Cell Biology, 2003. **4**(2): p. 140-156.
204. Filiano, A.J., et al., *Transglutaminase 2 protects against ischemic stroke.* Neurobiology of Disease, 2010. **39**(3): p. 334-343.
205. Chau, D.Y.S., et al., *The cellular response to transglutaminase-cross-linked collagen.* Biomaterials, 2005. **26**(33): p. 6518-6529.
206. Aeschlimann, D., et al., *Expression of Tissue Transglutaminase in Skeletal Tissues Correlates with Events of Terminal Differentiation of Chondrocytes.* Journal of Cell Biology, 1993. **120**(6): p. 1461-1470.
207. Borge, L., S. Demignot, and M. Adolphe, *Type II transglutaminase expression in rabbit articular chondrocytes in culture: Relation with cell differentiation, cell growth, cell adhesion and cell apoptosis.* Biochimica Et Biophysica Acta-Molecular Cell Research, 1996. **1312**(2): p. 117-124.
208. Rosenthal, A.K., B.A. Derfus, and L.A. Henry, *Transglutaminase activity in aging articular chondrocytes and articular cartilage vesicles.* Arthritis and Rheumatism, 1997. **40**(5): p. 966-970.
209. Summey, B.T., et al., *Tissue transglutaminase localization and activity regulation in the extracellular matrix of articular cartilage.* Journal of Orthopaedic Research, 2002. **20**(1): p. 76-82.
210. McHale, M.K., L.A. Setton, and A. Chilkoti, *Synthesis and in vitro evaluation of enzymatically cross-linked elastin-like polypeptide gels for cartilaginous tissue repair.* Tissue Engineering, 2005. **11**(11-12): p. 1768-1779.
211. Orban, J.M., et al., *Crosslinking of collagen gels by transglutaminase.* J Biomed Mater Res A, 2004. **68**(4): p. 756-62.

212. Zeugolis, D.I., et al., *An in situ and in vitro investigation for the transglutaminase potential in tissue engineering.* J Biomed Mater Res A, 2010. **92**(4): p. 1310-20.
213. Kashiwagi, T., et al., *Crystal structure of microbial transglutaminase from Streptoverticillium mobaraense.* Journal of Biological Chemistry, 2002. **277**(46): p. 44252-44260.
214. Garcia, Y., et al., *In Vitro Characterization of a Collagen Scaffold Enzymatically Cross-Linked with a Tailored Elastin-like Polymer.* Tissue Engineering Part A, 2009. **15**(4): p. 887-899.
215. Englert, C., et al., *Bonding of articular cartilage using a combination of biochemical degradation and surface cross-linking.* Arthritis Research & Therapy, 2007. **9**(3).
216. Koo, H.J., et al., *Antiinflammatory effects of genipin, an active principle of gardenia.* European Journal of Pharmacology, 2004. **495**(2-3): p. 201-208.
217. Kitano, A., et al., *Genipin suppression of fibrogenic behaviors of the alpha-TN4 lens epithelial cell line.* J Cataract Refract Surg, 2006. **32**(10): p. 1727-35.
218. Lima, E.G., et al., *Genipin enhances the mechanical properties of tissue-engineered cartilage and protects against inflammatory degradation when used as a medium supplement.* Journal of Biomedical Materials Research Part A, 2009. **91A**(3): p. 692-700.
219. Dare, E.V., et al., *Genipin Cross-Linked Fibrin Hydrogels for in vitro Human Articular Cartilage Tissue-Engineered Regeneration.* Cells Tissues Organs, 2009. **190**(6): p. 313-325.
220. Ferretti, M., et al., *Controlled in vivo degradation of genipin crosslinked polyethylene glycol hydrogels within osteochondral defects.* Tissue Engineering, 2006. **12**(9): p. 2657-2663.
221. Sung, H.W., et al., *Feasibility study of a natural crosslinking reagent for biological tissue fixation.* Journal of Biomedical Materials Research, 1998. **42**(4): p. 560-567.
222. Beamish, J.A., et al., *The effects of heparin releasing hydrogels on vascular smooth muscle cell phenotype.* Biomaterials, 2009. **30**(31): p. 6286-6294.
223. Elia, R., et al., *Stimulation of in vivo angiogenesis by in situ crosslinked, dual growth factor-loaded, glycosaminoglycan hydrogels.* Biomaterials, 2010. **31**(17): p. 4630-4638.
224. Jeng, L., B.R. Olsen, and M. Spector, *Engineering Endostatin-Producing Cartilaginous Constructs for Cartilage Repair Using Nonviral Transfection of Chondrocyte-Seeded and Mesenchymal-Stem-Cell-Seeded Collagen Scaffolds.* Tissue Engineering Part A, 2010. **16**(10): p. 3011-3021.
225. Farndale, R.W., D.J. Buttle, and A.J. Barrett, *Improved Quantitation and Discrimination of Sulfated Glycosaminoglycans by Use of Dimethylmethylene Blue.* Biochimica Et Biophysica Acta, 1986. **883**(2): p. 173-177.
226. Kitano, A., et al., *Genipin suppresses subconjunctival fibroblast migration, proliferation and myofibroblast transdifferentiation.* Ophthalmic Research, 2006. **38**(6): p. 355-360.
227. Tesche, F. and N. Miosge, *Perlecan in late stages of osteoarthritis of the human knee joint.* Osteoarthritis Cartilage, 2004. **12**(11): p. 852-62.
228. Harris, E.N., J.A. Weigel, and P.H. Weigel, *The human hyaluronan receptor for endocytosis (HARE/Stabilin-2) is a systemic clearance receptor for heparin.* Journal of Biological Chemistry, 2008. **283**(25): p. 17341-17350.
229. Vilar, R.E., et al., *Nitric oxide degradation of heparin and heparan sulphate.* Biochemical Journal, 1997. **324**: p. 473-479.

230. Raghuvanshi, S., et al., *Mycobacterium tuberculosis evades host immunity by recruiting mesenchymal stem cells.* Proceedings of the National Academy of Sciences of the United States of America, 2010. **107**(50): p. 21653-21658.
231. Fell, H.B., *The histogenesis of cartilage and bone in the long bones of the embryonic fowl.* Journal of Morphology and Physiology, 1925. **40**(3): p. 417-459.
232. Roy, S., *Ultrastructure of Articular Cartilage in Experimental Immobilization.* Annals of the Rheumatic Diseases, 1970. **29**(6): p. 634-&.
233. Langenskiold, A., J.E. Michelsson, and T. Videman, *Osteoarthritis of the Knee in the Rabbit Produced by Immobilization - Attempts to Achieve a Reproducible Model for Studies on Pathogenesis and Therapy.* Acta Orthopaedica Scandinavica, 1979. **50**(1): p. 1-14.
234. Eronen, I., et al., *Glycosaminoglycan Metabolism in Experimental Osteoarthrosis Caused by Immobilization.* Acta Orthopaedica Scandinavica, 1978. **49**(4): p. 329-334.
235. Akeson, W.H., et al., *Collagen Cross-Linking Alterations in Joint Contractures - Changes in Reducible Cross-Links in Periarticular Connective-Tissue Collagen after 9 Weeks of Immobilization.* Connective Tissue Research, 1977. **5**(1): p. 15-19.
236. Salter, R.B., et al., *The Biological Effect of Continuous Passive Motion on the Healing of Full-Thickness Defects in Articular-Cartilage - an Experimental Investigation in the Rabbit.* Journal of Bone and Joint Surgery-American Volume, 1980. **62**(8): p. 1232-1251.
237. Brosseau, L., et al., *Efficacy of continuous passive motion following total knee arthroplasty: A metaanalysis.* Journal of Rheumatology, 2004. **31**(11): p. 2251-2264.
238. Martin-Hernandez, C., et al., *Regenerated Cartilage Produced by Autogenous Periosteal Grafts: A Histologic and Mechanical Study in Rabbits Under the Influence of Continuous Passive Motion.* Arthroscopy-the Journal of Arthroscopic and Related Surgery, 2010. **26**(1): p. 76-83.
239. Nishino, T., et al., *Effect of Gradual Weight-Bearing on Regenerated Articular Cartilage after Joint Distraction and Motion in a Rabbit Model.* Journal of Orthopaedic Research, 2010. **28**(5): p. 600-606.
240. Roth, J.H., H.V. Mendenhall, and G.K. McPherson, *The effect of immobilization on goat knees following reconstruction of the anterior cruciate ligament.* Clin Orthop Relat Res, 1988(229): p. 278-82.
241. Breinan, H.A., et al., *Effect of cultured autologous chondrocytes on repair of chondral defects in a canine model.* J Bone Joint Surg Am, 1997. **79**(10): p. 1439-51.
242. Breinan, H.A., H.P. Hsu, and M. Spector, *Chondral defects in animal models: effects of selected repair procedures in canines.* Clin Orthop Relat Res, 2001(391 Suppl): p. S219-30.
243. Jackson, D.W., et al., *Spontaneous repair of full-thickness defects of articular cartilage in a goat model. A preliminary study.* J Bone Joint Surg Am, 2001. **83-A**(1): p. 53-64.
244. Driesang, I.M. and E.B. Hunziker, *Delamination rates of tissue flaps used in articular cartilage repair.* J Orthop Res, 2000. **18**(6): p. 909-11.
245. Jackson, D.W., et al., *Assessment of donor cell and matrix survival in fresh articular cartilage allografts in a goat model.* J Orthop Res, 1996. **14**(2): p. 255-64.
246. Butnariu-Ephrat, M., et al., *Resurfacing of goat articular cartilage by chondrocytes derived from bone marrow.* Clin Orthop Relat Res, 1996(330): p. 234-43.
247. Athanasiou, K., D. Korvick, and R. Schenck, *Biodegradable implants for the treatment of osteochondral defects in a goat model.* Tissue Engineering, 1997. **3**(4): p. 363-373.

248. Shahgaldi, B.F., et al., *Repair of Cartilage Lesions Using Biological Implants - a Comparative Histological and Biomechanical Study in Goats.* Journal of Bone and Joint Surgery-British Volume, 1991. **73**(1): p. 57-64.
249. Breinan, H.A., et al., *Autologous chondrocyte implantation in a canine model: change in composition of reparative tissue with time.* Journal of Orthopaedic Research, 2001. **19**(3): p. 482-492.
250. Schumacher, B.L., et al., *Immunodetection and partial cDNA sequence of the proteoglycan, superficial zone protein, synthesized by cells lining synovial joints.* Journal of Orthopaedic Research, 1999. **17**(1): p. 110-120.
251. Roberts, S., et al., *Lubricin: Its presence in repair cartilage following treatment with autologous chondrocyte implantation.* Cartilage, 2010. **1**(4): p. 298-305.
252. Swann, D.A., H.S. Slayter, and F.H. Silver, *The Molecular-Structure of Lubricating Glycoprotein-I, the Boundary Lubricant for Articular-Cartilage.* Journal of Biological Chemistry, 1981. **256**(11): p. 5921-5925.
253. Jones, A.R., et al., *Modulation of lubricin biosynthesis and tissue surface properties following cartilage mechanical injury.* Arthritis Rheum, 2009. **60**(1): p. 133-42.
254. Dorotka, R., et al., *Repair of articular cartilage defects treated by microfracture and a three-dimensional collagen matrix.* Biomaterials, 2005. **26**(17): p. 3617-29.
255. Kon, E., et al., *Arthroscopic Second-Generation Autologous Chondrocyte Implantation Compared With Microfracture for Chondral Lesions of the Knee Prospective Nonrandomized Study at 5 Years.* American Journal of Sports Medicine, 2009. **37**(1): p. 33-41.
256. Funayama, A., et al., *Repair of full-thickness articular cartilage defects using injectable type II collagen gel embedded with cultured chondrocytes in a rabbit model.* Journal of Orthopaedic Science, 2008. **13**(3): p. 225-232.
257. Wakitani, S., et al., *Human autologous culture expanded bone marrow mesenchymal cell transplantation for repair of cartilage defects in osteoarthritic knees.* Osteoarthritis and Cartilage, 2002. **10**(3): p. 199-206.
258. Kim, Y.J., et al., *Fluorometric Assay of DNA in Cartilage Explants Using Hoechst-33258.* Analytical Biochemistry, 1988. **174**(1): p. 168-176.
259. Ulbrich, C., et al., *Characterization of Human Chondrocytes Exposed to Simulated Microgravity.* Cellular Physiology and Biochemistry, 2010. **25**(4-5): p. 551-560.
260. Jones, A.R. and C.R. Flannery, *Bioregulation of lubricin expression by growth factors and cytokines.* Eur Cell Mater, 2007. **13**: p. 40-5; discussion 45.
261. Jay, G.D., D.E. Britt, and C.J. Cha, *Lubricin is a product of megakaryocyte stimulating factor gene expression by human synovial fibroblasts.* Journal of Rheumatology, 2000. **27**(3): p. 594-600.
262. Vickers, S.M., *Cell-seeded type II collagen scaffolds for articular cartilage tissue engineering*, in *Mechanical Engineering*. 2007, Massachusetts Institute of Technology: Cambridge. p. 241.
263. Chubinskaya, S., M. Hurtig, and D.C. Rueger, *OP-1/BMP-7 in cartilage repair.* Int Orthop, 2007. **31**(6): p. 773-81.
264. Chubinskaya, S., et al., *Age-related changes in cartilage endogenous osteogenic protein-1 (OP-1).* Biochim Biophys Acta, 2002. **1588**(2): p. 126-34.
265. Chubinskaya, S., et al., *Human articular chondrocytes express osteogenic protein-1.* J Histochem Cytochem, 2000. **48**(2): p. 239-50.

266. Soder, S., et al., *Antisense inhibition of osteogenic protein 1 disturbs human articular cartilage integrity.* Arthritis Rheum, 2005. **52**(2): p. 468-78.
267. Flechtenmacher, J., et al., *Recombinant human osteogenic protein 1 is a potent stimulator of the synthesis of cartilage proteoglycans and collagens by human articular chondrocytes.* Arthritis Rheum, 1996. **39**(11): p. 1896-904.
268. Huch, K., et al., *Effects of recombinant human osteogenic protein 1 on the production of proteoglycan, prostaglandin E2, and interleukin-1 receptor antagonist by human articular chondrocytes cultured in the presence of interleukin-1beta.* Arthritis Rheum, 1997. **40**(12): p. 2157-61.
269. Koepp, H.E., et al., *Osteogenic protein-1 (OP-1) blocks cartilage damage caused by fibronectin fragments and promotes repair by enhancing proteoglycan synthesis.* Inflamm Res, 1999. **48**(4): p. 199-204.
270. Im, H.J., et al., *Inhibitory effects of insulin-like growth factor-1 and osteogenic protein-1 on fibronectin fragment- and interleukin-1beta-stimulated matrix metalloproteinase-13 expression in human chondrocytes.* J Biol Chem, 2003. **278**(28): p. 25386-94.
271. Khalafi, A., et al., *Increased accumulation of superficial zone protein (SZP) in articular cartilage in response to bone morphogenetic protein-7 and growth factors.* J Orthop Res, 2007. **25**(3): p. 293-303.
272. Lee, S.Y., T. Nakagawa, and A.H. Reddi, *Induction of chondrogenesis and expression of superficial zone protein (SZP)/lubricin by mesenchymal progenitors in the infrapatellar fat pad of the knee joint treated with TGF-beta1 and BMP-7.* Biochem Biophys Res Commun, 2008. **376**(1): p. 148-53.
273. Yamane, S. and A.H. Reddi, *Induction of chondrogenesis and superficial zone protein accumulation in synovial side population cells by BMP-7 and TGF-beta1.* J Orthop Res, 2008. **26**(4): p. 485-92.
274. Kuo, A.C., et al., *Microfracture and bone morphogenetic protein 7 (BMP-7) synergistically stimulate articular cartilage repair.* Osteoarthritis Cartilage, 2006. **14**(11): p. 1126-35.
275. Cook, S.D., et al., *Repair of articular cartilage defects with osteogenic protein-1 (BMP-7) in dogs.* J Bone Joint Surg Am, 2003. **85-A Suppl 3**: p. 116-23.
276. Badlani, N., et al., *The protective effect of OP-1 on articular cartilage in the development of osteoarthritis.* Osteoarthritis Cartilage, 2008. **16**(5): p. 600-6.
277. Jelic, M., et al., *Regeneration of articular cartilage chondral defects by osteogenic protein-1 (bone morphogenetic protein-7) in sheep.* Growth Factors, 2001. **19**(2): p. 101-13.
278. Hurtig, M., et al., *BMP-7 protects against progression of cartilage degeneration after impact injury.* J Orthop Res, 2009. **27**(5): p. 602-11.
279. Ripamonti, U., et al., *Complete regeneration of bone in the baboon by recombinant human osteogenic protein-1 (hOP-1, bone morphogenetic protein-7).* Growth Factors, 1996. **13**(3-4): p. 273-89,color plates III-VIII,pre bk.
280. Linde, A. and E. Hedner, *Recombinant bone morphogenetic protein-2 enhances bone healing, guided by osteopromotive e-PTFE membranes: an experimental study in rats.* Calcif Tissue Int, 1995. **56**(6): p. 549-53.
281. Yoshida, K., et al., *Osteoinduction capability of recombinant human bone morphogenetic protein-2 in intramuscular and subcutaneous sites: an experimental study.* J Craniomaxillofac Surg, 1998. **26**(2): p. 112-5.

282. Hayashi, M., et al., *Weekly intra-articular injections of bone morphogenetic protein-7 inhibits osteoarthritis progression.* Arthritis Res Ther, 2008. **10**(5): p. R118.
283. Louwerse, R.T., et al., *Use of recombinant human osteogenic protein-1 for the repair of subchondral defects in articular cartilage in goats.* J Biomed Mater Res, 2000. **49**(4): p. 506-16.
284. Hidaka, C., et al., *Acceleration of cartilage repair by genetically modified chondrocytes over expressing bone morphogenetic protein-7.* J Orthop Res, 2003. **21**(4): p. 573-83.
285. Kong, H.J., et al., *Non-viral gene delivery regulated by stiffness of cell adhesion substrates.* Nat Mater, 2005. **4**(6): p. 460-4.
286. Kong, H.J., S. Hsiong, and D.J. Mooney, *Nanoscale cell adhesion ligand presentation regulates nonviral gene delivery and expression.* Nano Lett, 2007. **7**(1): p. 161-6.
287. Britt, J.C. and S.S. Park, *Autogenous tissue-engineered cartilage - Evaluation as an implant material.* Archives of Otolaryngology-Head & Neck Surgery, 1998. **124**(6): p. 671-677.
288. Abdollahi, A. and J. Folkman, *Evading tumor evasion: Current concepts and perspectives of anti-angiogenic cancer therapy.* Drug Resistance Updates, 2010. **13**(1-2): p. 16-28.

APPENDIX 1: The Biological Response Following Autogenous Bone Grafting for Large Volume Defects of the Knee

The material presented in this appendix was reproduced from the following:

Johnson LL, Jeng L, DeLano MC, Pittsley A, Gottschalk A, Spector M. The biological response following autogenous bone grafting for large volume defects of the knee: Index surgery through 12-21 years follow-up. In review.

Introduction

This report focuses on the biological events following autogenous bone grafting of large volume defects of the knee joint's femoral condyle secondary to osteochondritis dissecans (OCD) and osteonecrosis (ON). At the time this study was initiated the medical literature held no prospect for sustainable cartilage repair and the biological fate of various attempts at cartilage repair remains controversial.[1-7] The surgical treatment in the 1980's for large volume defects of the femoral condyle was a cadaver osteochondral allograft or total knee arthroplasty.[8, 9.]

At that time, physicians and patients were reluctant to consider cadaver allografts due to the unknown risk surrounding the discovery of A.I.D.S. in the early 1980's.[10] Total knee arthroplasty was an emerging technology without long term follow-ups at that time, so patients were reluctant to sacrifice the entire joint for a localized lesion. Most cartilage repair procedures were directed towards the two dimensional superficial loss of the articular cartilage.[11] Subsequently such procedures have been utilized for larger defects.[12-14] In recent years autogenous osteochondral grafts were introduced for large volume defects.[15] However, there are few long term reports of restoration of articular surfaces regardless of the treatment method, and histological studies of such cases are exceedingly rare.

The rationale for this novel approach was based upon past experience in the treatment of OCD. It was known that fixation of an osteochondral fragment without adding an underlying bone graft may fail to unite.[16] This knowledge lead to the use of adjunct autogenous bone grafting under such a lesion to insure union. Subsequently

autogenous bone graft was used as a matrix to fill the void adjacent to a partial OCD fragment replacement. The early positive results led to wider indications for the use of autogenous bone graft to fill large volume osteochondral defects of OCD and ON.

Precedent for neither this novel approach of arthroscopic assisted autogenous bone grafting of large osteochondral defects nor the long term biological outcome of this procedure was known to the authors at the onset. The purpose of this study was to examine the biological fate of autogenous bone grafting of large three dimensional osteochondral defects of the human knee with long term follow-up. It was hypothesized that the autogenous bone graft would integrate and the portion exposed to the articular surface would form fibrocartilage which would endure.

Material and Methods:

This study was initiated before the advent of Institutional Review Board (IRB) jurisdiction in our community. The subsequent clinical and radiological long term follow-up was under Michigan State University IRB approval. Between 9/29/1987 and 8/8/1994 there were fifty-one patients treated with autogenous bone grafting for large volume osteochondral defects. There were three pathological groups: OCD with a partial fragment (n=14); OCD without a fragment (n=13); and ON (n=24). Two patients in the ON group were iatrogenic. One was due to use of laser energy for an arthroscopic chondroplasty and the other was due to leukemia chemotherapy treatment including cortisone.

Patients with OCD and ON of any age, with large volume lesions were included in this study. Those with superficial cartilage lesions or defects of traumatic etiology were excluded. Patients with instability, ankylosis, or severe diffuse degenerative arthritis were excluded. There were twenty-five of the fifty-one patients available for this long term follow-up between twelve and twenty-one years. An electronic medical record existed for every patient. There were seven women and eighteen men in this group. The patients were thirteen to eighty-two years with average of forty-seven years. There were six patients with OCD with partial fragment fixation and eleven patients without a fragment. There were eight patients with ON.

All surgeries were performed by one surgeon. The index surgeries included other procedures; partial meniscectomy (15), abrasion arthroplasty (9), chondroplasty (8), resection osteophytes (2), wide synovectomy (1). The osteochondral crater was arthroscopically cleared of all necrotic tissue and the margins were under cut to physically secure the cancellous grafts. The surgical defects measured between 6-75 cubic centimeters. When present, the back of the hinged fragments of OCD were debrided. All chondral fragments were resected in ON. Twenty-nine percent of the fifty-one patients had an accompanying high tibial osteotomy when the lesion was medial and involved a large surface area and/or when there was a coexisting varus deformity. No osteotomy was performed in the OCD group when a fragment was replaced. Osteotomy was performed on two patients in the OCD group who had no fragment to replace. Forty percent of the twenty five patients in the ON group had associated tibial osteotomy.

The cancellous bone donor site was the proximal tibial metaphysis except in one patient with the largest defects. This patient had bilateral massive defects so it was

necessary to harvest additional cancellous graft from same side iliac crest. The cancellous grafts were held in place until a blood clot was formed.[17] Those patients with the cortical cancellous graft placed by open surgery had cancellous fragments packed adjacent to the interval between the graft and the host. The cortical cancellous grafts were held in place by screw fixation.

The post operative care included two months of non weight bearing ambulation with crutches including intermittent active range of motion exercises. Continuous passive motion was not used in any patient. There were no post operative infections that could have introduced a pathological tissue response.

Patient follow-up was routine on all patients through the first post operative year as well as opportunistic evaluations in the course of their care through six years. There was a hiatus in patient data until this formal follow-up was initiated in 2005. The long term follow-up process for the radiological evaluation was accomplished by tracking patients via the existing office medical records and an Internet search. Some participating patients who live out of state were financially compensated upon request for travel, lodging as well as loss of time off work by private funds. The follow-up radiological evaluations were performed without charge by the Department of Radiology at Michigan State University College of Human Medicine.

Radiological Imaging:

All had pre and post operative plain film radiographs. There were plain film radiological studies through out the course of patient care as well as at the time of the formal follow-up evaluations. The radiological documents included preoperative plain films in all cases taken in five views; bilateral standing AP, standing Rosenberg view,

Merchant view, supine notch view, and lateral. The long term radiological evaluation included the same plain films of both knees. MRI studies were obtained on twenty three patients between twelve and twenty one years. The long term biological fate of the donor and host sites were documented by MRI. One patient with a cardiac pacemaker had a CAT scan. One patient from Columbia, South America was too elderly to travel, but submitted follow-up history EMR modules and plain film x-rays.

Magnetic resonance imaging was performed at 3T, GE Healthcare with a quadrature knee coil. Structural imaging parameters were selected for characterization and differentiation of cartilage, subchondral and cancellous bone and joint fluid using the following sequences: axial proton density (TR 4166 ms/TE 37ms/ETL 20/FOV 14 cm/slice thickness 4 mm/interslice gap 0 mm/512 x 384 matrix), axial fat suppressed T2 (TR 2000 ms/TE 48 ms/ETL 11/FOV 14 cm/slice thickness 4 mm/interslice gap 0 mm/512 x 224 matrix), sagittal proton density (TR 1716 ms/TE 36 ms/ETL 7/FOV 16 cm/slice thickness 3.5 mm/interslice gap 0 mm/512 x 384 matrix), sagittal fat suppressed proton density (TR 1850 ms/TE 31 ms/ETL 7/FOV 16 cm/slice thickness 3.5 mm/interslice gap 0 mm/416 x 320 matrix), coronal proton density (TR 2716 ms/TE 36 ms/ETL 11/FOV 16 cm/slice thickness 3.5 mm/interslice gap 0 mm/512 x 384 matrix), coronal fat suppressed proton density (TR 2216 ms/TE 31 ms/ETL 11/FOV 16 cm/slice thickness 3.5 mm/interslice gap 0 mm/416 x 320 matrix). Imaging assessment of the joint and graft material included evaluation of 1) the presence of the subchondral bone plate, 2) continuity of trabecular bone features between underlying native cancellous bone and graft bone, 3) articular surface continuity over the graft and the adjacent native articular cartilage, 4) the signal characteristics of the graft bone compared to adjacent

native cortical and cancellous bone, and the presence of secondary degenerative changes in the neoarticular surface.

Photographic Documentation:

There was arthroscopic photographic and/or video documentation in all cases which was archived for identification of the site of the lesion and for observation of biological changes. Illustrative intra-operative findings were photographed. Surgical video tapes were saved through the end of this study to provide a means of review and clinical correlation.

Gross Pathology

Second look arthroscopy provided gross pathology inspection on the twenty nine patients at variable intervals for different patients between eight weeks to six years, with one opportunity for second look arthroscopy at twenty years. The gross pathological evidence was gathered during the scheduled screw removal in some cases and opportunistic second look in others. The twenty year follow-up opportunity presented when the patient injured what had been an asymptomatic knee.

Biopsy

There were twenty one post operative biopsies in fifteen patients between eight weeks and twenty years. Accurate targeting of the biopsy site was guided by review of the prior surgery on video tape. The biopsy specimens were taken with a Jamshidi 2 mm

diameter bone marrow biopsy needle. Routine histological preparations with hematoxylin and eosin (H&E) and Safranin-O were performed.

Twenty year biopsy histopathology:

Special attention was given to the twenty year biopsy samples. They were fixed, processed, and embedded in paraffin for microtomy. Sections were stained for hematoxylin and eosin (H&E), Safranin-O, or Masson's Trichrome using standard histological techniques. Sections allocated for immunohistochemical analysis were stained with the following mouse monoclonal antibodies: anti-lubricin (1:4800 dilution, Dr. T. Schmid, Rush University Medical Center, Chicago, Illinois;), anti-type II collagen (CIIC1, 1:20 dilution, Developmental Studies Hybridoma Bank, University of Iowa, Iowa City, IA), and anti-α-smooth muscle actin (SMA) (clone 1A4, 1:400 dilution, Sigma). The immunohistochemical staining was performed using the Dako Autostainer (DakoCytomation, Carpinteria, CA). Deparaffinized and rehydrated sections were digested in 0.1% protease for 40-45 mins to facilitate antibody penetration, followed by quenching of endogenous peroxidase with peroxidase blocking reagent (Dako) for 10 min. Nonspecific binding was blocked by incubation with 5% goat serum for 30 min. The primary antibody was applied at room temperature for 30 min. Negative controls were incubated with a mouse IgG and IgM cocktail (Dako), instead of the primary antibody. Peroxidase-based detection (Dako LSAB-2 System Kit, DakoCytomation, Carpinteria, CA) was used per the manufacturer's instructions. Briefly, sections were incubated with a biotinylated secondary antibody (goat anti-mouse IgG) for 10-15 mins, followed by application of streptavidin-HRP for 10-15 mins. Labeling was developed

with an aminoethyl carbazole (AEC) chromogen for 10 mins. Counterstaining was performed with Mayer's hematoxylin for 1.5 mins followed by application of coverslips.

Results:

The first cases were performed by arthroscopy, cancellous grafting and internal fixation with cannulated screw fixation of the existing partial OCD fragment. (**Fig.1A**) It was observed that the exposed cancellous bone was promptly covered with a blood clot. (**Fig. 1B**) At the time of screw removal there was maturing fibrous tissue on the surface of the autogenous bone graft. (**Fig. 1C**).

Early on it was not known if a subchondral cortical bone plate would develop following large volume cancellous bone grafting. Therefore the surgical approach evolved to open surgery using a cortical cancellous graft for OCD patients who had no fragment and for those with ON. (**Fig. 2**) The donor site included Gerty's tubercle with its convex surface to replicate the femoral condylar geometry.

Subsequently it was learned that the cancellous grafts did develop a subchondral bone plate, so larger defects were treated arthroscopically with multiple fragments of a cancellous graft. (**Fig. 3**) All bone grafts were recessed from the cartilaginous articular surface to be contiguous with the adjacent level of host bone.

Second look arthroscopy at eight weeks were accompanied by opportunistic biopsies of the repaired surfaces of these cases at eight weeks showed gross appearance and histomorphology similar to that observed after abrasion arthroplasty.[18] (**Fig. 1C, 2**) These observations prompted the consideration of autogenous bone graft as a matrix for large osteochondral defects in selected cases of ON and for OCD when the fragment was

absent. This rationale was supported by the recognition that fibrocartilage formed over surgically abraded exposed bone in the arthritic knee survived for two years.[18] It was further reasoned that the autogenous bone grafting method would avoid the risk of disease transmission and the autogenous bone graft matrix would fill the osteochondral defect. It was anticipated that the blood clot of the surface of the graft would convert to fibrocartilage.[17, 18]

The immediate biological response was blood clot formation in and on the autogenous bone graft. (**Fig. 1, 3D**) Opportunistic gross anatomical inspection was possible between eight weeks and twenty years. The regenerated graft surface was contiguous with and sealed to the adjacent normal cartilage, but remained soft to palpation at eight weeks and ten months compared to the adjacent normal articular cartilage. (**Fig. 2 G, 3 F**)

The gross appearance of the cortical-cancellous grafts had similar appearance as the solely cancellous grafts after similar post operative periods. However in the very large lesions the composite tibial and iliac crest graft was not sufficient volume to achieve a congruous articular surface at surgery. The incongruent and flat configuration remained unchanged. (**Fig. 4**) This same patient's biological response to the large bone grafts resulted in post operative loss of range of motion due to adhesions between the graft site and the joint lining. This resulted in two subsequent arthroscopic debridement procedures. Resection of the adhesions resolved the symptoms and restored motion.

A patient with an unsettled medical legal case due to iatrogenic osteonecrosis had two subsequent arthroscopies related to continuing complaints. The second look at six

years showed the gross anatomy to be firm to palpation and congruent with the adjacent surface without apparent pathological explanation for the symptoms. (**Fig. 5**)

The one patient (**Fig. 1**) seen at twenty years after an injury had mild degenerative change throughout the joint as well as the surface of the previous autogenous bone graft site. (**Fig. 1**)

Radiological Follow-up

Twenty five of the fifty one patients were available for radiological follow-up between twelve and twenty one years. During the course of the long term follow up evaluations it was apparent that there was a soft tissue covering seen on MRI over the area of the autogenous bone grafts. (**Fig. 1,2,3,4**) All donor bone sites healed. (**Fig. 6**) Continuity of trabecular bone detail with a smooth transition from graft bone to native cancellous bone was consistent with graft integration. However there were occasionally areas of cystic change seen in the grafts. Bone did not grow out beyond the level of the adjacent cortex. The surface tissue overlying the graft consistently had an MR appearance of intermediate signal intensity between that of joint fluid and meniscus, similar to that of hyaline cartilage remote from the area of grafting. The presence of mild signal heterogeneity in the articular surface on some of the subjects was present and was typical of degenerative change. There was osseous incorporation of the graft material in all groups of patients imaged including those with fixation of the native OCD fragment, combined cortical-cancellous grafts, and those with solely cancellous grafting procedures.

Histological Inspection

At eight weeks the cancellous grafts revealed a fibrovascular reparative tissue, approximately 3 mm in depth, overlying an active bone surface. The articular surface of the tissue, which appeared to be smooth, comprised a thin layer of cells at some locations (**Fig. 1F**). A few cells at the surface appeared rounded in lacunae, in a chondrocytic morphology. The superficial zone of the tissue (**Fig. 1F**) was hypocellular and hypovascular, relative to the underlying reparative tissue. Cells in this fibrocollagenous tissue generally appeared in fibroblast morphology (**Fig. 1F**). The surface region of the biopsy consisted of fibrous tissue, with many elongated, fibroblast-like cells; however, (**Fig. 1F**). The middle zone of the soft tissue portion of the biopsy was hypervascular, with small and large vessels distributed through a dense fibrocollagenous matrix populated with fibroblasts (**Fig. 1G**). In the deep region of the tissue, a transition from fibrous tissue to fibrocartilage was seen, with small but notable areas of rounded cells residing in lacunae within a fibrous matrix (**Fig. 1H**). The reparative tissue was in continuity with the underlying bone (**Fig. 1I**), and its overall appearance was consistent with a reparative response.

Opportunistic biopsy of an autogenous bone graft at 8 weeks revealed a fibrocartilagenous nature. (**Figs. 1F-I**) Similar histological findings were seen in one patient at 2 years. (**Fig. 3G**) The corticocancellous grafts maintained the intact cortex while the all cancellous grafts had no cortical bone at eight weeks. The cancellous grafts subsequently formed a subchondral bone plate as seen on biopsy.

The biopsy at twenty years comprised an osteochondral plug made up of deep zone of hyaline cartilage overlying a calcified cartilage layer and subchondral bone plate (**Fig. 1M**). Fibrocartilage was above the hyaline cartilage, and extended to the surface (**Fig. 1M**). The superficial zone of the plug was irregular with many fissures and areas of fragmentation (**Fig. 1N**). There were fewer cells in the surface zone which was more eosinophilic than the bulk of the cartilage (**Fig. 1N**). Of note was the absence of fibrous scar-like material in the biopsy. The cell number density and organization varied though the cartilaginous zone. Portions of the surface zone were acellular or only sparsely populated by cells (**Fig. 1N**). While cells throughout the section were generally rounded and in lacunae, some cells near the surface of the biopsy section exhibited a smaller fibroblastic appearance. Evidence of cartilage remodeling was noted in the middle of the cartilaginous tissue, where cells were seen in small clusters separated by a thin partition of matrix (**Fig. 1N**). Cells in the deeper areas above the tidemark exhibited a larger rounded morphology, resided within lacunae, and were arranged in a columnar pattern (**Fig. 1M**), characteristic phenotypes of chondrocytes in the deep zone of native articular cartilage. The areas surrounding the chondrocytic cells appeared more basophilic, a common feature of territorial matrix with large amounts of glycosaminoglycans (GAGs). Tidemark remodeling was also observed; the new tidemark could be distinctly seen above the old tidemark. Staining in the area below the tidemark revealed an extracellular matrix consisting of circumferential layers of lamellae, characteristic of bone. Some cells—osteocytes—could be seen in lacunae between the lamellae, while other cells—osteoblasts—could be seen on the surfaces of the bone. Examination of the histological sections by polarized light microscopy to reveal the collagen organization, demonstrated

the more fibrous appearance of the matrix in the fibrocartilaginous zone (**Fig. 1O**) superficial to the hyaline cartilage at the base (**Fig. 1P**). The polarized light microscopy also showed that collagen bundles were aligned perpendicular to the tidemark (**Fig. 1P**). The lamellar organization of the underlying bone was also revealed by polarized light microscopy (**Fig. 1P**).

A large portion of the section stained positive with Safranin-O (**Fig. 1Q**), indicating the presence of sulfated GAGs. The most intense positive staining was distributed as patches in the territorial matrices surrounding the cells in the deeper areas of the cartilaginous tissue (**Fig. 1R**). Generally, staining intensity decreased with increased distance from the cells, and little to no positive staining was seen in the interterritorial regions. Some areas at the surface of the section showed a noticeable decrease in staining intensity compared to the deeper regions, suggesting a lower local concentration of GAG (**Fig. 1Q**). Notably, some of the cells that displayed more of a fibroblastic phenotype were located in areas containing slight amounts of GAG. Closer inspection of the tidemark region revealed that positive staining was located largely above the newly remodeled tidemark (**Fig. 1R**).

The distribution of the staining intensities for type II collagen (**Fig. 1S**) was similar to that seen for Safranin-O. Positive staining was largely seen above the tidemark. Intense positive staining was primarily seen in the territorial matrices of the cells in the region right above the remodeled tidemark, where hyaline cartilage was located. Light to no staining was observed in the interterritorial areas. Staining intensity of the territorial

matrices gradually decreased towards the surface of the tissue section as cell morphology changed from chondrocytic to fibroblastic morphology. Positive staining was localized in the matrix, and no intracellular retention of type II collagen was noted (**Fig. 1T**). The negative controls did not stain for type II collagen.

Masson's trichrome staining revealed the presence of collagen in the majority of the extracellular matrix of the tissue above the tidemark (**Fig. 1U and V**). The bone tissue below the tidemark showed significant staining for cytoplasm, with small amounts of collagen scattered throughout the matrix. The staining pattern of the cartilaginous tissue adjacent to the bone appeared aligned, following the columns of cells and oriented perpendicular to the tidemark, whereas the staining near the surface showed no distinct alignment. Of note was the fact that while the surface of the biopsy tissue showed positive staining for collagen using Masson's trichrome (**Fig. 1U**), very little positive staining for type II collagen was seen in the same area (**Fig. 1V**), suggesting that the collagen located at the surface was primarily type I collagen. This is consistent with the finding that the tissue was fibrocartilaginous at the surface.

Of note was the consistent finding of a thin dense, discrete layer of positive staining for lubricin on the articulating surface of the biopsy section (**Fig. 1 W-Z**). The negative controls did not stain for lubricin. The freshly cut surfaces of the biopsy produced during trimming of the tissue did not stain for lubricin (**Fig. 1X**), indicating that the lubricin surface layer was not edge-effect artifactual staining. The discrete layer of lubricin covered the surfaces of the crevices and fissures through the tissue (**Fig. 1W and Y**) and

was on the surfaces of the fragments of the tissue (**Fig. 1Z**). Significant diffuse staining of the extracellular matrix was also located near the surface to variable depths ranging from 150 to 500 μm below the surface (**Fig. 1W**). Notably, no lubricin staining was seen in the deeper regions of the biopsy section. No detectable intracellular staining was observed.

Discussion

The biological fate of the autogenous bone graft matrix in this study showed integration to the host bone plus long term survival of the newly formed articular surface. The hypothesis was confirmed by planned MRI, opportunistic second look arthroscopy, biopsy, and histomorphological inspection.

Second look arthroscopy with biopsy at various intervals showed the early bone integration. (**Fig. 2,3**) The long term radiological study of the patient with the very large surgical defects showed the retention of the original incongruous contour of the bone graft geometry. (**Fig. 4**) This observation would suggest that future bone grafts for large surface lesions should replicate the normal articular contour, perhaps with use of the convex surface of Gerty's tubercle cortical cancellous graft for large defects.

The biopsies showed the articular surface to be fibrous tissue at eight weeks and conversion to fibrocartilage after several months. (**Fig. 1,2,3,4**) The MRI's showed there was long term maintenance of a soft tissue covering over the entire bone graft. The exact nature was not known until an opportunistic twenty year second look and biopsy

presented in one patient near the end of the follow-up study. (**Fig. 1**) This extensive histological analysis provides a rare opportunity to document the biological events following the use of an autogenous bone graft as matrix for a large volume osteochondral defect of the knee joint femoral condyle. Clinically the patient was asymptomatic for twenty years. The MRI taken prior to the injury showed integration of the bone graft although not completely homogeneous (**Fig 1-J**). Identification of the exact graft site was confirmed by review of the librariedprior surgical video tapes (**Fig. 1-D-E**). The gross anatomy the articular cartilage formation was congruent with the adjacent joint surface at eight weeks and twenty years (**Fig. 1-C, 2-E, 3-E**). The nature of the soft tissue covering of the bone graft identified by MRI was not known until the subsequent opportunistic biopsy (**Fig. 1 M-Z**). This single case showed the soft tissue covering to consist of mix of fibrous and hyaline cartilage despite the presence of subsequent mild diffuse degenerative arthritis as also seen in the remainder of the medial compartment (**Fig 1 O-V**). It was notable that the distribution of the important cartilage lubricating molecule (lubricin) was present on the twenty year biopsy surface (**Fig. 1 X-Z**). There was no intracellular staining of lubricin, suggesting that the possibility that the lubricin may have been produced outside the reparative tissue and diffused from the surrounding synovial fluid, rather than being produced by cells within the tissue itself. However, given the depth of some of the diffuse staining for lubricin in the extracellular matrix (up to 500 μm below the surface), it seems less likely that the molecule would have been absorbed from the joint fluid.

In retrospect it should have not been surprising that fibrocartilage has long term survival potential considering that the fibrocartilagenous meniscus is native to the

synovial joint. The meniscus survives under pressure and shear and provides a gliding surface. It was notable that the distribution of the important cartilage lubricating molecule (lubricin) was present on the twenty year biopsy surface. (**Fig. 1 W-Z**)

Animal studies show a similar biological fate of autogenous bone grafting to large osteochondral defects.[19, 20]

The surgical removal of the OCD fragment has poor outcomes.[21] Therefore the attempts at preservation have included in situ drilling, replacement, screw fixation, osteochondral autografts and allografts. [21-27] Present treatments for osteonecrosis include drilling, cancellous packing, uni-compartmental replacement, tibial osteotomy and total knee arthroplasty. [27-31]

Although various biological matrixes have been proposed in recent years, autogenous bone appears to be a cost effective readily available matrix for large osteochondral defects.[32-34] The autogenous nature removes the risk of complications of the allograft surgery while resulting in a long lasting biological solution for both the bone and articular surface.

The strengths of this report were the prospective design, long term follow-up, the high quality and consistent availability of an electronic medical record, and the archived video tapes for identification of locations of prior surgical sites for correlation with follow up imaging and arthroscopy, and the gross and microscopic pathology provided by opportunistic second look arthroscopy with biopsy. There were pathological studies ranging from eight weeks to twenty years supported by radiological evaluations. The MR examinations were performed with very high in plane resolution of 0.31 x 0.42 mm in the sagittal and coronal planes and 0.27 x 0.36 mm in the axial plane providing excellent

delineation of cartilage features with clear discrimination of articular surface tissue from subchondral bone and articular fluid.

The weaknesses of this study were the non-randomization and historical controls. Gross and microscopic studies were opportunistic and not at planned or staged intervals. There was the absence of cartilage specific MR sequences. The MR imaging for these examinations was a higher resolution version of imaging protocols which were considered advanced at the time our follow up study was initiated. Unfortunately we did not perform quantitative imaging of cartilage in our patients. This study was contemporaneous with the development of glycosaminoglycan imaging with delayed gadolinium enhancement MRI and was before this technique was performed at our institution.[35] Additionally, other measures of cartilage integrity, such as T2 mapping and magnetization transfer imaging, were not performed which may have offered insight into nature of the neoarticular tissue formed over these grafts. These methods may prove beneficial in future follow up assessments as this novel approach to the treatment of large osteochondral defects is further refined.

The clinical results will be the subject of separate report.

References

1. Mankin HJ, The reaction of articular cartilage to injury and osteoarthritis. N. Engl. J. Med., Dec 1974; 291(24):1285-92.
2. Mankin HJ, The reaction of articular cartilage to injury and osteoarthritis. N. Engl. J. Med., Dec 1974; 291(25):1335-40.
3. Mankin, HJ, The response of articular cartilage to mechanical injury. J Bone Bone Joint Surg. Am., Mar **1982**; 64: 460 - 466.
4. Buckwalter, JA, Integration of Science into Orthopaedic Practice: Implications for Solving the Problem of Articular Cartilage Repair
   J. Bone Joint Surg. Am., Apr 2003; 85: 1 - 7.
5. Buckwalter JA, Mankin HJ. Instructional Course Lectures, The American Academy of Orthopaedic Surgeons - Articular Cartilage. Part I: Tissue Design and Chondrocyte-Matrix Interactions. J. Bone Joint Surg. Am., Apr 1997; 79: 600 - 11.
6. Buckwalter JA, Mankin HJ, Instructional Course Lectures, The American Academy of Orthopaedic Surgeons - Articular Cartilage. Part II: Degeneration and Osteoarthrosis, Repair, Regeneration, and Transplantation. J. Bone Joint Surg. Am., Apr 1997; 79: 612 - 32.
7. Jakobsen RB, Engebretsen L, Slauterbeck JR. An analysis of the quality of cartilage repair studies. J. Bone Joint Surg. Am. 87:2232-2239.
8. Gross AE, Gross AE, Kim W, Las Heras F, Backstein D, Safir O, Pritzker KP. Fresh osteochondral allografts for posttraumatic knee defects: long-term follow-up. Clin Orthop Relat Res. 2008 Aug;466(8):1863-70. Epub 2008 May 9.

9. Mont MA, Rifai A, Baumgarten KM, Sheldon M, Hungerford DS. Total knee Arthroplasty for Osteonecrosis. J Bone Joint Surg. Am. Apr 2002; 84:599-603.

10. Gottlieb MS. *Pneumocystis carinii* pneumonia and mucosal candidiasis in previously healthy homosexual men: Evidence of a new acquired cellular immunodeficiency. *New England Journal of Medicine* 1981; 305:1425–1431.

11. Cole GJ, Pascual-Garrido C, Grumet RC. Surgical management of articular cartilage defects in the knee. J. Bone Joint Surg. Am. July 2009; 91:1778-90.

12. Brittberg M, Lindahl A, Nilsson A, Ohlsson C, Isaksson O, Peterson L. Treatment of Deep Cartilage Defects in the Knee with Autologous Chondrocyte Transplantation. N. Engl. J. Med., Oct 1994; 331: 889 - 895.

13. Peterson L, Minas T, Brittberg M, Lindahl A. Treatment of Osteochondritis Dissecans of the knee with autogenous chondrocyte transplantation. Results two to ten years. J Bone Joint Surg. Am. 2003: 85:17-24.

14. Zaslav K, Cole B, Brewster R, DeBerardino T, Farr J, Fowler P, Nissen C. A prospective study of autologous chondrocyte implantation in patients with failed prior treatment for articular cartilage defect of the knee. Results of the study of the treatment of articular repair (STAR) clinical trial. Am. J. Sports Med. , Jan 2009:37(1):42-55.

15. Hangody L, Fules P. Autologous Osteochondral Mosaicplasty for the Treatment of Full-Thickness Defects of Weight-Bearing Joints: Ten Years of Experimental and Clinical Experience. J. Bone Joint Surg. Am., Apr 2003; 85: 25 - 32.

16. Johnson, L. L., Uitvlugt, G., Austin, M. D., Detrisac, D. A., Johnson, C.: Osteochondritis Dissecans of the Knee: Arthroscopic Compression Screw Fixation. Arthroscopy 1990: 6(3):179-189.

17. Johnson, L. L.: Characteristics of Immediate Post-Arthroscopic Blood Clot Formation in the Knee Joint. Arthroscopy 1991; 7(1);14-22.

18. Johnson, L. L.: Arthroscopic Abrasion Arthroplasty Historical and Pathological Perspective: Present Status. Arthroscopy Journal, 2:54-69, 1986.

19. VanDyk GE, Dejardin LM, Flo G, Johnson, LL. Cancellous Bone Grafting of Large Osteochondral Defects: An Experimental Study in Dogs. Arthroscopy 1998;14:311-320.

20. Jackson DW, Lalor PA, Aberman HM, Simon TM. Spontaneous Repair of Full-Thickness Defects of Articular Cartilage in a Goat Model : A Preliminary Study. J. Bone Joint Surg. Am., Jan 2001; 83: 53.

21. Wright RW, McLean M, Matava MJ, Shively RA: Osteochondritis dissecans of the knee: Long-term results of excision of the fragment. Clin Orthop 2004; 424: 239-245.

22. Crawford DC, Safran MR. Osteochondritis Dissecans of the Knee. J. Am. Acad. Ortho. Surg., February 2006; 14: 90 - 100.

23. Mininder S. Kocher, Rachael Tucker, Theodore J. Ganley, and John M. Flynn Management of Osteochondritis Dessicans of the Knee: Current Concepts Review Am. J. Sports Med., Jul 2006; 34: 1181 - 1191.

24. Magnussen RA, Carey JL, Spindler KP. Does Operative Fixation of an Osteochondritis Dissecans Loose Body Result in Healing and Long-Term

Maintenance of Knee Function? Am. J. Sports Med., April 1, 2009; 37(4): 754 - 759.

25. HK Outerbridge, AR Outerbridge, and RE Outerbridge. The use of a lateral patellar autologous graft for the repair of a large osteochondral defect in the knee. J. Bone Joint Surg. Am., Jan 1995; 77: 65 - 72.

26. Emmerson BC, Gortz S, Jamail AA, Chung C, Amiel D, Bugbee WD. Fresh osteochondral allografting in the treatment of osteochondritis dissecans of the femoral chondyle. Am. J. Sports Med. 2007; 35(6): 907-914.

27. Wright JM, Crockett HC, Slawski DP, Madsen MW, Windsor RE. High Tibial Osteotomy. J. Am. Acad. Ortho. Surg., July/August 2005; 13: 279 - 289.

28. Marulanda G, Seyler TM, Sheikh NH, Mont MA. Percutaneous drilling for the treatment of secondary osteonecrosis of the knee. J Bone Joint Surg Br, Jun 2006; 88-B: 740 - 746.

29. Rijnen WHC, Luttjeboer JS, Schreurs BW, Gardeniers JWM. Bone Impaction Grafting for Corticosteroid-Associated Osteonecrosis of the Knee. J. Bone Joint Surg. Am., Nov 2006; 88: 62 - 68.

30. Myers TG, Cui Q. Kuskowski M, Mihalko WM, Saleh KJ. Outcomes of Total and Unicompartmental Knee Arthroplasty for Secondary and Spontaneous Osteonecrosis of the Knee. J. Bone Joint Surg. Am., Nov 2006; 88: 76 - 82.

31. Zywiel MG, McGrath MS, Seylre TM, Marker DR, Bonutti PM, Mont. Osteonecrosis of the knee: a review of three disorders. Orthop Clin North Am, 2009; 40 (2): 193-211.

32. Hak, DJ. The Use of Osteoconductive Bone Graft Substitutes in Orthopaedic Trauma. J. Am. Acad. Ortho. Surg., September 2007; 15: 525 - 536.

33. Marcacci M, Berruto M, Brocchetta D, Delcogliano A, Ghinelli D, Gobbi A, Kon E, Pederzini L, Rosa D, Sacchetti GL, Stefani G, Zanasi S. Articular cartilage engineering with Hyalograft C: 3-year clinical results. Clin Orthop Relat Res, Jun 2005; (435): 96-105.

34. Tognana E, Borrione A, De Luca C, Pavesio A. Hyalograft C: hyaluronan-based scaffolds in tissue-engineered cartilage. Cells Tissues Organs, Jan 2007; 186(2): 97-103.

35. Gillis A, Bashir A, McKeon B, Scheller A, Gray ML, Burstein D. Magnetic resonance imaging of relative glycosaminoglycan distribution in patients with autologous chondrocyte transplants. Invest Radiol. 2001 Dec;36(12):743-8.

Acknowledgement

Colleen Hammond, MSU radiology for coordination of IRB approval and patient scheduling for radiological evaluations while in fact facilitating the completion of this project.

Figure 1: A representative case of a patient with OCD who had screw fixation of a partial fragment plus a cancellous bone graft. This 36 year old man underwent arthroscopic surgery on 8/4/1987 for large volume osteochondral defect secondary to OCD. He had a small fragment remaining that was secured with screw fixation. An autogenous cancellous bone graft from the proximal tibial metaphysis was placed under and adjacent to the fragment.

The long term results of this patient showed the immediate post operative biological events, followed by planned and opportunistic second look arthroscopy and biopsy. He was asymptomatic at 19 years when an MRI was taken as part of the long term clinical followup on this cohort. He subsequently injured his knee that resulted in gross arthroscopic inspection at 20 years with correlated biopsy and extensive histochemical studies of the autogenous bone graft site.

(A) Index surgery showing partial fragment held with a screw and the adjacent exposed cancellous bone graft.

(B) Index surgery showing immediate post operative blood clot formation over the exposed cancellous bone graft.

(C) Eight weeks post op the arthroscopic view showed the fragment, the site of the screw removal as well as the biopsy site.

(D) Twenty years later the arthroscopy showed mild diffuse degenerative arthritis and the healed fragment and previously cancellous bone graft site.

(E) Arthroscopic confirmation of the prior bone graft site shows defect of the twenty year biopsy correlated perfectly with the prior archived video tape location of the graft.

(F) Micrographs of the 8-week biopsy showing the superficial area. Hematoxylin and eosin stain.

(G) Micrograph of the same histological section from the 8-week biopsy as F showing the middle zone. Hematoxylin and eosin stain.

(H) Micrograph of the same histological section from the 8-week biopsy as F showing the deep zone. Hematoxylin and eosin stain.

(I) Micrograph of the same histological section from the 8-week biopsy as F showing the transition to bone. Hematoxylin and eosin stain.

(J) MRI was taken at nineteen years when the patient was asymptomatic and member of a cohort of similar patients undergoing a long term clinical assessment. Sagittal MRI proton density images show incorporation of the cancellous bone graft material and the

thesteochondral fragment into the trabecular architecture of surrounding bone. The osseous component projects beyond the expected subchondral cortical bone plate contour, best seen on the sagittal images with preserved but thinned soft tissue isointense to surrounding cartilage overlying the surgical site 19 years after repair..

(K) Same MRI without fat suppression.

(L) Same MRI with fat suppression.

(M) Photomicrographs of the 20-year biopsy. Longitudinal section through the osteochondral biopsy; FC, fibrocartilage; HC, hyaline cartilage.

(N) Photomicrograph of the surface region of the same biopsy.

(O) Polarized light micrographs showing the collagen organization in the superficial zones. Hematoxylin and eosin staining.

(P) Polarized light micrographs showing the collagen organization in the deep zones of the biopsy. Hematoxylin and eosin staining.

(Q) Light micrograph of Safranin-O stained biopsy sections as seen in the cartilaginous region.

(R) Light micrograph of Safranin O in the tidemark regions. Sections were counterstained with fast green. Immunohistochemical staining of type II collagen (red chromogen) throughout the cartilaginous tissue and in greater detail in the extracellular matrix.

(S) Immunohistochemical staining of type II collagen (red chromogen) throughout the cartilaginous tissue.

(T) Higher magnification light micrographs of immunohistochemical staining of type II collagen in the biopsy sections as seen in greater detail of the extracellular matrix.

(U) Masson's trichrome staining for total collagen seen in global view of the cartilaginous tissue. Collagen, blue; nuclei stained black; and muscle and cytoplasm appeared red.

(V) Closer view of the Masson's trichrome surface staining. Collagen, blue; nuclei stained black; and muscle and cytoplasm appeared red.

(W) Immunohistochemical staining results for lubricin (red chromogen). A discrete layer of lubricin on the surface of the biopsied tissue.

(X) Freshly cut edges of the tissue produced during trimming (arrowheads) did not stain for lubricin.

(Y) Fragments of the surface were all coated with a layer of lubricin.

(Z) Fragments of the surface were all coated with a layer of lubricin.

Figure 2. Representative case of patient with a large defect filled with a cortical cancellous graft: This is a 26 year old male professional baseball player with OCD without a fragment due to previous surgical removal. A cortical cancellous graft from the convex Gerty's tubercle area was placed in the defect to insure presence of a subchondral bone plate.

A. Plain film radiograph shows the preoperative defect on medial femoral condyle.

B. Arthroscopic view of the defect of the left medial femoral condyle

C. Debridement performed by arthroscopy.

D. A Cortical Cancellous bone graft taken from Gerty's tubercle area was placed in the surgically developed defect via arthrotomy and held with a screw. Cancellous bone graft was packed around the main graft to bridge the void as shown here.

E. Gross appearance eight weeks following grafting at time of screw removal. The screw head which was placed by arthrotomy was too posterior for arthroscopic removal. Notice the red-white covering contiguous with the adjacent cartilage.

F. Photomicrograph of biological status of the graft at eight weeks shows a fibrovascular repair on the surface and integration of the bone graft below. Hematoxylin and Eosin X10.

G. An opportunistic second look arthroscopy at 10 months showed a well integrated graft surface still soft to palpation. This opportunity presented during an anesthesia for an opposite side knee meniscectomy.

H. Photomicrograph of the ten month biopsy. Notice the dense fibrocartilage on the surface in the right lower corner of the illustration. Hematoxylin and eosin. X100

I. Photomicrograph of the ten month biopsy. Notice the dense fibrocartilage on the surface to the right side of the illustration. Safranin O X200

J. Standing radiograph at 18 years post op.

K. MRI at 18 years post operation. There is minimal subchondral cystic degeneration within the cortical-cancellous graft. The hypertropic bone at the graft site has an intact soft tissue covering. Sagittal proton density image shows trabecular incorporation with continuity of the subchondral cortical bone.

Figure 3: A representative case of those in whom the defect was filled solely with autogenous cancellous bone. A 24 year old woman who had the large osteochondral defect after fragments of the OCD were removed by two previous arthroscopies.

A: This preoperative plain film reveals the large defect on the medial femoral condyle.

B. Arthroscopic view of the lesion after all soft tissue was debrided and the margins undercut to hold the cancellous bone graft.

C. Arthroscopic view of the cancellous bone graft being packed into the surgically created defect.

D. Arthroscopic view of the grafted area immediately after blood clot formation. After time elapsed for the clot to form the remaining blood was washed from the joint to document this biological event.
E. Arthroscopic view at two years following surgery when patient complained of some swelling in the knee. Notice the integrity of the graft surface and continuity with the adjacent normal cartilage.
F. Arthroscopic view of the graft site at time of the opportunistic biopsy. The subchondral bone is seen exiting the surface at the end of the biopsy needle.
G. Photomicrograph of fibrocartilage surface at 2 years. Notice the lacunae surrounding many of the cells. The cellular pattern is that of fibrocartilage. 100X Safranin O stain.
H. MRI at 16 years shows irregular pattern to the bone integration and soft tissue covering. Coronal proton density image demonstrates incorporation of the cancellous graft into the medial femoral condyle at the site of the defect. There is slight persistent depression of the articular surface at the repair site with intact but somewhat hyperintense surface tissue, likely reflecting some degree of degeneration. With fat suppression on the sagittal image there is mild subchondral edema at the repair site (Figure 3I3). This is supportive of the presence of subsequent degeneration rather than a primary effect of the repair procedure.
I, J, K. Comparison of pre operative (I) and sixteen year post op MRI sagittal proton density (J) and fat suppressed proton density (K) images. Similar location preoperative and sixteen year postoperative images of the osteochondral defect site and subsequent repair show relatively intact overlying cartilage at the repair. Low signal in the femoral condyle on the postoperative scan on the proton density weighted image is consistent with healing and sclerosis. Edema is seen on the fat suppressed sequence.

Figure 4: Representative case of patient with a large osteonecrosis defect. 26 year old man has massive osteonecrosis of both knees and ankles secondary to chemotherapy and cortisone treatment for acute leukemia.

A. The right knee defect was debrided arthroscopically and then opened for bone graft from both tibia and iliac crest because of the large size of the lesion.
B. The paucity of autogenous graft resulted in a flat contour to the surface, not replicating the normal convex femoral condylar geometry.
C: The plain films at 16 years post procedure on the right and 13 years post procedure, patient age 42 years. High tibial closing wedge osteotomies were performed on both sides due to the large size lesion.Medial compartmental degenerative changes are present bilaterally with mild irregularity of the articular surface and maintenance of the joint space. Subchondral mixed sclerotic and lucent regions are present in both medial femoral condyles in areas of incorporated graft material.
D. MRI sixteen years following surgery shows the maintenance of the original flat geometry of the autogenous bone graft. The soft tissue covering the articular surface is similar in signal intensity to the posterior condylar hyaline cartilage and distinct from the fibrocartilage low signal of the meniscus. Osseous signal heterogeneity within the medial condyle on the non-fat suppressed images is consistent with residual sclerosis and healing of the graft material and marrow fat continuity is seen between the graft and the remainder of the condylar marrow. Mild edema is seen anteriorly within the femoral condyle that is likely due to superimposed degenerative change. Coronal images demonstrate the sequellae of osteonecrosis involving both condyles and tibial epiphyseal regions. The articular surfaces of both the operative and nonoperative condyles have similar signal characteristics on the proton density and fat suppressed T2 weighted images.
The soft tissue covering the articular surface is similar in signal intensity to the posterior condylar hyaline cartilage and distinct from the fibrocartilage low signal of the meniscus. Osseous signal heterogeneity within the medial condyle on the non-fat suppressed images is consistent with residual sclerosis and healing of the graft material and marrow fat continuity is seen between the graft and the remainder of the condylar marrow. Mild edema is seen anteriorly within the femoral condyle that is likely due to superimposed degenerative change. Coronal images demonstrate the sequellae of osteonecrosis involving both condyles and tibial epiphyseal regions. The articular surfaces of both the operative and nonoperative condyles have similar signal characteristics on the proton density and fat suppressed T2 weighted images.

Figure 5. Representative case of patient with osteonecrosis. Opportunistic 2nd look arthroscopy at 6 years in medicolegal case showing healed surface, firm to probing. No biopsy was obtained at the time. This was the last arthroscopic view of the biological process during clinical care of this person as he subsequently died of natural causes.

Fig 6: The bone graft donor sites healed in the proximal tibial.

A. The cortex formed over the site of the prior removal of the cortical cancellous graft at Gerty's tubercle as illustrated by these MRI images.

B. The site of the transcutaneous harvest of the tibial metaphysis shows the cortex reformed, but small area of cancellous bone remains void in the central tibia.

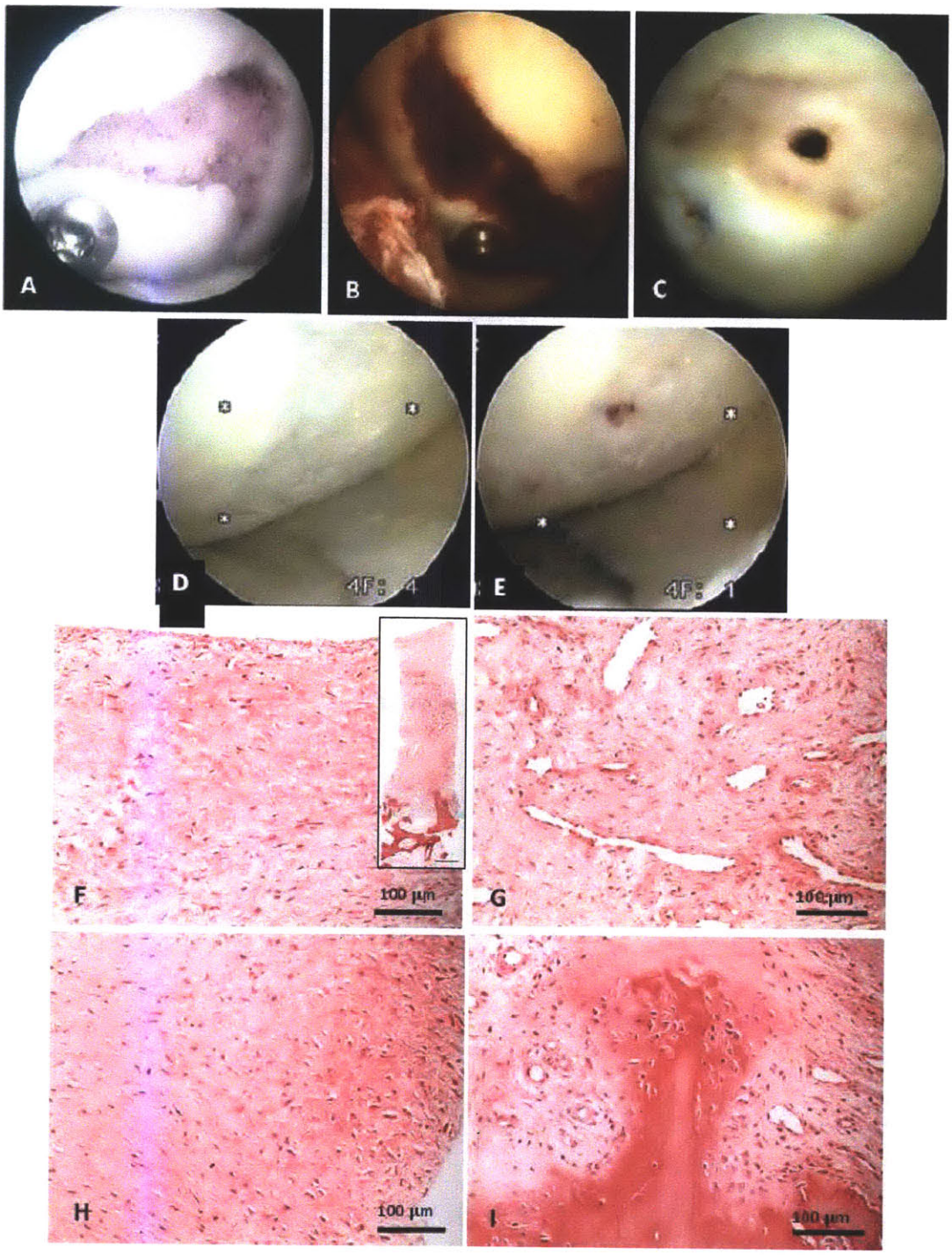

Arthroscopic Documented Biological Events and
Eight Week Histology
123x163mm (150 x 150 DPI)

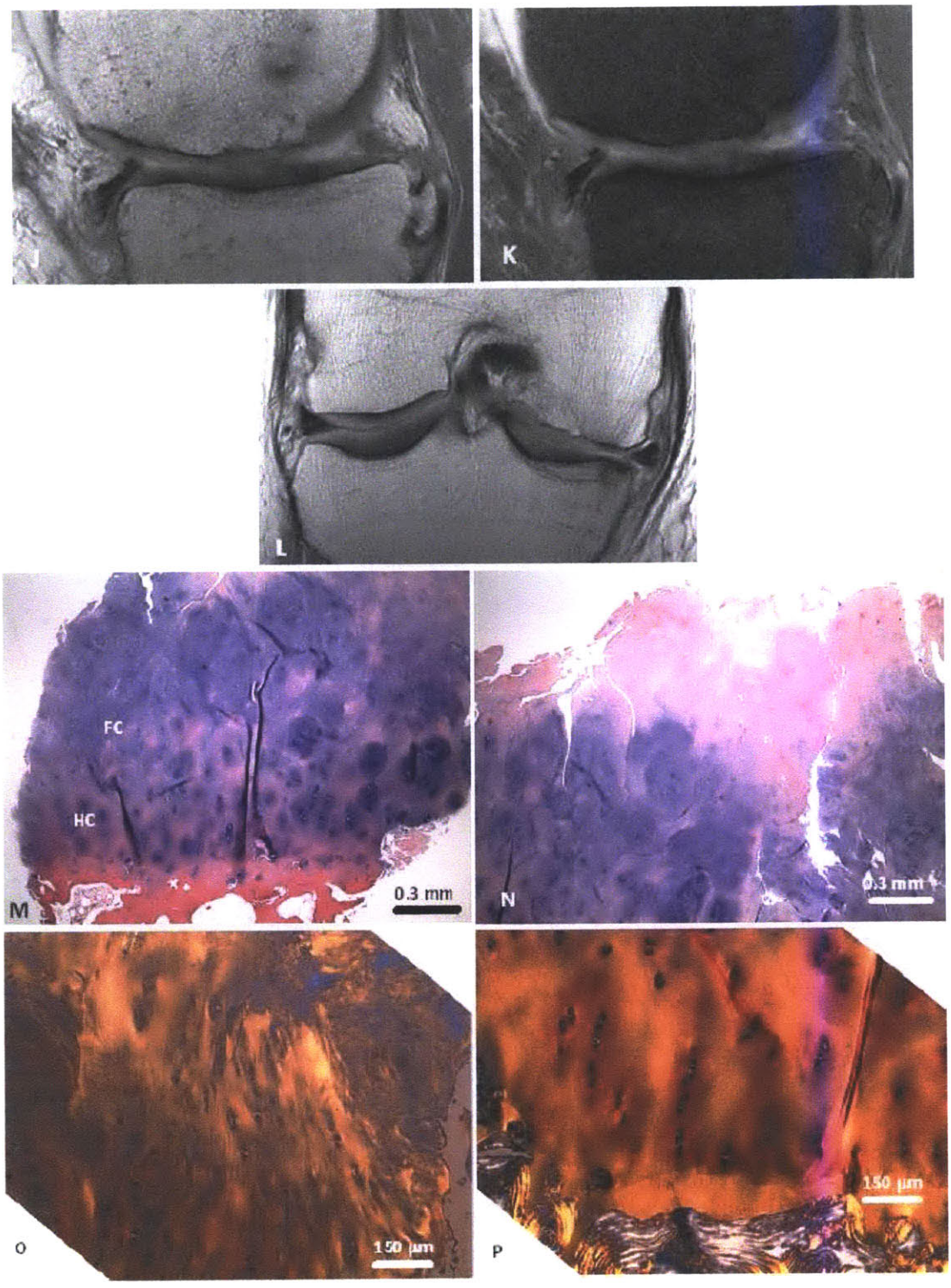

Documentation Long Term Biological Events; MRI and Extensive Histology
118x159mm (150 x 150 DPI)

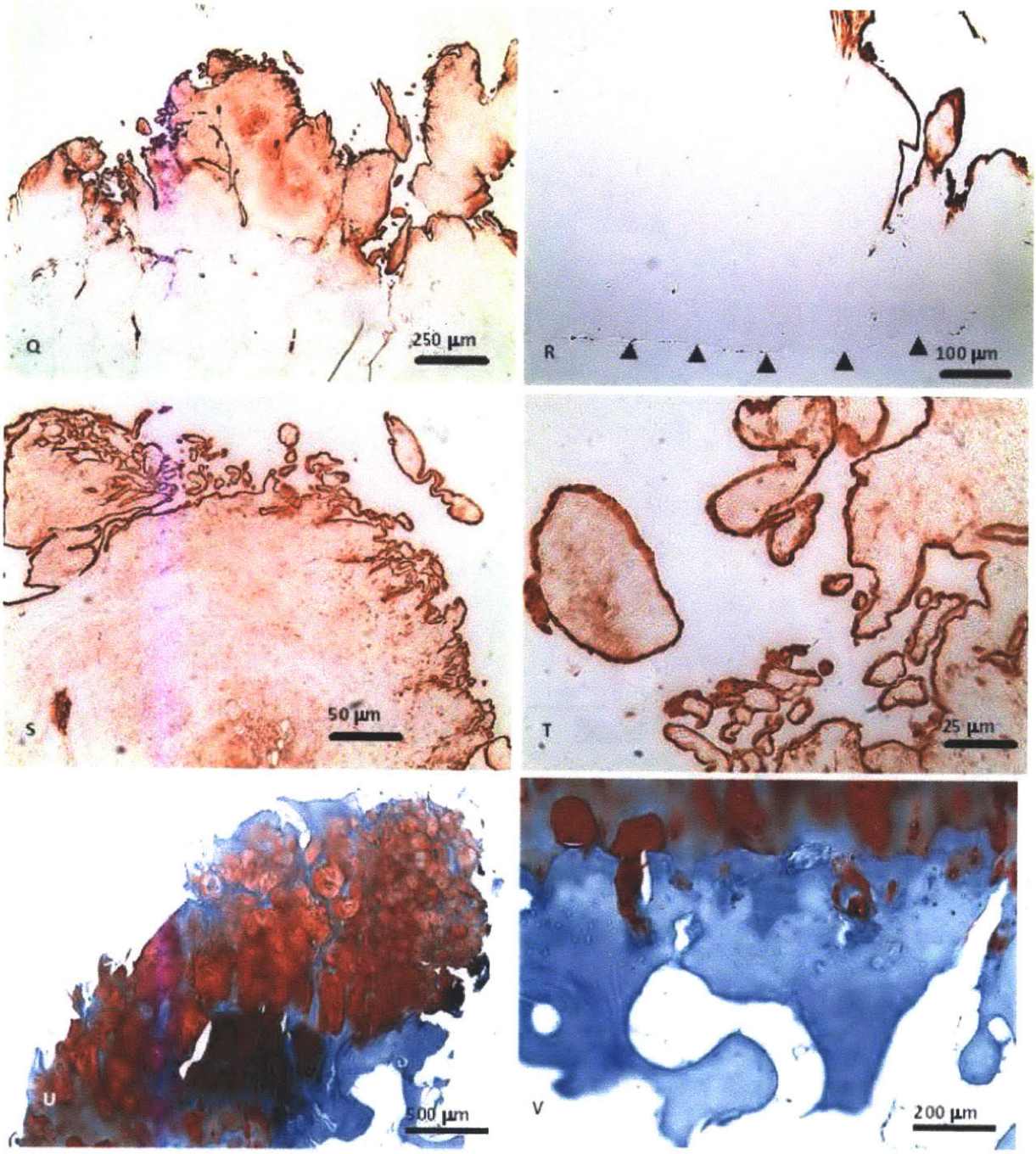

Histochemical Staining
121x135mm (150 x 150 DPI)

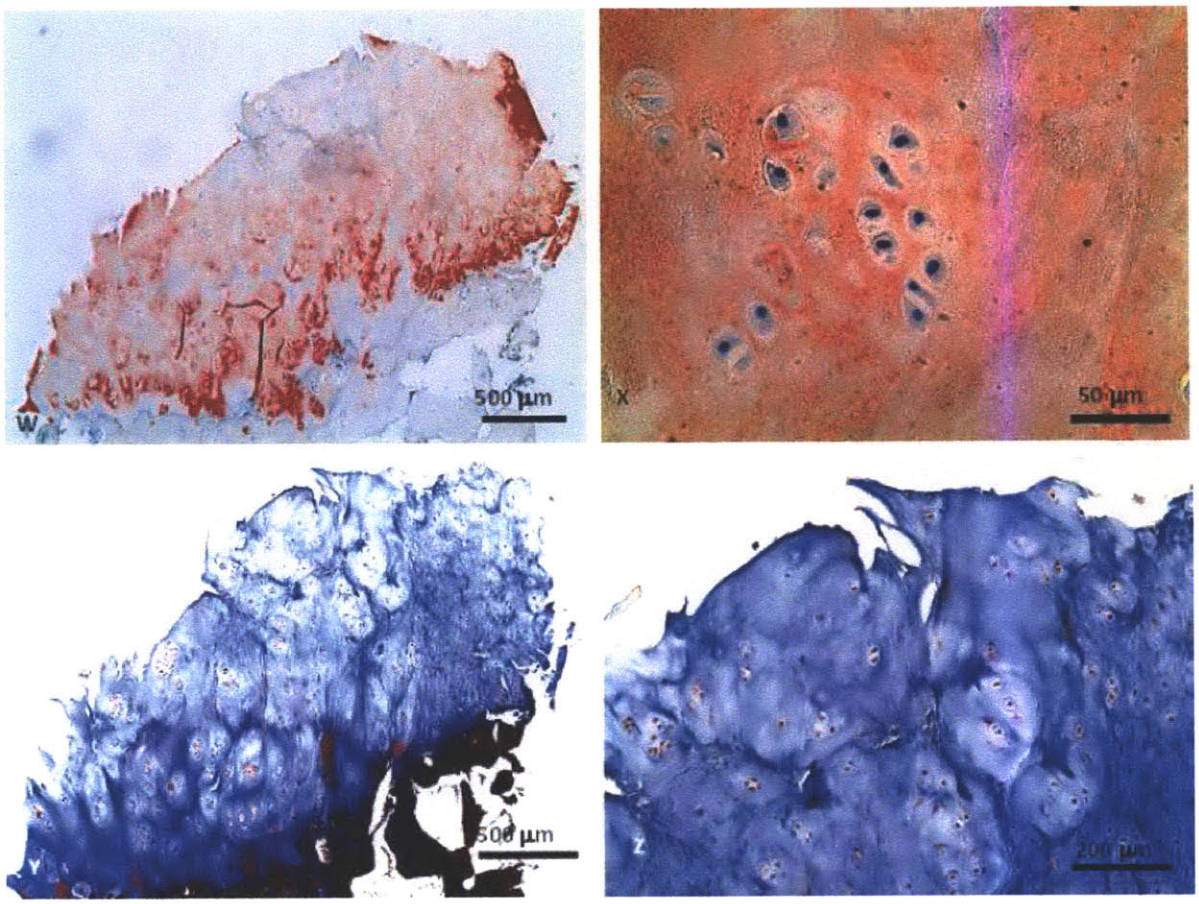

Histochemical Evidence of Lubricin at 20 years
116x87mm (150 x 150 DPI)

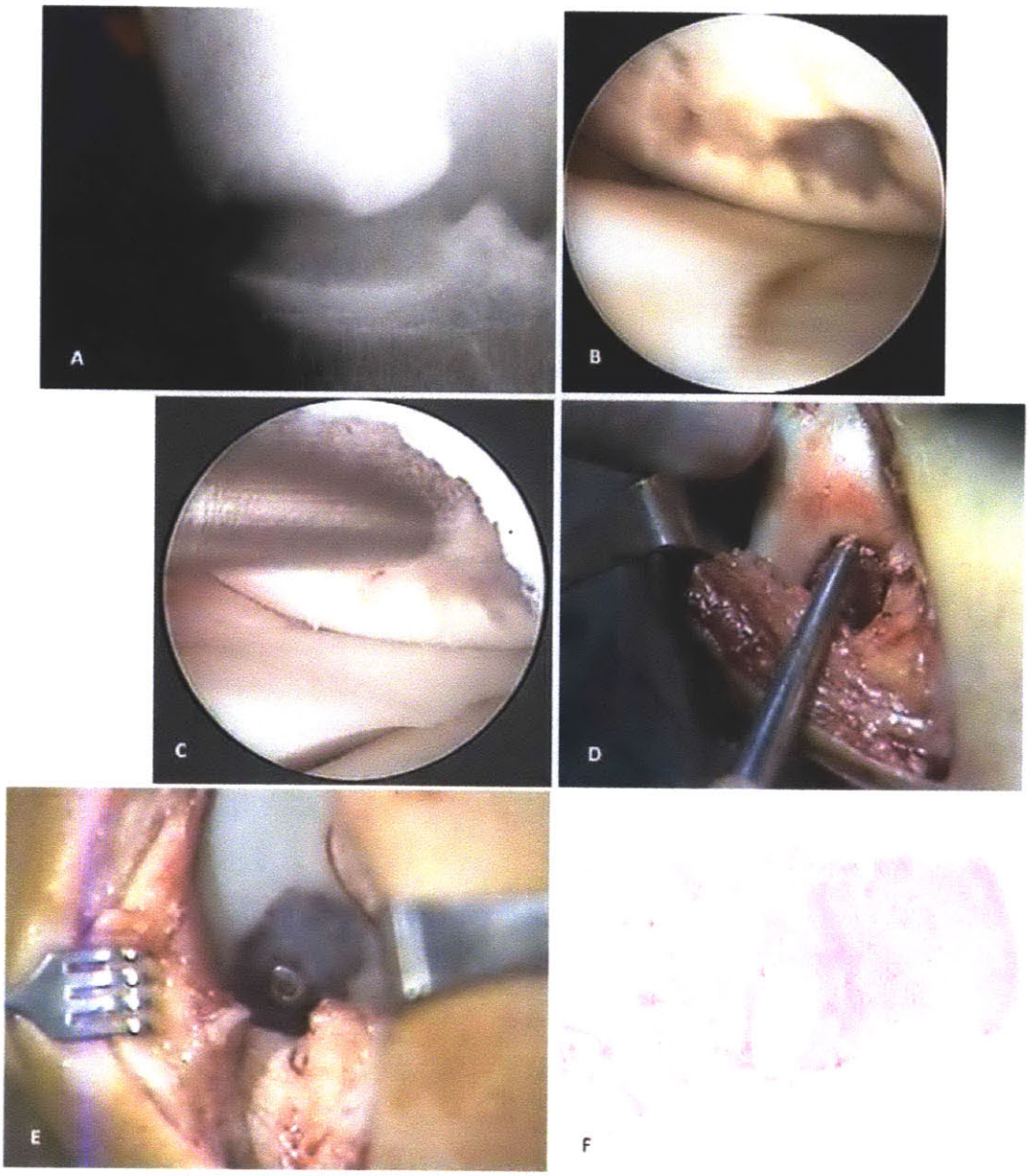

Cortical Cancellous Graft: Preop x-ray, arthrsocopic views, open surgery, 2nd look and 8 week histology.
112x127mm (150 x 150 DPI)

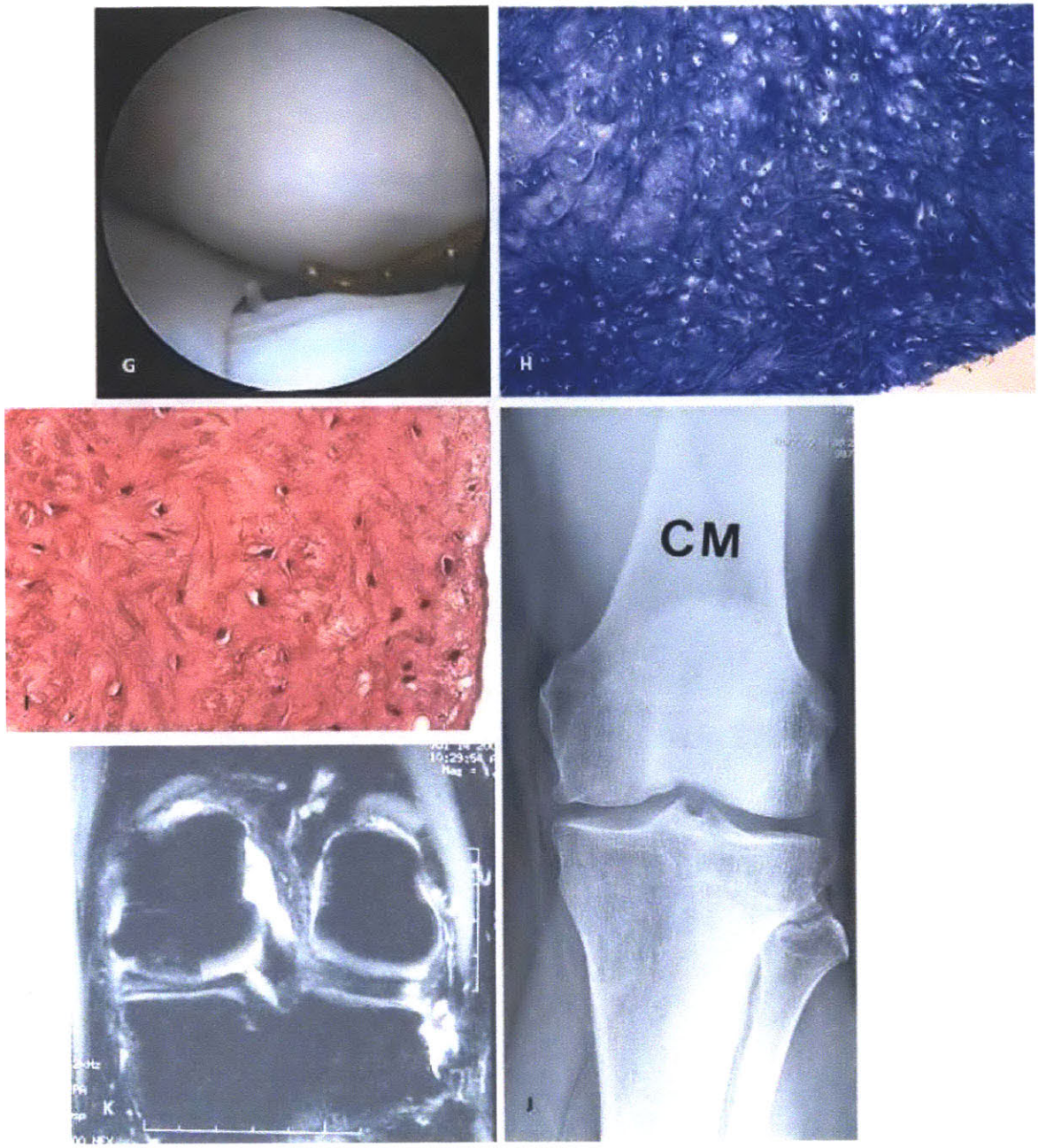

Correlative Documentation: arthroscopic view, 10 month histology, long term radiology.
112x126mm (150 x 150 DPI)

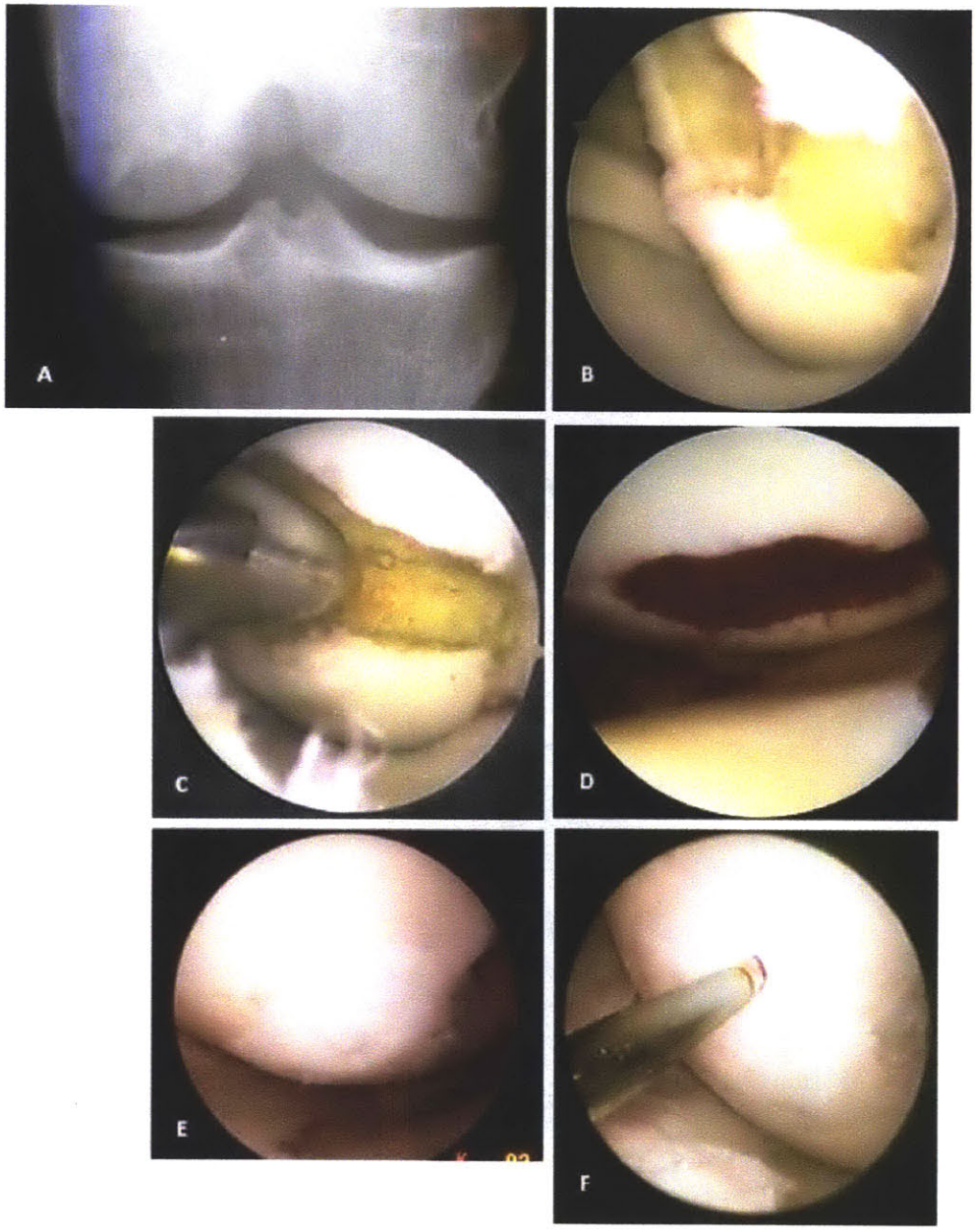

Pre op x-ray, arthroscopic surgery, intitial biological response of blood clost, 2 year second look and biopsy.
94x119mm (150 x 150 DPI)

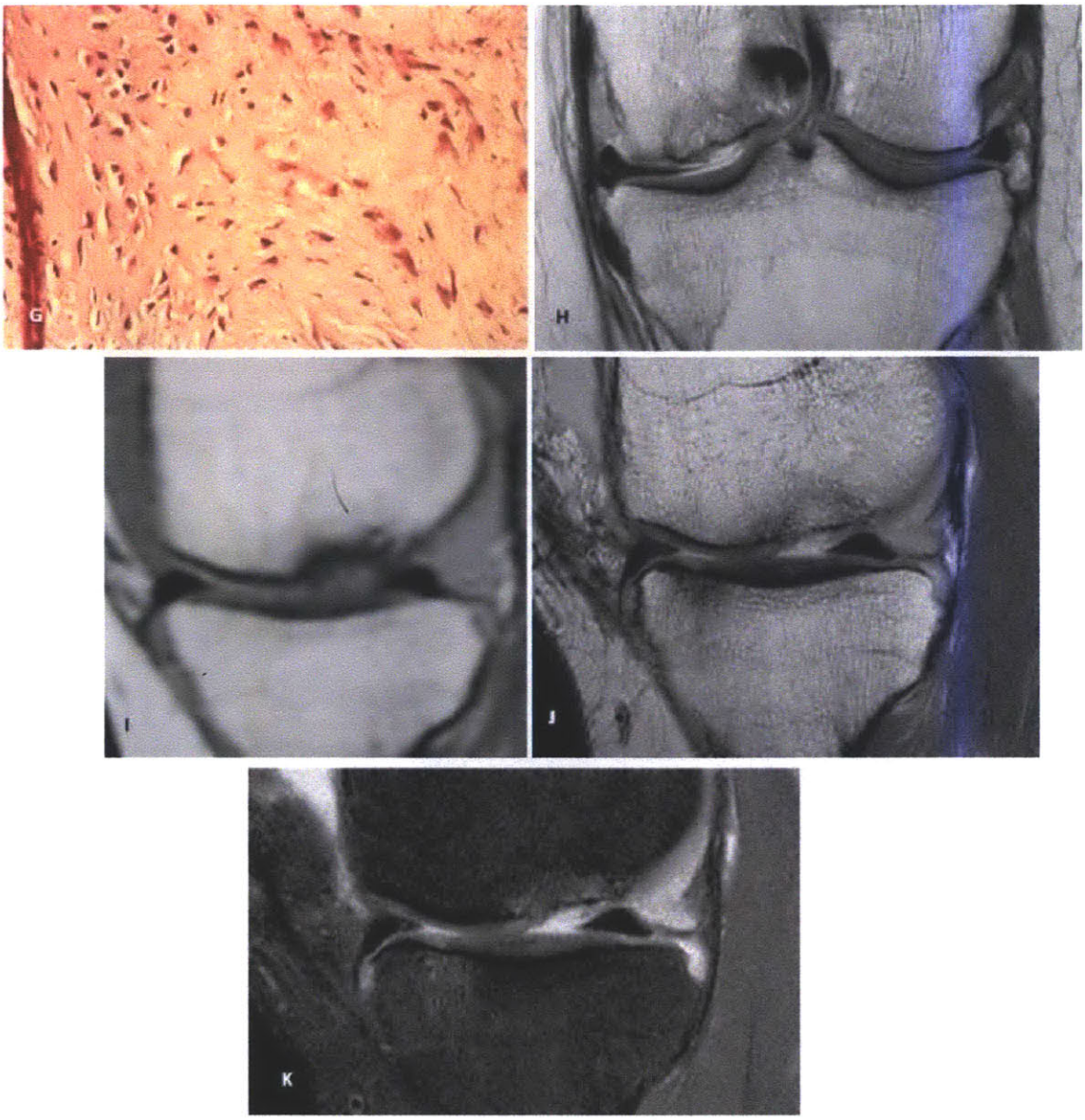

Histology, long term MRI studies.
119x123mm (150 x 150 DPI)

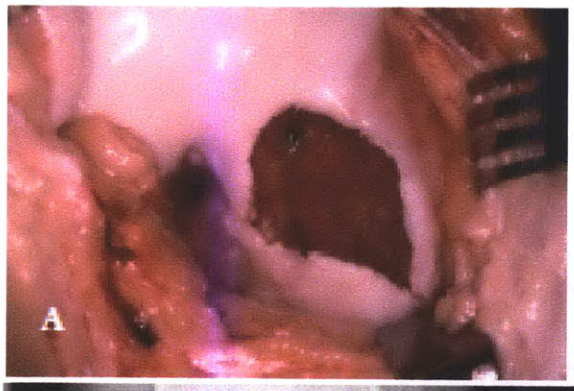
A

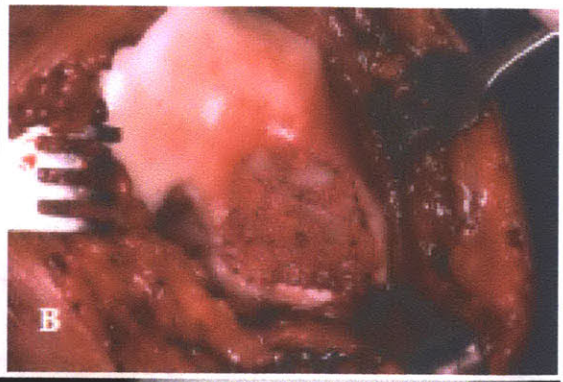
B

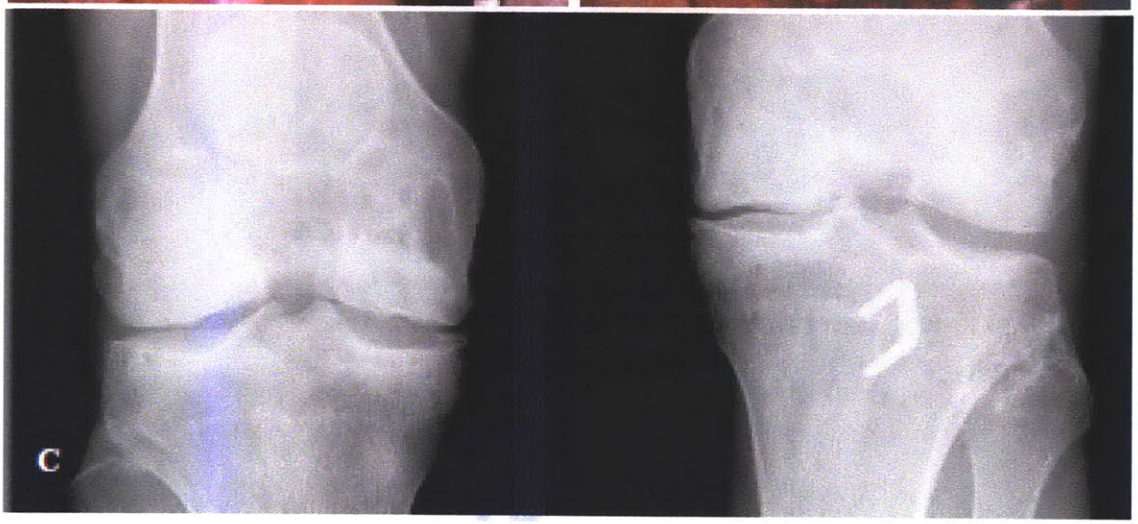
C

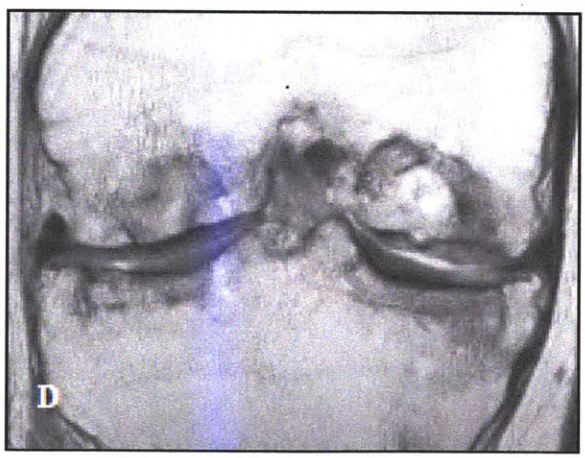
D

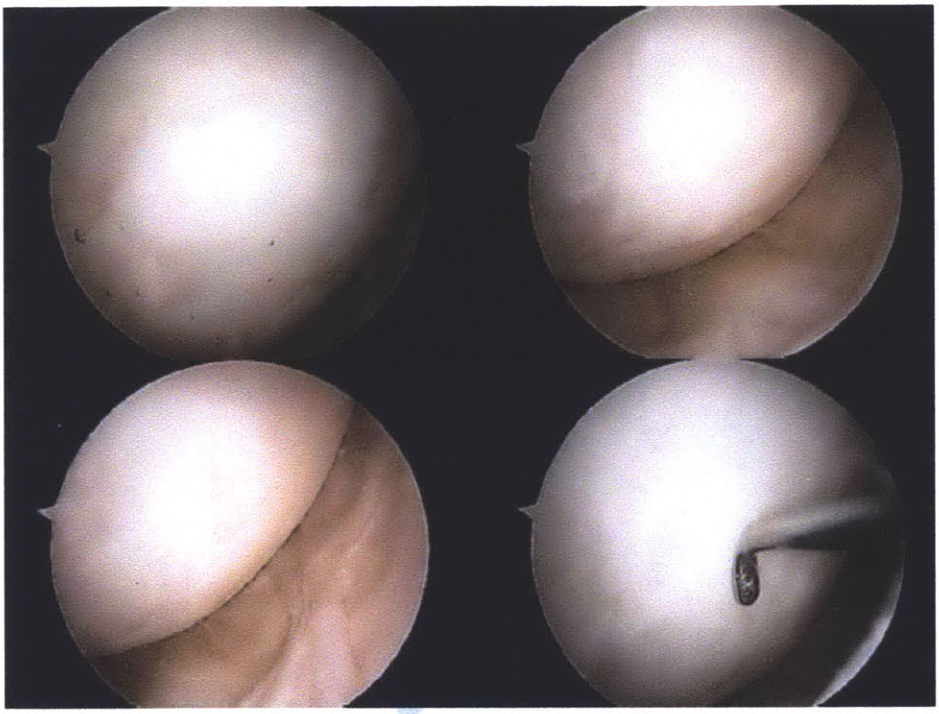

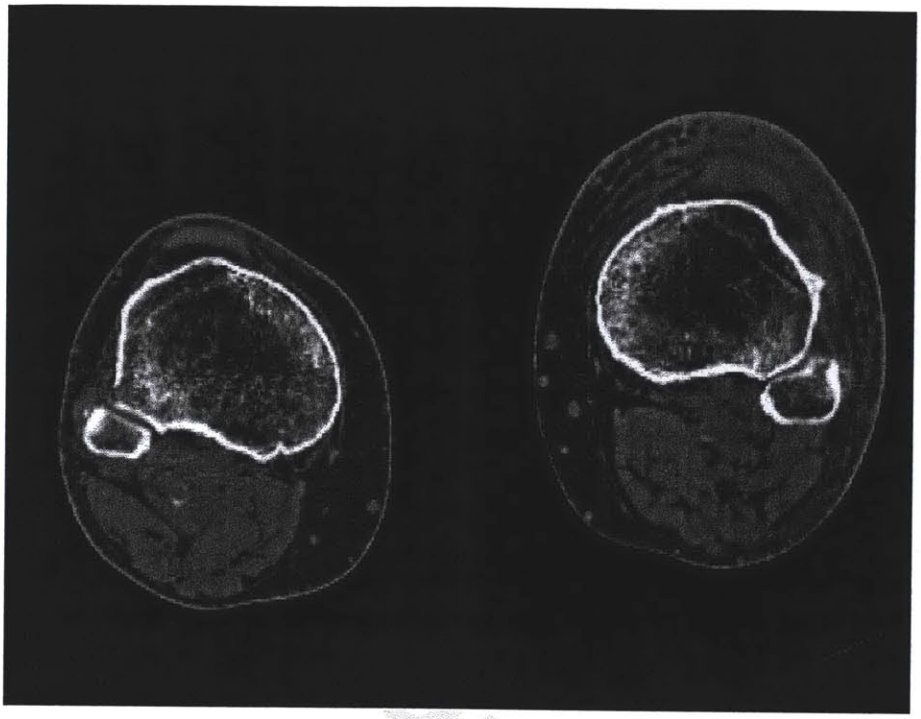

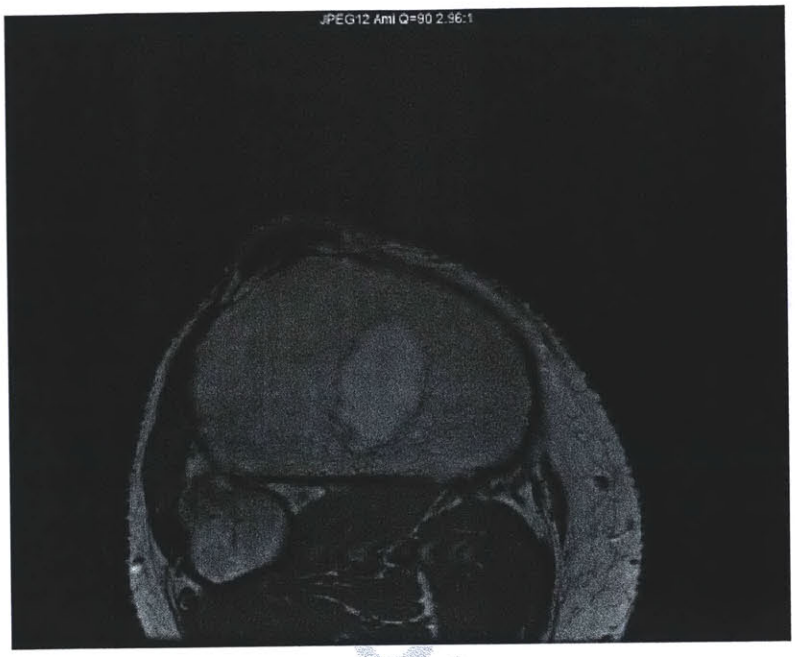

APPENDIX 2: Protocols

Adapted from Spector lab protocols.

Bacterial Transformation and Plasmid Isolation

Materials Needed:

- LB Medium (broth base) (From Invitrogen, Cat#12780-052): follow instructions on bottle, use 2L wide opening; make 4L, parafilm and shake, then foil cover and autoclave tape with a little opening and autoclave (program #2) and cool to room temperature and add Amp and store at room temperature
- LB Agar (From Invitrogen, Cat#22700-025): follow instructions on bottle; use 1L wide opening; plate in petri dishes overnight (store in cold room); make 1/2 L, autoclave (program #2) ~20 mins, then keep at 55°C until use, then add 500ul Carb in 500ml agar and dry in hood if needed and flip upside down to label
- Antibiotic (see chart below)
- Plasmid
- Mega QIAfilter™ Plasmid kit (Qiagen, Cat#12281)

See NE Biolabs website for info on restriction enzymes and buffer to use

TE buffer for plasmid storage:

- 1ml 1M Tris (pH=8) (From Invitrogen, Cat#15568-025)
- 0.2 ml 0.5M EDTA (pH=8) (From Invitrogen, Cat#15575-020)
- 98.8 ml dH_2O

Pouring Plates

1. 100mm tissue plates—cover bottom of plate
2. Spray ethanol on paper town and hold neck when pouring
3. 0.5L agar is enough for about 16 plates
4. Pass flame over agar to get rid of bubbles
5. Solidify for ~1h
6. Turn over and label with Carb
7. Dry and flick off lid
8. Can be stored at 4C for 1 month

Making Pipets for Streaking (if needed)

1. Turn on flame, prepare 400ml beaker with 70% ethanol
2. Seal tip of glass pipet in flame
3. Make 1st bend in glass using flame
4. Make 2nd bend in glass
5. Make sure tip is flat for streaking

Transformation Protocol Using Heat Shock

(Place LB agar plates in warm room)

1. Take competent E.coli cells (DH5α—from Invitrogen, Cat#18258-012, Max Efficiency small box with red lid) from –80C freezer and plasmid and epi tube and thaw them on ice (~20min).
2. Turn on bath to 42C.
3. Put 50ul competent cells in 1.5 ml tube (sterile Eppendorf or similar) for transforming a DNA construct.
4. Keep tubes on ice.
5. Add 0.5ul circular DNA into E.coli cells. Never exceed (1/10) of the total volume. Ideally add 5ul of construct to 50 ul of competent cells. Mix gently by swirling pipette tip in solution (DO NOT pipette up and down).
6. Incubate on ice for 30 min.
7. Put tube(s) with DNA and E.coli into water bath at 42C for 45 seconds.
8. Put tubes back on ice for 2 minutes to reduce damage to the E.coli cells.
9. Add 500 ul of pre-warmed LB (with no antibiotic added) (or SOC that comes with kits of DH5a)
10. Incubate tubes for 1 hour at 37C and shake, up to 300rpm.
11. Dip pipet in ethanol, flame, rub to cool tip before touching bacteria, then quickly spread about 100 ul (can include also a different spread volume on another plate—20 to 200ul) of the resulting culture on LB plates (with appropriate antibiotic added – usually Carb) in hexagon pattern.

12. Grow overnight at 37C in warm room, upside down to prevent condensation from dripping down, no parafilm.
13. Note: when making plates, wait until they are dry before storing in the cold room, or dry in the hood before use.
14. Pick and grow colonies about 12-16 hours later.

Bacterial Growth and Isolation

1. Place 5 ml of LB medium w/ Ampicillin (100ug/ml) in 15ml Flacon (round bottomed) culture tube.
2. Pick swipe of colonies w/ a sterile loop stick and place it in 5 tubes and single snap lid, not double snap (aeration).
3. Spin at 250rpm in the warm room for 6-8hrs (medium should look cloudy when ready).
4. For mega prep, transfer whole contents of 4 tubes into a sterilized 3000ml flask containing 1000ml of LB medium w/ antibiotic. One extra tube can be discarded.
5. Put on shaker (~260rpm—max to prevent severe shaking of bench) overnight.
6. Isolate plasmid w/ Qiagen Plasmid Purification kit (Mega QIAfilter™ Plasmid kit, Cat. 12281). Put RNase and blue dye in buffer 1.
7. Check amount of plasmid isolated w/ spectrophotometer and integrity w/ gel electrophoresis (cutting w/ appropriate restriction enzymes).

Antibiotics Used for GSCG Scaffolds

Antibiotic	Concentration	Storage	Working concentration (dilution)
Carb, 4°C (C9231)	100 mg/ml in water	–20°C	100 µg/ml (500ul of 100 mg/ml in 500ml)
Ampicillin, 4°C (From Sigma Cat#A8351)	100 mg/ml in water	–20°C	100 µg/ml (1/1000)
Kanamycin (From Invitrogen Cat#11815-024)	50 mg/ml in water	–20°C	50 µg/ml (1/1000)

**** Stored in 1ml aliquots at -20C and used 1 tube per 1L LB medium,***

Concentrations of Commonly Used Antibiotics

Antibiotic	Concentration	Storage	Working concentration (dilution)
*Ampicillin (sodium salt)	50 mg/ml in water	–20°C	100 µg/ml (1/500)
Chloramphenicol	34 mg/ml in ethanol	–20°C	170 µg/ml (1/200)
*Kanamycin	10 mg/ml in water	–20°C	50 µg/ml (1/200)
Streptomycin	10 mg/ml in water	–20°C	50 µg/ml (1/200)
Tetracycline HCl	5 mg/ml in ethanol	–20°C	50 µg/ml (1/200)

(From: http://www1.qiagen.com/plasmid/BacterialCultures.aspx?)

Preparing Bottles

13 Nalgene bottles, white lids, rubber gaskets, (4) 50ml grad cylinders, (8) 500ml wide opening Erlenmeyer flasks, (4) 500ml glass bottles, old long tubes, clear lids, normal glass bottle lids

1. Dishwasher first
2. Dry cycle
3. Cover with foil and autoclave

Isolating Plasmid

1. Prepare 6 Nalgene bottles—make sure white lid with autoclaved rubber gasket is sealed
2. Centrifuge (Sorvall RC5B): turn on machine, "DOOR" to open, put in rotor (line up 2 holes with 2 nails), balance bottles, speed 5 (RPM), time 5 min, make sure temperature is between 2 lines (otherwise machine won't start), tighten bottom part of lid 1st, then top pieces, both CCW, then "START"
3. Set up tip columns with blue piece in (4) 500ml Erlenmeyers and 500ml big regular filters on (4) 500ml glass bottles—equilibrate columns with QBT during wait
4. Pour into large Erlenmeyer with pellet on side—bleach and discard
5. Then 6 more bottles to spin (can reuse 2 Nalgenes)

6. 50ml buffer P1 in Nalgene with pellet, vortex to break up pellet, pour into 2nd Nalgene, vortex, 3rd Nalgene, vortex, 4th, vortex
7. 50ml P2 for no more than 5 mins, rock in hands GENTLY
8. 50ml P3 to stop reaction, put on ice until ready for normal filter
9. Normal large filter, 10 min, FWB2 wash buffer, stir, filter
10. Repeat until all 4 Erlenmeyers are centrifuged
11. Pour whole bottle into equil. column, then follow with buffer QC—liquid is ethanol waste, DNA on tip
12. Move tip (with DNA) to clean 500ml Erlenmeyer, then run QF through tip to elute DNA
13. Aliquot each Erlenmeyer into 2 old long plastic tubes, ~17.5ml/tube
14. Make 100ml of 70% ethanol
15. Rinse everything before putting it in dishwasher
16. Add 12.25ml isopropanol/tube
17. Change rotor for Sorvall, 45min, 12 RPM (precool rotor)
18. Beaker, Kimwipes, forceps to extract tubes
19. Decant (pour) isopropanol from tubes, making sure pellet is on the side (do this under bright light to help you see) (Kimwipes to drain upside down a little) (do not vortex/mix/pipet, do not dry entirely)
20. Add 10ml 70% ethanol/tube to wash pellet (do not vortex/mix/pipet, do not dry entirely)
21. 15min, 12 RPM
22. CAREFULLY pour off ethanol, mostly dry
23. 1x Tris EDTA pH 8 (TE), 1ml total to collect all plasmid
24. Put in sterilized epi tube, let it sit in fridge for a few days to really go into solution

Cutting Plasmid and Running Gel

1. Restriction digest:

   10x restriction buffer (buffer 3 for high salt like Not1)→ 1x (5ul)

   10x BSA→ 1x (5ul)

   DNA (last) (want 230ng) (1ul) [1/10, use ~1ul (depends on conc)]

   Water to get to 50ul (39ul)

   Not1 (do not add to uncut tubes)→ 1/2 ul (last)

2. Put mixture in bath at 37C for 1h (compare old plasmid to new and make sure bands run to same place on gel) (DO NOT VORTEX ONCE ENZYME IS ADDED; at most, finger flick to mix)
3. Pour 0.8% gel (Biorad #161-3101 agarose in 1xTBE / 0.5ug/ml EtBr) (to discard EtBr, run through special filter, discard filtered liquid in sink, put filter in SAA)
4. Make 200ml of gel by microwaving agarose 5 min, power 5, small Erlenmeyer in larger Erlenmeyer
5. Use narrow combs (purple), wide side closer to edge, pour gel with NO bubbles, set 1h (pour ~55C), discard gel in SAA when appropriate
6. Prepare 1kb ladder
7. Mix 20ul sample and 5ul orange G dye
8. Turn tray, pour buffer (1xTBE/EtBr) in, take out comb, load ~20ul sample/well and 5ul ladder/well
9. Plug in machine (run to red), constant V, 40mA (35), stop gel when blue ladder is halfway (~1h)

Viewing Gel

1. Make sure top lid up, EtOH filter with camer, gel in box
2. PCImage (may need to right click to open)
3. Acquire New Image
4. Turn on cabinet
5. Click on trans, save
6. To enlarge or reduce, click in/out under preview
7. When done, turn off box and clean

Culture Media

Reconstitution of growth factors

TFG-β1 (R&D 240-B, Recombinant Human)
"Purified recombinant human TGF-β1 is an extremely hydrophobic protein that adheres strongly to surfaces. To ensure recovery, lyophilized samples should be reconstituted with sterile 4mM HCl containing 1mg/ml BSA to a final TGF-β1 concentration of no less than 1μg/ml."

For 10μg of TGF-β1:

- Make 0.1N HCl (add 0.5ml of stock 12.1N HCl to 60.5ml dH_2O)
- Make desired amt. of 4mM HCl (ex. 0.5ml of 0.1N HCl to 12ml dH_2O)
- Add 166.5ul BSA solution (Gibco). Vorex and sterile filter.
- Add 10ml of 4mM HCl+BSA to 10μg TGF-β1 for stock concentration of 1μg/ml.
- Aliquot in sterile microtubes and store at -80°C up to 3 months. Avoid repeated freezing.

FGF-2 (R&D 233-FB, Recombinant Human FGF Basic)
"It is recommended that sterile phosphate-buffered saline containing at least 0.1% BSA be added to the vial to prepare a stock solution of no less than 10μg/ml of the cytokine."

For 25μg of FGF-2

- Add 33.3ul of sterile (7.5% g/ml) BSA to 2.5ml sterile PBS in 15ml Falcon tube
- Sterile filter
- Add 2.5ml of above solution to 25μg FGF-2 for stock concentration of 10μg/ml
- Aliquot in sterile microtubes and store at -80°C up to 3 months. Avoid repeated freezing.

PDGF-ββ (R&D # 220-BB, Recombinant Human)
"It is recommended that sterile 4mM HCl containing at least 0.1% (1mg/ml) BSA be added to the vial to prepare a stock solution of no less than 10μg/ml of the cytokine."

For 10μg of PDFG-ββ

- Make 0.1N HCl (add 0.5ml of stock 12.1N HCl to 60.5ml dH_2O)
- Make desired amt. of 4mM HCl (ex. 0.1ml of 0.1N HCl to 2.4ml dH_2O)
- Add 33.3ul of (7.5% g/ml) sterile BSA to 2.5ml 4mM HCl. Vortex and sterile filter.
- Add 1ml of 4mM HCl+BSA to 10μg PDGF-ββ for stock concentration of 10μg/ml.
- Aliquot in sterile microtubes and store at -80°C up to 3 months. Avoid repeated freezing.

Supplements

Dexamethasone (Dex: Sigma 4902, water soluble)
There is ~65mg dexamethasone per gram of powder. MW of dexamethasone = 392.5g/mol

- Make 10^{-3} M dexamethasone stock solution. Store for 1 year at -20°C.
    - Add 6.03mg Dex. powder to 1ml of 100% ethanol.

- Make 10^{-5} M dexamethasone stock solution in low-glucose (LG) DMEM.
  - Add 20µl of 10^{-3} M Dex. stock to 1.98ml LG-DMEM.
- Aliquot and store at -20°C.

L-Ascorbic acid 2-Phosphate

10µl of a 1/100 dilution of ascorbate 2-phosphate (Wako 013-12061, MW = 289.54g/mol)

- Add 37.5 mg ascorbate 2-phosphate + 10 ml Tyrodes salt solution (Sigma T2397)
  Liquid medium is no longer good if there is a pH change, precipitate or particulate matter throughout the solution, cloudy appearance, or a color change.
- Sterile filter the ascorbate 2-phosphate solution and store frozen in 2ml aliquots

MSC 2-D Expansion Medium: *(add growth factor just prior to use)*

Ingredient	Amount	Notes
DMEM	450ml	Low glucose (LG)
Fetal Bovine Serum (FBS: Gibco 10270-106 or equiv.)	~10%	Add 45ml FBS
PS	1%	Add 5ml
FGF-2 (R&D 233-FB-025)	10ng/ml	Add 1µl stock per 1ml media

Base Medium (Jakob base)

Ingredient	Amount	Notes
DMEM	500ml	High glucose (HG) w/o L-Glutamine
MEM Nonessential Amino Acids (Gibco 11140-050)	5.3ml	
HEPES Buffer (Sigma)	5.3ml	
PSG (Gibco 10378-016)	5.3ml	

Chondrocyte 2-D Expansion Medium

Add the following to 515ml Base Media (add growth factors just prior to use)

Ingredient	Amount	Notes
Fetal Bovine Serum (FBS: Gibco 10270-106 or equiv.)	~10%	Ex., add 50ml FBS to the 515ml base
TGF-β1 (R&D 240-B-002)	1ng/ml	Add 1µl stock per 1ml media

FGF-2 (R&D 233-FB-025)	5ng/ml	Add 0.5µl stock per 1ml media
PDGF-ββ (R&D 220-BB-010)	10ng/ml	Add 1µl stock per 1ml media

Chondrocyte and MSC 3-D Culture / Re-differentiation / Chondrogenic Medium
Add the following to 515ml Base Media (add supplements just prior to use); good for 2 weeks

Ingredient	Amount	Notes
ITS +1 (Sigma #I2521)	5ml	Liquid Media Supplememt (100X)
Bovine Serum Albumin (BSA)	9ml	1.25mg/ml of media
TGF-β1 (R&D 240-B-002)	10ng/ml	Add 10µl stock per 1ml media
Dexamethasone (Sigma)	100nM	Add 10µl stock per 1 ml media
L-Ascorbic acid 2-phosphate	0.1mM	Add 10µl stock per 1 ml media

MSC Harvest and Isolation

Materials

2x 50ml Falcon Tubes (per Goat)
12x 15ml Falcon Tubes (per Goat) (white cap, round bottom Falcon 352059)
1x DMEM-low glucose (Invitrogen cat# 11885-092) Stored in cold room at 4°C
1x FBS 45 ml (heat inactivated) (Invitrogen cat# 16000-044) Stored at -20°C
1x 10 ml Penicillin-Streptomycin (Invitrogen cat# 15140-122) Stored at -20°C
1x Phosphate Buffered Saline (PBS-Invitrogen cat# 14190-250) Stored at 4°C
1x Ficoll-Paque PLUS (GE Life Sciences cat#17-1440-02) Stored at 4°C
1x 20 ml syringe
1x 18 gauge needle
2x Jamshidi Bone Marrow Needles, 8G x 4 inches (10cm) manufacturer cat# DJ4008X Henry Schein cat # 9018239)
3x Heparin Lock Flush Solution 5 ml in 10ml syringe (BD cat# BD306510)
T-150 Culture Flasks (VWR cat# 15705-074)
T-75 Culture Flasks (VWR cat# BD353136)

Expansion Media

Make sterile media in the hood as follows:

- Get one 500 ml bottle of DMEM-low glucose and warm to 37C in the water bath
- Thaw one tube of 45 ml Fetal Bovine Serum and one tube of 10 ml Penicillin-Streptomycin
- Remove 50 ml of DMEM Bottle and save in a 50 ml in the refrigerator (4C)
- To the remaining 450 ml add:
- 45 ml (the whole tube) of FBS
- 5 ml 100X Pen/Strep
- Mix gently by inversion (avoid bubbles)
- Label bottle with date and 10%FBS, 1%P/S, and your name

Isolate MSC enriched Lymphocyte layer from Bone Marrow

- Warm **PBS** and **Ficoll-Paque** PLUS to **room temperature**
- Prepare a 50 ml aliquot of PBS in Falcon tube
- Prepare an 18 ml aliquot of Ficoll into one 50 mL Falcon tube
    - o The Ficoll comes in a bottle with a rubber seal. Take off the white top. Leave the aluminum.
    - o Take a 20 ml syringe and 18 gauge needle and put 5 ml air into the bottle
    - o Remove 18-20 ml into the syringe.
- Remove the needle and push the Ficoll into the 50 ml tube

Prepare the tubes for gradients as follows:

- Take 12 x 15 ml tubes and place in a rack with 6 tubes in front and 6 tubes behind
- Label the front tubes PBS or P and the back tubes Ficoll or F
- Using 1 ml pipetman, aliquot
    - o 2 ml PBS into each P tube (front) and
    - o 3 ml of Ficoll into the F tubes (back)

Note: the Ficoll is viscous so pull up in the 1 ml pipetman slowly

Bring to ARF OR: 2 x 50mL tubes for each goat, Jamshidi bone marrow needles (sterile)

Collect anticoagulated bone marrow from iliac crest placing each side in a tube. Collect no more than 2ml per side into 10ml Heparin containing syringe (Heparin/Bone Marrow Ratio 1:2)

Return to the tissue culture hood:

- Mix the aliquots form both sides into one 50ml Falcon tube
- Take 2 mL of anticoagulant treated blood and add to 2 mL of PBS, mix well
- A good draw will give you 12 mls or 6 tubes of BM+PBS
- Using p1000, **gently and slow** layer the 4 ml BM+PBS onto the 3 ml of Ficoll, don't mix
- This will give you 6 gradients to spin
- Spin in Allegra Tabletop Centrifuge at 3000 rpm, for 30 minutes, at 20C, **decel = 0**
- Label clean 50 mL Falcon tubes (sterile) one per goat
- Remove the gradient from Centrifuge and put back in the hood, **don't shake!**

The top should be a slight reddish color and the bottom should have the red blood cells pelleted

- Take the top 2 ml off with an aspirating pipet. This will take off the sticky white layer at the top containing most of the platelets.
- **DO NOT** come near the interface between plasma and Ficoll gradient
- Take p1000 and remove the whitish band at the interface and put in the 50 ml tube.
- Take two times 1 ml in total from the white layer, above and below

Avoid taking red clotted blood. It may be white, or it may have some red with it. Don't worry about the red. Just collect everything at the interface and make a note of what it looked like.

This is the low density "Lymphocyte layer" containing MSCs, Lymphocytes, Monocytes and some Platelets.

- Transfer all 6 "layers" for 1 animal into one 50 ml tube
- Add PBS to the 50 ml mark
- Invert to mix

Centrifuge 1500 rpm for 10 minutes, **decel = 3**, temp = 20C

- Aspirate supernatant, leaving a little so as not to disturb the pellet.
- Add 5 ml PBS, mix gently but thoroughly with the pipetaid
- Add PBS up to the 50 ml mark

Centrifuge 1500 rpm for 10 minutes, **decel = 3**, temp = 20C

- All Platelets should know be washed out of the cell pellet.
- Resuspend the pellet in 10 ml DMEM-lg, 10%FBS, P/S (at 37C)
- Count 5 ul + 195 ul Trypan Blue (1:40)

Depending on how big the pellet you may want to dilute sample to 15 or 30 ml and then dilute and count the cells. If the draw is good you will get 50-100 million cells.

Plate 50 million P0 cells in a T-75 with 15 ml of expansion media and 100 million cells in a T-150 with 30 ml of DMEM-LG (Density: 600,000 /cm_2)

Leave for 2 days before changing the media for the first time, you should see cells attaching and in a good prep there will be some cells starting to elongate after 2-3 days.

When you change the media, if you see attaching cells, rinse the flask with 37C PBS and then add the new media (also at 37C)

If you don't see attachment, don't rinse, just change the media.

Change the media every 2-3 days

At 80% confluence, freeze P0 cells at 1e6 cells /ml, 500 ul/tube = 5e5

Chondrocyte Harvest and Isolation

Materials

If removing only shavings (eg: for subsequent autologous seeding):
50 ml tubes with PBS
Scalpel handle (#3)
Scalpel blades (2 #10)
Sterile gloves

If removing whole joint
Surgical saw
Sterile specimen bags
Sterile towels/wrap
Sterile PBS to moisten towels
Sterile petri dish (100 mm)
Sterile spatula
Sterile forceps (2)
50ml centrifuge tubes
Small, sterile stir bar
Clean stir plate in incubator
PBS
T-75 and/or T-25 tissue culture flasks
Sterile cutting board

Solutions:

1) Protease solution (20 U/ml), ~ 40ml/2 joints (Sigma protease type XIV P5147)
· Dissolve appropriate amount of protease in media (usually use expansion base medium of DMEM-HG, NEAA, HEPES, PSG, no growth factors, without FBS)

$$pronase(mg) = \frac{V \times 20U/ml}{\#Units/mg\ (4.7)}$$

where V=volume of solution (usually ~ 40ml/2 joints).
· Sterile filter (0.22 μ m) solution (use syringe filter; allow time for protease to dissolve and it may be difficult to pass solution through filter).

2) Collagenase solution (200 U/ml), ~ 40ml/2 joints
· Dissolve appropriate amount of type II collagenase (Worthington Biochemical CLS2) in expansion base without FBS or growth factors (this dissolves quickly)

$$Collagenase(mg) = \frac{V \times 200U/ml}{\#Units/mg\ (varies)}$$

where V = volume of solution.

· Sterile filter solution using a 0.2 μ m syringe filter

Procedure

1. Open joint and remove slices of articular cartilage from joint surfaces. Place in PBS (or in tubes with PBS and store on ice if harvesting in OR).

· *Don't dig into the hard calcified cartilage or subchondral bone. Cartilage should offer little resistance to the blade; full thickness slices should be 0.5-1.5 mm thick depending on joint location*

· *If harvesting whole joint, open joint in sterile hood, cutting ligaments and removing menisci; take cartilage from tibial, femoral and patellar surfaces*

· *If slices are large, cut into pieces no larger than 3x3x1mm*

2. Using forceps and spatula, transfer cartilage pieces into tube/bottle with stir bar and protease solution. ***Cap loosely*** to allow air exchange.

3. Incubate 1hr (37° C, 5% CO_2) on spinner plate.

4. Centrifuge (10min, 1500rpm) the protease and tissue solution, remove the protease, and resuspend pellet
in collagenase solution.

5. Incubate overnight (maybe as short as 4-6 hours until all tissue is digested) on spinner plate. ***Make sure cap is loose***

6. Strain through 70 um pore strainer into new 50ml centrifuge tube.

7. Centrifuge (10 min @ 1500 rpm).

8. Aspirate media and resuspend pellet in complete expansion media with FBS; centrifuge again and resuspend in known amount of complete media to do cell count (usually 10-20ml).

9. Count cells and assess viability (usually 7-8 million cells/joint, >90% viability).

10. Plate freshly harvested cells (P0) in culture flasks, freeze when confluent at 1 ml per 2 million cells.

Passaging Cells

Materials:

Medium with FBS, no growth factors
Trypsin-EDTA
Sterile PBS
0.15 % (0.15g/100ml) collagenase II in sterile PBS
Glass and sterile plastic pipettes
Vacuum setup
Centrifuge tubes
Tissue culture flasks

Methods:

1. Warm the medium, trypsin, and PBS in 37° C water bath.

2. Remove medium from flasks with vacuum pipette (change for different animals), rinse with PBS (3 ml for 5 cm^2, 10 ml for 75 cm^2 flask, 20mL for 150 cm^2) to remove residual medium (trypsin will not detach the cells when in contact with the medium), then remove PBS.

3. Incubate cells with collagenase II solution (5-15 ml for 150 cm^2) for 5 mins.

4. Add trypsin/EDTA (5-15 ml for 150 cm^2) on top of the collagenase II solution already in flask.

5. Place in incubator for 5 more minutes.

6. Remove from incubator and tap on the sides of the flask to loosen the cells. Check under microscope to ensure the cells are no longer attached. If they are, return them to the incubator and check each minute until they are unattached.

7. Once the cells are floating, return to the hood and add medium with FBS to inactivate the trypsin (5-15 ml for 150 cm^2).

8. Using a sterile plastic pipette, transfer the cell suspension to a centrifuge tube (You can combine the contents of flasks from the same animal).

9. Balance the tubes and centrifuge at 1500 rpm for 10 minutes.

10. Once you have the cell pellet at the tube bottom, vacuum pipette off the medium.

11. Resuspend and count the cells (in about 1 ml for each million cells you think you have). While counting, centrifuge the cell suspension a second time to remove all trypsin.

12. Remove medium from second centrifugation and resuspend at desired density.

Cell Counting

Materials:

Medium
Pipette Aid
70% ethanol
Trypan Blue
Micropipetters
Calculator
Hemocytometer
Pipette tips

Methods:

1. Clean surface of hemocytometer and coverslip with 70% alcohol

2. The coverslip should rest evenly over the silver counting area.

3. Beginning with a cell pellet, suspend the cells in a known amount of medium (commonly used: 50mL)

4. Collect a 100 μL sample from the cell suspension and put in microcentrifuge tube. Dilute with 100 μL of trypan blue (dilution = 2).

5. Mix well and collect 10 μL of suspension in a micropipette tip.

6. Load the cell suspension into the hemocytometer, allowing it to be drawn under the coverslip.

7. Place hemocytometer on microscope stage, and view with standard 10X objective.

8. Count cells in each of the four corner and central squares (clear cells are viable, blue stained cells are dead). Avoid counting same cells for adjacent squares. For that, count cells that lie on the top and left lines but not those on the bottom or right lines of each square. Count living cells, and dead cells to report viability if necessary

9. Calculate total cell number from the following:

$$T = \frac{N_C}{N_S} \times D \times 10^4 \times V$$

T = Total number of cells in suspension
N_c = Number of cells counted
N_s = Number of squares counted
D = Dilution factor (2, in this case)
V = Volume of media used to suspend cell pellet (commonly 50ml)

The number 10^4 is the volume correction factor for the hemocytometer: each square is 1x1 mm and the depth is 0.1 mm.

10. Cell viability is calculated by:

$$100\% \times (\#\text{ live}/ (\#\text{live} + \#\text{dead}))$$

Freezing Cells

Materials

Expansion medium (make sure there is 10% FBS), without the growth factors
10% Dimethyl sulfoxide (DMSO; Sigma D2650)
Sterile, DMSO safe, syringe filters
Pipettes
Sterile cryogenic tubes
Nalgene Cryo 1° C Freezing Container (Cat #5100-0001)

Procedure

1. Determine amount of medium needed.
Sterilize the medium+DMSO solution by filtering through 0.22 μ m sterile filter.

3. Adjust cell concentration.

4. Pipette into cryogenic tubes (0.5-1 ml per 2 ml tube).

5. Place tubes in Nalgene freezing container in the -80° C freezer overnight. If Nalgene container is not available, place tubes at -20° C for 2-4 hours, then transfer to -80° C overnight.

6. Transfer to liquid nitrogen tanks.

Thawing Cells

Materials:

Frozen cell vials
medium
tissue culture flasks
15 or 50 ml tubes
Aspirating pipettes
Transfer pipettes
Vacuum suction
Pipette Aid

Methods:

1. Retrieve cells from the liquid nitrogen storage tank and place in 37°C water bath. Shake gingerly for 30-60 seconds while cells begin to thaw.

2. Just as liquid appears around the edges of the vial, remove from the water bath and bring into bio-safety hood.

3. Add warmed medium.

4. Transfer the cell suspension to a falcon tube, combining vials from the same animal. If desired, centrifuge for 10 minutes at 1500 rpm to remove the DMSO supplemented medium and resuspend in an appropriate dilution for cell counting.

5. Count the cells and resuspend at desired concentration for plating into tissue culture flasks.

Fabrication of Pre-Formed Sponge-Like Scaffold

Collagen I/III (0.5%) Slurry Preparation

Equipment
1 Beaker (250ml)
1 Stir bar
Pipette
Micropipette
Ph-meter
Spatula
Blender

Materials
HCl (6N)
Biogide Powder (collagen I/III)
dH_2O
Ice (to cool the collagen slurry during blending to protect protein)

Be sure to clean equipment before use

1. Prepare 200ml HCl solution at 0.001N
   a. *Add 50ul of 6N HCl to 3ml dH_20 to make 0.1N HCl*
   b. *Add 2ml of 0.1N HCl to 198ml dH_2O to make 0.001N HCl*
   c. *Stir*
   d. *(Adjust pH=3 by adding drops 6N HCl)*
2. Add 1g Biogide collagen powder while stirring
3. Adjust pH to 3 using 6N HCl
4. Blend at 15,000 rpm until particles are gone
5. Centrifuge at 1500 rcf for 2 mins, then remove bubbles on top using spatula
6. Pour 15ml in each plastic mold for freeze-drying

Collagen I/III (0.5%)-GAG (0.033%) Slurry Preparation

Equipment
1 Beaker (250ml)
1 Stir bar
Pipette
Micropipette
Ph-meter
Spatula
Blender

Materials

HCl (6N)
Biogide Powder (collagen I/III)
GAG (chondroitin sulfate, Sigma C4384; heparan sulfate, Sigma H7640)
dH_2O
Ice (to cool the collagen slurry during blending to protect protein)

Be sure to clean equipment before use

1. Prepare 200ml HCl solution at 0.001N
   a. *Add 50ul of 6N HCl to 3ml dH_20 to make 0.1N HCl*
   b. *Add 2ml of 0.1N HCl to 198ml dH_2O to make 0.001N HCl*
   c. *Stir*
   d. *(Adjust pH=3 by adding drops 6N HCl)*
2. Add 1g Biogide collagen powder while stirring
3. Adjust pH to 3 using 6N HCl
4. Blend at 15,000 rpm until particles are gone
5. Obtain a 15ml aliquot of blended slurry
6. Add 5mg GAG to slurry and blend at 15,000 rpm until particles are gone (may take 1-2 hours)
7. Centrifuge at 1500 rcf for 2 mins, then remove bubbles on top using spatula
8. Pour 15ml in each plastic mold for freeze-drying

Collagen II (1%) Slurry Preparation

Equipment
1 Beaker (250ml)
1 Stir bar
Pipette
Micropipette
Ph-meter
Spatula
Blender

Materials
HCl (6N)
Chondrocell (collagen II)
dH_2O
Ice (to cool the collagen slurry during blending to protect protein)

Be sure to clean equipment before use

1. Prepare 200ml HCl solution at 0.001N
   a. *Add 50ul of 6N HCl to 3ml dH_20 to make 0.1N HCl*

b. *Add 2ml of 0.1N HCl to 198ml dH_2O to make 0.001N HCl*
c. *Stir*
d. *(Adjust pH=3 by adding drops 6N HCl)*

2. Add 2g collagen while stirring
3. Adjust pH to 3 using 6N HCl
4. Blend at 15,000 rpm until particles are gone
5. Centrifuge at 1500 rpm for 2 mins, then remove bubbles on top using spatula
6. Pour 15ml in each plastic mold for freeze-drying

Freeze Drying and DHT

1. Put collagen slurry-filled molds in freeze dryer:
   i. Thermal treatment: hold at 15°C for 10 mins, ramp to -15°C in 30 mins, hold at -15°C for 240 mins
   ii. Freeze condenser vacuum: freeze at -15°C for 20 mins, -60°C condenser, 200mTorr vacuum
   iii. Drying cycle steps: hold at -5°C for 1200 mins, 200mTorr vacuum
   iv. Secondary drying: temperature of 20°C for 30 mins at 200mTorr (set point of 40°C)
2. Take scaffold sheets out of freeze dryer and put in aluminum foil
3. Put in DHT oven for 24 hours, 105°C, vacuum 30 inHg
4. Cut disks from sheets using an 8mm diameter sterile dermal biopsy punch

Cell Seeding and Transfection in Sponge-Like Scaffolds

EDAC1: [amount: 1:1:5 (EDAC:NHS:COOH)]

EDAC:	0.0184	[g]
NHS:	0.0111	[g]
Full water:	200	[ml]

Typical values for mass of 8mm scaffolds is 2 mg. There are 1.2mmol COOH per mole of collagen (see Olde Damink).

Methods

1. Dissolve the EDAC and NHS in dH_2O
   Notes: The amounts of EDAC and NHS required are frequently very small and difficult to weigh out, especially when only a small number of scaffolds are required. It is often easier to weigh out a larger amount of the chemicals, dissolve in dH2O, and dilute to the desired concentration.

2. Sterile filter EDAC/NHS solutions into sterile containers.

Supplementing Scaffold with Lipoplex

DNA concentration: varies
The volume of DNA diluent and serum-free medium is adjusted to make the final volume of the GenePORTER 2/DNA complexes be around 30ul/side.

Methods

1. Put the scaffold in normal well plate.
2. Hydrate each GenePORTER 2 lipid vial at room temperature with 1.5 ml (for T202015) of the Hydration Buffer. Vortex for 10 seconds at top speed before use. Store hydrated reagent at 4°C; vortex briefly before each use.
3. Dilute the DNA with DNA Diluent B (TE buffer can be kept in); mix well by pipetting and incubate at room temperature for 5 minutes (so it's better to prepare this right before use).
   NOTE: Do not vortex DNA Diluent B
4. Dilute the hydrated GenePORTER 2 reagent with serum-free DMEM-LG medium.
5. Add the diluted DNA to the diluted GenePORTER 2. Incubate at room temperature for 5 minutes to form lipid/DNA complexes (lipoplexes)
   NOTE: Do not incubate for more than 30 minutes.
6. Add lipoplexes (plasmid DNA + GenePORTER2) to each side of the scaffold and wait ~10 mins per side.
7. Add 1ml EDAC cross-linking. Wait for 30 min.
8. Remove EDAC/NHS solution with pipette or aspiration.
9. Rinse in sterile PBS (2ml PBS/well for 24-well plate) for at least 1 hour.

Agarose Coating for Well-plates (2% w/v)

Materials

Seaplaque agarose (#50100, Cambrex)

Distilled water
Bottle with cover

Methods

1. Filter 100ml (this amount should be decided by the well-plate type and numbers used) distilled water in the hood using 'sterile flip' (tube screwed on tube filter, then vacuum).
2. Add 2g agarose and shake.
3. Put the solution into a bottle with cover.
4. Put into the autoclave to dissolve agarose and for sterilization (option for liquid: 120°C, 20min).
5. Put 1ml in each 24-well plate in fridge to let it solidify. (After one hour, the liquid agarose will be solidified and can't spread in the well any more.)

Cell Seeding and Transfection in Scaffold

Cell density: 2M/side. The volume/side is about 20ul. So the concentration is 2M/20ul in DMEM-LG serum free medium.

1. Transfer the scaffold from normal well plate to agarose-coated well plate.
2. Remove extra PBS on the scaffolds with sterilized filter paper.
3. Add 20ul MSCs (2M cells) suspension (in DMEM-LG medium, **without serum**) to each side and incubate for ~20 mins per side.
4. Add DMEM-LG, **without serum,** to cover the scaffolds (0.5ml). ***Be careful to add medium so that the cells can stay on the scaffolds.***
5. Transfect for a total of 4 hours (lipoplexes will kill the cells after longer time) in incubator.
6. Add media to transfected scaffolds.

Transfection and Cell Seeding for Hydrogel Scaffolds

Transfection in Monolayer

Use 25μl of the DNA Diluent B per each 1μg of DNA according to GP2 protocol.

Methods

1. Hydrate each GenePORTER 2 lipid vial at room temperature with 1.5 ml (for T202015) of the Hydration Buffer. Vortex for 10 seconds at top speed before use. Store hydrated reagent at 4°C; vortex briefly before each use.
2. Dilute the DNA with DNA Diluent B (TE buffer can be kept in); mix well by pipetting and incubate at room temperature for 5 minutes. **NOTE: Do not vortex DNA Diluent B.**
3. Dilute the hydrated GenePORTER 2 reagent with serum-free DMEM-LG medium.
4. Add the diluted DNA to the diluted GenePORTER 2. Incubate at room temperature for 5 minutes to form lipid/DNA complexes (lipoplexes). **NOTE: Do not incubate for more than 30 minutes.**
5. When cells are expanded overnight in well-plate, rinse them with PBS.
6. Add the GenePORTER 2/DNA complexes directly to cells (15ml/T150 flask) and transfect at 37°C for 4 hours *(lipoplexes will kill the cells after longer time)* in incubator.
7. Add 15ml medium (DMEM low glucose + 10% FBS +1% antibiotic, no FGF-2) per T150 flask after the initial 4-hour incubation in serum-free media, to achieve higher transfection efficiencies. Do not remove the media already in the flasks.
8. Incubate overnight in preparation for cell seeding/gel casting.

Control Bead Preparation for Cell Seeding and Gel Casting (manufacturer's instructions)

Sepharose CL Gel Filtration Media from Sigma (84963 CL-4B), average bead size 45-165um

1. Cut tip of pipet tip, if necessary.
2. Pipet 2.496 ml (this is enough to cast 24 gels) of control beads in buffer (Sigma 84963 CL-4B, lot 050M1621) into tube.
3. Spin for 5 mins at 800-1000 rpm.
4. Remove liquid, add water, repeat step 3 another 4 times to wash beads.
5. After washing, resuspend the 1.92 ml of beads alone in 1.33 ml expansion base with no GFs.

Heparin Bead Preparation for Cell Seeding and Gel Casting (manufacturer's instructions)

Heparin-Agarose Type I Beads from Sigma (H6508), average bead size 45-165um

10. Cut tip of pipet tip, if necessary.
11. Pipet 3.84 ml (this is enough to cast 24 gels at 10% heparin) of heparin beads in buffer (Sigma H6508, lot 099K5156) into tube.
12. Spin for 5 mins at 800-1000 rpm.
13. Remove preservative, add water, repeat step 3 another 4 times to wash beads.
14. After washing, resuspend the 1.92 ml of beads alone in 1.33 ml expansion base with no GFs.

Solution Preparation for Cell Seeding and Gel Casting

15. Make 5x PBS by dissolving 1 packet (Sigma P3813) in 200 ml water and sterile filtering.
16. Make fresh 25mM stock genipin (MW 226.23 g/mol) solution by dissolving 56.56 mg genipin (Wako 078-03021) in 10ml of 5x PBS for 1h (may need to shake and incubate at 37C). Sterile filter genipin solution.
17. Make 1M NaOH by dissolving 2g (Fisher S318-5) in 50 ml water and sterile filtering. If NaOH is kept too long, it will crystallize.
18. Make 50mM Tris, pH 7.4 (MW 121.14 g/mol) by dissolving 0.3025 g of Tris (Invitrogen 15504-020) in 50ml of water. Adjust pH of solution with 0.1M NaOH and sterile filter.
19. Dissolve all (2.44mg) TG-2 (Sigma T5398, lot 119K7410V) in 1.22 ml of sterile 50mM Tris for final stock concentration of 2 mg TG-2/ml Tris.
20. Make 1M stock DTT (Sigma D-0623) (MW 154.25 g/mol) by dissolving 0.309g DTT in 2ml of deionized water and sterile filtering.
21. Make 1M stock calcium chloride (dehydrated) (Fluka 06991) (MW 110.98 g/mol) by dissolving 1.11g calcium chloride in 10ml of deionized water and sterile filtering.

Cell Seeding and Gel Casting

Cell density: 0.4M MSCs/well. Use 24-well plates, 0.5ml collagen gel-cell suspension per well. Use collagen I (BD Biosciences 354236) gel at final concentration of 2mg/ml.

22. Lift cells and resuspend in DMEM-LG/FBS/PS (no GFs). Collect 1 ml of the 30 ml expended media from flasks. Count
    live pGFP cells
    dead pGFP cells
    live pEndo cells
    dead pEndo cells.

23. Add materials in the order listed in chart, 1 tube for each of the listed groups. Make sure everything is sterile. **Keep collagen cold until ready for gelation. Note: <u>When pipetting, pipet collagen slowly and be careful not to introduce air bubbles!!</u>**

Group	**pEndo, 100ug/ml TG-2**	**pEndo, 100ug/ml mTG**
PBS (5x) (used as filler to bring up to desired total volume)	1.2 ml	1.2 ml
Expansion medium base (no GFs)	1.87 ml	1.66ml
Stock calcium chloride, final conc. 5mM	45 ul	
Stock DTT, final conc. 2mM	18 ul	
2mg/ml stock TG-2	450 ul	
mTG stock, orig. conc. 1.25 mg/ml		720 ul
1 M NaOH (added to keep neutral pH)	101.4 ul	101.4 ul
Rat tail collagen I stock (original conc. 3.91 mg/ml, already sterile)	4.6 ml	4.6 ml
Cell suspension (10M cells/ml)	**0.72 ml**	**0.72 ml**
Total volume	**9ml**	**9ml**

Group	**CM, pEndo, no crosslinker**	**CM, pEndo, 0.25 mM GP**
PBS (5x) (used as filler to bring up to desired total volume)	855 ul	750 ul
Expansion medium base (no GFs)	3.12 ml	3.12 ml
1 M NaOH (added to keep neutral pH)	123.5 ul	123.5 ul
Cell suspension (8.4 x 10^6 cells/800ul)	**800 ul**	**800 ul**
25mM genipin stock	0	105 ul
Rat tail collagen I stock	5.6 ml (orig. conc. 3.75 mlg/ml	5.4 ml (orig. conc. 3.89 mg/ml)
Total volume	**10.5 ml**	**10.5 ml**

Group	**0.25 mM GP, control beads**	**0.25 mM GP, heparin beads**
PBS (5x) (used as filler to bring up to desired total volume)	750 ul	750 ul
Expansion medium base (no GFs)	321.5 ul	321.5 ul
1 M NaOH (added to keep neutral pH)	123.5 ul	123.5 ul
Appropriate beads	3 ml	3 ml
Cell suspension (8.4 x 10^6 cells/800ul)	**800 ul**	**800 ul**
25mM genipin stock	105 ul	105 ul
Rat tail collagen I stock (original conc. 3.89 mg/ml, already sterile)	5.4 ml	5.4 ml
Total volume	**10.5 ml**	**10.5 ml**

24. Incubate for 1 hour at 37C to gel.
25. Add 1 ml media/well.

Homogenization Protocol

Equipment

Tissue-Tearor (Biospec Cat. No. 985-370)

Homogenizing Medium

1. Dissolve one tablet Complete™ Mini Protease Inhibitor cocktail (Roche 11836153001) per 7 mL PBS

Tissue Homogenization Protocol

1. Remove stored samples from freezer and weigh wet tissue, if desired.
2. Chop or cut tissue into small pieces (approx. 1 mm in length) using a safety razor blade.
3. Place tissue in homogenizing vessel (15ml round bottomed Falcon tube, cut down to size) containing 500 ul of homogenizing medium per sample.
4. Lower the probe tip into tissue suspension, turn on the Tissue-Tearor (for cell disruption, use the maximum speed setting) and operate for ~60 seconds. The homogenizing vessel should be placed in an ice bath during homogenization. Approx speeds of the Tissue Tearor are:

Switch Setting	Speed Range (RPM)
1	4500-8000
2	9000-11000
3	12000-17000
4	18000-24000
5	25000-30,000

5. Turn off the Tissue-Tearor before withdrawing from the homogenizing vessel. The Tissue-Tearor should be operated only in a liquid medium. Clean using water and detergent.
6. Transfer homogenates to 1.5ml Eppendorf tubes.
7. Centrifuge at 10,000-13,000 rcf for 5 mins to remove debris and insoluble materials.
8. Store supernatant at -80C until analysis.

DuoSet Endostatin ELISA (R&D Systems, DY1098)

Solutions:

PBS: 137 mM NaCl, 2.7 mM KCl, 8.1 mM Na2HPO4, 1.5 mM KH2PO4, pH 7.2-7.4
--Use 1 packet powdered PBS (Sigma P3813) + 1L DI water, 0.2□m filtered

Wash buffer: 0.05% Tween 20 in PBS, pH 7.2-7.4
--Make 20x wash buffer: 2 packets PBS (Sigma P3813), pH 7.4 + 1 ml Tween20 (BioRad 170-6531) in 100 ml water, 0.2□m filtered, store at 4C
--Dilute 1:20 in sterile filtered water to get 1x wash buffer for ELISA

Reagent Diluent: 1% BSA in PBS
--Make 5x reagent diluent: 1 packet PBS + 10g BSA (Sigma A7030) in 200 ml water, 0.2□m filtered, store at 4C
--Dilute 1:5 in sterile filtered water to get 1x for ELISA

Substrate Solution: 1:1 mixture of Color Reagent A (H2O2) and Color Reagent B (Tetramethylbenzidine) (R&D Systems Cat. # DY999)

Stop Solution: 2 N H2SO4 (R&D Systems, DY994)

Aliquots:

Capture Antibody: stock concentration 720ug/ml, reconstituted with 1ml PBS, rock gently for 2h at 4C, then aliquot 58ul/1.5ml epi tube, 17.2 tubes total, freeze aliquots for storage

Standard Endostatin: stock concentration 150ng/ml, reconstituted with 0.5ml reagent diluent, rock gently for 2h at 4C, then aliquot 16ul/1.5ml epi tube, 31.25 tubes total, freeze aliquots for storage

Detection Antibody: stock concentration 18ug/ml, reconstituted with 1ml reagent diluent, rock gently for 2h at 4C, then aliquot 58ul/1.5ml epi tube, 17 tubes total, freeze aliquots for storage

Methods:

Add 58ul stock capture antibody to 10.5ml PBS for 1 plate to get working concentration of 4ug/ml in PBS. Coat Spectraplates (High Binding, 96 wells) with 100 ul/well. Tap plate to remove any bubbles, cover plate with plate sealer, store overnight at room temperature.

Wash plate 3x with wash buffer—after last wash, invert plate and blot against clean paper towels

Block plates w/ reagent diluent, 300 µl/well
Cover plate, RT, 1 hr minimum

Wash plate 3x, invert and blot

Prepare endostatin standard dilutions:
9-point standard curve using 2-fold serial dilutions in Reagent Diluent w/ high standard at 4ng/ml, best fit for standard curve seems to be 2nd order polynomial:

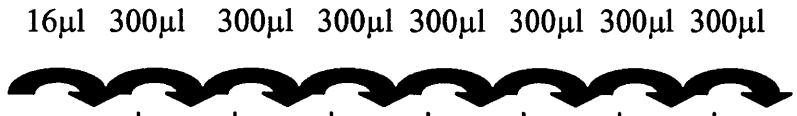

STOCK (150ng/ml)	8	7	6	5	4	3	2	1	Tube #
	584ul	300µl	300µl	300µl	300µl	300µl	300µl	300µl	**Reagent Diluent**
	4	2	1	0.5	0.25	0.125	0.0625	0.0313	**Std. Conc. (ng/ml)**

Add standards or samples (run standard in duplicate), 100ul/well
Include blank well w/ Reagent Diluent only
Cover plate, RT, 2 hrs

Wash plate 3x, invert and blot

Add 58ul stock detection antibody to 10.5ml reagent diluent for 1 plate to get working concentration of 0.1ug/ml in reagent diluent.
Add 100 µl/well
Cover plate, RT, 2 hrs

Wash plate 3x, invert and blot

Dilute stock solution of Streptavidin HRP 1:200 in Reagent Diluent (52.5ul of Streptavidin HRP in 10.5ml reagent diluent for 1 plate).
Add 100 µl/well
Cover plate, RT, 20 minutes—**Avoid direct light**

Store Streptavidin-HRP at 2-8℃ for up 6 months, ***DO NOT FREEZE***

Wash plate 3x, invert and blot

Substrate Solution: mix 1:1 Color Reagent A & Color Reagent B (5.2 ml A + 5.2 ml B for 1 plate).
Add 100ul/well
Cover plate, RT, 20 minutes—**Avoid direct light**

Add Stop Solution (DO NOT WASH BEFOREHAND)—50ul per well, gently tap plate to ensure thorough mixing

Determine optical density immediately using microplate reader set to 450 nm. Subtract readings at 540nm or 570 nm from 450nm readings for wavelength correction (corrects for optical imperfections in the plate). If samples fall above standard curve, dilute in reagent diluent and rerun ELISA.

Digesting Samples for Biochemical Analyses

Lyophilization

1. Remove stored samples from freezer; make sure each sample is in its own container (epi tube).
2. Poke a small hole in container.
3. Put samples in lyophilizer.
4. Turn on vacuum.
5. Turn on condenser to lower the temperature.
6. Leave samples overnight.

Proteinase K Digestion

1. Make Tris-HCl buffer: Dissolve 73.5 mg calcium chloride in 475 ml dH2O, then add 25ml 1M Tris, pH 8, to get 0.05M Tris.
2. Make 500 ug/ml proteinase K solution: Add 50mg proteinase K powder (Sigma P6556) to 100ml Tris-HCl buffer.
3. Add 1ml of proteinase K solution per sample.
4. Wrap sample in parafilm to make watertight.
5. Vortex sample.
6. Put in water bath, 60C, gentle rocking, overnight.
7. Freeze samples until analysis.

Picogreen dsDNA Quantitation Assay

Materials:

Quant-iT Picogreen dsDNA Assay Kit (Molecular Probes, Cat# P7589) contains:

- PicoGreen dye reagent (1mL solution in DMSO)—light sensitive (keep covered)
- 20X TE (25mL of 200mM Tris-HCl, 20mM EDTA, pH 7.5)
- Lambda DNA standard (1mL of 100 ug/mL in TE)

TE buffer for diluting samples:

- Prepare 1x TE buffer from the 20x TE stock, which is supplied in the Picogreen kit (to make 50 ml, add 2.5ml of 20x TE to 47.5ml sterile DNase-free dH2O)

96-well plate—Black Isoplate (Clear bottom plates, Wallac, Cat# 1450-571)

Procedure:

1. Thaw Picogreen dye at room temperature
2. DNA std working solution (2ug/ml): Add ***294ul of TE buffer*** + ***6ul DNA stock*** (100 ug/mL)
3. Vortex samples
4. Dilute all digested samples ***1:10*** with TE buffer (not from kit): ***180ul TE + 20ul digest*** (can be diluted in microcentrifuge tubes or 96-well plate)
5. Prepare the DNA standards as follows:

Standard No.	DNA Standard, 2ug/ml (ng/ml) (ul)	TE buffer (ul)	Well No.
Blank	0	100	1
1	1	99	2
2	5	95	3
3	10	90	4
4	25	75	5
5	50	50	6
6	75	25	7
7	100	0	8

6. Add 100ul of sample and diluted sample to each well
7. Dilute PicoGreen dye stock with TE buffer (from kit), ***200X***—*Prepare just before use*

   --100 ul of working dye solution needs to be added to well used

   --Make more working dye then needed (i.e. add solution for 5 additional wells)

   For example, if there are ***96 wells*** to fill, make enough dye for 110 wells:

   110 x 100ul = 11000ul (or 11ml); 11000/200 = ***55ul of PicoGreen stock + 11ml 1x TE***
8. Dispense 100 ul PicoGreen working dye solution to each well being used

Standard No.	Final Standards (ng/ml)
Blank	0
1	10
2	50
3	100
4	250
5	500
6	750
7	1000

9. Take fluorescence reading on microplate reader (WALLAC VICTOR^2 1420 Multilabel Counter, Perkin Elmer Life Sciences)): Protocol assigned in computer program under DNA Assay—"Fluorescein (485nm/535nm, 1.0s)" (includes a 5 min incubation period & shake)

* *If samples end up having a reading greater than the highest standard, samples need to be diluted more and re-run (fit standards with line)*

Dimethylmethylene Blue (DMMB) Assay for Sulfated Glycosaminoglycans

Materials:

Color Reagent

For 500ml of DMMB dye solution, mix the following:

- 425 ml dH_2O
- 1.52 g glycine (Sigma G8898)
- 1.19 g NaCl (Fisher S642)
  a. Adjust pH to 3.0 w/ concentrated HCl and NaOH
  b. Add more dH_2O to bring volume up to 500ml
- Add 8mg of DMMB dye
- Solution good for 3 months and should be kept in a light-protected bottle at 4°C (stir 30min prior to use)

TE buffer for diluting samples (can also use same 1x TE buffer that is used for Picogreen):

- 1ml 1M Tris (pH=8)
- 0.2 ml 0.5M EDTA (pH=8)
- 98.8 ml dH_2O

Procedure:

1. Stir DMMB dye working solution at least 30min before use
2. Prepare the Chondroitin Sulfate (CS) stock solution at 2 mg/mL in sterile filtered dH2O (keep in –20C freezer)
3. CS working solution (200µg/ml): Add 100 µl of CS stock + 900 µl dH_2O
4. Prepare the CS standards as follows: (Start w/ 7 labeled tubes filled w/ 200ul TE buffer)

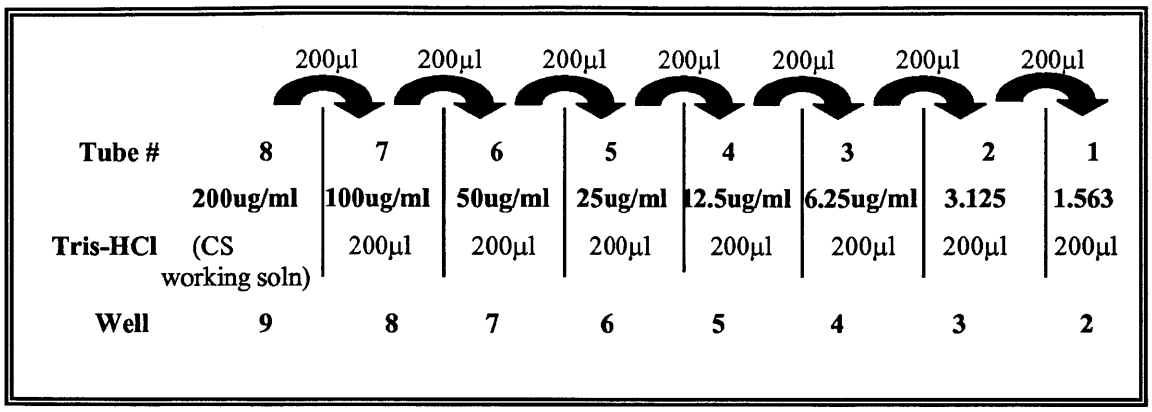

5. Thaw and vortex samples
6. Add 20ul of each standard and sample to the 96-well plate (Clear pates, Packard Bioscience Medium Binding Spectraplate-96, P12-106-043)—good to do this in duplicate, at least for the standard (Use 20ul aliquot of TE buffer as blank)
7. Dispense 200 µL of DMMB dye solution to each well used
8. Take reading at 530 nm—Protocol is already assigned on computer program for microplate reader under GAG Assay—"GAG-DMMB Assay protocol (530nm-1s)"

**** If sample reading is outside the standard curve range (or at the extremes of the standard curve), it is recommended that another dilution and reading of the sample be performed—the ideal is to have the reading land on the mid-range of the standard curve (usually a 2nd order polynomial is the best fit curve for this standard). Absorbance of highest standard usually ~0.5.***

Processing Samples for Histology

Fixation

1. Fix samples in 4% paraformaldehyde at 4°C for at least 3 hours.

Decalcification (if needed, for samples containing bone)

1. Make 25% EDTA:

- 1.9L dH2O
- 110g NaOH
- 625g EDTA
- ~80ml (36%) HCL
- pH adjusted to7.7
- add dH2O to bring total volume up to 2500ml

2. Put formalin-fixed tissue samples in EDTA at 4°C, changing EDTA ~2 times a week until sample is fully decalcified (check by feeling for hard bone and x-ray) (for goat knee samples, this could take several months).

Tissue Processing (Leica TP1020)

For samples in labeled cassettes (Fisher Cat. # 15-197-700E).

1. 70% alcohol, 10 min, room temperature
2. 80% alcohol, 90 min, room temperature
3. 95% alcohol, 90 min, room temperature
4. 95% alcohol, 90 min, room temperature
5. 100% alcohol, 90 min, room temperature
6. 100% alcohol, 90 min, room temperature
7. 100% alcohol (vacuum), 90 min, room temperature
8. Xylene, 90 min, room temperature
9. Xylene, 90 min, room temperature
10. Xylene, 90 min, room temperature

11. Paraffin (vacuum), 180 min, 58°C

12. Paraffin (vacuum), 180 min, 58°C

Embedding

1. Put a small amount of liquid paraffin in embedding mold.
2. Position sample in paraffin.
3. Freeze on cold plate for a few seconds.
4. Put labeled tissue cassette in mold.
5. Add more liquid paraffin in mold, to cover top of cassette.
6. Freeze on cold plate until solid.

Sectioning

1. Section samples using microtome, usually 6um.
2. Optional, for difficult to cut sections (such as decalcified sections): Soak paraffin blocks in water bath containing a few drops of ammonium hydroxide for at least an hour, then add ice to the water bath and soak blocks in ice water periodically during cutting.
3. Float paraffin sections in 40°C water bath.
4. Catch sections on slides (precoated slides work best for sample adhesion).
5. Let slides air dry.
6. Put slides on slide warmer, 60°C, for at least an hour, up to overnight.

Hematoxylin and Eosin (H&E) Staining

Solutions
Gill's Hematoxylin Solution (reuse): *Filter 200ml of stock solution into staining dish.*
Eosin Y Solution Aqueous (Sigma Cat# HT110-2-128).
Acid Alcohol: *0.5 % in 80% alcohol (199ml of 80% alcohol + 1 ml concentrated HCl)*
Cytoseal

Methods
1. Deparaffinize and rehydrate
Xylene 2 x 5 min.
100% alcohol 2 x 3 min.
95% alcohol 2 x 2min.
80% alcohol 1 min.
Quick rinse in gently flowing tap water

2. Hematoxylin, 3 min. *Note: be sure to filter hematoxylin prior to use!*

3. Wash in running tap water for 5 min.

4. Two quick dips in acid alcohol.

5. Wash in tap water for 5 min.

6. Eosin, 3 quick dips.

7. Dehydrate
100% alcohol 2 x 3 min.
Xylene 2 x 3 min.

8. Coverslip with Cytoseal.

Safranin-O Staining

Solutions

- Safranin-O (0.2% w/v): 0.2 g Saf-O + 1ml acetic acid + 100 ml dH_2O.
- Fast Green Stock Solution: 0.2g Fast green + 1 ml acetic acid + 100 ml dH_2O
- Fast Green Working Solution: 1:2 dilution of stock solution in dH_2O
- 0.5% Acetic Acid: 1 ml acetic acid in 199 ml dH_2O.

Procedure

1. Deparaffinize and rehydrate

Xylene	2 x 5 min.
100% alcohol	2 x 3 min.
95% alcohol	2 x 2min.
80% alcohol	1 min.

Quick rinse in gently flowing tap water

2. Hematoxylin, 3 min. Note: be sure to filter hematoxylin!

3. Wash in tap water for 5 min.

4. Fast green – 1 quick dip.

5. 0.5% acetic acid – 3 quick dips.

6. Safranin-O – 30 minutes

7. Dehydrate

95% alcohol	a few quick dips
100% alcohol	2 x 3 min.
Xylene	2 x 3 min.

8. Coverslip with Cytoseal.

Immunohistochemical Staining of Endostatin

Use DakoCytomation EnVision+ System-HRP (AEC) designed for Rabbit Primary Antibodies.

Standard setting uses 150ul per treated section of each slide and will treat 3 sections of slide (marked yellow).

Solution Preparation

Note: Amounts will vary depending on number of slides being stained

1. **Tris-Buffered Saline** (TBS) (Dako packets) Stored at RT in packets, 4°C in soln
   1 package (DakoS3001) to 1L dH_2O
   1 package (DakoS1969) to 5L dH20
2. **Wash Buffer with Tween 20** Stored at 4°C
   (DakoCytomation, S3006, 1000ml)
   500ml of 10x in 4500ml dH20
3. **0.1% Protease XIV** (Sigma P-5147) Stored at -20°C until use
   0.01g Protease
   10 ml TBS
4. **Peroxidase Blocking Reagent (Dako)** Stored at 4°C
   Ready-to-use 15ml/vial
5. **X0909 Blocking Solution (Dako)** Stored at 4°C
6. **Primary Endostatin Rabbit Polyclonal Antibody** Stored at 4°C
   Rabbit against human endostatin (Millipore AB1878)
   Concentration of product:
   Use 17 ug/ml final concentration
   Dilute primary antibody in universal AB diluent (Dako S0809) **(not TBS)**
7. **Dako Rabbit Immunoglobulin Negative Control** Stored at 4°C
   Concentration of product:
   Dilute to 17 ug/ml final conc in universal AB diluent
8. **Labelled Polymer-HRP Anti-Rabbit** Stored at 4°C
   Ready-to-use 15ml/vial (Dako)
9. **AEC PLUS** (Dako) Stored at 4°C
   Ready-to-use 15ml/vial
10. **Counterstain** Stored at RT
    Mayer's Hematoxylin Solution (Sigma MHS16)
    (filter before use)
11. **Aqueous Mounting Media** Stored at RT
    Faramount, Dako S3025

Methods ***Do not let the slides dry out during this process***

1. Put paraffin sections on slide warmer (setting 6 for 1 hour) (use human skin as control)
2. Turn on the computer and set up protocol on autostainer: on Desktop, click "DAKO Autostainer", login Dong, password Dong
3. To add slides, click on "Slides" and type in the number of slides you want to stain including all controls
4. Copy and paste the staining protocol by first clicking on "Copy" then on the slide you want to copy. Clicking on any slide will automatically "Paste" the protocol to any desired row.
5. Deparaffinize and rehydrate paraffin section via the following baths
    - Xylene 2 x 5 minutes
    - 100% alcohol 2 x 3 minutes
    - 95% alcohol 2x 2 minutes
    - 80% alcohol 1 minute
    - Running tap water 5mins
6. Load slides on the slide racks (make sure to keep slides wet with TBS) and reagent onto the reagent rack (white) with exact amount and placement the Autostainer requires.
7. Starting a run: click "Next" after loading slides, click on Prime Pump (water) and Prime Pump (buffer) and check if machine is really running.
8. Click on "Start Run"
9. Autostainer steps:
    - Rinse (TBS+Tween)
    - Proteolytic digestion to unmask antigenic sites with 0.1% (w/v) Protease XIV (40 min.)
    - Rinse
    - Endogenous peroxidase quench from Dako kit (10 min.)
    - Rinse
    - Block non-specific binding with X0909 Blocking Solution (10min.)
    - **NO RINSE**
    - Primary Antibody or Negative Control (30 min.)
    - Rinse
    - Polymer-HRP (30 min.)
    - Rinse
    - "switch"
    - Substrate- AEC Plus (10 min.)
    - Rinse
10. After Autostainer completed, immediately unload slides from machine and put in TBS to keep wet, click "Next".
11. Counter-stain with Mayers Hematoxylin for 1.5 minutes.
12. Rinse in running tap water (3 min).
13. Transfer slideholder into a container with tap water and immediately coverslip (don't let slides dry) with Aqueous Mounting Media (**do not use Cytoseal, it will take off AEC**).

Immunohistochemical Staining of Type I Collagen

Use DakoCytomation EnVision+ System-HRP (AEC) designed for Mouse Primary Antibodies.

Standard setting uses 150ul per treated section of each slide and will treat 3 sections of slide (marked yellow).

Solution Preparation

Note: Amounts will vary depending on number of slides being stained

12. **Tris-Buffered Saline** (TBS) (Dako packets) — Stored at RT in packets, 4°C in soln
    1 package (DakoS3001) to 1L dH_2O
    1 package (DakoS1969) to 5L dH20
13. **Wash Buffer with Tween 20** — Stored at 4°C
    (DakoCytomation, S3006, 1000ml)
    500ml of 10x in 4500ml dH20
14. **0.1% Protease XIV** (Sigma P-5147) — Stored at -20°C until use
    0.01g Protease
    10 ml TBS
15. **Peroxidase Blocking Reagent (Dako)** — Stored at 4°C
    Ready-to-use 15ml/vial
16. **X0909 Blocking Solution (Dako)** — Stored at 4°C
17. **Primary Collagen I Mouse Antibody** — Stored at 4°C
    Calbiochem I-8H5 CP17, mouse monoclonal IgG2a
    Concentration of product:
    Use 5 ug/ml final concentration
    Dilute primary antibody in universal AB diluent (Dako S0809) **(not TBS)**
18. **Dako Mouse Immunoglobulin Negative Control** — Stored at 4°C
    IgG2a (Dako X0943)
    Concentration of product:
    Dilute to 5 ug/ml final conc in universal AB diluent
19. **Labelled Polymer-HRP Anti-Mouse** — Stored at 4°C
    Ready-to-use 15ml/vial (Dako)
20. **AEC PLUS** (Dako) — Stored at 4°C
    Ready-to-use 15ml/vial
21. **Counterstain** — Stored at RT
    Mayer's Hematoxylin Solution (Sigma MHS16)
    (filter before use)
22. **Aqueous Mounting Media** — Stored at RT
    Faramount, Dako S3025

Methods ***Do not let the slides dry out during this process***

14. Put paraffin sections on slide warmer (setting 6 for 1 hour)
15. Turn on the computer and set up protocol on autostainer: on Desktop, click "DAKO Autostainer", login Dong, password Dong
16. To add slides, click on "Slides" and type in the number of slides you want to stain including all controls
17. Copy and paste the staining protocol by first clicking on "Copy" then on the slide you want to copy. Clicking on any slide will automatically "Paste" the protocol to any desired row.
18. Deparaffinize and rehydrate paraffin section via the following baths
    - Xylene 2 x 5 minutes
    - 100% alcohol 2 x 3 minutes
    - 95% alcohol 2x 2 minutes
    - 80% alcohol 1 minute
    - Running tap water 5mins
19. Load slides on the slide racks (make sure to keep slides wet with TBS) and reagent onto the reagent rack (white) with exact amount and placement the Autostainer requires.
20. Starting a run: click "Next" after loading slides, click on Prime Pump (water) and Prime Pump (buffer) and check if machine is really running.
21. Click on "Start Run"
22. Autostainer steps:
    - Rinse (TBS+Tween)
    - Proteolytic digestion to unmask antigenic sites with 0.1% (w/v) Protease XIV (40 min.)
    - Rinse
    - Endogenous peroxidase quench from Dako kit (10 min.)
    - Rinse
    - Block non-specific binding with X0909 Blocking Solution (10min.)
    - **NO RINSE**
    - Primary Antibody or Negative Control (30 min.)
    - Rinse
    - Polymer-HRP (30 min.)
    - Rinse
    - "switch"
    - Substrate- AEC Plus (10 min.)
    - Rinse
23. After Autostainer completed, immediately unload slides from machine and put in TBS to keep wet, click "Next".
24. Counter-stain with Mayers Hematoxylin for 1.5 minutes.
25. Rinse in running tap water (3 min).

Transfer slideholder into a container with tap water and immediately coverslip (don't let slides dry) with Aqueous Mounting Media (**do not use Cytoseal, it will take off AEC**).

Immunohistochemical Staining of Type II Collagen

Use DakoCytomation EnVision+ System-HRP (AEC) designed for Mouse Primary Antibodies.

Standard setting uses 150ul per treated section of each slide and will treat 3 sections of slide (marked yellow).

Solution Preparation

Note: Amounts will vary depending on number of slides being stained

23. **Tris-Buffered Saline** (TBS) (Dako packets) — Stored at RT in packets, 4°C in soln
    1 package (DakoS3001) to 1L dH_2O
    1 package (DakoS1969) to 5L dH20
24. **Wash Buffer with Tween 20** — Stored at 4°C
    (DakoCytomation, S3006, 1000ml)
    500ml of 10x in 4500ml dH20
25. **0.1% Protease XIV** (Sigma P-5147) — Stored at -20°C until use
    0.01g Protease
    10 ml TBS
26. **Peroxidase Blocking Reagent (Dako)** — Stored at 4°C
    Ready-to-use 15ml/vial
27. **X0909 Blocking Solution (Dako)** — Stored at 4°C
28. **Primary Collagen II Mouse Antibody** — Stored at 4°C
    CIICI-a 4/6/06 mouse IgG2a
    Concentration of product:
    Use 4 ug/ml final concentration
    Dilute primary antibody in universal AB diluent (Dako S0809) **(not TBS)**
29. **Dako Mouse Immunoglobulin Negative Control** — Stored at 4°C
    Concentration of product:
    Dilute to 4 ug/ml final conc in universal AB diluent
30. **Labelled Polymer-HRP Anti-Mouse** — Stored at 4°C
    Ready-to-use 15ml/vial (Dako)
31. **AEC PLUS** (Dako) — Stored at 4°C
    Ready-to-use 15ml/vial
32. **Counterstain** — Stored at RT
    Mayer's Hematoxylin Solution (Sigma MHS16)
    (filter before use)
33. **Aqueous Mounting Media** — Stored at RT
    Faramount, Dako S3025

Methods ***Do not let the slides dry out during this process***

26. Put paraffin sections on slide warmer (setting 6 for 1 hour) (a good positive control tissue to use is goat cartilage)
27. Turn on the computer and set up protocol on autostainer: on Desktop, click "DAKO Autostainer", login Dong, password Dong
28. To add slides, click on "Slides" and type in the number of slides you want to stain including all controls
29. Copy and paste the staining protocol by first clicking on "Copy" then on the slide you want to copy. Clicking on any slide will automatically "Paste" the protocol to any desired row.
30. Deparaffinize and rehydrate paraffin section via the following baths
    - Xylene 2 x 5 minutes
    - 100% alcohol 2 x 3 minutes
    - 95% alcohol 2x 2 minutes
    - 80% alcohol 1 minute
    - Running tap water 5mins
31. Load slides on the slide racks (make sure to keep slides wet with TBS) and reagent onto the reagent rack (white) with exact amount and placement the Autostainer requires.
32. Starting a run: click "Next" after loading slides, click on Prime Pump (water) and Prime Pump (buffer) and check if machine is really running.
33. Click on "Start Run"
34. Autostainer steps:
    - Rinse (TBS+Tween)
    - Proteolytic digestion to unmask antigenic sites with 0.1% (w/v) Protease XIV (40 min.)
    - Rinse
    - Endogenous peroxidase quench from Dako kit (10 min.)
    - Rinse
    - Block non-specific binding with X0909 Blocking Solution (10min.)
    - **NO RINSE**
    - Primary Antibody or Negative Control (30 min.)
    - Rinse
    - Polymer-HRP (30 min.)
    - Rinse
    - "switch"
    - Substrate- AEC Plus (10 min.)
    - Rinse
35. After Autostainer completed, immediately unload slides from machine and put in TBS to keep wet, click "Next".
36. Counter-stain with Mayers Hematoxylin for 1.5 minutes.
37. Rinse in running tap water (3 min).
38. Transfer slideholder into a container with tap water and immediately coverslip (don't let slides dry) with Aqueous Mounting Media (**do not use Cytoseal, it will take off AEC**).

Immunohistochemical Staining for Collagen IV

Use DakoCytomation EnVision+ System-HRP (AEC) designed for Rabbit Primary Antibodies.

Standard setting uses 150ul per treated section of each slide and will treat 3 sections of slide (marked yellow).

Solution Preparation
Note: Amounts will vary depending on number of slides being stained

34. **Tris-Buffered Saline** (TBS) (Dako packets) — Stored at RT in packets, 4°C in soln
    1 package (DakoS3001) to 1L dH_2O
    1 package (DakoS1969) to 5L dH20
35. **Wash Buffer with Tween 20** — Stored at 4°C
    (DakoCytomation, S3006, 1000ml)
    500ml of 10x in 4500ml dH20
36. **0.1% Protease XIV** (Sigma P-5147) — Stored at -20°C until use
    0.01g Protease
    10 ml TBS
37. **Peroxidase Blocking Reagent** — Stored at 4°C
    (Dako)
    Ready-to-use 15ml/vial
38. **X0909 Blocking Solution** — Stored at 4°C
39. **Primary CIV Rabbit Polyclonal Antibody** — Stored at 4°C
    (abcam ab6586)
    Concentration of product:
    Use 17ug/ml diluted in universal AB diluent (Dako S0809) **(not TBS)**
40. **Dako Negative Rabbbit Control (Normal)** — Stored at 4°C
    Dako X0903
    Concentration of product:
41. **Labelled Polymer-HRP Anti-Rabbit** (Dako) — Stored at 4°C
    Ready-to-use 15ml/vial
42. **AEC PLUS** (Dako) — Stored at 4°C
    Ready-to-use 15ml/vial
43. **Counterstain** — Stored at RT
    Mayer's Hematoxylin Solution (Sigma MHS16)
    (filter before use)
44. **Aqueous Mounting Media** — Stored at RT
    Faramount, Dako S3025

Methods ***Do not let the slides dry out during this process***

39. Put paraffin sections on slide warmer (setting 6 for 1 hour) (use goat skin as control)
40. Turn on the computer and set up protocol on autostainer: on Desktop, click "DAKO Autostainer", login Dong, password Dong, "Program", "File", "Open", "endostat"
41. To add slides, click on "Slides" and type in the number of slides you want to stain including all controls
42. Copy and paste the staining protocol by first clicking on "Copy" then on the slide you want to copy. Clicking on any slide will automatically "Paste" the protocol to any desired row.
43. Deparaffinize and rehydrate paraffin section via the following baths
    - Xylene 2 x 5 minutes
    - 100% alcohol 2 x 3 minutes
    - 95% alcohol 2x 2 minutes
    - 80% alcohol 1 minute
    - Running tap water 5mins
44. Load slides on the slide racks (make sure to keep slides wet with TBS) and reagent onto the reagent rack (white) with exact amount and placement the Autostainer requires.
45. Starting a run: click "Next" after loading slides, click on Prime Pump (water) and Prime Pump (buffer) and check if machine is really running.
46. Click on "Start Run"
47. Autostainer steps:
    - Rinse (TBS+Tween)
    - Proteolytic digestion to unmask antigenic sites with 0.1% (w/v) Protease XIV (40 min.)
    - Rinse
    - Endogenous peroxidase quench from Dako kit (10 min.)
    - Rinse
    - Block non-specific binding with X0909 Blocking Solution (10min.)
    - **NO RINSE**
    - Primary Antibody or Negative Control (30 min.)
    - Rinse
    - Polymer-HRP (30 min.)
    - Rinse
    - "switch"
    - Substrate- AEC Plus (10 min.)
    - Rinse
48. After Autostainer completed, immediately unload slides from machine and put in TBS to keep wet, click "Next".
49. Counter-stain with Mayers Hematoxylin for 1.5 minutes.
50. Rinse in running tap water (3 min).
51. Transfer slideholder into a container with tap water and immediately coverslip (don't let slides dry) with Aqueous Mounting Media (**do not use Cytoseal, it will take off AEC**).

Immunohistochemical Staining for Laminin

Use DakoCytomation EnVision+ System-HRP (AEC) designed for Rabbit Primary Antibodies.

Standard setting uses 150ul per treated section of each slide and will treat 3 sections of slide (marked yellow).

Solution Preparation
Note: Amounts will vary depending on number of slides being stained

45. **Tris-Buffered Saline** (TBS) (Dako packets) — Stored at RT in packets, 4°C in soln
    1 package (DakoS3001) to 1L dH_2O
    1 package (DakoS1969) to 5L dH20
46. **Wash Buffer with Tween 20** — Stored at 4°C
    (DakoCytomation, S3006, 1000ml)
    500ml of 10x in 4500ml dH20
47. **0.1% Protease XIV** (Sigma P-5147) — Stored at -20°C until use
    0.01g Protease
    10 ml TBS
48. **Peroxidase Blocking Reagent** — Stored at 4°C
    (Dako)
    Ready-to-use 15ml/vial
49. **X0909 Blocking Solution** — Stored at 4°C
50. **Primary Laminin Rabbit Polyclonal Antibody** — Stored at 4°C
    (abcam ab11575)
    Concentration of product:
    Use 27ug/ml diluted in universal AB diluent (Dako S0809) **(not TBS)**
51. **Dako Negative Rabbbit Control (Normal)** — Stored at 4°C
    Dako X0903
    Concentration of product:
52. **Labelled Polymer-HRP Anti-Rabbit** (Dako) — Stored at 4°C
    Ready-to-use 15ml/vial
53. **AEC PLUS** (Dako) — Stored at 4°C
    Ready-to-use 15ml/vial
54. **Counterstain** — Stored at RT
    Mayer's Hematoxylin Solution (Sigma MHS16)
    (filter before use)
55. **Aqueous Mounting Media** — Stored at RT
    Faramount, Dako S3025

Methods ***Do not let the slides dry out during this process***

52. Put paraffin sections on slide warmer (setting 6 for at least 1 hour) (use goat skin as control)
53. Turn on the computer and set up protocol on autostainer: on Desktop, click "DAKO Autostainer", login Dong, password Dong, "Program", "File", "Open", "endostat"
54. To add slides, click on "Slides" and type in the number of slides you want to stain including all controls
55. Copy and paste the staining protocol by first clicking on "Copy" then on the slide you want to copy. Clicking on any slide will automatically "Paste" the protocol to any desired row.
56. Deparaffinize and rehydrate paraffin section via the following baths
    - Xylene 2 x 5 minutes
    - 100% alcohol 2 x 3 minutes
    - 95% alcohol 2x 2 minutes
    - 80% alcohol 1 minute
    - Running tap water 5mins
57. Load slides on the slide racks (make sure to keep slides wet with TBS) and reagent onto the reagent rack (white) with exact amount and placement the Autostainer requires.
58. Starting a run: click "Next" after loading slides, click on Prime Pump (water) and Prime Pump (buffer) and check if machine is really running.
59. Click on "Start Run"
60. Autostainer steps:
    - Rinse (TBS+Tween)
    - Proteolytic digestion to unmask antigenic sites with 0.1% (w/v) Protease XIV (40 min.)
    - Rinse
    - Endogenous peroxidase quench from Dako kit (10 min.)
    - Rinse
    - Block non-specific binding with X0909 Blocking Solution (10min.)
    - **NO RINSE**
    - Primary Antibody or Negative Control (30 min.)
    - Rinse
    - Polymer-HRP (30 min.)
    - Rinse
    - "switch"
    - Substrate- AEC Plus (10 min.)
    - Rinse
61. After Autostainer completed, immediately unload slides from machine and put in TBS to keep wet, click "Next".
62. Counter-stain with Mayers Hematoxylin for 1.5 minutes.
63. Rinse in running tap water (3 min).
64. Transfer slideholder into a container with tap water and immediately coverslip (don't let slides dry) with Aqueous Mounting Media (**do not use Cytoseal, it will take off AEC**).

Immunohistochemical Staining of vWF (Factor VIII-Related Antigen)

Use DakoCytomation EnVision+ System-HRP (AEC) designed for Rabbit Primary Antibodies.

Standard setting uses 150ul per treated section of each slide and will treat 3 sections of slide (marked yellow).

Solution Preparation
Note: Amounts will vary depending on number of slides being stained

56. **Tris-Buffered Saline** (TBS) (Dako packets) — Stored at RT in packets, 4°C in soln
    1 package (DakoS3001) to 1L dH_2O
    1 package (DakoS1969) to 5L dH20
57. **Wash Buffer with Tween 20** — Stored at 4°C
    (DakoCytomation, S3006, 1000ml)
    500ml of 10x in 4500ml dH20
58. **0.1% Protease XIV** (Sigma P-5147) — Stored at -20°C until use
    0.01g Protease
    10 ml TBS
59. **Peroxidase Blocking Reagent (Dako)** — Stored at 4°C
    Ready-to-use 15ml/vial
60. **X0909 Blocking Solution (Dako)** — Stored at 4°C
61. **Primary vWF Rabbit Polyclonal Antibody** — Stored at 4°C
    Rabbit against human vWF (Dako A0082)
    Concentration of product:
    Use 16.5 ug/ml final concentration
    Dilute primary antibody in universal AB diluent (Dako S0809) **(not TBS)**
62. **Dako Rabbit Immunoglobulin Negative Control** — Stored at 4°C
    Dako X0936 (solid phase absorbed)
    Concentration of product:
    Dilute to 16.5 ug/ml final conc in universal AB diluent
63. **Labelled Polymer-HRP Anti-Rabbit** — Stored at 4°C
    Ready-to-use 15ml/vial (Dako)
64. **AEC PLUS** (Dako) — Stored at 4°C
    Ready-to-use 15ml/vial
65. **Counterstain** — Stored at RT
    Mayer's Hematoxylin Solution (Sigma MHS16)
    (filter before use)
66. **Aqueous Mounting Media** — Stored at RT
    Faramount, Dako S3025

Methods ***Do not let the slides dry out during this process***

65. Put paraffin sections on slide warmer (setting 6 for 1 hour) (a good positive control tissue to use is goat skin)
66. Turn on the computer and set up protocol on autostainer: on Desktop, click "DAKO Autostainer", login Dong, password Dong
67. To add slides, click on "Slides" and type in the number of slides you want to stain including all controls
68. Copy and paste the staining protocol by first clicking on "Copy" then on the slide you want to copy. Clicking on any slide will automatically "Paste" the protocol to any desired row.
69. Deparaffinize and rehydrate paraffin section via the following baths
    - Xylene 2 x 5 minutes
    - 100% alcohol 2 x 3 minutes
    - 95% alcohol 2x 2 minutes
    - 80% alcohol 1 minute
    - Running tap water 5mins
70. Load slides on the slide racks (make sure to keep slides wet with TBS) and reagent onto the reagent rack (white) with exact amount and placement the Autostainer requires.
71. Starting a run: click "Next" after loading slides, click on Prime Pump (water) and Prime Pump (buffer) and check if machine is really running.
72. Click on "Start Run"
73. Autostainer steps:
    - Rinse (TBS+Tween)
    - Proteolytic digestion to unmask antigenic sites with 0.1% (w/v) Protease XIV (40 min.)
    - Rinse
    - Endogenous peroxidase quench from Dako kit (10 min.)
    - Rinse
    - Block non-specific binding with X0909 Blocking Solution (10min.)
    - **NO RINSE**
    - Primary Antibody or Negative Control (30 min.)
    - Rinse
    - Polymer-HRP (30 min.)
    - Rinse
    - "switch"
    - Substrate- AEC Plus (10 min.)
    - Rinse
74. After Autostainer completed, immediately unload slides from machine and put in TBS to keep wet, click "Next".
75. Counter-stain with Mayers Hematoxylin for 1.5 minutes.
76. Rinse in running tap water (3 min).
77. Transfer slideholder into a container with tap water and immediately coverslip (don't let slides dry) with Aqueous Mounting Media (**do not use Cytoseal, it will take off AEC**).

Immunohistochemical Staining of CD31 (PECAM-1)

Use DakoCytomation EnVision+ System-HRP (AEC) designed for Rabbit Primary Antibodies.

Solution Preparation

Note: Amounts will vary depending on number of slides being stained

67. **Tris-Buffered Saline** (TBS) (Dako packets) — Stored at RT in packets, 4°C in soln
    1 package (DakoS3001) to 1L dH_2O
    1 package (DakoS1969) to 5L dH20
68. **Wash Buffer with Tween 20** — Stored at 4°C
    (DakoCytomation, S3006, 1000ml)
    500ml of 10x in 4500ml dH20
69. **10mM Tris/ 1 mM EDTA**, pH 9.0 — Stored in cabinet in 224
    1.21 g Tris (Invitrogen 15504-020)
    0.37 g EDTA (Sigma E-5513)
    (Ethylenediaminetetraacetic acid disodium salt dihydrate, $C_{10}H_{14}N_2Na_2O_8 \cdot 2H_2O$, MW 372.24)
    1000 ml DI water
70. **Peroxidase Blocking Reagent** — Stored at 4°C
    (Dako)
    Ready-to-use 15ml/vial
71. **X0909 Blocking Solution** — Stored at 4°C
    Ready-to-use
72. **Primary Antibody** — Stored at 4°C
    Abcam 28364 or negative (Dako X0903)
    Dilute to 21ug/ml final concentration
73. **Antibody Diluent** (Dako S0809) — Stored at 4°C
74. **Labelled Polymer-HRP Anti-Rabbit** — Stored at 4°C
    Ready-to-use 15ml/vial (Dako)
75. **AEC PLUS** (Dako) — Stored at 4°C
    Ready-to-use 15ml/vial
76. **Counterstain** — Stored at RT
    Mayer's Hematoxylin Solution (Sigma MHS16)
    (filter before use)
77. **Aqueous Mounting Media** — Stored at RT
    Faramount, Dako S3025

Methods ***Do not let the slides dry out during this process***

78. Put paraffin sections on slide warmer (use goat skin as control)
79. Deparaffinize and rehydrate paraffin section via the following baths
    - Xylene 2 x 5 minutes
    - 100% alcohol 2 x 3 minutes
    - 95% alcohol 2x 2 minutes
    - 80% alcohol 1 minute
    - Rinse in tap water
80. Mix Tris and EDTA and DI water and check pH (usually doesn't need adjustment).
81. Incubate slides in Tris/EDTA for 10 mins in decloaker set at 90C. Make sure solutions are nearly boiling (~95°C) the whole time.
82. Remove slides from decloaker and leave slides in solutions for 20 minutes to cool down to room temperature.
83. Steps:
    - Rinse (TBS+Tween)
    - Endogenous peroxidase quench from Dako kit (10 min.)
    - Rinse
    - Block non-specific binding with X0909 Blocking Solution (10min.)
    - **NO RINSE**
    - Primary Antibody or Negative Control (30 min.)
    - Rinse
    - Polymer-HRP (30 min.)
    - Rinse
    - Substrate- AEC Plus (10 min.)
    - Rinse
84. Counter-stain with Mayers Hematoxylin for 1.5 minutes.
85. Rinse in running tap water (3 min).
86. Transfer slideholder into a container with tap water and immediately coverslip (don't let slides dry) with Aqueous Mounting Media (**do not use Cytoseal, it will take off AEC**).

Immunohistochemical Staining of Lubricin

Use DakoCytomation EnVision+ System-HRP (AEC) designed for Mouse Primary Antibodies.

Standard setting uses 150ul per treated section of each slide and will treat 3 sections of slide (marked yellow).

Solution Preparation
Note: Amounts will vary depending on number of slides being stained

78. **Tris-Buffered Saline** (TBS) (Dako packets) — Stored at RT in packets, 4°C in soln
    1 package (DakoS3001) to 1L dH_2O
    1 package (DakoS1969) to 5L dH20
79. **Wash Buffer with Tween 20** — Stored at 4°C
    (DakoCytomation, S3006, 1000ml)
    500ml of 10x in 4500ml dH20
80. **0.1% Protease XIV** (Sigma P-5147) — Stored at -20°C until use
    0.01g Protease
    10 ml TBS
81. **Peroxidase Blocking Reagent (Dako)** — Stored at 4°C
    Ready-to-use 15ml/vial
82. **X0909 Blocking Solution (Dako)** — Stored at 4°C
83. **Primary Lubricin Mouse Antibody** — Stored at 4°C
    Mouse monoclonal S.679
    Concentration of product:
    Use 4.6 ug/ml final concentration
    Dilute primary antibody in universal AB diluent (Dako S0809) **(not TBS)**
84. **Dako Mouse Immunoglobulin Negative Control** — Stored at 4°C
    IgG2b
    Concentration of product:
    Dilute to 4.6 ug/ml final conc in universal AB diluent
85. **Labelled Polymer-HRP Anti-Mouse** — Stored at 4°C
    Ready-to-use 15ml/vial (Dako)
86. **AEC PLUS** (Dako) — Stored at 4°C
    Ready-to-use 15ml/vial
87. **Counterstain** — Stored at RT
    Mayer's Hematoxylin Solution (Sigma MHS16)
    (filter before use)
88. **Aqueous Mounting Media** — Stored at RT
    Faramount, Dako S3025

Methods ***Do not let the slides dry out during this process***

87. Put paraffin sections on slide warmer (setting 6 for 1 hour) (a good positive control tissue to use is goat cartilage)
88. Turn on the computer and set up protocol on autostainer: on Desktop, click "DAKO Autostainer", login Dong, password Dong
89. To add slides, click on "Slides" and type in the number of slides you want to stain including all controls
90. Copy and paste the staining protocol by first clicking on "Copy" then on the slide you want to copy. Clicking on any slide will automatically "Paste" the protocol to any desired row.
91. Deparaffinize and rehydrate paraffin section via the following baths
    - Xylene 2 x 5 minutes
    - 100% alcohol 2 x 3 minutes
    - 95% alcohol 2x 2 minutes
    - 80% alcohol 1 minute
    - Running tap water 5mins
92. Load slides on the slide racks (make sure to keep slides wet with TBS) and reagent onto the reagent rack (white) with exact amount and placement the Autostainer requires.
93. Starting a run: click "Next" after loading slides, click on Prime Pump (water) and Prime Pump (buffer) and check if machine is really running.
94. Click on "Start Run"
95. Autostainer steps:
    - Rinse (TBS+Tween)
    - Proteolytic digestion to unmask antigenic sites with 0.1% (w/v) Protease XIV (40 min.)
    - Rinse
    - Endogenous peroxidase quench from Dako kit (10 min.)
    - Rinse
    - Block non-specific binding with X0909 Blocking Solution (10min.)
    - **NO RINSE**
    - Primary Antibody or Negative Control (30 min.)
    - Rinse
    - Polymer-HRP (30 min.)
    - Rinse
    - "switch"
    - Substrate- AEC Plus (10 min.)
    - Rinse
96. After Autostainer completed, immediately unload slides from machine and put in TBS to keep wet, click "Next".
97. Counter-stain with Mayers Hematoxylin for 1.5 minutes.
98. Rinse in running tap water (3 min).

Transfer slideholder into a container with tap water and immediately coverslip (don't let slides dry) with Aqueous Mounting Media (**do not use Cytoseal, it will take off AEC**).

Histomorphometry

Open the desired H&E image in ImageJ.

Measure area:
• Select the POLYGON SELECTION TOOL. You can change the width of the line drawn with the pencil tool by "Edit" "Options" "Line Width" "5". To change the color, double click the COLOR PICKER (dropper) button.
• Draw the outline of the area of interest (Ctrl+D to make outline permanent).
• Select the WAND (TRACING) TOOL.
• Click on the line you just drew. The area of interest will be selected.
• Select Analyze, Measure. The results box will list the number of pixels in the area selected. Record this number. You may wish to save the image at this point.
• Change to a new color by double-clicking the COLOR PICKER button for each new tissue type/area of interest and repeat.

Measure bonding:
• Select SEGMENTED LINE SEGMENTS and trace the line of interest.
• Select "Analyze" "Measure".
• Record length.